Development of DNMT2 inhibitors for the selective manipulation of the epitranscriptome

Dissertation

zur Erlangung des Grades

„Doktor der Naturwissenschaften"

im Promotionsfach Chemie

am Fachbereich Chemie, Pharmazie,

Geographie und Geowissenschaften

der Johannes Gutenberg-Universität Mainz

Tim Fischer, M.Sc.

geboren am 18.02.1993 in Speyer

Mainz, April 2022

JOHANNES GUTENBERG UNIVERSITÄT MAINZ

JG|U

Dekanin: ████████████████

1. Gutachter: ██████████████

2. Gutachterin: ████████████████

Datum Dissertation: 7. Juni 2022

D77 (Dissertation Mainz)

Die vorgelegte Dissertation wurde am Institut für Pharmazeutische und Biomedizinische Wissenschaften der Johannes Gutenberg-Universität in Mainz zur Erlangung des Grades "Doktor der Naturwissenschaften" unter der Betreuung von ████████████ und ████████████████ angefertigt.

1. Gutachter

████████████████

Fachbereich Chemie, Pharmazie, Geographie und Geowissenschaften

Institut für Pharmazeutische und Biomedizinische Wissenschaften

Johannes Gutenberg-Universität Mainz

2. Gutachterin

██████████████████

Fachbereich Chemie, Pharmazie, Geographie und Geowissenschaften

Institut für Pharmazeutische und Biomedizinische Wissenschaften

Johannes Gutenberg-Universität Mainz

Hiermit versichere ich eidesstattlich:

1. Ich habe die jetzt als Dissertation vorgelegte Arbeit selbst angefertigt und alle benutzten Hilfsmittel (Literatur, Apparaturen, Material) in der Arbeit angegeben.

2. Ich habe oder hatte die jetzt als Dissertation vorgelegte Arbeit nicht als Prüfungsarbeit für eine staatliche oder andere wissenschaftliche Prüfung eingereicht.

3. Ich hatte weder die jetzt als Dissertation vorgelegte Arbeit noch Teile davon bei einer anderen Fakultät bzw. einem anderen Fachbereich als Dissertation eingereicht.

| Ort, Datum | Unterschrift |

'Nature does nothing uselessly.'

– Aristotle.

'The ballot is stronger than the bullet.'

- Abraham Lincoln.

Acknowledgements

Content

Abstract

The research discipline of epitranscriptomics dealing with ribonucleic acid (RNA) modifications has gained increased popularity over the last decade. With the discovery of their contribution to numerous physiological and pathophysiological pathways, RNA modifications are now considered as highly pertinent field in biological and biomedical research.

Methylations hold particular interest, since they represent the most widespread RNA modification and thus are involved in a huge variety of cellular regulations. Methyl groups are attached to RNA by the enzyme family of RNA methyltransferases (MTases). Due to the association of RNA methylations with several malignancies, the corresponding MTases shifted into the focus of medicinal chemists as potential drug targets.

One specifically interesting RNA MTase is DNA methyltransferase 2 (DNMT2), which exact biological function remains enigmatic. However, increasing amounts of data indicate a participation of this enzyme in pathophysiological processes. Accordingly, modulators of DNMT2 activity were developed within the scope of this thesis by following two converging approaches. Firstly, small molecule inhibitors were designed and assessed, while secondly, RNA aptamers were evolved and analysed.

The small molecule inhibitors evaluated herein are based on the structure of the natural cofactor *S*-adenosyl-L-methionine (SAM), which was chemically derivatised to yield Y-shaped structures. A systematic overview of structure-activity relationships for these inhibitors was provided by two distinct surveys leading to profound insights into molecular architectures recognised by DNMT2. Thus gained perceptions were backed and complemented by *in silico* analyses further broadening the understanding of molecular recognition.

These efforts resulted in compounds with moderate affinities for the enzyme, which presumably compete with SAM for the identical binding site. Beyond this, more sophisticated inhibition mechanisms for specific inhibitors were revealed, such as time-dependent inhibition or RNA competition. Intriguingly, for selected compounds even partial selectivity towards other MTases was observed.

The generation of RNA aptamers for DNMT2 commenced with analysing systematic evolution of ligands by exponential enrichment (SELEX) evolved pools employing next generation sequencing (NGS) and a subsequent bioinformatics pipeline. Therefore, not only promising sequences were chosen for further characterisation, but highly conserved nucleotides among these were likewise identified. Subsequent *in vitro* experiments exposed one aptamer with higher inhibitory efficacy compared to the complete RNA pools and first truncation experiments of this sequence added knowledge about its structure-activity relationship.

x

Zusammenfassung

Der Wissenschaftszweig der Epitranskriptomik, welcher sich mit Ribonukleinsäure (RNA) Modifikationen beschäftigt, hat in den vergangenen zehn Jahren zunehmend an Popularität gewonnen. Durch die Verbindung von RNA Modifikationen mit verschiedenen physiologischen und pathophysiologischen Stoffwechselvorgängen sind diese nun ein bedeutsames Feld für biologische und biomedizinische Wissenschaften. In diesem Zusammenhang sind besonders Methylierungen von Interesse, da sie die meistverbreiteten Modifikationen darstellen und dementsprechend in vielfältiger Weise an der zellulären Regulation mitwirken. Methylgruppen werden von der Enzymfamilie der RNA Methyltransferasen (MTasen) auf RNA übertragen. Da RNA Methylierungen mit diversen Krankheiten in Zusammenhang gebracht wurden, sind die dazugehörigen MTasen nun in den Fokus von medizinischen Chemiker*innen als potentielle *drug targets* gerückt.

Eine außergewöhnliche MTase ist die DNA methyltransferase 2 (DNMT2), von welcher die genaue biologische Funktion noch nicht vollständig aufgeklärt wurde. Allerdings deutet immer mehr darauf hin, dass das Enzym an pathophysiologischen Prozessen beteiligt ist. Dementsprechend wurden im Zuge dieser Arbeit Modulatoren für die DNMT2 Aktivität entwickelt, indem zwei konvergente Strategien verfolgt wurden. Erstens wurden *small molecule* Inhibitoren entwickelt und untersucht, während zweitens RNA Aptamere generiert und analysiert wurden.

Die *small molecule* Inhibitoren, welche in dieser Arbeit evaluiert wurden, basieren auf der Struktur des natürlichen Cofaktors *S*-Adenosyl-L-Methionin (SAM). Dieser wurde chemisch derivatisiert, sodass Y-förmige Strukturen erzeugt wurden. Ein systematischer Überblick über Struktur-Wirkungsbeziehungen für diese Inhibitoren wurde durch zwei Studien generiert. Diese gewähren einen detaillierten Einblick in die von DNMT2 erkannten molekularen Architekturen. So gewonnene Erkenntnisse konnten durch *in silico* Modelle unterfüttert werden, sodass das Verständnis über die molekularen Interaktionen erweitert werden konnte.

Diese Ansätze führten zu Molekülen mit moderaten Affinitäten für das Enzym und konkurrieren wahrscheinlich mit SAM um die gleiche Bindetasche. Weiterhin wurden differenziertere Inhibitionsmechanismen, wie zeitabhängige Inhibition oder RNA Konkurrenz, offenbart. Interessanterweise wurde für einige Inhibitoren sogar partielle Selektivität gegenüber anderen MTasen beobachtet.

Für die Generierung von DNMT2 RNA Aptameren wurden zunächst RNA Mischungen, welche durch *systematic evolution of ligands by exponential enrichment* (SELEX) entstanden, durch Hochdurchsatzsequenzierung (NGS) und anschließenden bioinformatischen Methoden analysiert. Hierdurch wurden nicht nur vielversprechende Kandidaten für weitere Charakterisierung ausgewählt, sondern auch über alle Sequenzen hochkonservierte Nukleotide identifiziert. Nachfolgende *in vitro* Experimente zeigten, dass ein isoliertes Aptamer stärkere Inhibition als die kompletten RNA Mischungen aufwies und erste Verkürzungsexperimente lieferten ein fundiertes Wissen über Struktur-Wirkungsbeziehungen für die Aptamere.

List of Figures

List of Tables

Abbreviations

^{3}H-SAM	tritium labelled *S*-adenosyl-L-methionine
5-FU	5-fluorouracil
5mC	5-methylcytosine
A	adenosine/adenine
A. thaliana	*Arabidopsis thaliana*
aaRS	aminoacyl-tRNA synthase
ACS	american chemical societey
AF4	assymetric flow-field flow fractionation
Am	2'-*O*-methyladenosine
AML	acute myeloid leukaemia
APS	ammonium persulfate
ASLC	azacitidine sensitive leukaemia cells
Asn	asparagine
Asp	aspartate
ATP	adenosine triphosphate
B. subtilis	*Bacillus subtilis*
BSA	bovine serum albumin
C	cysteine
C	cytidine/cytosine
C. albicans	*Candida albicans*
CADD	computer aided drug design
COSMIC	catalogue of somatic mutations in cancer
CD	circular dichroism
Cm	2'-*O*-methylcytidine
COMT	catechol-*O*-MTase
CRISPR	clustered regularly interspaced short palindromic repeats
CTP	cytidine triphosphate

Cys	cysteine
D. discoideum	*Dictyostelium discoideum*
D. melanogaster	*Drosophila melanogaster*
DENV	*dengue virus*
DKFZ	Deutsches Krebsforschungszentrum
DMSO	dimethyl sulfoxid
DNA	deoxyribonucleic acid
DNMT1	DNA methyltransferase 1
DNMT2	DNA methyltransferase 2
DNMT3	DNA methyltransferase 3
dNTP	deoxynucleoside triphosphate
DTT	dithiothreitol
dsRNA	double stranded RNA
E	glutamate
E. coli	*Escherichia coli*
E. cuniculi	*Encephalitozoon cuniculi*
E. histolytica	*Entamoeba histolytica*
EDTA	ethylenediaminetetraacetic acid
EMSA	electrophoretic mobility shift assays
Erm	erythromycin resistance methyltransferase
FRET	Förster resonance energy transfer
FBDD	fragment-based drug discovery
FDA	federal drug agency
G	glycine
G	guanosine/guanine
Gln	glutamine
Glu	glutamate
Gly	glycine

xvi

Gm	2'-*O*-methylguanosine
GTP	guanosine triphosphate
H. sapiens	*Homo sapiens*
HEK cells	human embryonic kidney cells
HIV	human immunodefficiency virus
hnRNPK	heterogeneous nuclear ribonucleoprotein K
HPLC	high-performance liquid chromatography
HTRF	homogenous time-resolved fluorescence
HTS	high throughput screenings
HCoV-OC43	*human coronavirus*-OC43
i^6A	N^6-isopentenyladenosine
i.c.	*in cellulo*
i.s.	*in silico*
i.vt.	*in vitro*
i.vv.	*in vivo*
IC_{50}	half maximal inhibitory concentration
ICB	intracellular buffer
ICMT	isoprenylcysteine carboxyl methyltransferase
IEX	ion exchange chromatography
IMAC	immobilised metal ion affinity chromatography
ITC	isothermal titration calorimetry
IVT	*in vitro* transcription
JEV	*japanese encephalities virus*
JGU	Johannes Gutenberg-University
K_D	dissociation constant
kDa	kilo dalton
K_i	equilibrium constant of the enzyme-inhibitor complex
LBDD	ligand-based drug design

Leu	leucine
LNA	locked nucleic acids
LTS	low throughput screening
−M	negative mesomeric effect
m^{6}A	N^6-methyladenosine
m^{3}C	3-methylcytidine
m^{5}C	5-methylcytidine
m^{7}G	N^7-methylguanosine
m^{1}Ψ	N^1-methylpseudouridine
miRNA	microRNA
mRNA	messenger RNA
MS	mass spectrometry
ms^{2}i^{6}A	2-methylthio-N^6-isopentenyladenosine
MST	microscale thermophoresis
mt-tRNA	mitochondrial tRNA
MTase	methyl transferase
MTHF	N^5,N^{10}-methylenetetrahydrofolate
MSA	multiple sequence alignment
N	asparagine
NGS	next generation sequencing
neg	negative control
NMR	nuclear magnetic resonance
NTP	nucleoside triphosphate
PAGE	polyacrylamide gel electrophoresis
PAINS	pan-assay interference compounds
PARPi	poly-ADP-ribose-polymerase inhibitors
PCR	polymerase chain reaction
PDB	protein data bank

PEG	polyethylene glycol
pH	*potentia hydrogenii*
Ph. Eur.	european pharmacopoeia
Phe	phenyl alanine
pK_a	acid dissociation constant
pos	positive control
Pro	proline
Ψ	pseudouridine
Q	glutamine
Q	queuosine
R	arginine
RdRp	RNA dependent RNA polymerase
RNA	ribonucleic acid
rRNA	ribosomal RNA
RT-PCR	reverse transcriptase PCR
S	serine
S. cerevisiae	*Saccharomyces cerevisiae*
S. frugiperda	*Spodoptera frugiperda*
S. pombe	*Schizosaccharomyces pombe*
SAH	*S*-adenosyl-L-homocysteine
SAM	*S*-adenosyl-L-methionine
SARS-CoV-2	*severe acute respiratory syndrome coronavirus* 2
SAR	structure activity relationship
SBDD	structure-based drug design
SEC	size exclusion chromatography
SFG	sinefungin
siRNA	small interference RNA
SELEX	systematic evolution of ligands by exponential enrichment

Ser	serine
sncRNA	small non-coding RNA
SPA	scintillation proximity assay
SPR	surface plasmone resonance
S_NAr	nucleophilic aromatic substitution
T	threonine
T	thymidine
t^6A	N^6-threonylcarbamoyl adenosine
TBE	tris-borate-EDTA buffer
TCA	trichloroacetic acid
TEMED	tetramethylethylenediamine
TIM barrel	triose-phosphate isomerase barrel
tRF	tRNA fragment
tRNA	transfer RNA
TSA	thermal shift assay
tsRNA	tRNA derived small RNA
U	uridine/uracil
Um	2'-O-methyluridine
ULR	ultra low range DNA ladder
UTP	uridine triphsophate
UV	ultraviolet
Val	valine
VEGF	vascular endothelial growth factor
v_i	initial velocity
VS	virtual screening
v_s	steady-state velocity
WNV	*west nile virus*
X	random amino acid/nucleotide
xx	

|	
XNA	xeno nucleic acids
yW	wybutosine
ZIKV	*zika virus*

1 Introduction

1.1 Epitranscriptomics

Ribonucleic acid (RNA) is a ubiquitous biopolymer and the most pivotal player in protein biosynthesis, best known for its three main representatives: messenger RNA (mRNA), transfer RNA (tRNA) and ribosomal RNA (rRNA) (1). In recent years, various additional functionalities of RNA were unveiled alongside novel RNA species conferring increased significance and importance to RNA beyond its classical task in protein translation (1–6). Notable examples are small interfering RNAs (siRNAs) capable of gene silencing by targeted mRNA degradation (6–8) or tRNA derived small RNAs (tsRNAs also called tRNA fragments (tRFs)) affecting multiple physiological processes, e.g. epigenetic regulation (9, 10).

With the 2020 Nobel Prize in chemistry awarded to Jennifer Doudna and Emmanuelle Charpentier, two discoverers of the clustered regularly interspaced short palindromic repeats (CRISPR)-Cas9 system (11, 12), together with the federal drug agency's (FDA) emergency approval of the first mRNA-based vaccines in the same year (13), RNA has emerged as a main focus in biological and medical research. Although RNA is capable of adopting highly complex three-dimensional structures (14), its composition is rather limited at first sight, as it consists of only four different nucleotides mainly interacting via canonical Watson–Crick–Franklin base pairing (15). In contrast, proteins comprise 20 canonical amino acids giving them an extended interaction scope (16).

However, interactions between bases are not restricted to Watson–Crick–Franklin base pairing, non-canonical interactions as Wobble or Hoogsteen base pairings are also feasible. This enables more complex arrangements of RNAs and thus permits their diverse functionalities (15). In addition, all four bases occurring in RNA, namely adenine (A), guanine (G), cytosine (C) and uracil (U), as well as the ribose moieties are chemically modified, which considerably expands the diversity of these building blocks.

Well over 150 RNA modifications have been described to date, with their number steadily increasing (17). Modifications range from simple chemical attachments as the methyl group to more complex molecules like i^6A or t^6A, bearing isopentenyl or threonyl derivatives, (18, 19) to highly sophisticated base alterations such as queuosine (Q) or wybutosine (yW), which are presented in Figure 1 (20, 21).

Modifications are found at several positions of all four canonical bases (indicated by descriptors before the base letter) and moreover at the 2'-position of the ribose (indicated by an m behind the base letter, Figure 1). Over the past ten years, the field of RNA modifications became increasingly popular, sparked by the precise mapping of m^6A (structure displayed in Figure 1) on mRNA (22, 23) and was dubbed "epitranscriptomics", in analogy to epigenetics (24, 25).

As the epitranscriptome became more prevalent, the enzymes associated with it became increasingly recognised, roughly dividing into 'writers' (implement modifications), 'readers' (decode modifications) and 'erasers' (remove modifications) (26). The existence of erasers already indicated the dynamics underlying this layer of information reflecting their multiple functions *in vivo* (27, 28).
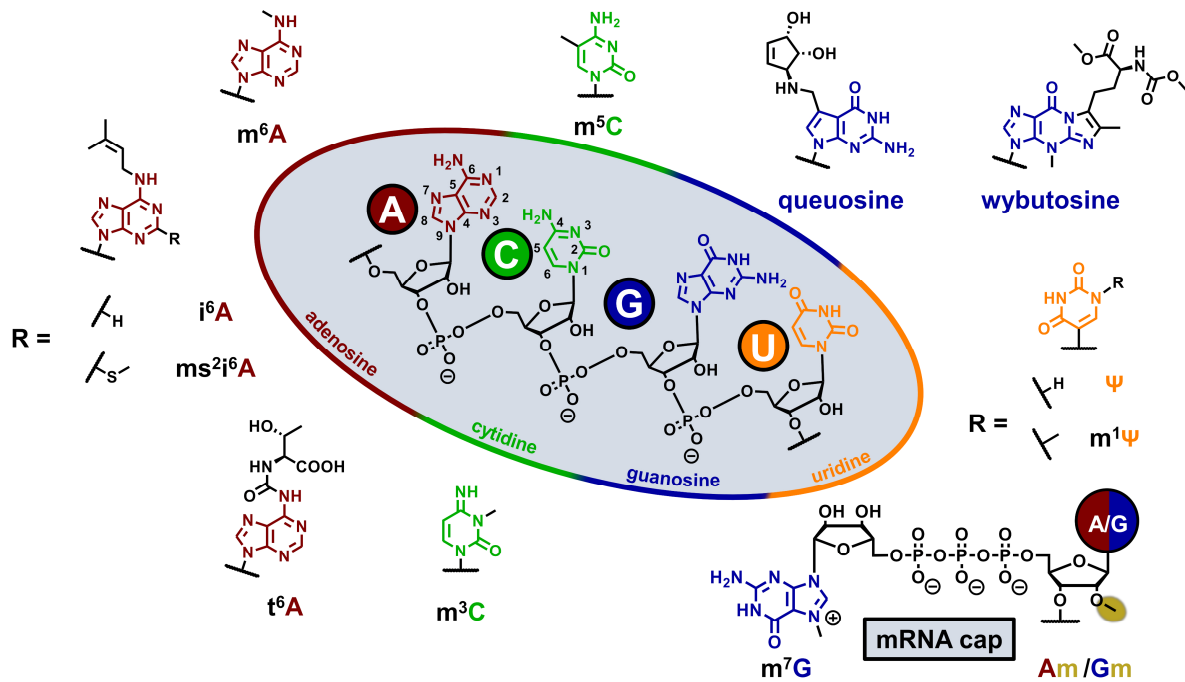
Figure 1. Epitranscriptomics. Structure of the four canonical RNA bases as well as selected examples of RNA modifications with a representative image of an mRNA cap.

RNA modifications and their machinery participate in biological regulation by numerous and diverse pathways with many of them not fully understood (29, 30) and importantly they have been found to contribute to pathological phenotypes (31). In this context, m⁶A is arguably the most famous and well-studied modification. It is highly abundant on mRNA, where it influences translation, alternate splicing as well as stability and thus directly affects the production of corresponding proteins (32–34). Accordingly, it is not surprising that m⁶A was associated with progression of cancers, such as acute myeloid leukaemia (AML) (31, 35–39) or development of the nervous system (40).

The epitranscriptome is also utilised by the innate immune system to distinguish between endo- and exogenous RNA and consequently to recognise pathogens (41). In this regard, pseudouridine (Ψ, or rather its methylated form m¹Ψ, see Figure 1) is particularly worth mentioning, since it is incorporated into the mRNA vaccines of BioNTech/Pfizer and Moderna for its immunomodulatory qualities (13, 42).

1.2   RNA methylation

Despite the vast divergence of RNA modifications, one of the most relevant members is also the simplest one: the methyl group. Next to the above mentioned m⁶A, methyl groups have been found on all major types of RNA as well as on various positions on the RNA scaffold, with prominent members such as m⁵C, m⁷G or 2'-*O*-methylations as depicted in Figure 1 (43). As can be expected, the biological functions exhibited by RNA methylations are as diverse as their occurrence on RNA.

Already half a century ago, RNA methylations were identified on the 5'-cap of mRNAs in which a m⁷G bearing guanosine is linked to the RNA via a 5'-5' triphosphate bridge, while additional to this, 2'-*O*-methylations can be found at the first nucleotides of the corresponding mRNA (Figure 1) (44–48). These modified mRNA caps have an impact on mRNA translation (49, 50), stability (51), transport (52,

53) and influence various different functions (47, 48, 54), while additionally they are also crucial for the discrimination of exogenic from endogenic RNA by the innate immune system (55–58).

RNA methylations also impact the structural integrity of tRNAs and rRNAs, e.g. by blocking of Watson–Crick–Franklin base pairing and therefore add an additional layer of translational control (59).

Interestingly, RNA methylations can also facilitate the incorporation of other modifications. For instance, the 2'-O-methylations Cm located at position 32 and Gm at position 34 (Cm_{32} and Gm_{34}) are crucial for robust hypermodification of m^1G_{37} to wybutosine (yW) on tRNA^{Phe} in *Schizosaccharomyces pombe* and *Saccharomyces cerevisiae* (60, 61). The other way around, the incorporation of methyl groups can be triggered by different modifications, as in *Escherichia coli* tRNA^{Leu} in which i^6A_{37} facilitates Cm or Um incorporation at position 34 (43, 62, 63).

An impressive and recent example for the possible impact of RNA methylations is given by the m^3C_{32} modification found on mitochondrial (mt)-tRNA^{Thr} and mt-tRNA$^{Ser(UCN)}$ in humans. The modification is implemented by the enzyme METTL8, in particular if RNA position A_{37} is modified with t^6A_{37} (mt-tRNA^{Thr}), i^6A_{37} or $ms^2i^6A_{37}$ (mt-tRNA$^{Ser(UCN)}$). Modified mt-tRNA adopts a different conformation compared to RNA lacking m^3C and slightly alters translation (64, 65). As this process is localised in the mitochondria, the methylation leads to increased respiratory chain activity and intriguingly the corresponding writer, METTL8, is overexpressed in pancreatic cancer cell lines (66).

1.3 RNA methyltransferases

Methyl groups are grafted onto their respective targets by methyltransferases (MTases) (67). These targets include not only RNA (68), but also deoxyribonucleic acid (DNA) (69), proteins (70) and small molecules (71) and most of them are utilising S-adenosyl-L-methionine (SAM) as cofactor which is converted into S-adenosyl-L-homocysteine (SAH) during the methylation reaction (Figure 2) (67).

After adenosine triphosphat (ATP), SAM is one of the most abundant cofactors found in cells, and accordingly, SAM-dependent MTases were observed in all three domains of life (72). Classically, the enzyme family was sorted into five different classes (67, 73, 74), however, the discovery and structural assessment of novel MTases further expanded the scope to nine classes (75–80). Allocation of enzymes to the classes is based on their structure and characteristic folds rather than on their phylogenetic assignment (81–83). In Table 1 selected examples are presented with references to representative crystal structures.

Class I is the most abundant group of MTases and is named after its characteristic Rossmann-fold (67, 73, 74, 84). Another noteworthy MTase class is class V, which contains a so-called SET domain and is usually associated with protein MTases (85). Of special interest are MTases of class VII, which include a TIM barrel and use radical mechanisms for methylation of their respective targets (86, 87). Class IV enzymes, also dubbed SPOUT or SpoU-TrmD MTases exclusively contain RNA MTases (83, 88), which are also found in classes I, VII, VIII, and IX.
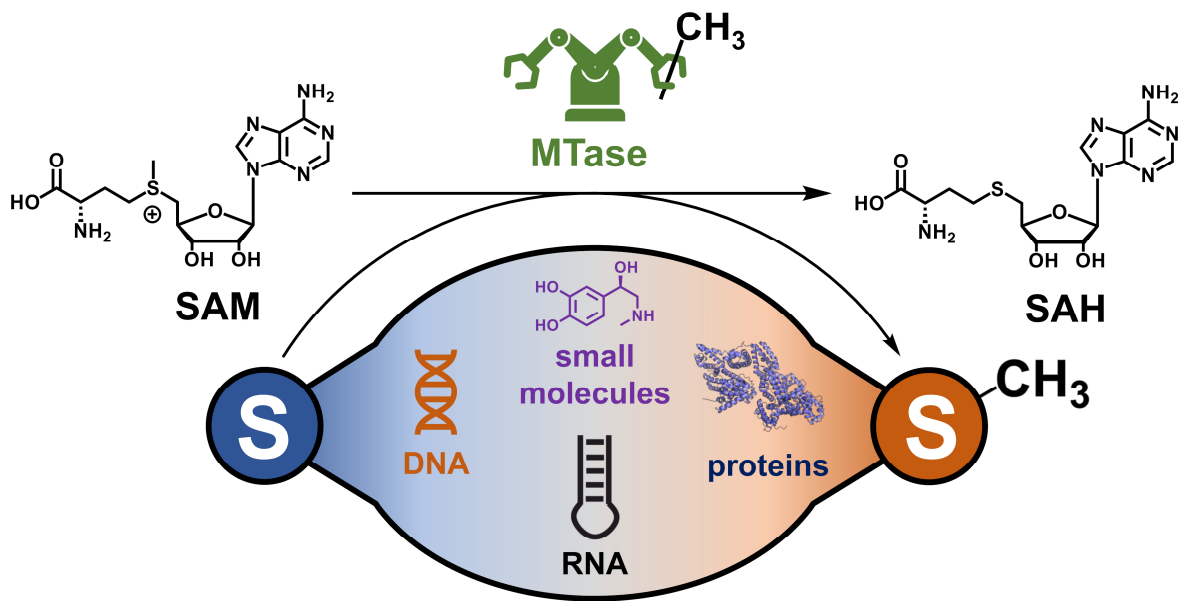
Figure 2. RNA MTases. Transfer reaction as catalysed by MTases on RNA, DNA, proteins and small molecules.

Even though most MTases utilise SAM as a cofactor, some exceptions use N^5,N^{10}-methylenetetrahydrofolate (MTHF) for methylation reactions (89–92). MTHF-dependent MTases are not classified in a commonly accepted system as their SAM-dependent counterparts, but they are known to methylate a variety of targets including RNA, proteins and especially small molecules and further occur in all three domains of life (93–96). One prominent member is the thymidylate synthase, which is a clinically relevant anti-cancer target and is addressed by the drug 5-fluorouracil (5-FU) (94, 95).

Table 1. MTase classes. Listed are various MTase classes together with their unique structural features and representative examples. Table adapted from Fischer *et al.* (97) for which is was created with ██████████ and ██████████.

Name	Structure	Representative crystal structure
Class I Rossmann-fold MTases (98–101)	An αβα-sandwich formed by seven β-sheets flanked by three α-helices on each side	nsp10-nsp16 methyltransferase complex SARS-CoV-2 PDB 6YZ1 (100)
Class II (102)	A characteristic central, antiparallel β-sheet, flanked by eight central β-sheets framed by several α-helices at both ends	MetH methionine synthase *E. coli K12* PDB 1MSK (102)
Class III (103)	Two α β-clusters containing four α-helices with five central β-sheets	CbiF cobalt-precorrin-4 transmethylase *Priestia megaterium* PDB 1CBF (103)
Class IV SPOUT (SpoU-TrmD) MTases (83, 104)	C-terminal knot; seven α-helices surrounding a six-stranded parallel β-sheet	RlmB 2'-*O*-methyltransferase *E. coli* PDB: 1GZ0 (104)
Class V SET-domain containing proteins (85, 105)	C-terminal pseudoknot surrounded by a combination of three β-sheet constructions consisting of three β-strands	SET7/9 lysine methyltransferase *H. sapiens* PDB: 1MT6 (105)
Class VI Transmembrane MTases (76, 106)	C-terminal catalytic subdomain comprising an α-helix and containing five transmembrane α-helices with a cofactor-binding pocket	Isoprenylcysteine carboxyl methyltransferase (ICMT), *Methanosarcina acetivorans* PDB 4A2N (76)
Class VII TIM barrel MTases (77, 107)	Partial or full TIM barrel with a [4Fe-4S] cluster	MiaB radical methylthiotransferase *Bacteroides uniformis* PDB: 7MJV (77)
Class VIII (78, 79)	Six-stranded anti-parallel β-barrel, sheets interconnected with extended loops	TrmO/YaeB tRNA methyltransferase *Archaeoglobus fulgidus* PDB: 2NV4 (78, 79)
Class IX (80)	A concave surface formed by two four-stranded antiparallel β-sheets with five α-helices at the opposite side	SsTaw3 tRNA-yW N-4 methyltransferase *Saccharolobus solfataricus* PDB: 1TLJ (80)

1.4 DNA methyltransferase 2

Due to its close structural resemblance to DNA methyltransferases, DNA methyltransferase 2 (DNMT2) was long thought to act on DNA (69, 108–110). However, at best low DNA methylating activity was detected but still this remains controversial (111). The lack of activity was surprising, especially since DNMT2 is highly conserved in a lot of eukaryotic organisms (112–114) and can also be found in some prokaryotes (115). In 2006, Goll *et al.* finally revealed DNMT2 to be an RNA MTase methylating tRNA^{Asp} at position C_{38} leading to m^{5}C$_{38}$, depicted in Figure 3A (116).
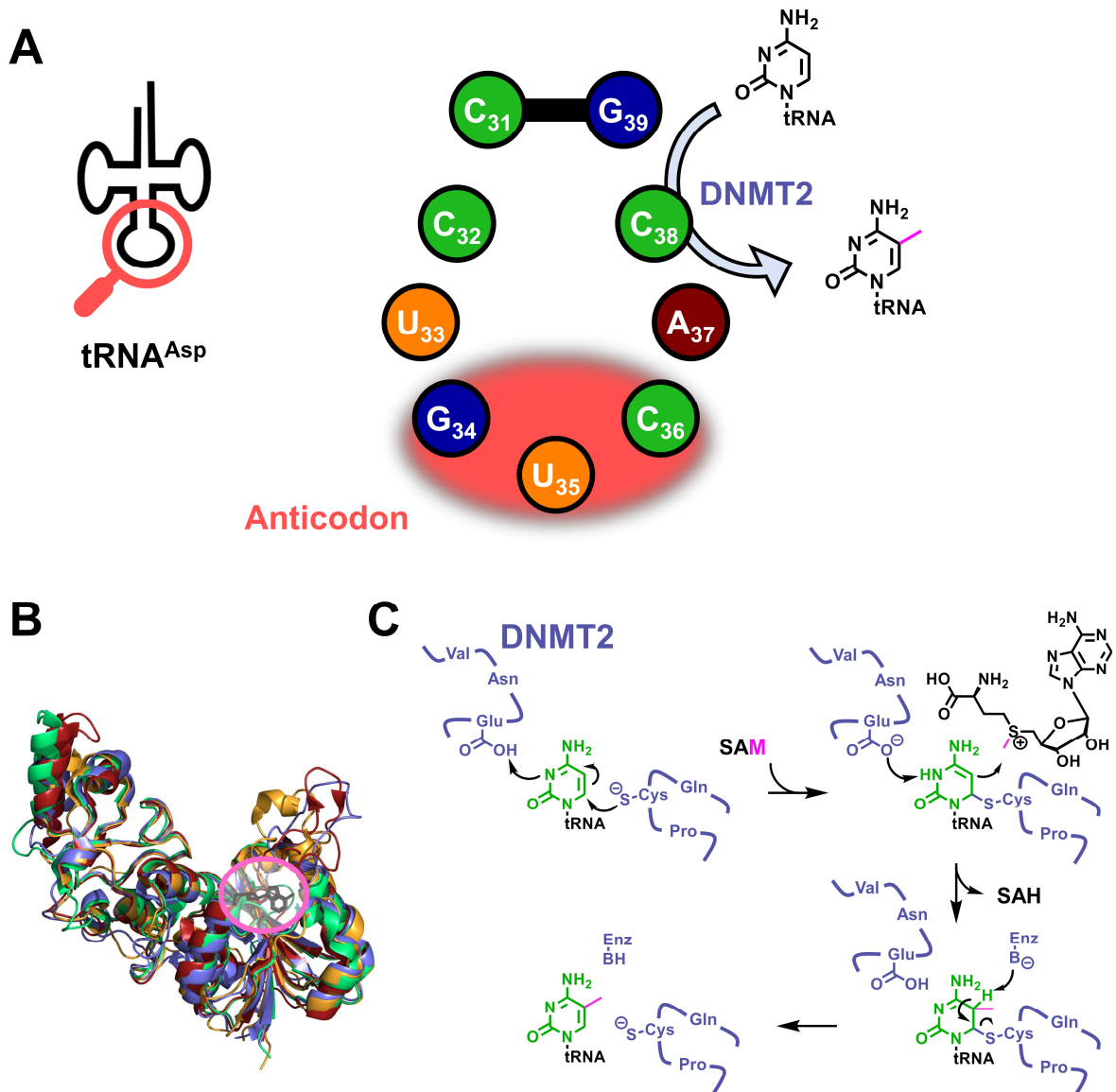
Figure 3. DNMT2 basics. A) Zoom-in to the anticodon loop of tRNA^{Asp}, which is methylated at position C_{38} by DNMT2 leading to m^{5}C. B) Overlay of all published crystal structures of DNMT2. DNMT2 homologue of human in green, PDB: 1G55 (117), of *S. frugiperda* in red, PDB: 4H0N (118), *E. histolytica* in orange, PDB: 3QV2 (119) and *S. pombe* in blue, PDB: 6FDF (120), co-crystallised SAH is displayed in black in the pink circle. Protein structures created with PyMOL (121). C) Catalytic mechanism of DNMT2 (marked in blue) in which the catalytic cysteine attacks position 6 of the cytosine base (displayed in green), while N^3 is protonated by a glutamate, which leads to activation of C^5. The activated carbon atom can then attack the methyl group (displayed in pink) provided by the cofactor SAM and after deprotonation of the C^5 position by an unknown base m^{5}C modified tRNA is released.

1.4.1 Structure and catalytical mechanism of DNMT2

As mentioned above, DNMT2 is structurally closely related to DNMT1 and DNMT3 (69), thus it is proposed that these enzymes evolved from a common ancestor and DNMT2 changed its substrate specificity from DNA to RNA during evolution (112). Consisting of less than 400 amino acids, DNMT2 is a rather small protein, especially in comparison with its catalytically active protein-siblings DNMT1 (around 1600 amino acids) and DNMT3 (around 900 amino acids). Both proteins contain regulatory domains at their N-termini, while DNMT2 only consists of the catalytic domain (69).

A detailed insight into the structure of DNMT2 is given by the four different crystal structures published so far. These include homologues from human (PDB: 1G55 (117)), *Spodoptera frugiperda* (PDB: 4H0N (118)), *Entamoeba histolytica* (PDB: 3QV2 (119)) and *S. pombe* (PDB: 6FDF (120)) (Figure 3B).

These structures revealed a Rossmann-fold, allocating DNMT2 to class I MTases (117–120, 122). Furthermore, motives I to X, associated to the catalytic activity of DNMTs, were found (113, 117, 118, 123) and are utilised by the enzyme according to a DNMT-like mechanism. This makes DNMT2 the only m^5C RNA MTase known following this kind of mechanism and not an m^5C RNA MTase like mechanism (124, 125).

For the successful transfer of a methyl group from the cofactor SAM to the 5-position of the cytosine base, the position must be activated in a first step due to the electron-poor character of cytosine. Therefore, DNMT2 utilises a catalytic cysteine residue located in motif IV (proline-cysteine-glutamine, PCQ) attacking position six of the base (123). The nucleophilic attack is facilitated by the protonation of N^3 by a glutamate residue of motif VI (glutamate-asparagine-valine, ENV) and leads to the formation of a covalent protein-RNA complex, which is activated on the 5-position of the attacked cytosine. The activated C^5 atom can now act as a nucleophile itself and attacks the methyl group provided by SAM. The catalytic cysteine is eliminated after deprotonation of C^5 and subsequent rearomatisation leads to the release of the methylated tRNA as well as SAH (111). Additional to motives IV and VI, aspartate residues in motif VIII (arginine-random amino acid-arginine, RXR) were identified to be crucial for DNMT2 activity (124). The detailed mechanism is depicted in Figure 3C.

Albeit the mechanism utilised by other m^5C RNA MTases, also known as the NSUN family, looks very similar at first glance, some differences occur. Here, the catalytic cysteine is located on motif VI (threonine-cysteine-serine/threonine, TCS/T), while no glutamate residue in motif IV is used for protonation of N^3, but an aspartate located in motif IV. Also, deprotonation of C^5 is performed by a cysteine residue on motif IV (125–127).

1.4.2 Substrates of DNMT2

This DNMT-like mechanism in an RNA MTase, together with the structural similarities between DNMT2 and the other, 'real' DNMTs leads to the question if the enzyme is also able to modify DNA. Interestingly, this question has not been conclusively clarified yet (124). While some studies describe low levels of DNMT2 related DNA methylation, especially in DNMT2-only organism such as *D. melanogaster* or *Dictyostelium discoideum* (128–137), other reports dispute this (116, 138–140).

To resolve this contradiction, it was proposed that low levels of 5mC might indeed be artifacts or occur due to suboptimal experimental conditions, as incomplete bisulfite conversion (138–140). Another explanation could be the low abundance of DNMT2 homologues in organisms with disputed 5mC

occurrence leading to hardly reproducible results (111). Furthermore, DNMT2 homologue expression was shown to be higher in wild-type strains compared to laboratory strains for *D. discoideum* (141). Differences between constant, mild lab and varying, more challenging natural conditions might therefore provide another explanation for the differences in potential occurring 5mC modifications (111).

An unchallenged substrate is tRNA$^{Asp}_{GUC}$, which is methylated at C_{38} by DNMT2, close to the anticodon loop. Depending on the species, further DNMT2 substrates are tRNA$^{Gly}_{GCC}$, tRNA$^{Glu}_{U/CUC}$ and tRNA$^{Val}_{AAC}$ being methylated at the same position (111, 141–144).

More recent studies imply DNMT2 activity in the context of DNA damage and propose a function on mRNA or RNA:DNA duplexes (145–147). DNMT2 was also shown to methylate deoxynucleotides if they were embedded into the tRNA^{Asp} structure even with higher affinity than all-ribo tRNA^{Asp} (148).

Multiple bases in the T- and D-loops of tRNA$^{Gly}_{GCC}$ were identified as crucial for successful *in vitro* methylation and furthermore a $C_{32}U_{33}X_{34}X_{35}C_{36}A_{37}C_{38}$ motif in the anticodon loop was suggested as potential consensus motif recognised by DNMT2, depicted in Figure 3A (144).

The same question was also addressed from the protein's point of view, which led to the identification of eight basic amino acid residues on the protein surface important for DNMT2 activity. Based on this, a tRNA binding-site on the protein was proposed (149).

Although these studies provide a first insight into the interaction between protein and RNA, for a detailed insight a co-crystal structure of DNMT2 and an RNA substrate would be most beneficial, which is yet to be resolved (111).

1.4.3   Biological functions of DNMT2

Biological function of an enzyme is often closely related to its subcellular localisation, e.g. DNMT1 and 3 are mostly found in the nucleus, alongside their substrate (DNA) (150, 151). However, DNMT2 is found in the nucleus as well as in the cytoplasm (116, 152–154) which might reflect the dynamic localisation of tRNAs (114, 155), but might also depend on exogenous factors such as stress (156).

The position of the m^{5}C modification introduced by DNMT2 at C_{38} close to the anticodon region already hints a potential role of DNMT2 in translation, especially since RNA modifications here were shown to impact proper protein production (157, 158). Indeed, in double knock-out mice lacking both DNMT2 and NSUN2 (another tRNA m^{5}C MTase) activity, a reduction of protein translation was detected besides the loss of m^{5}C. Importantly, no changes in mRNA levels were measured, while the level of certain tRNAs was reduced backing a tRNA related mechanism (159).

Additional to this, loss of the m^{5}C modification at C_{38} lowered aminoacylation of tRNA^{Asp} *in vitro* and *in cellulo*, which led to a reduction of poly-Asp proteins in cells (Figure 4A). These proteins are localised in the nucleus and are important for protein expression, indicating an influence of DNMT2 activity on expression of poly-Asp containing proteins and therefore an influence on overall gene regulation (160).
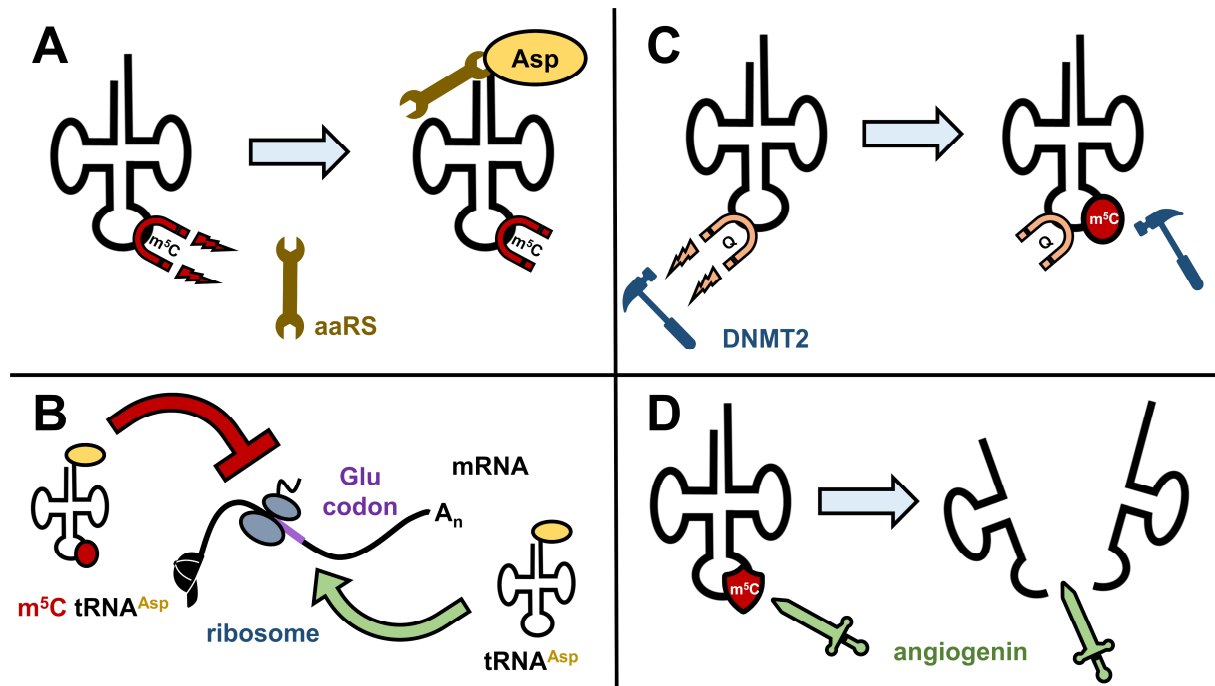
Figure 4. DNMT2 functions. A) DNMT2 mediated m^5C modification leads to higher degree of amino acylation of tRNA^{Asp}. aaRS = aminoacyl-tRNA synthase. B) DNMT2 mediated m^5C modification leads to higher translational precision by better distinctiveness of Asp and Glu codons for tRNA^{Asp}. C) Modification of tRNA^{Asp} with Q enhances DNMT2 activity and elevates m^5C levels. D) DNMT2 mediated m^5C modification stabilises RNA against the endonuclease angiogenin. m^5C displayed in red, aaRS displayed in brown, aspartate displayed in yellow, queuosine displayed in orange, DNMT2 displayed in blue, and angiogenin displayed in green.

Another function of DNMT2 and its implemented m^5C_{38} modification was unveiled in DNMT2 knockout mice, in which the ability of tRNAs to distinguish between aspartate and glutamate codons was reduced, as depicted in Figure 4B. These findings point to DNMT2 having an influence on translational fidelity and thus on protein integrity (161).

One more modification found in the anticodon region of tRNA$^{Asp}_{GUC}$ is Q (structure presented in Figure 1) at the wobble position G_{34}, which boosts activity of DNMT2 homologues in *S. pombe* and *D. discoideum in vivo* and *in vitro*, therefore providing a further example of crosstalk between modifications (*vide supra*, see Figure 4C) (120, 162).

Another well-known stress reaction in cells is tRNA fragmentation (163) being significantly impacted by tRNA modifications (164). The aforementioned study of Tuorto *et al.* (159) did not only reveal an influence of DNMT2 mediated tRNA methylation on translation, but also on RNA stability. This was also demonstrated for *D. melanogaster* tRNA^{Asp}, tRNA^{Gly} and tRNA^{Val} which were favourably cleaved by the endonuclease angiogenin in the absence of m^5C_{38}, as can be seen in Figure 4D (142). Herein, cleavage leads to the generation of tRNA fragments (tRFs), a class of small non-coding RNAs exhibiting numerous regulatory functions (9). For example, tRFs repress protein translation (165) and are thought to have effects in adipogenesis (166) and on the epigenetic inheritance (10).

In *Dnmt2* mutant *D. melanogaster*, tRFs linked to DNMT2 activity were found to influence siRNA-dependent pathways after heat shocking the flies. In this case, higher amounts of tRFs were found to be present, dsRNA accumulation was observed, and the corresponding siRNA pathways were downregulated. These siRNA pathways downregulate the stress response under normal conditions and accordingly, *Dnmt2* mutant flies showed prolonged stress response compared to wild-type flies (167).

1.4.4 Involvement of DNMT2 in (patho)physiological processes

Knockout of *Dnmt2* in *D. melanogaster*, *Arabidopsis thaliana* or mice led to viable phenotypes with no morphological abnormalities (116). However, in *Dnmt2* knockdown zebrafish growth defects were detected (154).

DNMT2 activity was linked to stress conditions and resistance (141, 156, 168–172), e.g. *D. melanogaster Dnmt2* mutants were more prone to heat stress (142) indicating DNMT2 to be involved in stress responses, while on the contrary overexpression of the enzyme led to stress resistance and prolonged lives in lower organisms (173–175).

Further, the *DNMT2*-gene is upregulated in numerous tumour samples, according to the catalogue of somatic mutations in cancer (COSMIC) data base (176), for example in cervical cancer (177) or lymph node metastases (178). Alterations of the gene were also shown to modulate the enzyme's activity with some mutations sharply increasing enzyme activity (179). Silencing of *DNMT2* sensitised tumour cells for radiation and the treatment with poly-ADP-ribose-polymerase inhibitors (PARPi) (145) and let to upregulation of tumour suppressor micro RNAs (miRNAs) with antiproliferative effects in human fibroblasts (169). Antiproliferative effects after *DNMT2* loss were also investigated for human embryonic kidney (HEK) 293 cells (146). Additionally, knockdown of *DNMT2* in cancer cells enhanced drug-induced cell senescence meaning a potential sensitisation for cancer drugs but also likely an aggravation of side effects (180).

Another link between cancer and DNMT2 was found in leukaemia cells. On the one hand, levels of m^5C and DNMT2 were increased in azacitidine (a well known m^5C MTase inhibitor used in cancer therapy, *vide infra*) resistant leukaemia cell lines compared to azacitidine sensitive leukaemia cells (ASLCs). On the other hand, DNMT2 was shown to form a complex with another RNA m^5C MTase NSUN3 and the RNA binding protein hnRNPK (from the heterogeneous nuclear ribonucleoprotein family) and knockdown of either of these three proteins led to reduced ASLC viability. Furthermore, this complex seems to be involved in the recruitment of RNA polymerase II, which is participating in the formation of azacitidine sensitive chromatin regions and thus links DNMT2 to successful cancer therapy in leukaemia (181).

DNMT2 homologues were also linked to the regulation of retrotransposons in *D. melanogaster* and *D. discoideum* (135, 136), albeit these findings remain disputed (138, 139).

Increasing amounts of studies propose DNMT2 to regulate viral replication, though in arbitrary ways (182). In *D. melanogaster* and its cells, DNMT2 was linked to inhibition of proliferation of different viruses (168, 183), while the DNMT2 homologue in *Aedes* cells and mosquitos was associated with higher viral replication (183–185). In human cell lines, overexpression of *DNMT2* leads to deregulation of genes usually involved in viral infections (156), while DNMT2 overexpression in human cells which were infected with the human immunodeficiency virus (HIV) led to elevated levels of viral RNA. The corresponding knockdown led to a reduction of viral RNA. In this case, a direct interaction between DNMT2 and viral mRNA as well as methylation of viral RNA by the enzyme was observed and proposed as mechanism for enhanced viral replication (147).

Next to an influence in viral replication, connections between DNMT2 and responses to bacterial and parasite infections were drawn, however not much is known in this context so far (137, 186).

Inheritance of certain phenotypes, which does not come along with changes in DNA sequence is called epigenetic inheritance and mediated by modifications on DNA and histones, certain RNA species and also by RNA modifications (187–192). Transmission by RNA species is particularly described for metabolic (190, 193–197) and mental disorders (198–201).

Noteworthy, the heredity of metabolic disorders in mouse models was linked to elevated levels of m^2G and m^5C on small non-coding RNAs (sncRNAs) (190), with DNMT2 playing a crucial part (193). Knockdown of the corresponding gene in mice reduced the epigenetic transmission of phenotypes, which are caused by sperm sncRNA and induced by a high-fat diet (193).

Another example of DNMT2-mediated heritage was described for phenotypes linked to *Kit* and *Sox9* genes in mice. The *Kit* gene encodes a tyrosine kinase and is responsible for white coloured tails, while *Sox9* encodes a transcription factor and stimulates enhanced growth in the animals. Knockout of the *Dnmt2*-gene leads to abolishment of the corresponding phenotypes, implying a possible function of the RNA MTase (202).

1.4.5 The DNMT2 enigma - is it solved already?

The DNMT2 enigma, as described by Schäfer and Lyko over 10 years ago in 2010, first arose with the contradiction between the high conservation of DNMT2 over several species and its lack of activity on DNA substrates (114). The identification of tRNA being the main substrate of DNMT2 certainly was a breakthrough, which let to numerous publications related to this enzyme (116).

The m^5C incorporated by DNMT2 was shown to enhance translation (159), as well as amino acylation of tRNAs (160) and increased the ability of tRNA^{Asp} to discriminate between codons (161). All these functions are important for synthesis of proteins in adequate amounts and with appropriate quality. Importantly, m^5C_{38} has an impact on tRNA stability (142, 159) and therefore directly influences the occurrence of tRFs and also of siRNA (167), with both RNAs being able to regulate cell physiology (9). This broadens the influence which DNMT2 may have on cellular processes significantly. As described above, DNMT2's involvement in the stress response and resistance was reported by numerous studies (141, 142, 156, 168–175) and is thus commonly accepted by the scientific community (111). Very remarkable is the role the enzyme plays in the epigenetic transmission of certain phenotypes (193, 202) opening a door in which borders between epigenetics and epitranscriptomics are vanishing.

However, even while some important and interesting questions are addressed, many functions and effects mediated by DNMT2 remain still elusive. Starting on a basic level, this includes substrate specificity. Without question various tRNAs are well investigated substrates of DNMT2 (111, 141–144), but the question if DNA can be methylated by the enzyme is still not finally answered, with occasionally published studies claiming evidence for DNMT2 mediated DNA methylation (128–137) and thus contradicting other reports (116, 138–140). Dependency on experimental conditions was proposed but not ultimately clarified (111). Also, in several recent publications mRNA is described as substrate for DNMT2 implying an even broader spectrum of functions executed by DNMT2 (145–147).

Somehow related to the question of substrate specificity is the issue with DNMT2 and viral proliferation. Here, effects mediated by DNMT2 seems to be dependent on the species and potentially on the virus investigated (147, 168, 183–185). While in some studies a methylation of viral mRNA by DNMT2 is described (147), other mechanisms mediated by tRFs or siRNA seem plausible as well (167).

The role the enzyme plays in cancer is slowly uncovered but still not solved completely. With upregulation of the corresponding gene in cancer cell lines (176) and its role in modulation of cell proliferation (146, 180), DNMT2 seems to be involved to some degree in cancer progression. Furthermore, it was demonstrated that lack of DNMT2 sensitises cancer cells for subsequent treatments (145). Additionally, it was proposed that DNMT2 forms a complex with NSUN3 and hnRNPK which modulates chromatin structures (181).

Taken the paragraphs mentioned above into account the DNMT2 enigma still remains. However, especially considering its role in viral and cancer progression, it becomes evident that interest in DNMT2 research is not only restricted to basic research, but an application in medicinal chemistry is of interest.

1.5   Small molecule inhibitors for RNA MTases

As outlined in the chapters above, RNA methylations, and with them RNA MTases, participate in several biological and physiological pathways. This alone is very remarkable, though their involvement in pathophysiological processes adds another layer of significance to this enzyme family shifting it into the focus of the pharmaceutical industry. This is because targeting RNA MTases with drugs might lead to novel antiviral compounds, antibiotics or cancer treatments. The interest becomes evident not only when considering the growing number of related publications, but also by the foundation of multiple start-up companies, which dedicated themselves to the manipulation of the epitranscriptome (203–206).

The following chapters are based on the review article 'Chemical biology and medicinal chemistry of RNA methyltransferases' published in Nucleic Acids Research in 2022 (97).

1.5.1   Activity assays used for MTases

For a successful drug development campaign, one basic requirement is a robust enzyme activity assay. In the case of MTases several possibilities have been described, which often rely on the detection of SAH, the by-product of the enzymatic reaction (Figure 2) (207, 208). These methods have the big advantage of its generic applicability for basically all SAM-dependent MTases. SAH detection and quantification usually utilises high-performance liquid chromatography (HPLC) methods coupled with a huge variety of different detection methods. These include ultraviolet (UV) (209), fluorescence (210–212), electrochemical (213) and most importantly mass spectrometry (MS) detection (214).

While the ability to build a generic MTase assay using HPLC based methods is certainly a huge advantage, the high consumption of time and materials limits its throughput. Therefore, methods as the staggered parallel scheme were developed to allow high-throughput screenings (HTS) in combination with HPLC based assays. Here, multiple HPLC systems are connected to one MS detector and analyte retention times are adjusted to have a time delay. This enables the detector to switch between the different HPLC systems depending on incoming analytes maximising its working time and thus enhancing the throughput drastically (215, 216).

Another approach for applying MS for HTS in combination with MTases is the RapidFire technique. In this approach the column usually applied in HPLC is replaced with an automated solid-phase-extraction, which has a very brief turnaround time (217, 218). The RapidFire system was utilised in HTS projects to reveal novel RNA MTase inhibitors (219, 220).

Besides the direct quantification of SAH utilising HPLC, the molecule can be enzymatically converted to obtain compounds which can be detected by absorption (221–223), fluorescence (224) or luminescence (225, 226). This allows continuous measurement of the enzyme reaction usually in a well-plate format with a fluorescence reader.

The most classical method to detect MTase activity is the tritium incorporation assay, which is still widely utilised. In this assay, MTases transfer a ^{3}H-labelled methyl group of ^{3}H-SAM onto their substrates. First, the substrates are precipitated on a filter paper and after discarding unreacted cofactor by washing, incorporated ^{3}H-labelled methyl groups on the substrates are quantified using liquid scintillation counting (Figure 5) (148, 227). As an alternative to precipitation and scintillation counting, small molecular fragments such as nucleotides obtained from digesting RNA can be separated using thin layer chromatography and subsequently quantified by means of the radioactive label (228–230).
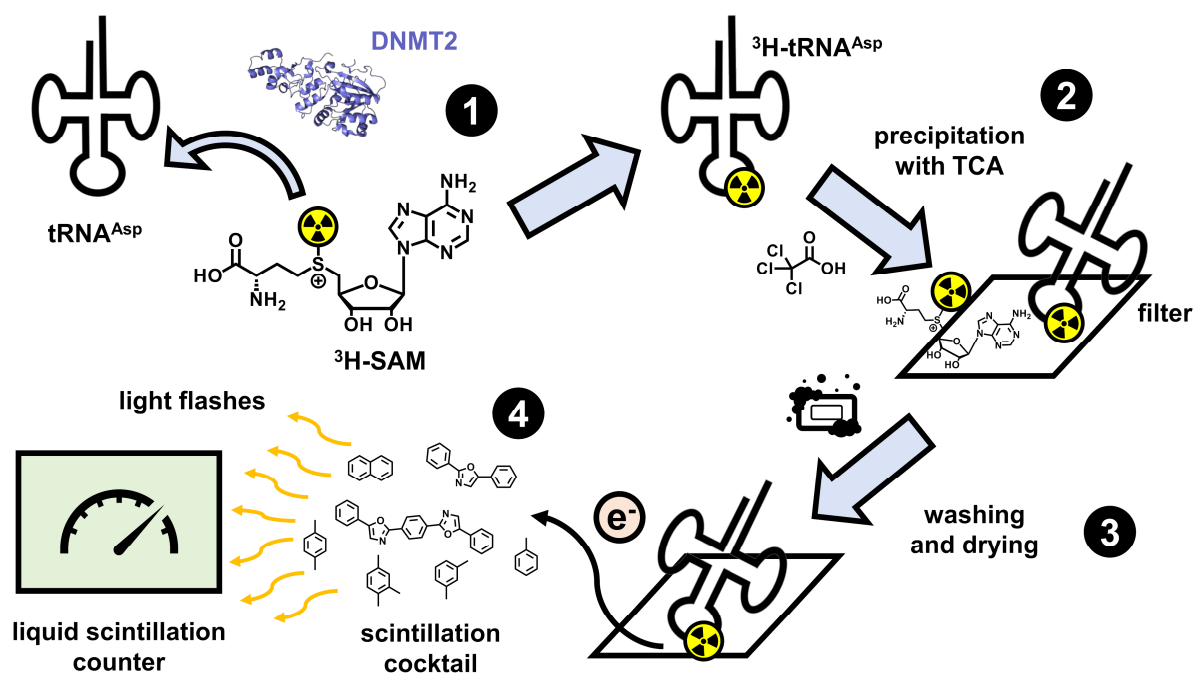
Figure 5. Tritium incorporation assay. Workflow of a typical tritium incorporation assay using the example of the RNA MTase DNMT2 (148, 227). DNMT2 transfers a ^{3}H-labelled methyl group from ^{3}H-SAM to the tRNA marking it radioactively (**1**). After precipitation of the tRNA with trichloroacetic acid (TCA) on a filter paper (**2**), residual ^{3}H-SAM is removed by washing (**3**) and built-in tritium is quantified using liquid scintillation counting (**4**). Protein structure was created with PyMOL (121) and PDB: 1G55 (117).

As HPLC based assays, tritium incorporation assays are also limited by their low throughput numbers. When working with radioactivity the turnover can be enhanced when utilising scintillation proximity assays (SPA), which are usually carried out in well-plate formats. Here, the ^{3}H-methylated substrate is purified by binding to scintillation beads (e.g., by unspecific electrostatic or biotin/streptavidin interactions). Afterwards, the radioactive decay excites the scintillation cocktail in the beads leading to an emission which can be quantified (231–233).

As non-generic alternatives, quantification of the methylated target by various specific methods is possible (207, 234, 235). An example is the utilisation of a fluorescent cap analogue as substrate for N^7-G mRNA cap MTases changing its fluorescence properties after being methylated (236).

1.5.2 Early research on small molecule MTase inhibitors

While research on RNA MTases became increasingly popular in the last few years, connections between this enzyme family and cancer or viral infectiousness were already drawn half a century ago (50, 237). This knowledge led to an early wave of development of small molecules targeting RNA MTases, albeit in the form of crude enzyme extracts rather than purified enzymes due to a lack of methodology (238–246).

While the activity of these early compounds was modest at best, early structure activity relationship (SAR) studies could be drawn with the knowledge gained through small screenings (247–249). Furthermore, the concept of bisubstrate inhibitors, in which one molecule competes with both SAM and substrate RNA, was successfully applied (250), while selectivity for specific MTase extracts was described (251, 252). The substructures of these early compounds were almost exclusively based on the two most prominent pan MTases inhibitors: SAH and sinefungin (SFG), both displayed in Figure 6.
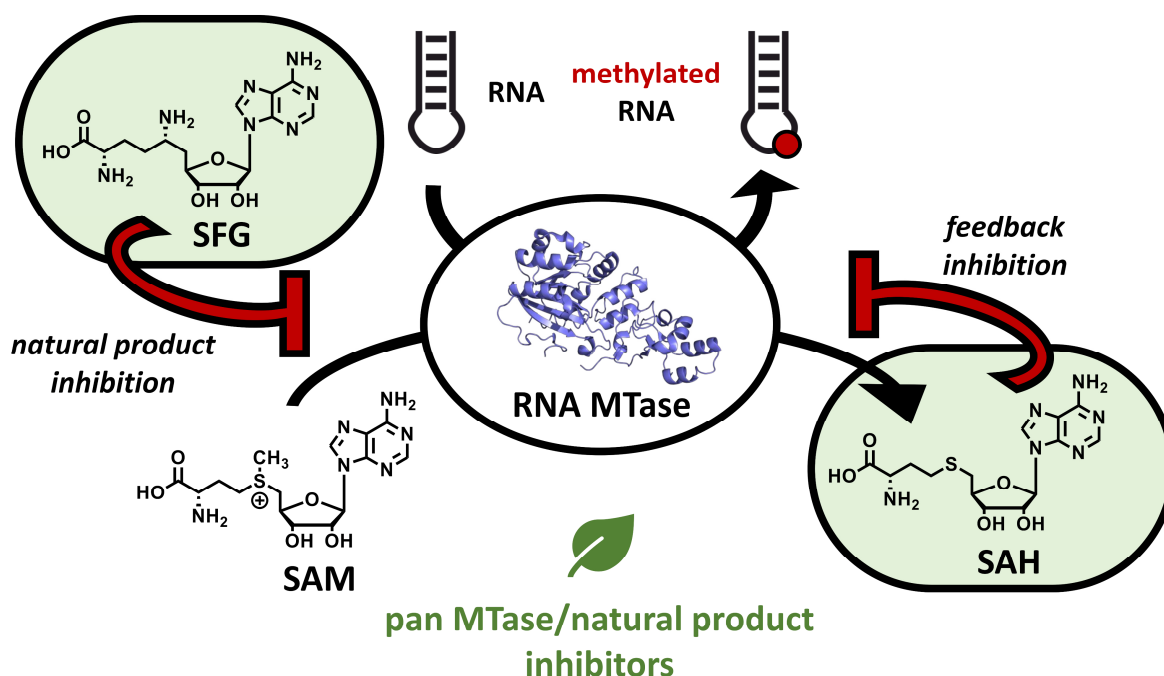
Figure 6. Pan MTase inhibitors. Displayed are the natural products and pan MTase inhibitors sinefungin (SFG), which can be extracted from *Streptomyces griseolus*, and SAH, the by-product of the methylation reaction acting as a feedback inhibitor. Figure adapted from Fischer *et al*. (97). Protein structure created with PyMOL (121) and PDB:1G55 (117).

SAH, the demethylated form of SAM, is the by-product of the methylation reaction and acts as a feedback inhibitor for MTases (253). Sinefungin's molecular structure is closely related to that of SAM and is a natural product which was identified in *Streptomyces griseolus* from which it can be extracted (254). Both molecules are still widely applied in MTase drug research, for example as starting points for early drug design or as reference inhibitors during assay development (208).

1.5.3 General development of small molecule inhibitors

For the identification of novel small molecule inhibitors several techniques may be applied. Usually this is a gradual process, in which at first suitable hits are identified and subsequently being further optimised. A widely used method for hit identification are high-throughput screenings (HTS), in which great numbers of compounds (up to a million) are subdued to an assay system and by chance more or less promising compounds are identified (255).

A more rational approach is the fragment-based drug discovery (FBDD). As in HTS, also FBDD starts with a screening, but in contrast the molecular weight of the screened compounds usually does not exceed 300 Da, hence the term 'molecular fragment'. For the initial screening, typically biophysical methods with high sensitivity are applied and determination of a detailed binding mode of the fragments (e.g. by X-ray crystallography) is of high priority (256). Even if the resulting hits generally display only limited affinities to their respective targets, their ligand efficiency is very high because most atoms of the corresponding molecule participate in the binding event (257).

Also, due to the more limited chemical space of smaller fragments, the screening libraries used in FBDD are considerably smaller, saving valuable time and money. The hit identification in FBDD is followed by fragment growing, which expands the fragment structures into the binding site based on the resolved co-structure. If successful, this step can be conducted until a novel enzyme inhibitor with desired properties is developed. Identifying multiple fragments with distinct but adjacent binding sites enables fragment linking utilising both hits for subsequent drug development. Additional to smaller screening libraries, another advantage of FBDD is the detailed knowledge of inhibitor-enzyme interaction from the very beginning of the drug development process allowing a better finetuning of chemical, physical and biological properties (256–258).

A third pillar of hit identification are *in silico*-based methods, such as virtual screenings (VS). Here, even greater numbers of molecules than in HTS (ranging up to 10^{15}) are screened by computational methods before they are investigated in wet lab experiments (259–261). In this regard two different approaches are categorised: ligand-based drug design (LBDD) and structure-based drug design (SBDD). In LBDD, optimisation of ligands is based on known molecular structures, e.g. by artificial intelligence algorithms, whereas in SBDD the target's three dimensional structure is exploited for improvement, particularly by molecular docking (262).

Prior to screenings, either virtual or 'real' ones, the corresponding libraries ought to be filtered according to criteria such as lead- or drug-likeness and obtained results should be considered with the appreciation of pan-assay interference compounds (PAINS) to enhance chances of success (263–267).

1.5.4 Prokaryotic MTase inhibitors

With the emergence of antibiotic treatments, millions of lives were saved taking away parts of the horrors inflicted by bacterial infections. This perceived safety led to a gap in innovation for novel antibiotics, which, in combination with the misuse of antibiotics, led to the current 'antibiotic resistance crisis' (268). Therefore, strategies for overcoming antibiotic resistances as well as developing novel antibiotics are urgently needed. Prokaryotic MTases are a suitable, yet mostly unexploited target which might fulfil these requirements. A detailed overview over prokaryotic MTase inhibitors is summarised in Table 17 in the Appendix adapted from Fischer *et al.* (97).

The name of the erythromycin resistance methyltransferase (Erm) family already links antibiotic resistances to methyltransferases and thus non-surprisingly was identified as a valid drug target. As can be seen in Figure 7, enzymes of the Erm family methylate rRNA at the binding site for antibiotics as macrolides, streptogramin or lincosamides impeding binding of these molecules. Therefore, addressing this enzyme family might cope with various antibiotic resistances at once (269).
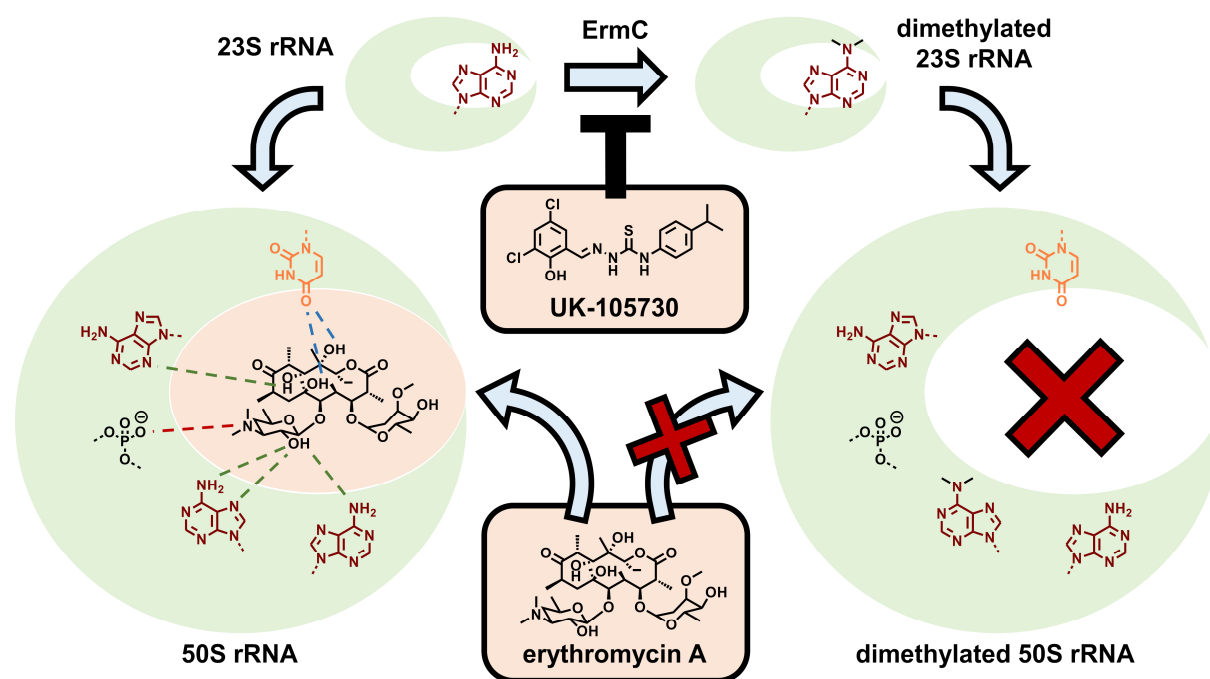
Figure 7. ErmC inhibition. Mechanism of ErmC inhibitors. The dimethylation of an adenosine in the 23S rRNA prevents binding of the antibiotic erythromycin A to 50S rRNA in which it is incorporated. ErmC inhibitors as UK-105730 (IC$_{50}$ =0.45 µM) have the ability to prevent this methylation and therefore allow erythromycin A to fulfil its activity suggesting a combination therapy. Figure adapted from Fischer *et al.* (97), for which it was created by ▮▮▮▮▮▮▮▮▮.

The enzyme which is best studied in this context is ErmC (270), for which inhibitors were identified after applying VS (271–273) or HTS (274). Among others, this led to the identification of UK-105730 with an IC$_{50}$ value of around 0.45 µM exposing resistant bacteria strains to azithromycin (274). For ErmAM a nuclear magnetic resonance (NMR) screening with subsequent optimisation led to SAM-competitive inhibitors with low micromolar affinity (275). Even though these findings sound promising, there is no substantial interest to pursue this development further into clinical studies so far.

1.5.5 MTase inhibitors for single cell eukaryotes

Inhibitors for RNA MTases of single cell eukaryotes are nearly absent in the literature, despite the fact of sinefungin's name implying antifungal activity. The molecule inhibits Ecm1 in *E. cuniculi* (236) and Ccm1 in *C. albicans* (276), both enzymes involved in the implementation of mRNA caps. Additional to sinefungin, Ecm could be addressed by SAH and closely related analogues (277, 278). An overview about the literature is summarised in Table 18 in the Appendix adapted from Fischer *et al.* (97).

1.5.6 MTase inhibitors for the treatment of non-infectious human diseases

As described above, the epitranscriptome is involved in numerous physiological and pathophysiological pathways. While 2'-*O*-methylations, m5C and m6A were linked to neuronal development and malignancies (279, 280) and partly also to epigenetic inheritance (192, 193), the main focus of drug development for human RNA MTases is focused on cancer treatment. Here, numerous modifications could be linked to diseases, such as m6A (31, 36–38, 40, 281), m5C (282), m3C (283), or m7G (284–286) rendering the respective MTases as promising cancer targets (287). In this regard, m6A with its writer complex METTL3-METTL14 is by far the most investigated system to date, which is why it is elaborated in further detail below. A broader overview about the published literature is summarised in Table 19 in the Appendix adapted from Fischer *et al.* (97).

While various METTL3-METTL14 inhibitors could be identified (220, 288–290) a combination of *in silico* and *in vitro* methods identified activators for the complex (291). Another hit identified by an *in silico* screening contained an internal spiro moiety (289, 292), which activity could be boosted from the low micromolar to the low nanomolar range after conducting a SAR study. The final compounds were further able to reduce m6A levels in a cellular context (292).

By far the most promising RNA MTase inhibitor so far was developed by the start-up company STORM Therapeutics targeting METTL3-METTL14 for the treatment of AML. The original hit arose from a HTS and was improved to yield compound STM2457 exhibiting an *in vitro* IC$_{50}$ value in the low nanomolar range. Additionally, the binding mode of STM2457 is exceptionally well understood, due to the resolved co-crystal structure (depicted in Figure 8) revealing its exact position in the SAM binding pocket.
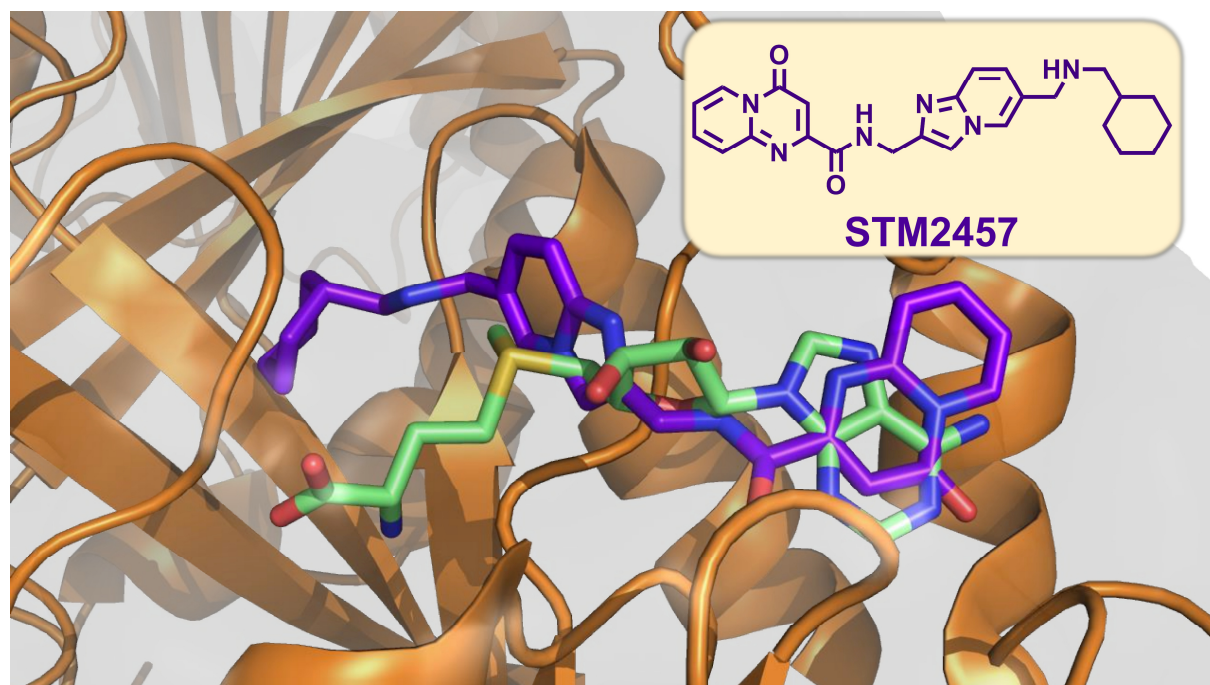
Figure 8. METTL3-METTL14 inhibition. Co-crystal structure of STM2457 (purple) overlaid with SAM (green) in complex with METTL3-METTL14 (orange ribbons). Molecular structure of STM2457 is displayed on the top right. Figure adapted from Fischer *et al.* (97), for which it was created by ▮▮▮▮▮▮▮▮. Image created with PyMOL (121), with PDBs: 7O2I (220) and 5L6E (293).

Naturally it shows remarkable selectivity, even when compared to various MTases, and most importantly it was able to impair AML development in mice and enhance the survivability of AML-transplanted animals (220).

Interestingly, this compound was able to reduce viral replication of *severe acute respiratory syndrome coronavirus* 2 (SARS-CoV-2) and *human coronavirus* (HCoV)-OC43 (a seasonal flue coronavirus) in cell culture presumably by disrupting viral scavenging of the host MTase machinery (294).

1.5.7   MTase inhibitors as antiviral drugs

The impact of the SARS-CoV-2 pandemic clearly demonstrated the danger imposed by RNA viruses. This becomes even more evident when considering other epidemics caused e.g., by the *zika* (ZIKV) or *dengue viruses* (DENV) (295–297). As mentioned above, the innate immune system utilises RNA modifications to distinguish between exo- and endogenous RNA (41). For this reason, viruses code for their own MTases modifying viral RNA caps. Modification takes place after the attachment of an unmodified guanosine at the 5' end of the mRNA via an 5'-5' triphosphate bridge. In the next step, an m^7G modification is attached to this first guanosine, while afterwards the following nucleotide in the RNA sequence is methylated at its 2'-*O*-position as can be seen in Figure 1.

Both methylations require their own MTase functionality, which in some cases is located on the same enzyme, as in flaviviruses (298). Modification of viral RNA is not only crucial for evading the host's immune system, but also stimulates the translation of viral proteins (55–58) making these enzymes interesting targets for the development of novel antiviral drugs (56, 299, 300).

Early work in this direction was successful in inhibiting viral MTases with SAH, SFG and corresponding analogues with some compounds indeed displaying antiviral activity (239, 241, 301, 302). In comparison to prokaryotic and eukaryotic RNA MTase inhibitors, a substantial amount of research was published, which is summarised in Table 20 in the Appendix adapted from Fischer *et al.* (97). In the following paragraphs significant examples are presented in more detail.

Flaviviral inhibitors. A very relevant class of viruses are flaviviruses, which causes around 400 million infections per year. It includes members as the *dengue, zika or west nile viruses* (WNV) being responsible for diseases like hepatitis, encephalitis and even fetal death (303). In flaviviruses, both N^7- and 2'-*O*-MTase functionalities are found on the NS5 protein, which additionally contains an RNA-dependent RNA polymerase (RdRp) and a guanylyl transferase functionality. To fulfil its various tasks, the enzyme has several substrate binding sites including guanosine triphosphate (GTP), RNA and SAM binding sites with the two latter ones being important for MTase activity (304–306).

Both MTase functions are essential for viral replication, but in different manners. The N^7-functionality was linked to efficient translation of viral proteins (307–309), whereas the 2'-*O*-methylation was shown to suppress the host's innate immune response (58, 310) making both MTase functions attractive drug targets.

It is also possible to inhibit both MTase functions with a single small molecule, as was demonstrated with SAM analogues on DENV NS5. These compounds were modified at the adenine N^6-position with hydrophobic residues to address a previously identified, conserved site on the protein (311). This led to inhibitors with K_i values in the sub micromolar range and a higher potency than SAH. Additionally, selectivity against human MTases was observed (312).

In a remarkable campaign, a FBDD was conducted for the development of novel DENV NS5 inhibitors. Using a thermal shift assay (TSA), 500 fragments were screened, which led to the discovery of 32 hits. With seven of these fragments, a co-crystal structure could be resolved, whereas five of them inhibited at least one of the two MTase functions. Interestingly, the fragments bound to four different binding sites in the enzyme, with only one, the GTP binding site, previously known. Two of these novel, presumably allosteric, cavities were located close to each other and were found direct next to the SAM binding site (313).

Since these binding pockets were in close proximity to each other, the fragments embedded here were linked and afterwards subjected to further fragment growing to fill out the respective binding sites. Thus developed compounds did not protrude in the SAM binding pocket and also did not reduce N^7-MTase activity. However, they were able to inhibit the 2'-*O*-MTase function of DENV, ZIKV and WNV with IC$_{50}$ values in the three-digit micromolar range (314, 315). To further optimise these compounds, a focused library was created *in silico*, centred around the essential scaffold and applied to a computational docking pipeline. Resulting inhibitors had improved IC$_{50}$ values as low as 20 µM against DENV and ZIKV 2'-*O*-MTase functions but displayed no antiviral properties (Figure 9) (316).
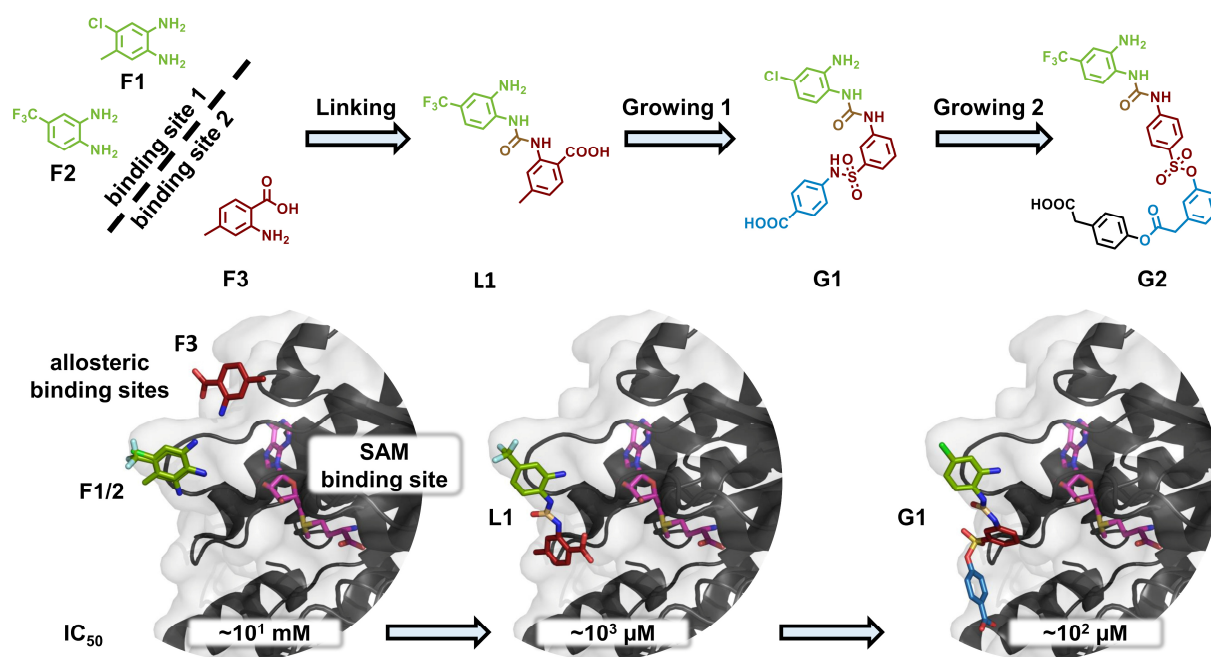
Figure 9. Flaviviral MTase inhibition. FBDD strategy applied to flaviviral NS5 MTase which led to 2'-*O*-MTase inhibitors. IC$_{50}$ values were improved by fragment linking and growing strategies from the millimolar range (F1-F3), to around 100 µM (G1) and lower to approximately 20 µM (G2). Figure adapted from Hernandez *et al*. (316) and Fischer *et al*. (97). SAM is displayed in pink. Protein structures were created with PyMOL (121). PDB IDs used: 5EKX, 5EIW, 5EIF, 5EHG, 5E9Q, 5EHI (314), 5WZ2 (317).

Coronaviral inhibitors. Since the start of the century, members of the coronaviral family were responsible for three infamous epi- and pandemics (318). Especially the emergence of SARS-CoV-2 in late 2019 revealed the vulnerability of modern, globalised societies leading to an urgent need of novel antiviral treatments. Unlike flaviviruses, coronaviruses need a total of three enzymes for their two RNA MTase functions. The N^7-MTase function is located on the nsp14 protein and additional to the typical N^7-MTase function of enabling efficient viral RNA translation and replication, nsp14's function was also

linked to the viral evasion of the innate immune system (319–322). The catalytic site of the 2'-*O*-MTase is located on nsp16 which forms a complex with nsp10 to conduct its function (323, 324). As for flaviviruses, both enzymes were addressed for drug-development.

In the relatively short time period since the outbreak of the SARS-CoV-2 pandemic an enormous number of *in silico* studies was published dealing with the design of potential inhibitors for either RNA MTase activity (see Table 20 in the Appendix). Alternatively, the exploitation of the SAM substructure was used for the design of inhibitors for nsp14 and nsp16 leading to compounds with IC_{50} values as low as the nanomolar range (325–327). Some of these compounds were competing with both, SAM and RNA and thus follow a bisubstrate mechanism (327, 328).

In a completely different approach, a screening of around 1800 approved drugs was able to identify nitazoxanide as a moderate nsp14 inhibitor with an IC_{50} value of around 10 μM displaying selectivity towards the human MTase hRNMT. Additionally, a previous screening revealed the drug's antiviral properties in cell culture (Figure 10) (219). Although the antiviral properties are likely not only attributed by its effect on MTase functions, its promising effects launched nitazoxanide into clinical trials against coronavirus disease 2019 (COVID-19) (NCT04486313, NCT04459286, NCT04348409, NCT04746183, as of 03/2022).
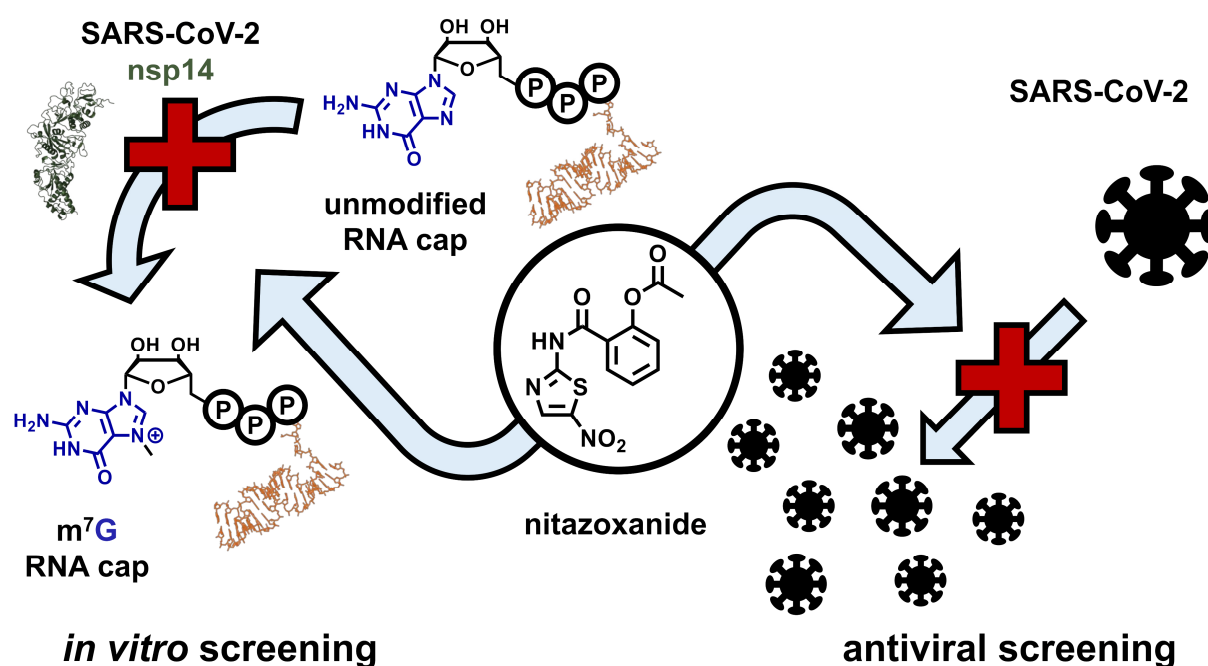
Figure 10. Coronaviral MTase inhibition. The broad-spectrum antiviral drug nitazoxanide arose from an *in vitro* drug repurposing screening targeting nsp14 while a second, antiviral screening revealed it to inhibit SARS-CoV-2 propagation (219). Figure adapted from Fischer *et al.* (97). Protein and RNA structures were created with PyMOL (121). PDB ID used: 7N0B (329).

1.5.8 Further RNA MTase inhibitors

One of the most famous and clinically relevant RNA MTase inhibitors is the drug azacitidine (Figure 11A), which is used for the treatment of leukaemia and myelodysplastic syndrome.
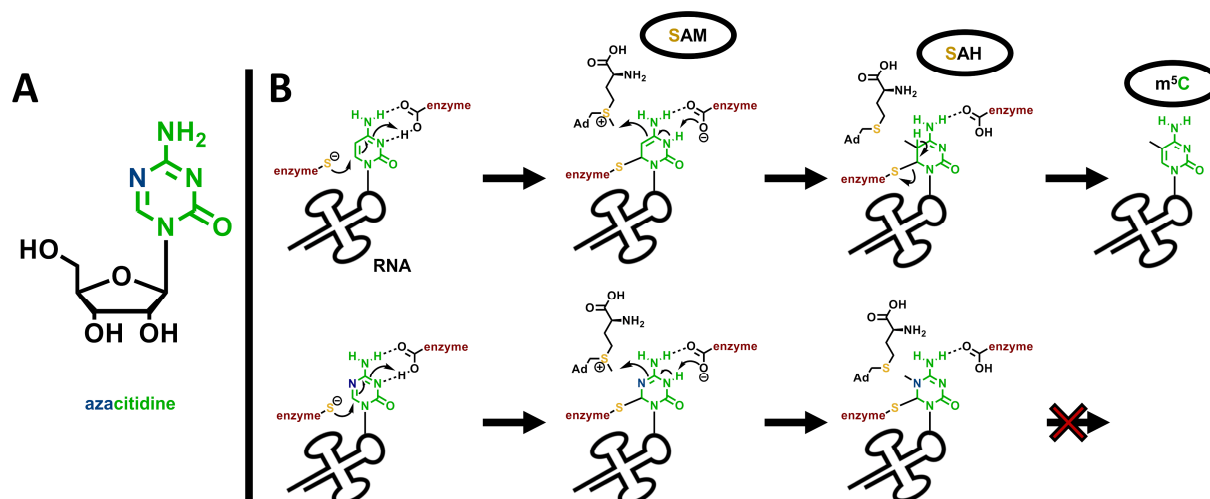
Figure 11. Azacitidine inhibition. A) Molecular structure of azacitidine. B) In the upper panel, the mechanism of m^{5}C MTases is displayed illustrating that a catalytic cysteine of the corresponding MTase attacks at C^6 of the cytidine base. After methylation of C^5, this cysteine residue is eliminated again leading to the m^{5}C modified base. In the lower panel, the same mechanism is displayed with an incorporated azacitidine. In contrast to the native cytidine, azacitidine prevents the release of the catalytic cysteine and traps the enzyme on the RNA, thereby inactivating it. Ad = adenosine. Figure adapted from Fischer *et al.* (97).

In vivo, this cytidine analogue is incorporated into RNA and DNA, where it traps the corresponding MTases and thereby inhibiting them. The trapping occurs due to the electron deficient ring which prevents elimination of the catalytic cysteine used by the MTases for methylation (*vide supra* and Figure 11B) (330, 331). This distinct mechanism of action proves azacitidine to be a macromolecular inhibitor, even if it is administered in form of a small molecule. Two RNA m^{5}C MTases, DNMT2 and NSUN2, were shown to be inhibited by azacitidine (332–334).

An additional example for macromolecular RNA MTase inhibitors are peptides, which are able to disrupt the formation of the nsp10-nsp16 complex in SARS-CoV, hence inhibiting 2'-*O*-MTase function (335, 336).

1.5.9 Aptamers as RNA MTase inhibitors

The use of aptamers offers yet another viable option for regulating RNA MTase activity. Aptamers are short, single-stranded and highly structured nucleic acids, which are able to bind their respective targets with high selectivity and affinity (337). They can be generated by systematic evolution of ligands by exponential enrichment (SELEX) for a variety of targets. This procedure was first reported by two independent groups in 1990 (338, 339). Meanwhile, numerous variants of SELEX have been developed, such as capillary electrophoresis SELEX (340) or asymmetric flow-field flow fractionation (AF4) SELEX (341–343). The basic concept of the original process however remains the same and is depicted in Figure 12A.
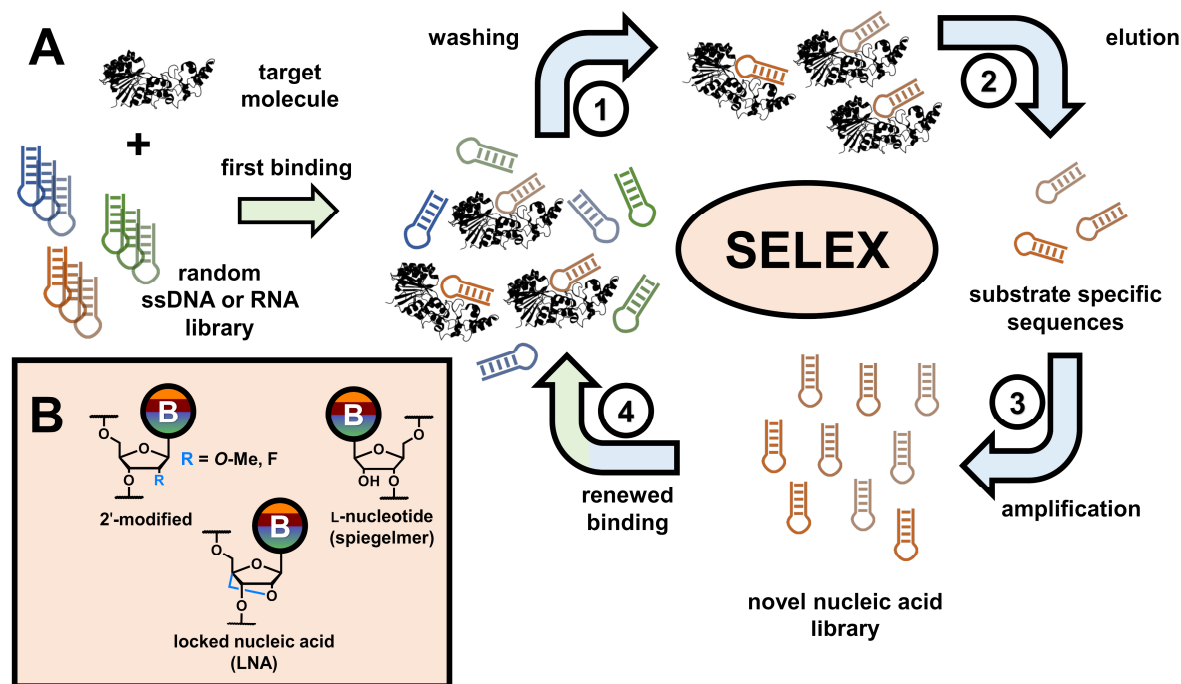
Figure 12. SELEX procedure. A) Depicted is the general SELEX procedure. At first the target molecule is incubated with a random oligonucleotide library. Afterwards, unbound sequences are discarded by washing (**1**) and subsequently bound sequences are eluted (**2**). In step three, these sequences are amplified, either by RT-PCR and IVT in the case of RNA or by PCR followed by strand separation for DNA (**3**). The newly generated pool is then subjugated to binding again and the cycle is repeated several times (**4**). B) Nucleotides which can be incorporated into RNA to enhance stability of aptamers.

During this process, a high number of varying RNA or DNA sequences ($> 10^{15}$) is subjected to the target of interest. After removal of non-binding sequences, bound molecules are eluted from the target and amplified by reverse transcriptase polymerase chain reaction (RT-PCR) and *in vitro* transcription (IVT) in case of RNA or with PCR with subsequent strand separation in the case of DNA. This new oligonucleotide pool is then used in the next round of SELEX and the cycle is repeated several times (337). Analysis of the produced pools is usually done by sequencing to select promising candidates from the vast nucleic acid pools (344).

Aptamers generated during this process usually display high specificity and affinity, and can act as inhibitors, agonists or might not affect the enzyme's activity rendering them interesting candidates for drug development or delivery (345, 346). Indeed, Macugen (also known as Pegaptanib), an aptamer binding to the vascular endothelial growth factor (VEGF), was approved by the FDA in 2004 for the treatment of neo-vascular age-related macular degeneration (347). Since then, however, no new aptamer-based drugs were approved, although numerous candidates reached late clinical stages (346). This observation can be explained by low half-lives, immunogenicity and toxicity concerns as well as problems with cellular uptake and localisation of aptamers (337, 346).

Low half-lives are due to the fast degradation of oligonucleotides *in vivo* mediated by nucleases or cyclic phosphate formation. This can be circumvented by incorporation of several modifications into the RNA backbone as exchanging the 2'-OH group in RNAs with 2'-F or by introducing various sugar derivatives, like xeno nucleic acids (XNA) (348) as locked nucleic acids (LNA) (349) or spiegelmers (L-variant of nucleotides, Figure 12B) (350, 351). In addition to their fast degradation, aptamers are excreted relatively fast by the liver and kidneys, which can be bypassed by PEGylation, describing attachment of

polyethylene glycol (PEG) chains (352, 353). While this indeed leads to higher circulation times, PEG was associated to allergic reactions, thereby causing its own problems (354).

Despite their drawbacks, aptamers are seen as promising candidates for future therapeutics, not least because they can be tailored for a huge variety of targets, even if these are hard to address by small molecules. With a high dynamic in the ongoing research of aptamers, the above-mentioned problems are expected to be avoided to achieve higher performance of aptamers in clinical studies (337, 346).

Since there is a high conservation of SAM binding sites between various MTases, selectivity for this class of enzymes is not trivial to achieve leaving aptamers a promising approach to detour this problem. However, literature for aptamers directed against MTases, and RNA MTases in particular, is very scarce. Even not related to RNA MTases, one promising aptamer candidate was described for the DNA MTase DNMT1, which displayed high affinity, good inhibition of activity and moreover a high selectivity against the structurally closely related DNMT3. Furthermore, it was able to reduce enzyme activity in cell culture experiments (341).

For RNA MTases of DENV and the *japanese encephalities virus* (JEV) the SELEX approach led to aptamers which displayed the characteristic high affinity and were further able to reduce both N^7- and 2'-*O*-MTase activities. In cells previously infected with a viral genome, co-expression of the aptamers impeded replication of viral RNA, pointing to a potential antiviral activity (355, 356).

1.5.10   RNA MTase inhibitors, what's next?

As described in the chapters above, the research field of epitranscriptomics gained considerable attention over the last decade due to its interesting and complex properties. Since RNA modifications were linked to numerous diseases, the enzymatic machineries behind them were revealed as possible drug targets. This resulted not only in an increased interest in academia, but also in the industry as can be seen by the foundation of various start-up companies (203–206).

However, compared to other enzyme families, research around RNA MTase inhibitors is still in its infancy with a lot of studies focussing on SAM derivatives to obtain first insights into SAR. Nevertheless, modern approaches in drug design were scrutinised to develop compounds based on scaffolds detached from SAM.

Especially promising molecules were identified for METTL3-METTL14 and with compound STM2457 without doubt a breakthrough was achieved. The developing company is expected to move forward to clinical studies in 2022 with yet another, more promising candidate (357, 358), which most likely will give the field a further push in popularity. Regardless of the compound's success in clinical studies, crucial insights on the field of epitranscriptomics are probably gained facilitating further research attempts. The newly earned impetus will hopefully not be restricted to the development of novel cancer therapies but include strategies to develop new antiviral and antibiotics or overcome corresponding resistances. For these, a solid foundation was built with prior research efforts.

Additionally, with improvements in aptamer research, especially concerning their *in vivo* efficacy, this class of molecules is of particular interest for RNA MTases. Applying this technique would circumvent selectivity issues which are expected to cause problems in small molecule research. With aptamers developed against DNMT1 (a DNA MTase), as well as JEV and DENV NS5, first examples are provided for effective MTase aptamers with all three displaying promising *in cellulo* activity.

2 Motivation and Objectives

As outlined in the introduction, RNA modifications and with them RNA modifying enzymes have significant impact in cellular regulation (29, 30) and in the progression of malignancies (31). In this regard, RNA methylations are the most relevant modifications and are implemented by RNA MTases (43). Inhibitors for RNA MTases are considered promising drug targets, with recent developments focused on cancer treatment now heading towards clinical trials (220).

One particular interesting RNA MTase is DNMT2 methylating tRNA^{Asp} (and others) at position 38 which leads to a m^{5}C modification (116). While the impact of this modification on tRNA properties as stability and translation was demonstrated (111), numerous functions of DNMT2 remain puzzling. From its exact substrate specificity (116, 138–140) over the role it plays in epigenetic inheritance (193, 202), to a potential influence on viral replication (147, 168, 183–185) many questions remain. Furthermore, links between DNMT2 and cancer were drawn (145, 146, 176, 180, 181).

For these reasons the motivation of this work was the development of novel DNMT2 inhibitors. Due to its involvement in cancer progression, DNMT2 is a viable drug target, especially since it was shown that abolishment of DNMT2 activity leads to sensitisation of cancer cells towards radiation or PARP inhibitors (145) and the upregulation of tumour supressing miRNAs (169). Additional to this, DNMT2 inhibitors can facilitate solving the DNMT2 enigma by functioning as structural probes in cellular experiments. In this study, a cornerstone for future drug development projects for DNMT2 and other is to be set. Next to the establishment of a robust activity assay, the focus should be laid on early structure activity relationship studies to assess, if the enzyme is druggable at all and to obtain a general idea of preferences for the enzyme. Therefore, two approaches are followed, either by addressing the SAM pocket of DNMT2 with small molecules or its RNA binding site by an RNA aptamer. It is also considered to address the catalytical cysteine with the small molecule inhibitors to obtain covalent inhibitors.

A valid starting point for early small molecule drug design is the ubiquitous methyl donor SAM (359), which was derivatised by members of the ████████ group to increase its affinity. This strategy has already been successfully applied to the development of inhibitors for various MTases, such as the catechol-*O*-MTase (COMT) (360–362), the histone MTase DOT1L (363), and also for RNA MTases such as METTL3-METTL14 (288–290) or the viral RNA cap MTases nsp14 and nsp16 of SARS-CoV-2 (326). Remarkably, the SAH derivative Pinometostat, a DOT1L inhibitor, even reached the stage of clinical trials for the treatment of leukaemia (326) (NCT03724084, 03/2022). Accordingly, this method was chosen as initial design strategy for potential DNMT2 inhibitors.

To address DNMT2's RNA binding site, RNA aptamers should be scrutinised due to their unique properties. For this, SELEX generated RNA pools ought to be analysed by next-generation sequencing and subsequently by *in silico* and *in vitro* methods. Thereby, suitable sequences should be pinpointed and further evaluated by aptamer truncation.

3   Results and Discussion

3.1   Rational design and testing of first DNMT2 inhibitors

3.1.1   Design strategy

As the starting point for the design of DNMT2 inhibitors, the SAM scaffold was selected. In the case given, the amino acid side chain on the 5' end was derivatised, while the adenosine scaffold with its adenine base and ribose was not altered. To obtain a detailed insight into the structure-activity relationship of DNMT2, derivatives in several successions were constructed, as can be seen in Figure 13. Most design ideas were developed by ▉▉▉▉▉▉▉▉▉ from the group of Professor ▉▉▉▉▉▉▉, JGU Mainz.
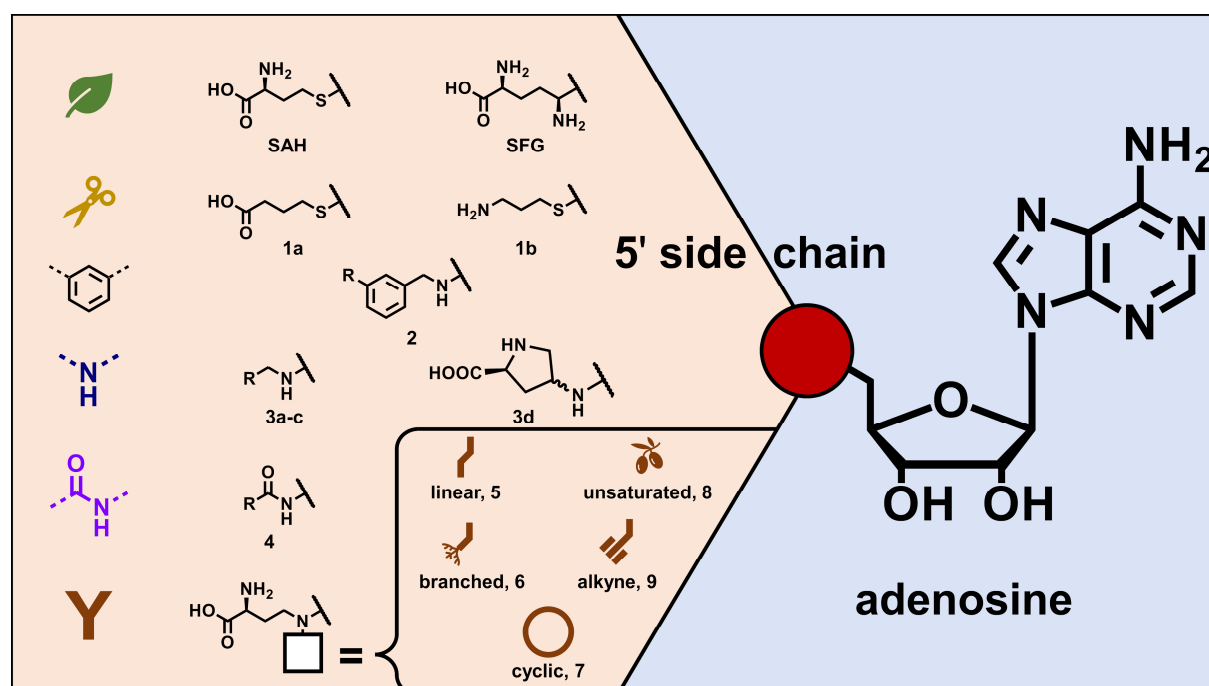
Figure 13. Design strategy for the first DNMT2 inhibitors. The natural products SAH and SFG were used as reference substances (green leave). The 5' side chain of SAM was altered either by truncating it (yellow scissors, **1**), using aromatic moieties (black, **2**), amine (blue, **3**) or amide (lilac, **4**) linkers as well as tertiary amines or 'Y-shaped' compounds (brown, **5–9**). For the Y-shaped compounds linear **5**, branched **6**, saturated cyclic **7**, unsaturated **8** or alkyne **9** residues were studied.
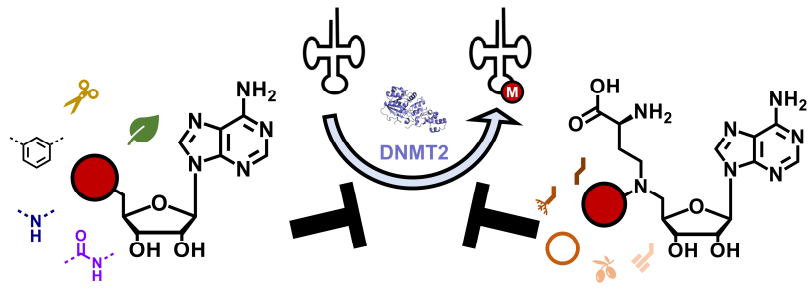
Naturally the well-known pan MTase inhibitors SAH and SFG were included in the investigation. First synthetic efforts for creating potential DNMT2 inhibitors were aimed at truncation of the amino acid side chain (**1**) or by altering it with aromatic moieties (**2**). Further experiments attempted to exchange the thioether linker by amines (**3**) or amides (**4**). Finally, derivatives were investigated in which the sulphur atom was replaced by a tertiary amine, resulting in Y-shaped molecules resembling the positive charge of SAM depending on the pH value and potentially addressing the cytidine binding site of DNMT2 (**5–9**). All compounds were synthesised by ▉▉▉▉▉▉▉▉ and in the course of their master theses by ▉▉▉▉▉▉▉, ▉▉▉▉▉▉ (both supervised by ▉▉▉▉▉▉▉▉) and ▉▉▉▉▉▉▉ (supervised by ▉▉▉▉▉▉▉▉ and myself) from the group of Professor ▉▉▉▉▉▉, JGU Mainz.

3.1.2   Compound evaluation on DNMT2
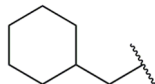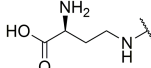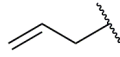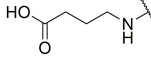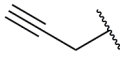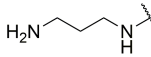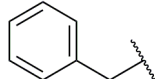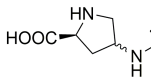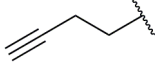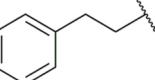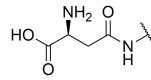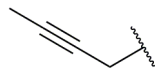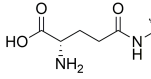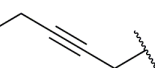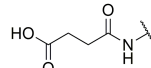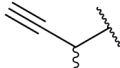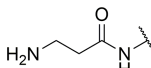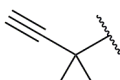
The ability of the compounds to modulate DNMT2 activity was measured using a tritium incorporation assay, which workflow is depicted in Figure 5 (148, 227). This assay was chosen since implementation of a HPLC based assay with either electrochemical or MS/MS detection was not possible due to instrumental restrictions. Substrate tRNA^{Asp} was produced by *in vitro* transcription (IVT) with a PCR amplified template and purified by gel elution or ion exchange chromatography (IEX). DNMT2 was recombinantly expressed in *E. coli* cells and purified threefold using immobilised metal ion affinity chromatography (IMAC) exploiting the His6 Tag of the protein, IEX and size exclusion chromatography (SEC). Recombinant protein expression and purification was conducted by ███████████████, group of Professor ████████████, JGU Mainz. For initial screening, the synthesised compounds were subjected to the activity assay at concentrations of 100 μM. To verify the activity assay's screening results with an orthogonal method, binding of the molecules was assessed with microscale thermophoresis (MST) (364) at a concentration of 100 μM (conducted by ████████████████, group of Professor ████████████, JGU Mainz). Results of these experiments are presented in Table 2.

Table 2. Overview of first DNMT2 inhibitors. DNMT2 binding and inhibition of the compounds at 100 µM as determined by MST and the tritium incorporation assay. Inhibition is displayed as mean values ± standard deviation of three independent measurements. Table ranges over multiple pages. Figure schematically depicts inhibition of DNMT2 by the various investigated compounds. Protein structure was created with PyMOL (121) and PDB: 1G55 (117).

Compound	Binding at 100 µM (MST)	Inhibition at 100 µM [%]	Compound	Binding at 100 µM (MST)	Inhibition at 100 µM [%]
Natural products			**Y-shaped linear**		
SAH	✓	85.7 ± 1.7	5a	✓	30.3 ± 1.9
SFG	✓	83.5 ± 1.1	5b	✓	n.i.
Truncated compounds			5c	✗	n.i.
1a	✗	n.i.	5d	✗	n.i.
1b	✗	n.i.	**Y-shaped branched**		
Aromatic linkers			6a	✓	44.0 ± 2.7
2a	✗	n.i.	6b	✗	n.i.
2b	✗	n.i.	6c	✗	n.i.
2c	✗	n.i.	**Y-shaped cyclic**		
2d	✗	n.i.	7a	✓	27.5 ± 0.4
2e	✗	n.i.	7b	✓	32.0 ± 2.0
2f	✗	n.i.	7c	✓	24.5 ± 8.5

	Amine linkers			**7d**	X	n.i.
3a		✓	n.i.		**Y-shaped unsaturated**	
3b		X	n.i.	**8a**	✓	53.9 ± 6.4
3c		X	n.i.	**8b**	✓	72.2 ± 1.2
3d		X	n.i.	**8c**	✓	56.8 ± 6.8
	Amide linkers			**8d**	✓	30.2 ± 0.8
4a		X	n.i.	**8e**	✓	23.2 ± 8.2
4b		X	n.i.		**Y-shaped alkyne**	
4c		X	n.i.	**9a**	✓	61.3 ± 2.1
4d		X	n.i.	**9b**	✓	62.8 ± 0.1
				9c	✓	81.6 ± 2.1
				9d	✓	17.3 ± 1.4

IC_{50} values were determined for selected compounds exhibiting both binding in the MST assay and a sufficient strong inhibition in the activity assay using the tritium incorporation assay. The IC_{50} value of **9c** was determined by ▮▮▮▮▮▮ in the course of his master thesis. For fitting of experimental data the two-parameter logistic function was used, even though for some compounds saturation at low doses was not at 100% enzyme activity following the recommendation of Copeland (365).

Additionally, compound binding was characterised in more detail using isothermal titration calorimetry (ITC, conducted by ▮▮▮▮▮▮▮▮ group of Professor ▮▮▮▮▮▮, JGU Mainz) (366). These values are displayed in Table 3 with dose-response curves given in Figure 14.

Table 3. Characterisation of selected DNMT2 inhibitors. K_D values as determined by ITC and IC_{50} values as determined by the tritium incorporation assay of the most potent DNMT2 inhibitors. Values are displayed as mean values ± standard deviation (K_D) or ± standard error (IC_{50}) of three independent measurements. The K_D value of SAH is displayed as mean value ± standard deviation of six independent measurements. Figure schematically depicts binding and inhibition of DNMT2 by the various investigated compounds. Protein structure was created with PyMOL (121) and PDB: 1G55 (117).
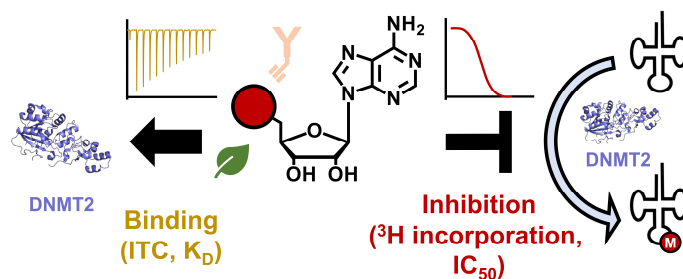
Compound		K_D [µM]	IC_{50} [µM]
SAH		13.6 ± 4.4	15.8 ± 1.5
SFG		7.5 ± 3.5	13.2 ± 0.8
8b		11.4 ± 2.4	77.1 ± 5.3
9a		10.4 ± 2.2	39.7 ± 9.2
9b		10.5 ± 3.3	32.2 ± 4.3
9c		8.1 ± 1.4	12.9 ± 1.9

For both natural products, SAH and SFG, inhibition of around 85% was assessed and both were classified as binders in the MST assay. IC_{50} values were similar with 16 µM and 13 µM respectively and also K_D values were comparable with 14 µM for SAH and 8 µM for SFG.

Both truncated versions of SAH, **1a** and **1b**, displayed neither binding nor inhibition at 100 µM. The same held true for all compounds with aromatic linkers **2a–e** and the phthalimide derivative **2f**. Furthermore, molecules **3a–d** bearing amine linkers did not show any inhibition and only **3a** was binding DNMT2 according to the MST assay. To further explore **3a** it was applied to the tritium incorporation assay at an elevated concentration of 1 mM where it displayed DNMT2 inhibition of 44%. None of the compounds bearing amide linkers **4a–d** were categorised as binders nor inhibitors.
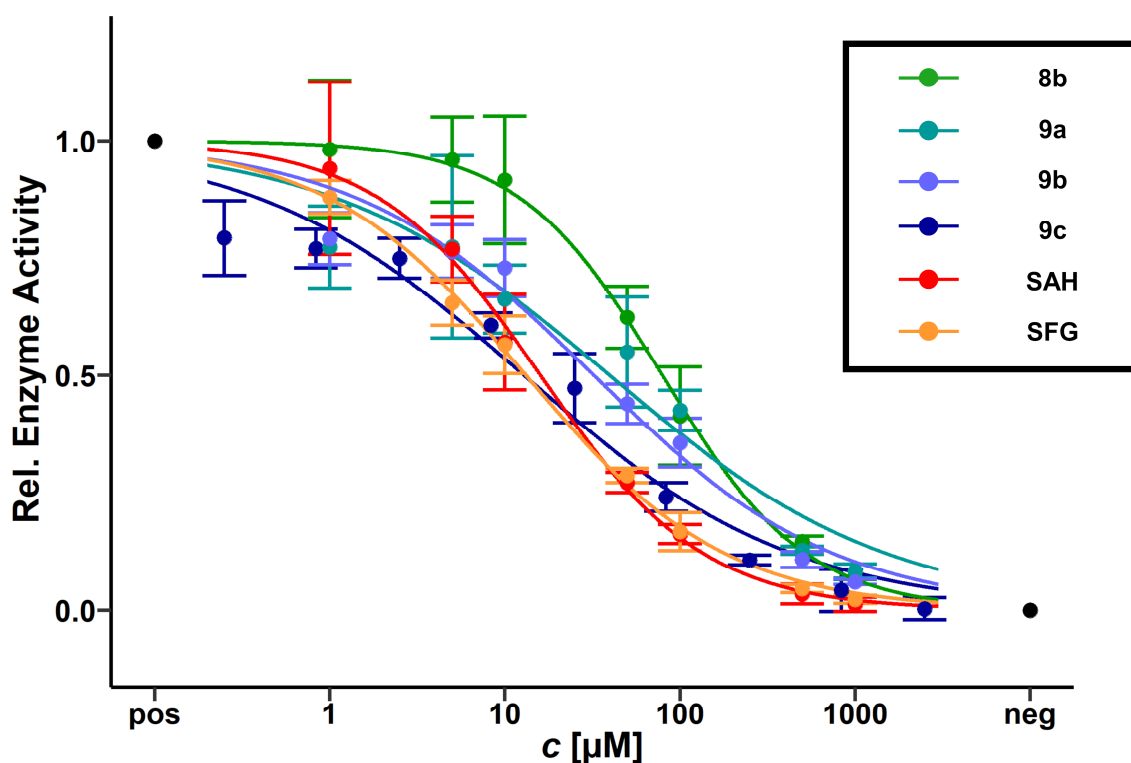
Figure 14. Dose-response curves I. Dose-response curves of SAH, SFG, as well as compounds **8b**, **9a**, **9b** and **9c** for IC_{50} calculation as determined by the tritium incorporation assay. "pos" refers to control experiments conducted in the absence of inhibitor and "neg" refers to experiments conducted in the absence of inhibitor and tRNA^{Asp}. Displayed are mean values and standard deviations of experimental triplicates.

However, the simplest Y-shaped structure **5a**, bearing a methyl group, was binding to DNMT2 and inhibited its activity by 30%. Exchanging the methyl group to an ethyl group as in compound **3b** let to an abolishment of inhibition, while binding was measured via MST. Attaching longer *n*-propyl or -butyl side chains resulted in molecules **5c** and **5d**, which exhibited no binding and inhibition of the enzyme. Derivative **6a** bearing a branched isopropyl side chain was binding to the target and also diminished its activity by 44%, whereas for larger branched moieties **6b** and **6c** no binding and inhibition could be measured.

For compounds **7a–c** carrying cyclopropyl, -butyl and -pentyl rings the MST assay displayed binding, while inhibition of 28%, 32% and 25% was determined respectively. Molecule **7d** with a cyclohexyl residue was classified as a non-binder and did not reduce the enzymatic activity.

All Y-shaped derivatives with unsaturated side chains were classified as binders according to MST. Compounds **8a**, **8b** and **8c,** which were derivatised with allyl, propargyl and benzyl residues, were diminishing DNMT2 activity by 54%, 72% and 57%. A K_D value of 11 µM was determined for propargylic derivative **8b**, which is comparable to SAH and SFG, while the IC_{50} value of approximately 80 µM was significantly higher. **8d** and **8e**, derivatives of **8b** and **8c** containing ethyl linkers, showed inhibition of 30% and 23%. If the terminal carbon chain of **8b** was extended with a methyl (**9a**) or ethyl group (**9b**) the inhibition at 100 µM was 61% or 62%, while IC_{50} values were around 40 µM and 32 µM. The K_D values with 11 µM and 10 µM were highly similar and in the range of SAH and SFG.

At last, the branched monomethyl compound **9c** displayed a strong inhibition of 82%. The additional methyl group in the side chain of **9c** makes the α-carbon atom asymmetric and thus, **9c** describes a 1:1

mixture of two epimers with different configurations ((R) and (S)). The dimethyl derivative **9d** inhibited DNMT2 by 17%. Due to its strong activity in the tritium incorporation assay, K_D and IC_{50} values were determined for **9c**. The K_D of 8 µM was comparable to other investigated compounds, but its IC_{50} value of 13 µM was remarkably low.

A first glance at the data presented above clearly illustrates a good agreement between the MST and activity assays. All compounds displaying inhibition at 100 µM were also revealed as binders, while only two molecules classified as binders did not exhibit inhibition resulting in a correlation of 90% between non-binders and non-inhibitors. Interestingly, **3a** was classified as a binder but not as inhibitor at 100 µM and showed inhibition at a higher concentration of 1 mM exposing this compound to be a weak inhibitor. Thus, MST is likely to be more sensitive towards weak-interacting molecules and compounds displaying binding but no inhibition at 100 µM might be in fact weak inhibitors.

Since the truncated and aromatic SAM derivatives **1** and **2**, lacking the amino acid functionalities, were not able to reduce the activity of DNMT2 and did not exhibit binding, the amino acid side chain seems to be crucial for interaction with the enzyme.

Exchanging the thioether moiety with either secondary amines or amides appears to be poorly tolerated since **3a** was the only compound from this series binding DNMT2 according to MST. As described above, inhibition for **3a** was only measured at higher concentrations, whereas at 100 µM none of the compounds inhibited the enzyme. To exclude the possibility that the loss of affinity was induced by a shortened side chain instead of the exchange from the sulphur atom with the amide moiety, different chain lengths were evaluated. Indeed, after the comparison between **4a** and **4b** this was ruled out since both molecules were inactive against DNMT2.

Only after turning to Y-shaped compounds synthetic inhibitors were identified, which allowed a first structure activity relationship study for DNMT2. In all comparisons between derivatives bearing unsaturated side chains, either of linear (**5a–d**), branched (**6a–c**) or cyclic (**7a–d**) nature, a preference for smaller residues was clearly determined. Still, the potency of these compounds remained well out of the range of SAH and SFG.

The implementation of unsaturated residues on the other hand led to inhibitors with higher affinities (**8a–8e**), with alkyne **8b** exhibiting the most potent inhibition. Still, its IC_{50} value of around 80 µM was significantly higher compared to IC_{50} values of SAH and SFG, but the K_D of 11 µM was comparable to the ones obtained from SAH and SFG of 14 and 8 µM. The promising inhibition of propargyl and benzyl derivatives **8b** and **8c** with 72% and 57% at 100 µM could not be enhanced by elongating the connecting methylene groups to ethylene groups, actually inhibition decreased in both cases (**8d** and **8e**). However, extending the terminus of **8b** with methyl or ethyl groups yielded inhibitors **9a** and **9b** with IC_{50} values of 40 µM and 32 µM, while the K_D values remained around 10 µM, which in both cases is comparable to **8b**.

To combine the moderate inhibition exhibited by **6a** and **8b**, both substructures present in the side chains were merged, as can be seen in Figure 15A leading to derivatives **9c** and **9d** (original idea by ▇▇▇▇ ▇▇▇▇▇▇). While the dimethyl derivative **9d** reduced DNMT2 activity only by 17%, the monomethyl derivative **9c** inhibited the enzyme effectively with an IC_{50} value of 13 µM. The respective value was in the range of IC_{50} values for SAH and SFG, making it the most potent synthetic inhibitor of DNMT2

identified by this compound series. However, the K_D value of 8 µM did not change significantly compared to other derivatives.
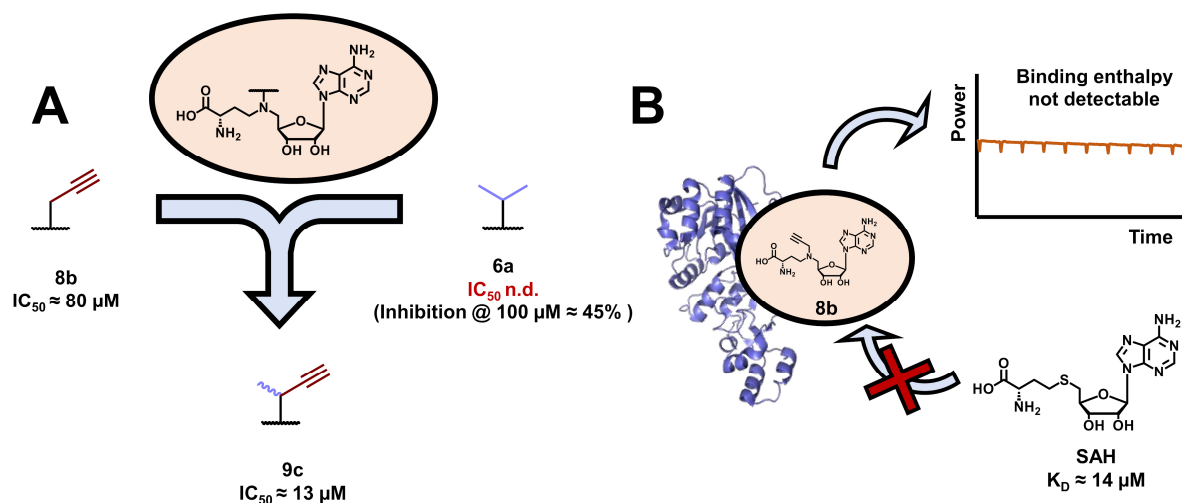
Figure 15. Inhibitor merging and binding site. A) Merging of substructures of **8b** and **6a** led to compound **9c** showing substantial inhibition. B) Exploring the potential binding site of synthetic SAM derivatives by titrating SAH against DNMT2 preincubated with **8b** in an ITC experiment. No binding enthalpy was detected in contrary to experiments without preincubated enzyme. Protein structure was created with PyMOL (121) and PDB: 1G55 (117).

As presented in Table 3, the measured K_D values are relatively similar, while IC_{50} values differ significantly leading to inconsistent ratios between the two values. The IC_{50}/K_D ratio is around one for SAH and 1.5 for **9c** but for the other compounds it is generally higher with roughly two for SFG, three for **9b**, four for **9c** and seven for **8b**. This indicates, that binding to DNMT2 does not result in consistent inhibition. A possible explanation is that both experiments were conducted under different conditions using distinct buffer components and pH values. This is potentially leading to slight variations in surface charges or hydration shells and thus to different binding behaviours of the inhibitors. Also, IC_{50} values are strongly dependent on the experimental conditions, as substrate or enzyme concentration adding another potential source for variations (367). The most pronounced discrepancy among both assays is tRNA^{Asp}, which is absent in the ITC assay. Binding of such a large and strongly charged molecule can induce conformational changes in the enzyme and might change its surface charge significantly, thus providing a feasible explanation for the different ratios. However, based on the available data, a satisfying clarification cannot be provided. A detailed discussion for treating this phenomenon is given further below.

The close structural resemblance between synthetic inhibitors and the natural cofactor SAM already suggests that they can compete for the same binding site. For further elucidation, SAH was titrated against DNMT2 preincubated with compound **8b** using ITC (experiment conducted by ██████ ████████████, Figure 15B). In this case, no binding enthalpy was measured supporting the previously stated hypothesis of a shared binding site.

Due to the additional methyl group, compound **9c** is a mixture of two epimers raising the question if one of the epimers is more active towards DNMT2 than the other. To examine this, the mixture was separated by ██████████████ and inhibition was compared at 100 µM in the tritium incorporation assay by ████████████ in the course of his master thesis. An exact allocation to either the (R) or (S)

epimer was not possible. However, no significant difference was observed between the inhibition of the separated epimers, instead both reduced DNMT2 activity similar as the epimeric mixture (Figure 16A).
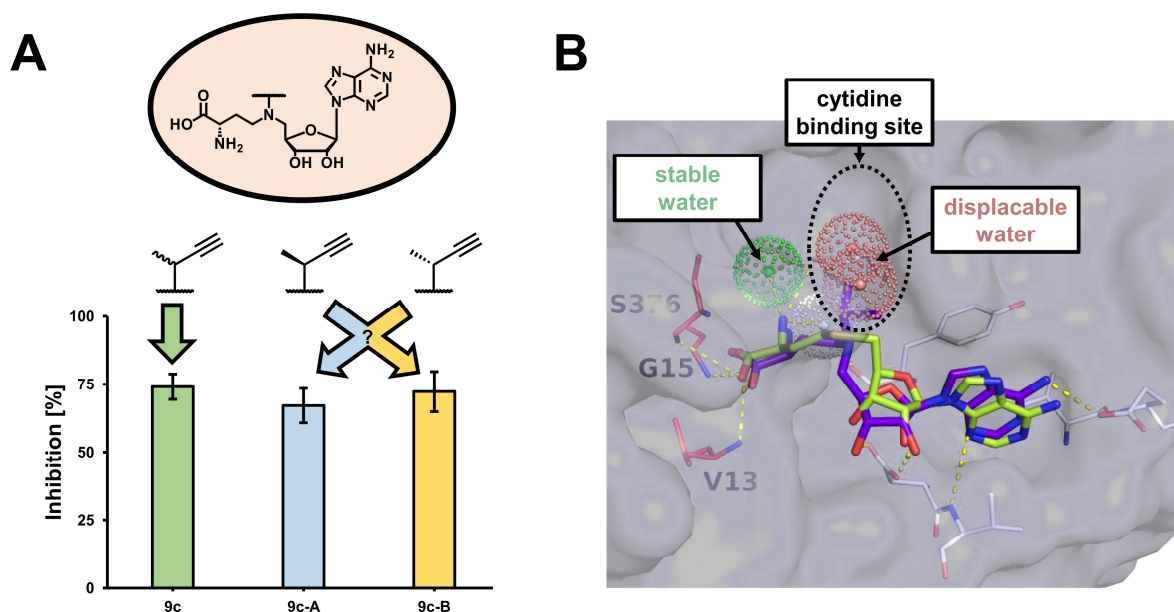
Figure 16. Epimer inhibition and *in silico* analysis. A) Inhibition of epimeric mixture **9c** and the separated epimers **9c-A** and **9c-B** at 100 μM as determined by the tritium incorporation assay. Displayed are mean values and standard deviations of experimental triplicates. B) Predicted binding mode of **9c** ((*R*)-epimer, purple) with DNMT2, overlaid with the co-crystallised structure of SAH (light green). Amino acids interacting with the compound's acid moieties are displayed in dark red, the cytidine binding site is indicated with a dotted line in black, energetically unfavoured water molecules potentially displaced by Y-shaped inhibitors are coloured in light red and the energetically favoured water molecule possibly interacting with the compound's amino group is shown in green. Docking studies were conducted by Dr. ███████████. Figure was created with PyMOL (121) and PDB: 1G55 (117).

Noteworthy, docking studies conducted by Dr. ███████████ supported and complemented the experimental data. The predicted binding modes for the docked ligands corresponded strongly with the binding mode of the reference ligand SAH adding further evidence for a shared binding site and also backed the original assumption of addressing the cytidine binding site with Y-shaped compounds, as can be seen in Figure 16B. Computational solvent analysis revealed that the additional group of the Y-shaped compounds might be able to displace energetically unfavoured water molecules suggesting a reason for their higher potency. Furthermore, the docking studies provide a possible explanation for the importance of the amino acid side chain. While the acid group of the co-crystallised SAH was shown to interact with the amide backbone of Val-13 and Gly-15 and the side chain of Ser-376, the amino group was predicted to interact with water molecules that are firmly embedded in the crystal structure. A more precise overview about the docking procedure and its results is given in Schwickert, Fischer, Zimmermann *et al.* (currently under revision).

3.1.3 Selectivity of alkyne derivatives towards various SAM-dependent MTases

As a consequence of the close structural resemblance to the ubiquitous MTase substrate SAM, a key interest is the selectivity of the synthesised compounds towards other SAM-dependent MTases. To assess the selectivity, enzymatic activity assays of various MTases were conducted using the tritium incorporation assay with compounds listed in Table 3, including the natural products SAH and SFG at a concentration of 100 µM. MTases used for selectivity experiments included DNMT3A-3L, since it exhibits high structural homology to DNMT2 (69). Furthermore, the functional related tRNA m^5C MTases NSUN2 and NSUN6 (368–370), were investigated alongside the SAM-dependent histone MTase G9a (371). DNMT3A-3L, NSUN2 and G9a assays were conducted by ███████████ in the course of his master thesis. The results are provided in Table 4.

Table 4. Selectivity of DNMT2 inhibitors. Inhibition of SAH, SFG and alkyne derivatives **8b** and **9a–c** against a panel of SAM-dependent MTases. Inhibition was measured with the tritium incorporation assay at a compound concentration of 100 µM. Displayed are mean values ± standard deviations of three independent measurements. For **a** the mean value ± standard deviation of two independent measurements are displayed. Figure schematically depicts inhibition of several MTases by the various investigated compounds. Protein structures were created with PyMOL (121) and PDB: 1G55 (DNMT2) (117), PDB: 6F57 (DNMT3A-3L) (372), PDB: 4NVQ (G9a) (373), PDB: 5WWQ (NSUN6) (374), AF: F-Q08J23-F1 (NSUN2) (375, 376).
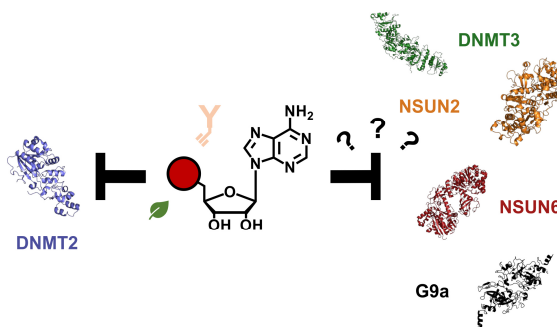
Compound		Inhibition at 100 µM [%]				
		DNMT3A-3L	NSUN2	NSUN6	G9a	DNMT2
SAH		96.7 ± 3.2	97.3 ± 0.3	99.6 ± 4.6	94.3 ± 0.8	85.7 ± 1.7
SFG		98.0 ± 2.3	76.8 ± 1.7	70.2 ± 1.8	43.0 ± 9.7	83.5 ± 1.1
8b		92.6 ± 1.4	n.i.	25.9 ± 3.5	22.2 ± 1.9[a]	72.2 ± 1.2
9a		88.2 ± 1.7	n.i.	12.9 ± 7.6	31.9 ± 14.8	61.3 ± 2.1
9b		90.7 ± 0.8	n.i.	22.7 ± 4.9	37.6 ± 5.1	62.8 ± 0.1
9c		84.2 ± 0.8	n.i.	n.i.	71.0 ± 5.9	81.6 ± 2.1

34

The DNMT3A-3L construct was inhibited more strongly by all investigated compounds than DNMT2. The highest inhibition at 100 µM was observed for SAH and SFG, which was around 100% for both. Synthetic compounds **8b**, **9a** and **9b** lowered the enzyme's activity by 93%, 88% and 91% respectively, while the weakest inhibition was evaluated for **9c** with 84%.

Also, NSUN2 and NSUN6 were inhibited by SAH around 100%, but SFG exhibited a weaker inhibition of 77% and 70% correspondingly. While all synthetic compounds investigated did not reveal significant inhibition towards NSUN2, **8b**, **9a** and **9b** reduced NSUN6 activity slightly, whereas **9c** showed no significant activity towards either of these tRNA MTases.

As for DNMT3A-3L, the enzymatic activity of G9a was lessened by all inhibitors considered. Again, SAH displayed profound inhibition of 94% but SFG only reduced G9a activity by 43%. For **8b**, **9a** and **9b** weak inhibition in the range between 20% to 40% was assessed, **9c** however reduced G9a activity around 70%.

The potent inhibition of DNMT3A-3L by the synthetic compounds undoubtedly proves that selectivity for the compounds is not given yet. Since DNMT2 and DNMT3A both exhibit high structural similarities, this observation is not surprising, particularly when considering the close structural resemblance of the synthetic molecules compared to the ubiquitous cofactor SAM. Also, both SAH and SFG are reported to reduce DNMT3A activity with IC_{50} values in the low to sub micromolar range (377, 378), which was also observed for DNMT3B with IC_{50} values < 500 nM (379, 380). This profound inhibition by SAH and SFG poses a feasible reason for the synthetic SAM analogues not to be selective comparing DNMT2 and DNMT3A-3L.

Remarkably, all synthetic inhibitors reduced NSUN2 and NSUN6 activities only weakly or not at all, with **9c** showing no activity towards neither enzyme. Since a slight preference for SFG towards SAH was detected, this behaviour may be credited to the Y-shaped structure of these compounds.

In contrast to other investigated MTases, inhibition of G9a by SFG was relatively weak with only 40%. Reported IC_{50} values for G9a vary strongly between the low micromolar range to over 500 µM, rendering this observation plausible (381–383). Importantly, the reported trend between SAH and SFG inhibition, which is stronger for SAH, was reproduced (382). In the comparison between DNMT2 and G9a at best moderate selectivity was observed, with **8b**, **9a** and **9b** displaying a slight preference for DNMT2, while **9c** reduced both enzyme activities to a comparable degree.
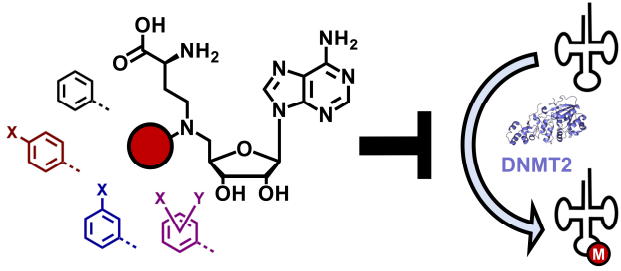
Unsurprisingly, only limited selectivity of the investigated inhibitors was observed, which is likely attributed to the high similarity of the synthetic compounds and the ubiquitous cofactor SAM. This is most obvious for DNMT3A-3L, since both proteins share significant structural likeness (69). Although not investigated here, selectivity is not expected for DNMT1, which is structurally closely related to DNMT2 and DNMT3A (69). Comparable to DNMT3A and DNMT3B, IC_{50} values in the low- to sub-micromolar range are reported for SFG, SAH and SAH analogues towards DNMT1 (379, 380, 384, 385). G9a was inhibited by all investigated compounds albeit less strong compared to DNMT3A-3L. In the comparison between DNMT2 and NSUN2 or NSUN6 however, only weak inhibition or even no inhibition was observed for synthetic inhibitors, hinting that partial selectivity was achieved.
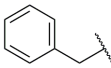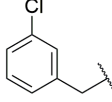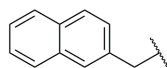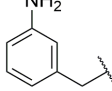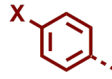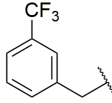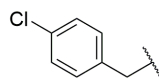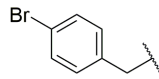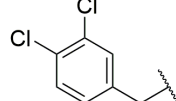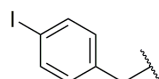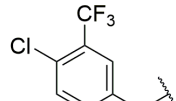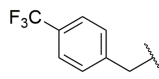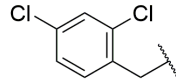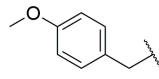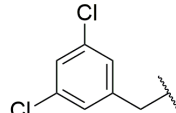
3.2 Rational design and testing of DNMT2 inhibitors with arylic side chains

3.2.1 Aromatic DNMT2 inhibitors with methylene linkers

As described in the chapter above, the Y-shaped SAM analogue **8c** bearing a benzylic residue in its side chain was able to inhibit DNMT2 around 57% at a concentration of 100 µM. Aromatic groups hold great potential since they can be derivatised easily and in a diverse manner. On that account, another series of Y-shaped SAM-like compounds was designed by ███████████ and synthesised by ██████████ during the course of her master thesis, supervised by ███████████. All compounds were derivatised with various aromatic moieties as tertiary residues at the amino group linking adenosine and amino acid, which were connected via a benzylic linker. Inhibition and binding of these compounds towards DNMT2 was assessed by the tritium incorporation and MST assays at a concentration of 100 µM as described above (MST assays were conducted by ███████████, group of Professor ██████████). The results of this compound series are depicted in Table 5.

Table 5. Overview of benzylic DNMT2 inhibitors. DNMT2 binding and inhibition of the compounds at 100 µM as determined by MST and the tritium incorporation assay. Inhibition is displayed as mean values ± standard deviation of three independent measurements. Figure schematically depicts inhibition of DNMT2 by the various investigated compounds. Protein structure was created with PyMOL (121) and PDB: 1G55 (117).

Compound	Binding at 100 µM (MST)	Inhibition at 100 µM [%]	Compound	Binding at 100 µM (MST)	Inhibition at 100 µM [%]
no substitution			**3-substitution**		
8c	✓	56.8 ± 6.8	**12a**	✓	67.2 ± 3.4
10	✓	55.4 ± 1.7	**12b**	✗	n.i.
4-substitution			**12c**	✓	60.6 ± 3.0
11a	✓	85.8 ± 2.3	**disubstitution**		
11b	✓	67.3 ± 3.4	**13a**	✓	73.8 ± 3.5
11c	✓	75.5 ± 0.8	**13b**	✓	86.2 ± 3.0
11d	✓	51.1 ± 6.6	**13c**	✓	47.0 ± 3.2
11e	✓	64.0 ± 3.1	**13d**	✓	59.6 ± 4.6

All compounds were classified as binders by MST and inhibited DNMT2 at 100 µM, except for derivative **12b** with an amino group at its 3-position, which exhibited neither binding nor inhibition at this concentration. The inhibition of 57% and 55% at 100 µM for **8c** and **10** bearing unsubstituted ring systems with varying sizes was very similar. Arranging chloro, bromo or iodo residues at the 4-position of the benzylic ring led to compounds **11a–c**, reducing DNMT2 activity by 86%, 67% and 76%

respectively. Derivatives **11d** and **11e** bearing either trifluoromethyl and methoxy residues at this position inhibited the enzyme by 51% and 64%.

Besides the 4-position, the 3-postion of the benzylic ring was substituted with chloro-, amino- or trifluoromethyl groups. As described above, attachment of an amino-group at the 3-position as in compound **12b** abolished affinity towards DNMT2. Contrary to that, compounds **12a** and **12c** with chloro- or trifluoromethyl groups inhibited DNMT2 by 67% and 61%.

Additionally, a subset of derivatives bearing disubstituted benzylic rings were analysed. While the 3,4-dichloroderivative **13a** reduced DNMT2 activity by 74%, **13b** with a 4-chloro-3-trifluoromethyl substitution displayed 86% inhibition. Furthermore, 1,4- and 2,5-dichloroderivatives **13c** and **13d** were investigated and lowered the activity by 47% and 60%.

When inspecting the results displayed in Table 5, a correlation of 100% between MST and activity assays is observed, which is in line with findings described above (Table 2). Exchanging the phenyl to a naphthyl ring seems to be well tolerated indicating no sterical clash. This further becomes evident when considering other inhibitors with bulky groups such as **11b** and **11c** with bromine or iodine residues at the 4-position. In general, substitutions at the 4-position are well tolerated, since all compounds in this series display inhibition comparable or higher to the unsubstituted derivative. Interestingly, no trend in inhibition for halogenide residues was examined indicating a mechanism of inhibition which is not solely based on either size or partial charge due to electronegative differences. Since compound **11d** displays a rather low inhibition compared to other compounds, which are substituted at position 4, it becomes clear, that a strong negative partial charge at this position is not leading to higher affinities of the compounds.

In contrast to this, derivatives with modifications at the 3-position did not lead to a significant increase in inhibition, an amino group here even led to a complete loss of affinity. Unlike the other investigated residues, amino groups are strong electron donors in arylic rings due to their +M effect, which might be an explanation for the observed behavior.

If additionally to a 4-chloro residue another chloro- or a trifluoromethyl-group was attached to the 3-position, inhibition remains similar to the monosubstituted 4-chloro derivative suggesting that effects of substituents at positions 3 and 4 do not add up, but rather that the 4-chloro residue is responsible for the higher affinity. This is further emphasised by compound **13d,** which has no 4-chloro residue while its inhibition is comparable to the unsubstituted benzylic compound **8c**. Modification of the 2-position with an extra chlorine atom additional to a 4-chloro moiety (**13c**) drops inhibition from 85% to around 50% revealing substitutions at this position as hindering.

The acquired results can also be considered regarding the Topliss scheme (proposed by ███████ ███████████), which provides a decision tree for improving aromatic substitution patterns in the context of medicinal chemistry (386). The steps of the workflow are depicted in Figure 17.
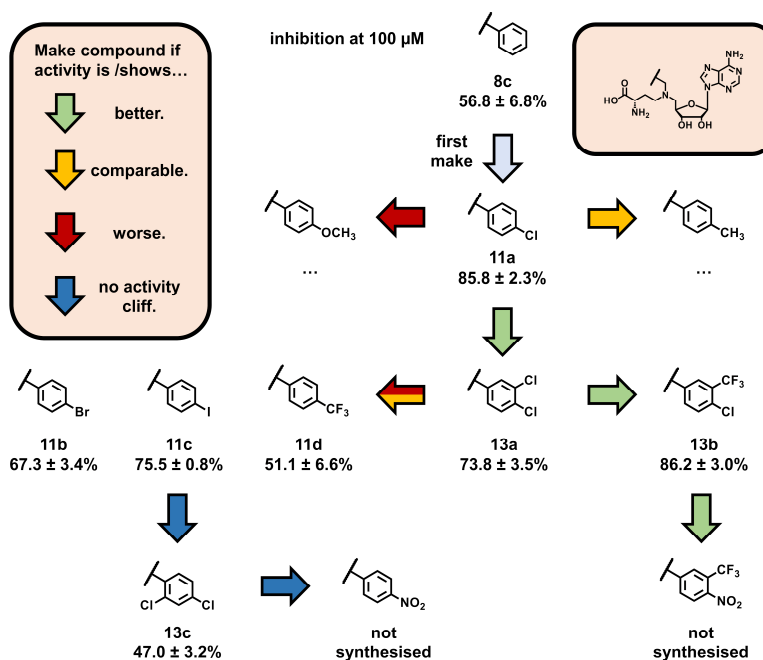
Figure 17. Topliss scheme. Representation of the Topliss scheme (386). The scheme provides a decision tree for the improvement of aromatic substitution patterns in medicinal chemistry. Here, activities of different compounds are compared and based on the results, novel molecules with varying substitution patterns can be designed in a rational way. Comparisons discriminate between better, comparable, worse or activity cliffs. As activity measure for comparison, inhibition at 100 µM was used. Only relevant paths are shown for simplicity. Representation inspired by (387).

In the Topliss scheme, the starting point is the comparison between the unsubstituted aromatic ring and a 4-chloro substituted ring. Since the chloro derivative **11a** exhibits stronger inhibition, the green arrow was followed to the 3,4-dichloro compound **13a**, which inhibition did not exceed the one of **11a**. Accordingly, compounds **11b–11d** were investigated, but none of these molecules provided an activity cliff, which was also true for the 2,4-dichloro derivative **13c**. In this case, activity cliff refers to a strong improvement in inhibition of the novel compound compared to the preceding one. Following the Topliss scheme, the next step would be evaluating the 4-nitro derivative, which has not been sythesised so far. Even if it does not follow the scheme's suggestion taking the path from **13a** to **13b** resulted in an inhibition of 86%. Here, the next step would lead to a 4-nitro-3-trifluoromethyl substitution pattern, which was also not synthesised yet.

Once comparing the inhibition of later compounds in this scheme to the chloro-derivative **11a,** it becomes evident that further improvement was not achieved. The limitation of the scheme is revealed when regarding the paths taken from compound **13a**. The path proposed by the scheme led to compounds **11b–d** with comparable or lower affinities towards DNMT2, while following the "wrong" path to **13b** led to a compound with a strong inhibition at 100 µM, comparable to the one of **11a**.

The nitro compounds ending the workflow might lead to enhanced inhibition. However, from an electronic point of view this is not likely, since the nitro group acts in a similar fashion (electron withdrawing) as the trifluoromethyl group, which did not display a significant advance in inhibition. Nevertheless, the exceptional characteristics of nitro groups could result in higher affinities towards DNMT2. Though it is worth mentioning that especially nitro-substituted aromatic rings should be considered with caution in drug design, since nitro groups along with their metabolites exhibit multiple unwanted properties (388).

3.2.2 Aromatic DNMT2 inhibitors with sulphonamide linkers

To broaden the understanding of arylic, Y-shaped SAM analogues, sulphonamides were tested as alternative linkers between SAM scaffold and aromatic ring. As methylene groups, the sulphur atom of sulphonamides is sp^3 hybridised (389), but considerably larger containing different and more pronounced partial charges (390) (Figure 18A). Furthermore, sulphonamides possess electron withdrawing properties by mesomeric and inductive effects (391–394). While resonance formulas with C-S and S-N double bonds are possible (Figure 18B), the π-character of both C-S (390, 395, 396) and S-N (395, 397) bonds seems to be rather low. Especially in the case of S-N bonds, the π-character depends on the electronic surroundings of the corresponding sulphonamides, i.e. electron withdrawing residues at the sulphur atom lead to a more profound π-proportion in the bonding (398, 399). This results in a relatively free rotation around the respective bonds (395, 399). The additional electron withdrawing effect of this group is of interest, since electron deficient aromatic ring systems can act as warheads and thus, they can be exploited for the design of potential covalent inhibitors (400–404).
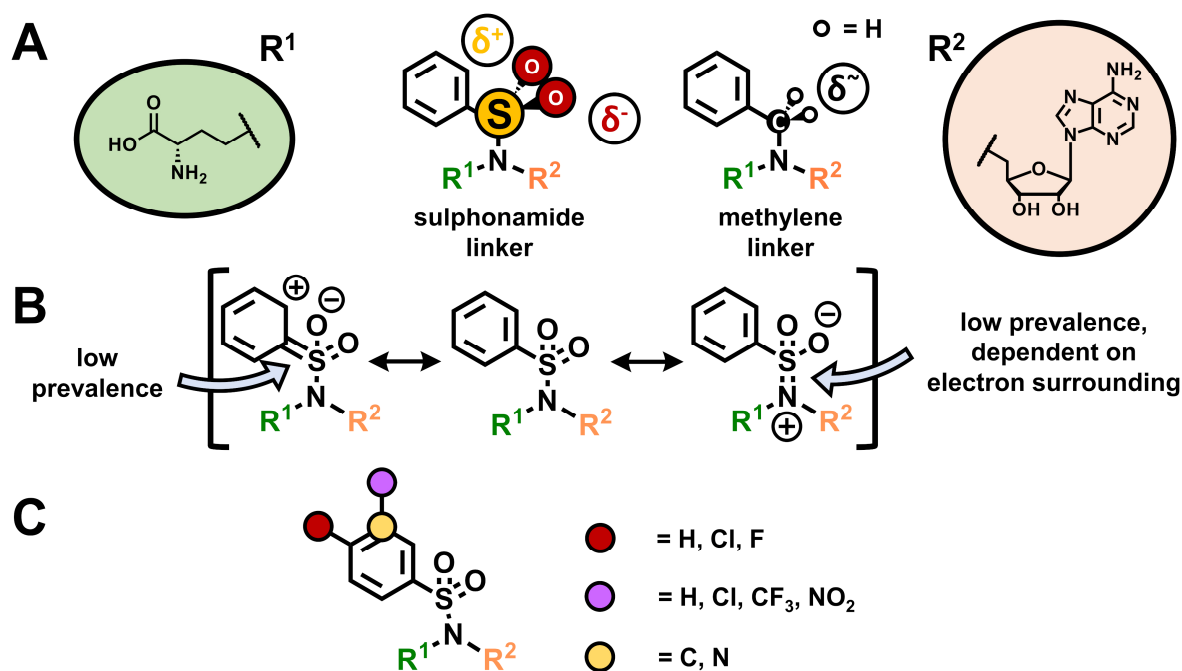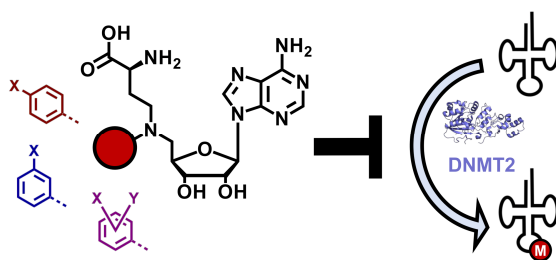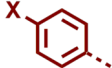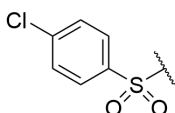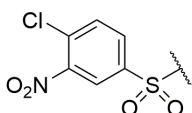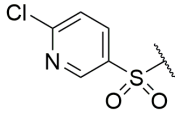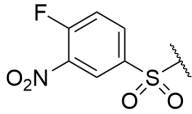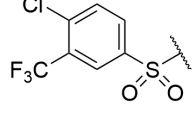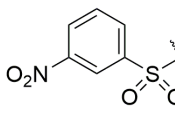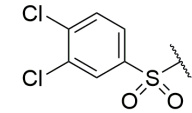
Figure 18. Sulphonamide properties. A) Different size and partial charges (δ) of sulphonamides compared to methylene groups. δ˜ refers to no significant partial charge difference. B) Possible resonance formulas for aromatic sulphonamides. C) Design strategy for sulphonamide derivatives.

In this regard, a third set of compounds was designed bearing aromatic rings as tertiary residues at the 5' amino group, this time connected via a sulphonamide linker. Additionally, several electron withdrawing groups were attached to the ring, namely 4-fluoro, 3-nitro, 3-trifluoromethyl as well as 3- and 4-chloro residues. As an alternate electron poor system, a central pyridyl ring was examined (Figure 18C). This compound series further enabled direct comparisons between benzyl and sulphonamide derivatives. Most compounds were designed by ▮▮▮▮▮▮▮▮ and synthesised by ▮▮▮▮▮▮▮ and ▮▮▮▮▮ in the course of his master thesis, supervised by ▮▮▮▮▮▮. Inhibitory evaluation was conducted using the tritium incorporation assay at a concentration of 100 μM and results of these experiments are displayed in Table 6.

Table 6. Overview of sulphonamide DNMT2 inhibitors. DNMT2 inhibition of sulphonamide compounds at 100 µM as determined by the tritium incorporation assay. Inhibition is displayed as mean values ± standard deviation of three independent measurements. Figure schematically depicts inhibition of DNMT2 by the various investigated compounds. Protein structure was created with PyMOL (121) and PDB: 1G55 (117).

Compound	Inhibition at 100 µM [%]	Compound	Inhibition at 100 µM [%]
	4-substitution		**3,4-disubstitution**
14a	n.i.	**16a**	100 ± 6.7
14b	33.2 ± 1.9	**16b**	n.i.
	3-substitution	**16c**	54.3 ± 3.7
15	n.i.	**16d**	27.8 ± 17.0

Sulphonamide derivative **14a** with a 4-chloro residue did not inhibit DNMT2, whereas exchange of the phenyl to a pyridyl ring led to compound **14b** displaying weak inhibition of 33% at 100 µM. For the third monosubstituted molecule, the 3-nitroderivative **15**, no significant inhibition at a concentration of 100 µM was determined.

Combination of structures **14a** and **15** led to compound **16a** displaying quantitative inhibition. The exchange of its 4-chloro to a 4-fluoro residue (**16b**) however abolished the inhibition completely. Keeping the 4-chloro residue constant and exchanging the 3-nitro group to either trifluoromethyl- or chloro-moieties resulted in **16c** and **16d** inhibiting DNMT2 by 54% and 28% at 100 µM. Due to the high inhibition displayed at 100 µM, the IC_{50} value of **16a** was determined to be 6.3 ± 0.8 µM, the dose-response-curve for IC_{50} determination is presented in Figure 19.

The IC_{50} value of **16a** is comparable to IC_{50} values of SAH, SFG and **9c** (around 15 µM). However, it should be stated that the dose-response curve can be enhanced when considering multiple lower concentrations.
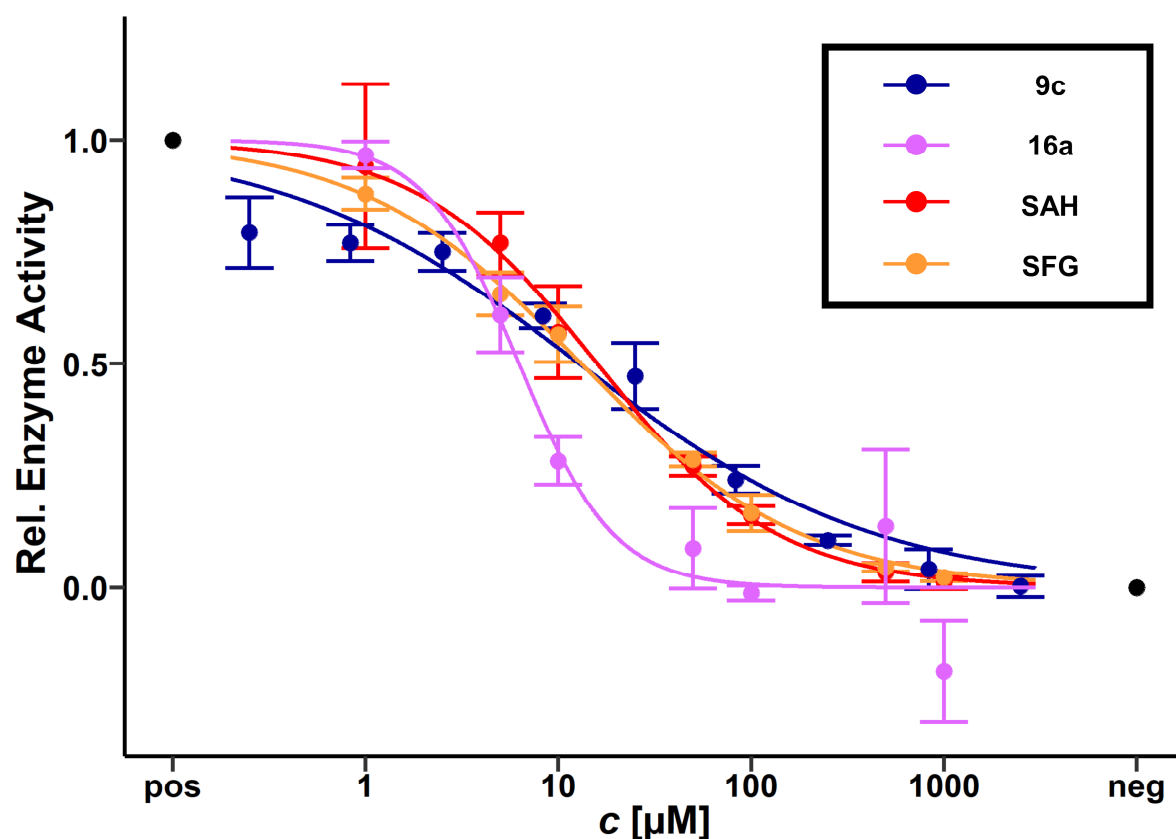
Figure 19. Dose-response curves II. Dose-response curve of **16a** in comparison with **9c**, **SAH** and **SFG** for IC$_{50}$ calculation as determined by the tritium incorporation assay. "pos" refers to control experiments conducted in the absence of inhibitors and "neg" refers to experiments conducted in the absence of inhibitor and tRNA^{Asp}. Displayed are mean values and standard deviations of experimental triplicates.

Comparing the corresponding pairs of **14a** and **11a**, **16d** and **13a** as well as **16c** and **13b** only differing in their linking moieties (Figure 20A) reveals a clear preference for benzylic linkers (Figure 20B). This might be attributed to the different sizes, partial charges and the slightly impeded turnability of the sulphonamide compared to the methylene group as described above and depicted in Figure 19A.

Figure 20B demonstrates that the inhibition of investigated benzylic compounds is comparable, while inhibition of sulphonamide derivatives strongly depends on their substitution pattern. One difference between the substituents is their ability to withdraw electrons from the ring. If only one chloro residue is present on the molecule at the 4-position (**14a**), no significant inhibition is detected. Adding an additional chlorine atom as a mild electron withdrawing group at the 3-position (as in **16d**) lead to minor inhibition (28%), whereas compound **16c** bearing the stronger electron withdrawing trifluoromethyl moiety displayed moderate inhibition of 54%. A complete inhibition at a concentration of 100 µM was achieved with **16a** including the strong electron withdrawing nitro group.
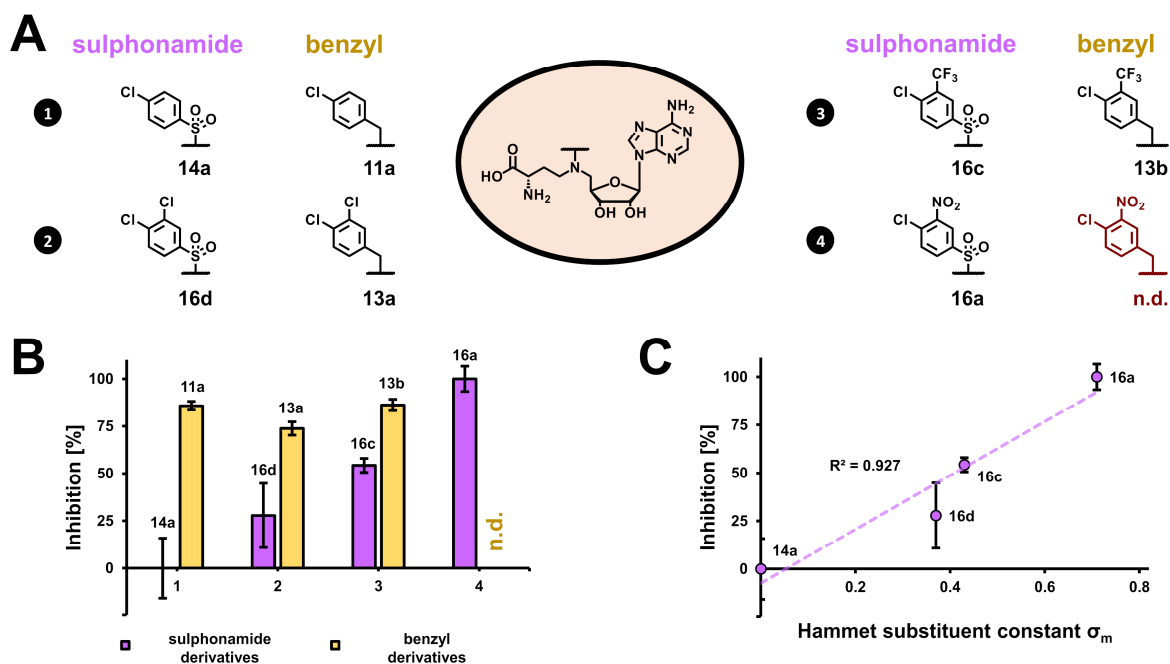
Figure 20. Arylic inhibitors. A) Investigated compound pairs differing only in their respective linker moieties. B) Inhibition at 100 µM of various compounds with aromatic residues as determined by the tritium incorporation assay. Displayed are mean values and standard deviations of experimental triplicates. C) Inhibition at 100 µM as determined by the tritium incorporation assay plotted against Hammet substituent constants σ_m. σ_m is calculated from pK_a values of corresponding substituted benzoic acids in aqueous solution. Displayed are mean values and standard deviations of experimental triplicates. n.d. = not determined.

Comparing inhibition of these compounds with the ability of their respective residues to withdraw electrons at the 3-position reveals a correlation between higher inhibition and stronger electron withdrawing capabilities, as can be seen in Figure 20C. To quantify the electron withdrawing capabilities, the Hammet substituent constant σ_m was chosen, which is calculated from pK_a values of the corresponding substituted benzoic acids in aqueous solution (392). This phenomenon becomes even more evident when comparing compounds **14a** and **14b**, both having a chlorine residue at the 4-position but differing in their ring architecture, with only the electron inferior derivative **14b** displaying inhibition, albeit a weak one.

The assessment of **16a** and **16b**, similar molecules with only the 4-position of the aromatic ring being exchanged from a chloro to a fluoro residue, further supports the above proposed importance of a 4-chloro moiety. Here, the chloro derivative **16a** displays 100% inhibition at 100 µM, while the fluoro molecule **16b** does not exhibit any significant inhibition. This comparison also suggests that the 3-nitrogroup mainly exerts its effect due to its electron withdrawing effect instead of direct interactions with the enzyme.

The preceding considerations hint that the higher activity of **16a** is plausibly based on the electron-deficient aromatic ring carrying two residues with negative mesomeric (−M) effects (nitro- and sulphonamide-groups). The 4-chloro residue exhibits an additional electron pulling activity but appears to exert its main impact through direct interaction with the enzyme. Since the substituents differ in several other variables than their electron pulling capabilities, more data needs to be gathered for a definite statement.

3.2.3   Time-dependent enzyme inhibition

To further investigate the influence of the electron-deficient aromatic rings on the interaction between small molecules and enzyme, inhibition of compounds at certain concentrations was investigated with varying preincubation times of compound and enzyme. SAH, SFG and compounds **8b** and **16a** were either subjected directly to the enzymatic reaction or preincubated with DNMT2 for 75 minutes before initiating the enzymatic reaction. As can be seen in Figure 21A, SAH, SFG and **8b** do not inhibit DNMT2 in a time-dependent manner, but the inhibition of derivative **16a** displayed time-dependent behaviour. Of all investigated compounds only **16a** displays time-dependency. This might be attributed to the electron-deficient aromatic ring, but other reasons cannot be ruled out.
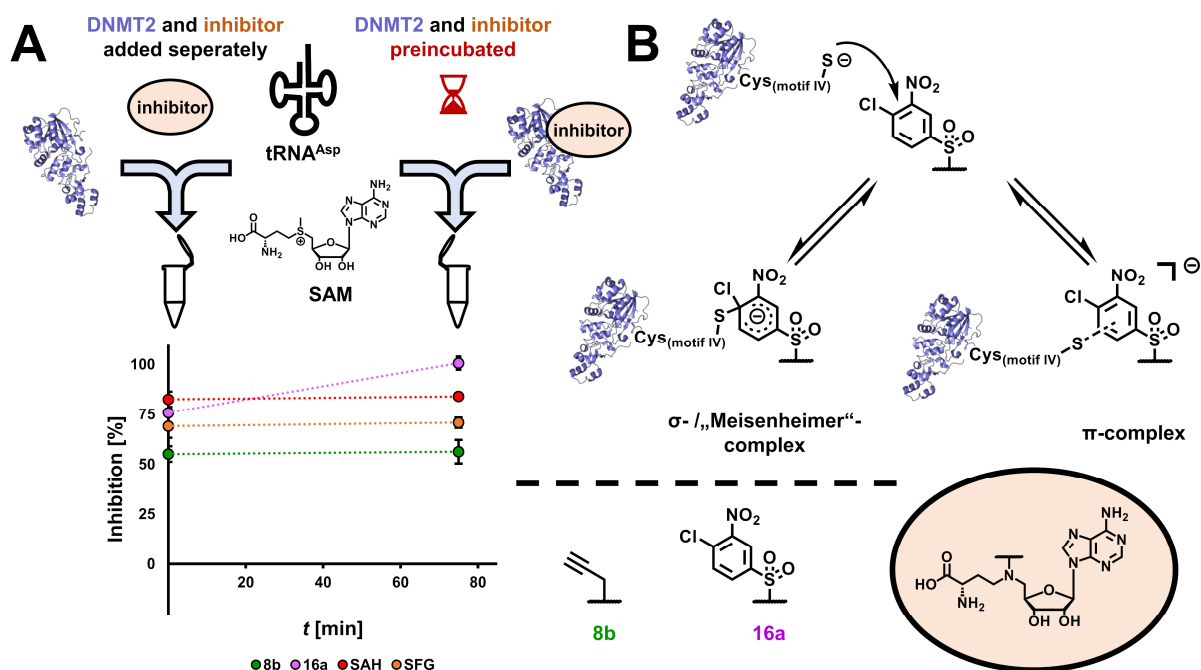
Figure 21. Time-dependent inhibition. A) Inhibition at 100 µM of SAH, SFG and **8b** or at 5 µM of **16a** in dependency of preincubation time of DNMT2 and compound as determined by the tritium incorporation assay. Displayed are mean values and standard deviations of experimental triplicates. B) Possible interactions of DNMT2's catalytic cysteine with the electron-deficient aromatic ring of **16a**. Protein structures were created with PyMOL (121) and PDB: 1G55 (117).

It remains unclear whether the observed time-dependency is based on a slow, tight, or irreversible binding. However, from a mechanistical point of view an irreversible covalent bond formation is unlikely in case of a nucleophilic aromatic substitution (S_NAr) reaction. In this case, the highest reactivity would be expected with a fluorine atom present, but this could not be confirmed as derivative **16b** did not exhibit any inhibition towards DNMT2 (Table 6) (405). Due to the close proximity of the catalytic cysteine to the SAM binding site, it is possible that the aromatic moiety of the inhibitor interacts with the cysteine. This can happen either by the formation of σ- (Meisenheimer) or π-complexes (Figure 21B), which is also discussed for protease inhibitors (406). To clarify the binding mechanism additional experimental data is required.

3.2.4   RNA competition

Another possible explanation for the comparably strong inhibition of compound **16a** is its voluminous aromatic residue. According to the anticipated binding mode (*vide supra,* Figure 16) this residue should intrude inside the binding site of the cytosine base and possibly competing with the RNA substrate. To elucidate a potential competition, the tritium incorporation assay was conducted in the presence of inhibitors SFG, SAH, **8b**, **8c**, **11a** and **16a** with varying concentrations of tRNA (Figure 22A).
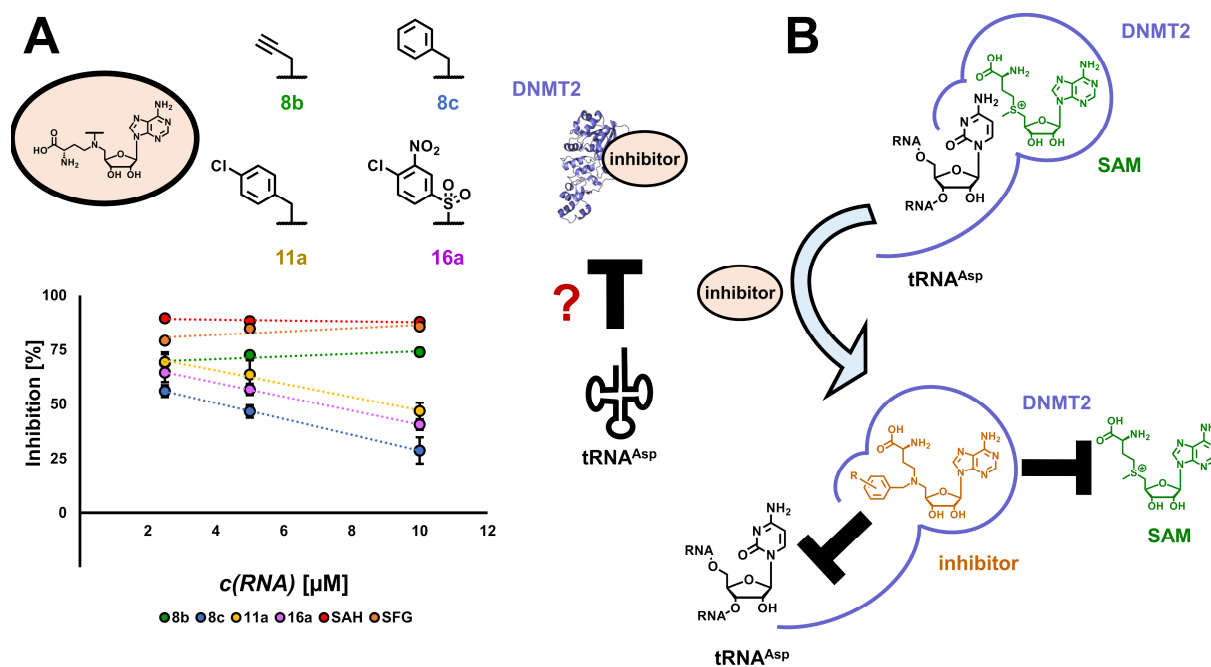
Figure 22. RNA competition. A) Inhibition of DNMT2 at 100 µM (**8b**, **8c**, **11a**, SAH, SFG) or 2.5 µM (**16a**) in dependency of various RNA concentrations as determined with the tritium incorporation assay. Displayed are mean values and standard deviations of experimental triplicates. B) Possible mechanism of action for arylic compounds competing with RNA as well as SAM. Protein structure was created with PyMOL (121) and PDB: 1G55 (117).

While the inhibition of SAH, SFG and compound **8b** was independent of the RNA concentration, all three aromatic derivatives **8c**, **11a** and **16a** displayed less inhibition with elevated concentrations of RNA indeed emphasising competition between inhibitors and RNA. As can be seen in Figure 22A, the dependency of inhibition and RNA concentration for these three compounds is linear. Applying a linear fit to the data reveals similar values for the corresponding slopes of 32, 36 and 31 nM^{-1} for **8c**, **11a** and **16a** respectively. Thus, no different competition potencies between the investigated substitution patterns and linker moieties seems to occur. Since the RNA competition was detected for all investigated aromatic compounds regardless of their substitution pattern and linkers, it is plausible that the aromatic ring alone is sufficient for the competition.

While the results described above reveal RNA competition for the compounds bearing aromatic side chains, **8b** was shown to compete for the SAM binding site using ITC (as described above). Considering the close structural resemblance of the aromatic derivatives to **8b** and SAM, a bisubstrate mechanism for the aromatic SAM analogues as depicted in Figure 22B is possible, although SAM competition for these kinds of molecules must be confirmed in additional experiments to draw a definite conclusion.

3.3 Summary and Outlook

As described above, inhibitors for DNMT2 based on the SAM scaffold have been developed and investigated using a tritium incorporation activity assay together with the biophysical methods MST and ITC (conducted by ████████████████). In a first set of compounds (**1–9**), synthesised by ██████ ████████████████████████████████, a so-called Y-shape of the amino acid side chain was revealed to be crucial for inhibition. Especially unsaturated residues, like benzyl or propargyl moieties, proved themselves as useful for the design of DNMT2 inhibitors. Furthermore, ITC measurements conducted by ████████████████ validated competition between synthetic analogue **8b** and SAH for the same binding site (Figure 15), while docking studies by Dr. ████████████ backed and complemented the experimental findings (Figure 16).

In compound series two (**10–13**) and three (**14–16**), synthesised by ████████████████████████ ████████████, molecules with arylic rings were evaluated, which were linked to the SAM scaffold either by methylene- or sulphonamide-groups. For benzylic derivatives, particularly a 4-chloro substitution demonstrated promising inhibition. Inhibition by sulphonamide derivatives was found to correlate with the ability of substituents to withdraw electrons from the aromatic ring (Figure 20) proposing a possible explanation for the time-dependent inhibition of compound **16a** (Figure 21). All investigated arylic compounds competed with the substrate tRNA hinting to a bisubstrate mechanism (Figure 22).

Two of the synthetic compounds were capable of inhibiting DNMT2 with comparable potency as the natural products SAH and SFG. Namely **9c** and **16a** exhibiting IC_{50} values of 13 µM and 6 µM compared to 16 µM and 13 µM of SAH and SFG. In addition, further promising candidates were identified (e.g. **11a–c**, **13a** or **13c**). For a better assessment and a profound statement, determination of their IC_{50} values is crucial. For complementing the data gathered for the aromatic compounds, K_D values using ITC are to be measured in analogy to experiments conducted for the first set of compounds. Furthermore, verifying the screening results for sulphonamide derivatives with MST adds significance to the data.

As already discussed above, screening data gathered with MST and the activity assay correlated well, but discrepancies between the ratios of various K_D and IC_{50} values were observed. Potential causes could be different experimental conditions including the presence of tRNA^{Asp} in the tritium incorporation assay, which is absent in ITC measurements. To further investigate this discrepancy, a good starting point is the reproduction of both values with varying reaction conditions and orthogonal assay methods like MST or SwitchSENSE® (407) for K_D determination or HPLC based activity assays (408), to exclude experimental biases. For the comparison of potential conformational changes of DNMT2 upon tRNA binding, the most detailed insight would be given by the evaluation of crystal structures of the enzyme in the presence or absence of tRNA (374, 409). Since it is not trivial to obtain these (410, 411), potential conformational changes can also be explored with techniques such as circular dichroism (CD) spectroscopy (412), NMR (413) or the use of suitable Förster resonance energy transfer (FRET) pairs (414).

The merging of compounds **6a** and **8b** to **9c** improved the ability to inhibit DNMT2 significantly (Figure 15A). It is thus a viable option to adapt this strategy to different compounds, such as **11a–c**, **13a** or **13c** to check if their potency can be increase as well (Figure 23A). Another interesting perspective

would be testing compound **17a**, a benzylic variant of the most potent inhibitor **16a**, due to the higher overall potency of benzylic linkers. The synthesis of this compound was done by ████████████ ████████, but the final molecule proved unstable and could not be evaluated further. A branched version of this compound, **17b**, as proposed above, might improve its stability (Figure 23B).
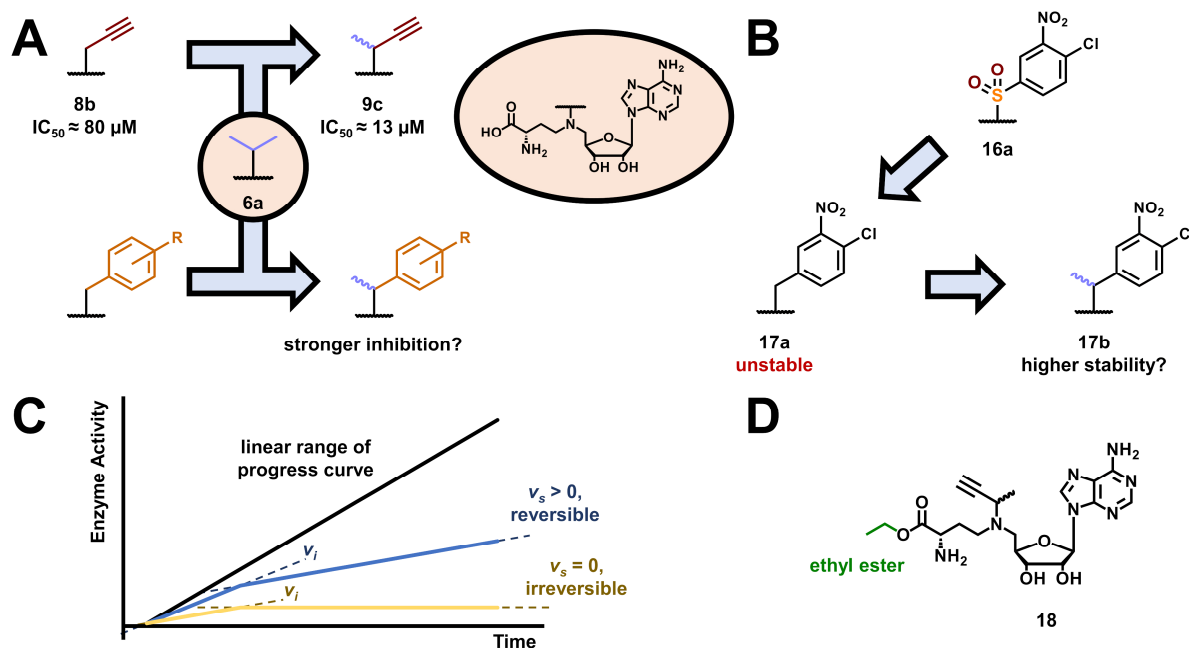
Figure 23. Outlook small molecule inhibitors. A) Applying the merging strategy used for alkyne derivative **8b** and **6a** might lead to benzylic derivatives with stronger potency. B) Due to the higher effectiveness exhibited by benzylic derivatives investigating **17a** is of interest, but the molecule was found to be unstable. Branched compound **17b** might exhibit higher stability due to its additional methyl group. C) Progress curves for time-dependent inhibitors. Initial velocity v_i is followed by steady-state-velocity v_s which equals zero for irreversible inhibition and is greater zero for reversible inhibitors. D) Ethyl ester prodrug **18** as used in cell assays.

To broaden the knowledge of SAR, different linker moieties can be investigated. Especially carboxyamides are of interest, since they can be synthesised easily and possess interesting and differing properties from methylene- or sulphonamide-groups including a profound −M effect as well as a planar sp^2 hybridisation (415). In this regard, derivatisation of the ribose and adenine base in addition to the amino acid side chain will add more detailed information of SAR.

A correlation between inhibition and electron deficiency of the aromatic ring was observed for sulphonamide derivatives (Figure 20) and intriguingly compound **16a** displayed time-dependent inhibition (Figure 21). This opens the question if other compounds such as **14b**, **16c**, **16d** or benzylic derivatives **13a** and **13b** bearing electron poor aromatic rings also display time-dependent inhibition.

Another concern is the reversibility of **16a**. Insights here would give important knowledge for the mechanism of action of the inhibitor. To explore this, dilution or dialysis experiments with preincubated enzyme-inhibitor complexes can be conducted. In the case of irreversible inhibition strong dilution or dialysis should not change the potency of the inhibitor, whereas enzymatic activity is expected to be restored for reversible inhibitors (416–418). Further hints for the characterisation of the complex can be collected using protein MS (419–422) or by investigating a potential biphasic behaviour of the progression curve of the enzymatic reaction. Here, two velocities appear due to the slow enzyme-

inhibitor-complex formation: an initial velocity (v_i) and a steady-state velocity (v_s). V_i is present before the equilibrium of enzyme-inhibitor-complex formation is reached and v_s after the equilibrium is reached. In the case of an irreversible inhibitor $v_s = 0$, while for reversible inhibition $v_s > 0$ (Figure 23C) (365, 419, 423). Understanding the detailed mechanism of action of the time-dependent inhibition would allow a better characterisation of the compounds using K_i values, since IC_{50} values hold only limited significance in this case (365).

One additional important observation which can give a more detailed understanding of the mechanism of action is the competition of arylic compounds and RNA. This hints for a bisubstrate mechanism, but to confirm this, competition experiments with SAH or SAM need to be conducted. While further docking studies will provide an additional layer of information, a co-crystal structure of inhibitor and DNMT2 would be well-suited to offer a definite answer along with providing a template for a more rational approach for drug design.

Two further concerns are the potency of the designed compounds in a biological context, with *in cellulo* activity as the next logical step, as well as their selectivity towards other enzymes, especially different MTases.

First cellular experiments were conducted by ▆▆▆▆▆▆▆▆ in cooperation with the ▆▆▆ group, DKFZ Heidelberg, but only minor effects contributed to the inhibitors have been investigated so far, even if an ester prodrug **18** of compound **9c** was used (data not shown, Figure 23D). Optimisation of the cell-assay procedure along with confirming cell permeability of the highly polar molecules is important for further successful experiments.

As described above, selectivity of selected compounds was observed for the m5C RNA MTases NSUN2 and NSUN6, but not for other investigated MTases (DNMT3A-3L, G9a). Due to the close structural resemblance of the compounds with the natural cofactor SAM and the high homology of SAM binding sites for multiple MTases (208), profound selectivity is not expected for most other SAM-dependent MTases. Developing selectivity along multiple MTases is not trivial but can be achieved as described in literature (220, 292, 424, 425).

Due to the ubiquitous biological appearance of SAM as well as its poor pharmacological properties, both, weak cellular effects as well as poor selectivity, can at least partly be attributed to the SAM substructure of the compounds. While biologically active and selective SAM derivatives were developed (424), further research should also consider the identification of novel scaffolds for potential DNMT2 inhibitors. This might pose a challenge, not least because of the low throughput of the activity assay making larger screening approaches less feasible. The workflow can be accelerated by applying MST as a primary screening method, especially since high correlations between activity and MST screenings were observed. Even higher throughputs can be achieved when using plate-based assays. Binding assays in this case might be based on fluorescent SAH derivatives (426, 427) using fluorescence polarisation (428, 429) or quenching (430–432) assays, currently developed by ▆▆▆▆▆▆▆▆, while activity assays may apply specific techniques such as homogenous time-resolved fluorescence (HTRF) (433, 434) or enzymatic conversion of the reaction byproduct SAH (*vide supra*) (221, 223, 225).

In silico methods, such as virtual screenings, can also be used for the prediction and identification of novel scaffolds (435–437). This technique was applied by Dr. ▆▆▆▆▆▆▆▆ and together with ▆▆▆▆ ▆▆▆▆▆▆▆ compounds were identified binding DNMT2 depending on their concentration, albeit none

of these compounds was able to inhibit DNMT2 at a concentration of 100 μM (data not shown). Nevertheless, applying comparable strategies together with the knowledge gained from the above described and future SAR studies is crucial for the development of next-generation inhibitors for DNMT2, potentially exhibiting higher selectivity and biological activity.

3.4 Development of RNA aptamers as inhibitors for DNMT2

The enzymatic function of DNMT2 can not only be modulated by small molecules, but also by directly addressing its RNA binding site e.g., with aptamers. These short and single stranded nucleic acids exhibit high specificity and affinity towards their respective targets, rendering them as promising enzyme inhibitors (346).

In the following section, the development of an DNMT2 inhibiting RNA aptamer is described. This includes the generation of the aptamer via SELEX (conducted by the group of Professor ████, university of Bonn), sequencing of the final SELEX pool (conducted by ██████████ and ██████ ████████, Biopôle Nancy), as well as selection of promising aptamer sequences via bioinformatic methods. The most encouraging sequences were investigated regarding their inhibition efficiency in enzyme activity assays and a first attempt of aptamer truncation was carried out.

3.4.1   SELEX procedure

To generate RNA aptamers against DNMT2, an automated SELEX process was conducted by the group of Professor ██████, university of Bonn (438).

The initial library used for the enrichment procedure consisted of a section of 40 random nucleotides flanked by two constant primer binding regions. In total, two selections were performed, one under standard conditions and one in the presence of heparin (80 ng μL^{-1}). Due to its polyanionic structure (Figure 24A), heparin acts as an unspecific inhibitor for RNA-protein interactions and therefore might influence the outcome of the selection process (439, 440).

For both selections, the randomised starting library was subjected to a total of 12 rounds of SELEX. Agarose gel analysis of PCR products after each round indicated a successful enrichment (Figure 24B) alongside further evidence for an interaction between selected RNA of rounds 1, 6 and 12 with DNMT2 provided by a filter retention assay (Figure 24C, both experiments were conducted by the group of Professor ██████, university of Bonn). In this assay, various amounts of DNMT2 are incubated with ^{32}P-labelled RNA and sucked through a filter. While unbound RNA passes through the filter, the RNA-enzyme complex is retained and can be quantified according to ^{32}P-induced radioactivity.

The potential of the generated RNA pools to inhibit DNMT2 activity was validated with IVT synthesised RNA from the final round of SELEX for both selections. The enzymatic activity was reduced around 50% by both RNA pools at a concentration of 370 ng μL^{-1} using 3 μM substrate tRNA^{Asp} (Figure 24D).

The results presented above demonstrate that the SELEX procedure for DNMT2 yielded enriched RNA pools that are capable of binding the enzyme and further have the potential to modulate its activity. The outcomes of binding as well as inhibition assays are comparable for RNA evolved in the presence or absence of heparin indicating a similar selection profile.
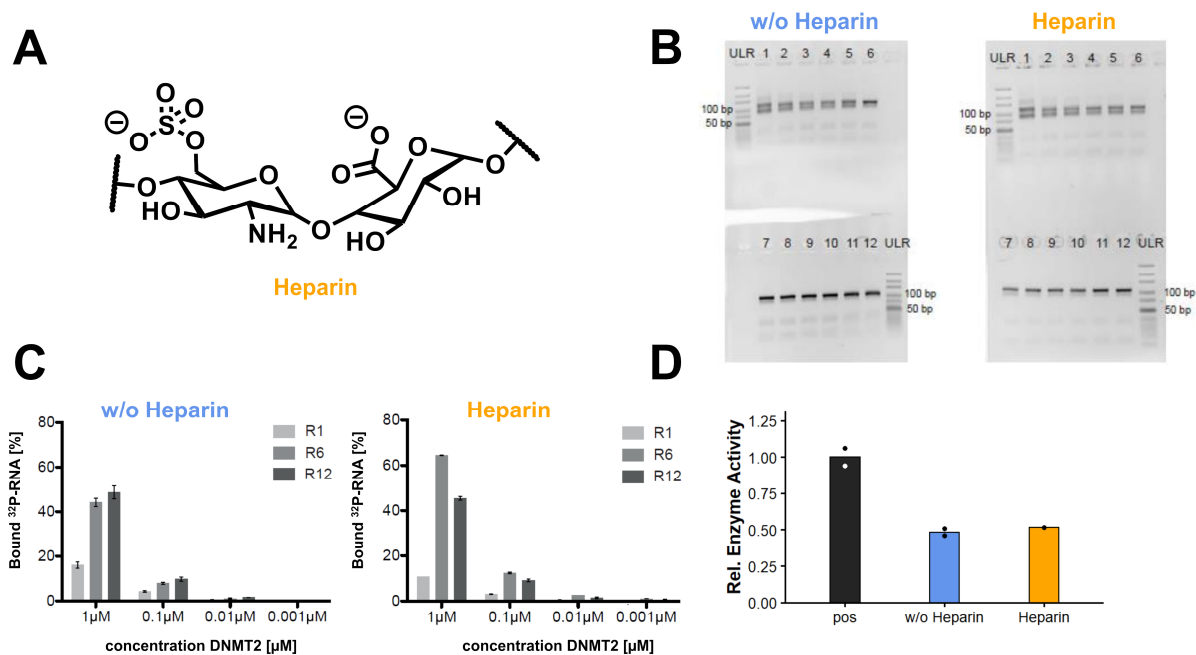
Figure 24. Outcome aptamer selection. A) Molecular structure of heparin. B) Agarose gel picture of PCR products obtained by the SELEX procedure. Numbers refer to selection round, ULR = ultra low range DNA ladder. Experiments conducted by the research group of Professor ▮▮▮▮, Bonn. C) Results of filter retention assays for selections in the absence or presence of heparin for SELEX rounds 1, 6, and 12. Displayed are mean values and standard deviations of experimental triplicates. Experiments conducted by the research group of Professor ▮▮▮▮, Bonn. D) Relative enzyme activity as determined by the tritium incorporation assay in the presence of complete RNA pools of SELEX round 12 (370 ng µL^{-1}) using 3 µM tRNA^{Asp}. Bar diagrams of experiments "pos" and "w/o Heparin" refer to average values of experimental duplicates.

3.4.2 Sequencing of RNA pools

To determine the exact composition of the selected RNAs, the PCR products of the 12th cycles were analysed by next generation sequencing (NGS). The sequencing library was prepared by one-step elongation PCR, implementing all sequences required for NGS in a single step. The sequencing runs were conducted by ▮▮▮▮▮▮ and ▮▮▮▮▮▮▮▮, Biopôle Nancy (441, 442).

Quantification of unique sequences using the FastAptamer (443) software revealed two highly enriched sequences which were identical in the two different enrichment experiments. The most abundant sequence was present in 72% of SELEX round 12 without heparin addition and in 75% of SELEX round 12 with heparin addition, whereas the second most frequent sequence accounted for 5% and 3%, respectively.
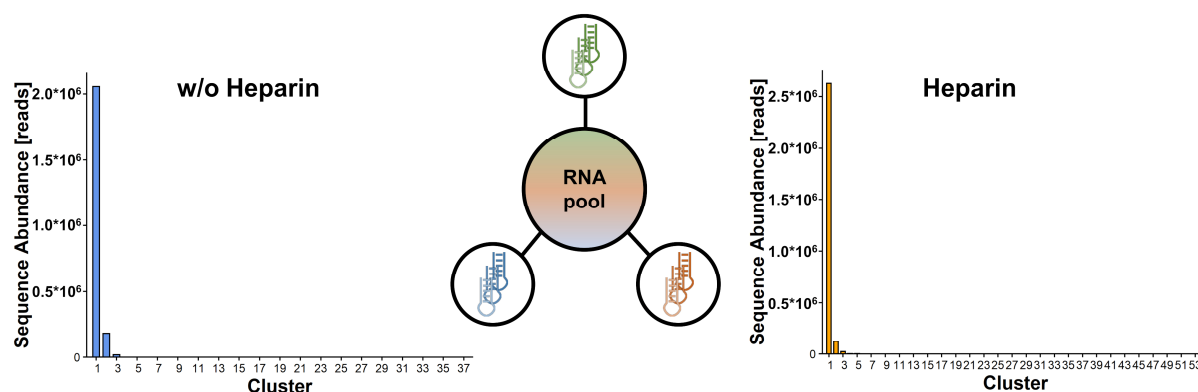
Figure 25. Cluster analysis. Sequence abundance of each cluster. Analysed were the 12th rounds of SELEX conducted in the absence and presence of heparin using FastAptamer (443) with a Levenshtein distance of 4.

For a more detailed comprehension of the pool anatomy, sequences with a Levenshtein distance (444) up to 4 were clustered (Figure 25). Cluster 1, containing the most enriched sequence, accounted for more than 90% in both SELEX pools, while cluster 2 amounted to 8% and 4% in RNA obtained without and with heparin addition. Thus, the two most abundant sequences with their corresponding clusters made up 98% or 99% of the complete pools. In all cases, the third most abundant cluster corresponded to the same representative sequence and added up to $8*10^{-1}$%. In contrast, following clusters differed in their representative sequences between both selections and further were only present in traces below $5*10^{-2}$%. An overview of the distribution for the four most abundant clusters and their representative sequences is given in Table 7.

Table 7. Aptamer sequence distribution. Overview of the distribution for the four most abundant clusters and their representative sequences for selections in the absence and presence of heparin as identified by the NGS cluster analysis using FastAptamer (443).

Cluster	w/o heparin		heparin	
	Representative sequence abundance [%]	Cluster abundance [%]	Representative sequence abundance [%]	Cluster abundance [%]
1	72	91	75	94
2	6	8	3	4
3	$6*10^{-1}$	$8*10^{-1}$	$4*10^{-1}$	$8*10^{-1}$
4	$8*10^{-3}$	$1*10^{-2}$	$4*10^{-2}$	$4*10^{-2}$

Analysis of the sequencing data revealed similar sequence distributions in both selection pools, which, combined with the similar behaviour in the *in vitro* assays (Figure 24B, C, D), points out that heparin had no major effect on the pool distribution and behaviour of SELEX round 12.

The high enrichment of two sequences, particularly one, during the SELEX process is unusual and a broader distribution of multiple sequences and clusters was expected (341, 445). A possible explanation would be high affinities of the selected sequences towards DNMT2, replacing other competing sequences during the selection. Moreover, the DNA and RNA polymerases used during the SELEX procedure tend to have preferences for specific substrates, which possibly has a substantial influence on the outcome. A higher preference of the DNA polymerase towards specific sequences would also lead to a bias during the PCR based library preparation for NGS sequencing. To further understand the exact mechanisms behind this strong enrichment, DNA pools of other SELEX rounds may be sequenced. This would enable precise tracking of certain sequences over the SELEX process providing a better understanding how different sequences evolve during the selection.

3.4.3 Multiple sequence alignment

To identify conserved nucleotide positions among the evolved sequences, a multiple sequence alignment (MSA) was carried out using Jalview (446). Due to the high similarity between the sequence distributions, no difference among the two pools was expected and thus, MSA was only done for the selection conducted in the absence of heparin.

If all sequences were taken into account for the MSA, the large quantity of similar sequences present in the pool would lead to a generally high conservation. This could lead to an overrepresentation of certain positions. In addition, the high amount of input sequences prevented the MSA from running, why low abundant sequences had to be discarded. However, if only unique sequences were considered regardless of their abundance, the alignment might be biased since in this case low frequency-sequences affect the results as much as highly enriched ones.

MSA was run in both instances to check if substantial differences occur. Regardless of aligning all or only unique sequences, the fixed primer binding regions showed a conservation of around 100% (Figure 26). The overall sequence conservation of the MSA with all sequences was very high (around 90%, Figure 26A), while it was about 75% if only unique sequences were investigated regardless of their abundance (Figure 26B). Remarkably, both alignments identified the same eight positions in the variable region with a conservation of around 100%, suggesting that both methods are valid options.

Being conserved nearly 100%, these eight nucleotides are likely to play crucial roles in the interaction between the RNA with DNMT2, thus giving a valuable insight in the structure-activity relationship of the aptamer, which can be exploited for the generation of truncated RNA sequences (*vide infra*). The primer binding sites are identical in all sequences, which means that no nucleotides can be identified as important for binding in these regions using MSA.
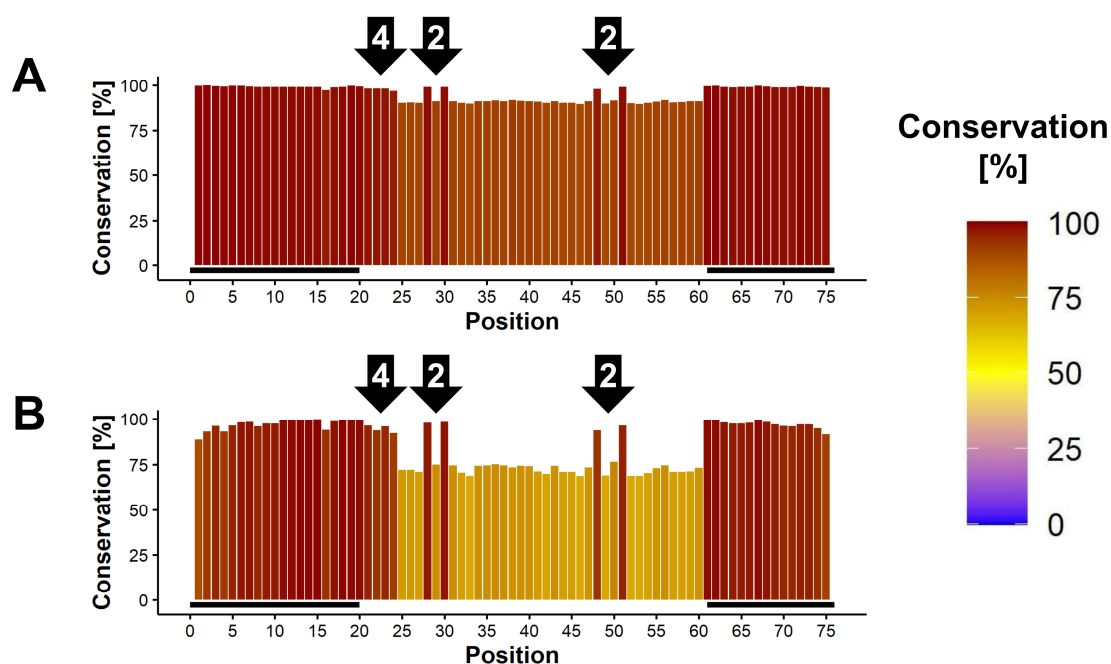
Figure 26. Multiple Sequence Alignment. A) MSA considering all sequences. B) MSA considering only unique sequences regardless of their abundance. Black bars indicate constant primer binding regions on the template. Black arrows display the eight conserved positions with the digits inside specifying the numbers of nucleotides which are referred to. The MSA was conducted using Jalview (446).

3.4.4 Inhibition analysis of the aptamers

After the *in silico* analysis of the two 12th SELEX rounds, the properties of the sequences were to be determined in *in vitro* experiments. Therefore, the representative sequences of the four most abundant clusters were chosen as an initial starting point. While there was no difference for the first three representative sequences, the fourth representative sequence differed between the pools enriched in the presence and absence of heparin. The fourth most abundant sequence constituted to a greater percentage in the RNA pool selected with heparin, which was around one magnitude higher ($4*10^{-2}$% vs. $8*10^{-3}$%, see Table 7), hence the sequence was chosen from this pool. The allocation of the representative sequences and their respective abundance can be found in Table 8.

Table 8. Aptamer sequence abundance. Overview of the sequences used for *in vitro* experiments.

Aptamer name	w/o heparin		heparin	
	Cluster	Sequence Abundance [%]	Cluster	Sequence Abundance [%]
A1	1	72	1	75
A2	2	6	2	3
A3	3	$6*10^{-1}$	3	$5*10^{-1}$
A4	7	$6*10^{-3}$	4	$4*10^{-2}$

RNAs were synthesised using IVT and purified via PAGE excision. In a first experiment the potential of the aptamers to act as substrates for DNMT2 instead of tRNA^{Asp} was determined at a concentration of 50 µM using the tritium incorporation assay. Enzyme activity could not be measured for any of the synthetic aptamers, implying that they cannot function as substrates (Figure 27A).
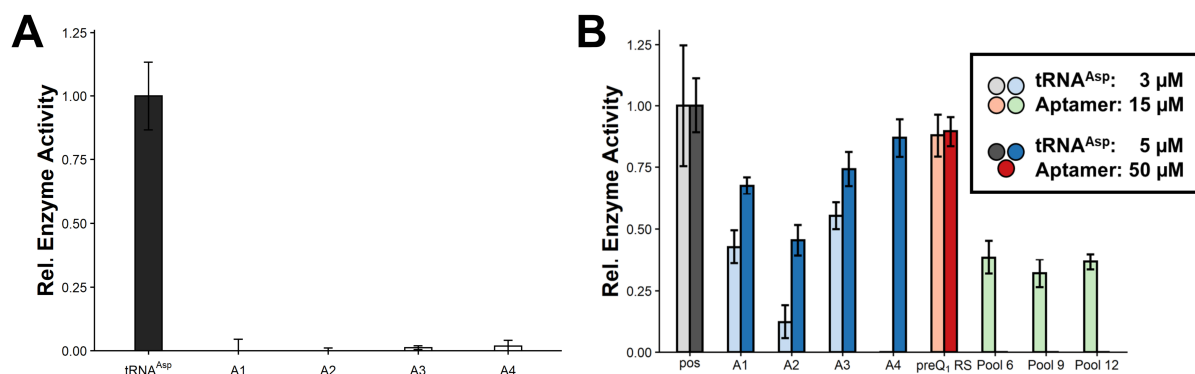
Figure 27. Aptamer *in vitro* evaluation. A) Relative enzyme activity as determined by the tritium incorporation assay in the presence of either tRNA^{Asp} (5 µM) or A1–4 (50 µM). Displayed are mean values and standard deviations of experimental triplicates. B) Relative enzyme activity as determined by the tritium incorporation assay either using 5 µM substrate tRNA^{Asp} with addition of 50 µM aptamer RNA (dark colours) or using 3 µM tRNA^{Asp} with addition of 15 µM aptamer RNA (bright colours). Displayed are mean values and standard deviations of experimental triplicates.

Next, the ability of the aptamers to reduce DNMT2 activity was investigated by adding 50 µM of the corresponding aptamer to enzyme reactions carried out in the presence 5 µM substrate tRNA^{Asp}. The aptamer domain of the preQ$_1$ riboswitch of *B. subtilis* (447) was used to investigate the effect of a non-specific RNA on the enzymatic activity of DNMT2.

With this assay setup, A1, the most abundant sequence in the pool, inhibited the enzyme activity around 33%, A2 displayed an inhibition of roughly 55%, whereas A3 reduced the relative enzyme activity about 26%. A4 however, only inhibited DNMT2 activity by 13%, which is comparable to the unspecific inhibition of the preQ$_1$ riboswitch, indicating that A4 interacts only non-specifically with the enzyme (Figure 27B, dark colours).

The inhibition was weaker than expected under these conditions, which is possibly caused by the high concentration of 5 µM of substrate tRNA^{Asp} in the assay, as it presumably competes with the aptamers. Another possible explanation for the comparably weak inhibition is that highly effective sequences were not identified with the bioinformatic analysis due to their low prevalence in the pool.

To lessen a possible competition between substrate and inhibitory RNA, the concentration of tRNA^{Asp} was reduced to 3 µM while the concentration of the aptamers was decreased to 15 µM in the activity assay. Furthermore, A4 was excluded from the experiment due to its weak inhibition, which did not exceed the unspecific one of the preQ$_1$ riboswitch. Additionally, IVT synthesised RNA of SELEX pools 6, 9 and 12 was analysed at a concentration of 420 ng µL^{-1} (~15 µM, exact molecular weight unknown) to determine how the inhibition of the defined sequences compare to the inhibition of complete RNA pools. With this comparison the ability of the *in silico* analysis to identify potent RNA sequences can be ensured.

As depicted in Figure 27B (bright colours), the trends for aptamer inhibition remained the same with lower RNA concentrations. A1 and A2 inhibited DNMT2 by 57% and 88% respectively, A3 decreased DNMT2 activity around 45%, while the inhibition of the preQ$_1$ riboswitch (12%) was comparable as in the previous experiment. The complete RNA pools of SELEX cycles 6, 9 and 12 reduced the enzyme's activity around 60 to 70% under these conditions.

Inhibition by A1 is in the range of the inhibition by cycle 12 RNA, which could be expected, since A1 makes up over 70% of this pool, its closely related sequences (see cluster 1) even over 90%. A2 exhibited stronger inhibition than the complete pool, demonstrating that the bioinformatic analysis was able to pinpoint one aptamer that was more potent than the complete pool. Naturally, further, more powerful aptamers might not have been identified by the *in silico* pipeline due to their low prevalence in the complete pool.

A stronger inhibition was observed when using 3 µM substrate instead of 5 µM, even with a lower concentration of 15 µM of aptamer compared to 50 µM, proposing that inhibitor and substrate RNA are competing each other. As in total only two different concentrations were studied, these findings should be considered with caution until a larger amount of varying RNA concentrations is studied. Furthermore, it should be stated that this competition is not necessarily a specific one e.g. competition for the identical binding site, but may also be unspecific since the RNA species used are relatively large (~25 kDa) compared to the size of the enzyme (~44 kDa) leading to sterical hinderances. Further, RNAs bear a strong negative charge, making them natural repellents (448). Previous findings demonstrate that tRNA^{Asp} binds to positively charged amino acid residues over a rather large area on the surface of DNMT2 which is likely to result in at least partially overlapping binding sites and thus opposing an unspecific competition mechanism (149).

The inhibition of RNAs of cycles 6, 9 and 12 are very similar and differ only in the range of measurement accuracy, matching the observations of the filter retention assay (Figure 24C, conducted by the group of Professor ▮▮▮▮, Bonn), which demonstrated that the binding affinity of RNA remained constant from cycle 6 to cycle 12 (SELEX without heparin) or even decreased (SELEX with heparin). This suggests that RNA potency was not increased in terms of its inhibition and binding potential in the second half of SELEX progression. This observation would give a plausible explanation for the strong enrichment of only two sequences in the final pools when considering secondary effects such as overamplification by DNA or RNA polymerases, as described above. To fully comprehend these issues, sequencing of multiple SELEX cycles is beneficial to investigate the enrichment behaviour of single sequences during the selection process. Additionally, *in vitro* data of multiple IVT transcribed RNA pools can add up to sequencing results, possibly enabling the identification of previously neglected, more potent sequences.

3.4.5 Aptamer truncation

During the process of aptamer truncation, nucleotides contributing not or only to a minor extend are discarded, thus improving the overall affinity of aptamer sequences towards their respective targets, and further providing information on SAR (341, 449).

In the case at hand, A2 is the most potent of the selected aptamers and a good starting point for the procedure of truncation. Suitable positions for sequence partitions were selected based on the predicted secondary structure of A2 using the RNAFold webserver (450–452) and considering the highly

conserved positions identified by MSA (*vide supra*, Figure 26A). This led to the generation of five novel sequences, each containing the terminal loop L1 with varying amounts of nucleotides on the 5' and 3' ends while excluding the internal loop L2 (Figure 28A and B).
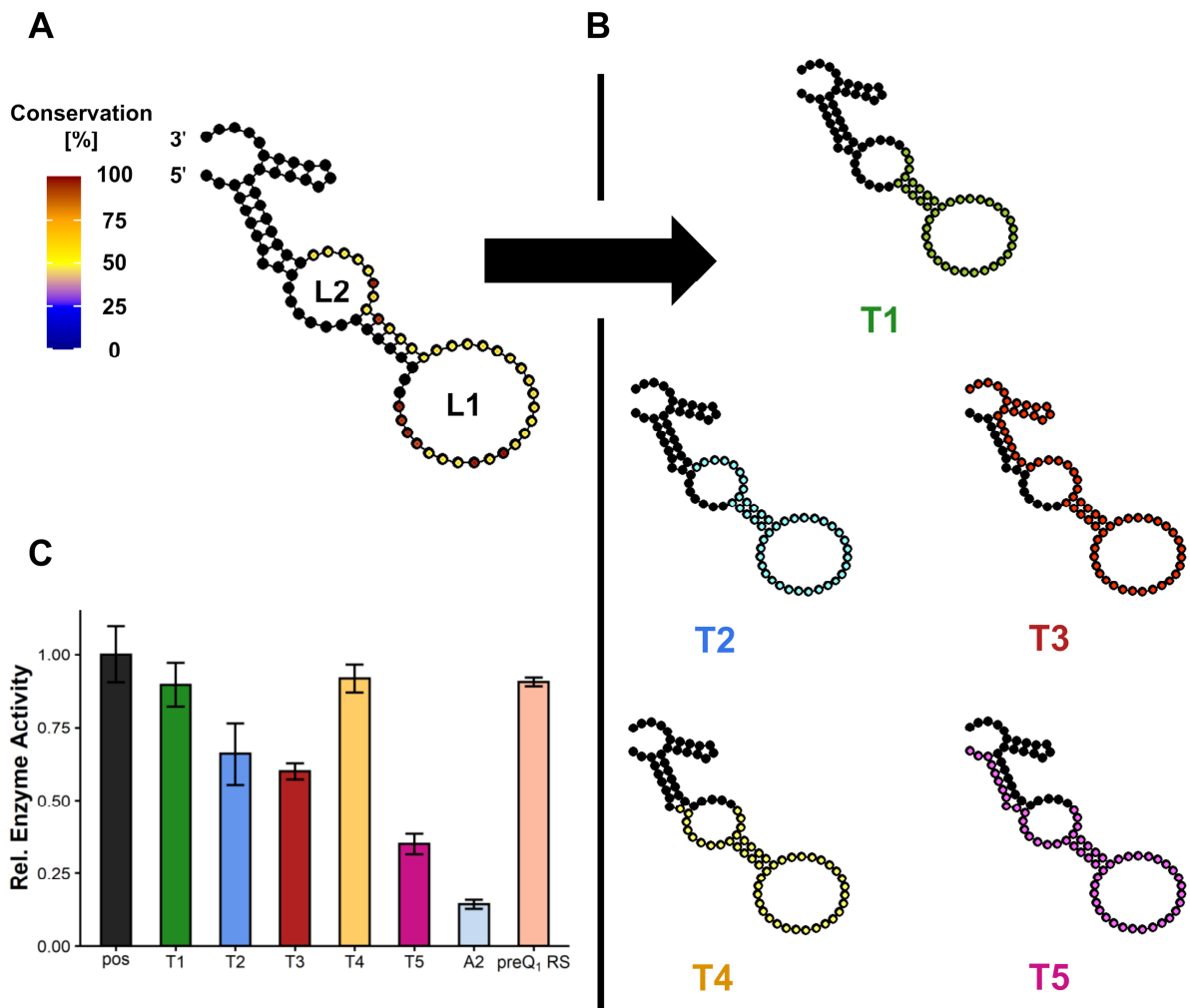
Figure 28. Aptamer Truncation. A) Predicted secondary structure of A2. Colours indicate the conservation of the corresponding nucleotide in the complete sequence. The fixed primer binding regions are marked in black. L1 and L2 refer to the predicted terminal and internal loops on the RNA structure. B) Predicted secondary structure of A2. Coloured regions highlight sequence parts chosen for truncation while black parts were discarded. T1–5 allocate to the truncated aptamer species. C) Relative enzyme activity as determined by the tritium incorporation assay in the presence of 15 μM truncated aptamer, A2 or the preQ$_1$ riboswitch using 3 μM substrate tRNA^{Asp}. Displayed are mean values and standard deviations of experimental triplicates.

The IVT synthesised RNAs were investigated in the tritium incorporation assay at a concentration of 15 μM using 3 μM substrate tRNA^{Asp}. All truncated sequences inhibited DNMT2 activity less than the full-length aptamer A2 (inhibition of 88%). Sequences T1 and T4 did not show a stronger inhibition than the RNA of the preQ$_1$ riboswitch. Inhibition of T2 and T3 was only moderate at 34% and 40%, respectively, whereas T5 decreased DNMT2 activity by 65% showing the strongest effect of all truncated sequences. (Figure 28C).

With this first truncation series, no sequences with higher inhibitory effect on DNMT2 compared to A2 could be generated, nonetheless, information on SAR were received. Based on the weak inhibition of T1, it can be clearly excluded that L1 alone is sufficient for DNMT2 inhibition even if all conserved nucleotides are included in this sequence. Furthermore, the comparably strong inhibition of T5,

especially in comparison to T1 and T4, suggests that the 5' end, or parts thereof, play a crucial role in the interaction between RNA and enzyme. Comparing T1, T2 and T3 a longer 3' end, at least until partition position of T2, seems to be beneficial for a stronger inhibition. While the optimal length of the 3' and 5' ends remain elusive, L2 may be of some importance for a strong RNA-protein interaction considering the predicted secondary structure in light of the above discussed results. Another approach to improve the aptamer's potency to inhibit DNMT2 would be to scale down L1, as most nucleotides in this structural element have an overall low conservation rendering them as potentially expandable.

Another possibility for the low activities of the shortened sequences might be incorrect structure prediction. Secondary structure predictions for RNA purely based on sequence information are error prone (453) and thus the original assumption for the truncation process might already be biased.

For a more detailed insight into the minimal aptamer structure, further shortened RNAs can be designed referring to knowledge gained by this first experiment. Errors originating from secondary structure prediction can be omitted if the design is based on the sequence alone but this approach restricts rational attempts for designing novel sequences to a minimum.

3.4.6 Summary and Outlook

As described in the paragraphs above, the SELEX process was utilised successfully for DNMT2. Here, the addition of heparin to the SELEX procedure did not alter the outcome significantly, instead two highly enriched sequences were identified in both selections using NGS. Furthermore, applying MSA on the sequencing data led to the identification of eight highly conserved nucleotide positions among all sequences. Based on the bioinformatic cluster analysis, four sequences were selected for *in vitro* experiments. While none of them acted as a substrate for DNMT2, one aptamer, namely A2, displayed moderate inhibition towards DNMT2. However, attempts to enhance its potency with truncation experiments failed, but the results from this research gave a detailed insight into SAR.

To generate more efficient aptamers, two possibilities might be considered: identifying novel sequences in the pools given or enhancing identified ones. The urgent question persists whether A2 is one of the strongest sequences or whether sequences with higher affinities remain unidentified. To answer this question, multiple rounds of SELEX may be sequenced and tested for their ability to interact with DNMT2, as discussed above.

Initial attempts to improve A2 were already made by shortening its sequence, but without success so far. Considering the information of SAR gained through the first set of truncation experiments, additional trimmed sequences can easily be designed and tested to construct a novel aptamer that might outperform A2.

Another possibility for improving an existing aptamer's performance is a reselection, which additionally provides information about SAR. Here, a doped library based on an already characterised aptamer is synthesised, which sequences differ only in one or two nucleotides compared to the original. This novel RNA pool is then subjugated to a limited number of SELEX cycles. If successful, more potent sequences are generated and further conclusions regarding the importance of specific nucleotides can be drawn according to their conservation during this process (454–456). Moreover, this data can be helpful for a future truncation procedure. Since it exhibits the highest potency to date, A2 is a suitable candidate for reselection.

For a detailed characterisation of the aptamers, binding experiments are crucial. Inhibition and binding data are likely comparable but might differ in the case of an allosteric aptamer binding, which does not interfere in substrate tRNA binding. Also, affinities between aptamers and native substrate can only be compared in binding assays.

The use of MST and electrophoretic mobility shift assays (EMSA, conducted by ███████████ during her bachelor thesis) have been evaluated for this purpose, but both methods had drawbacks, hence they were not pursued further.

The implementation of a plate based biochemical binding assay using biotinylated proteins with streptavidin coated well plates (457) is in process and was executed by ████████ during his master thesis. Also, biophysical methods as ITC (458), surface plasmon resonance (SPR) (457) or SwitchSENSE® (459) can be utilised for the determination of binding constants and, with especially the latter two, providing data about binding kinetics.

In analogy to small molecule inhibitors, the selectivity of the optimised aptamer is of major concern, although SELEX generated sequences usually display high selectivity towards their respective targets (346, 460). To assess this, the potential of inhibiting and binding other enzymes of the generated aptamer can be examined using the assays described above.

The next logical step after optimising the aptamer *in vitro* is to evaluate its functionality in a cellular context, where it might not only function as an enzyme inhibitor but may also be exploited to probe DNMT2 function in cells. However, use of RNA aptamers *in cellulo* requires overcoming their rapid degradation by nucleases and their limited uptake by cells (461).

A well-established method to enhance stability of RNA aptamers is to derivatise the 2' positions of their structural riboses with either 2'-*O*-Me or 2'-fluoro residues or by using more sophisticated approaches, as derivatisation with locked nucleotides (351).

Transfection with cationic lipids such as lipofectamine (461) is a standard method for delivering RNA into cells, yet transfection efficiency can vary in different experiments, posing a potential drawback to this method. The problem of poor cell permeability can be circumvented by expressing the corresponding RNA directly in cells using plasmids, though the rapid degradation of RNA prevents the accumulation of expressed aptamers. Specific expression systems such as the Tornado plasmid, which generates cyclic RNA species with higher intracellular stability, bypass this problem and are able to introduce substantial amounts of target RNA into cells to study their biological function in a cellular context (462).

4 Conclusion and Perspectives

In the present study, attempts for the development of modulators for DNMT2 activity are outlined. Therefore, two approaches were pursued: In a first effort, small molecules were developed to address the SAM binding site of the enzyme, while the second method aimed at blocking substrate tRNA binding with the use of an aptamer.

The development of small molecule inhibitors was conducted in close cooperation with ████ ███.

Here, derivatives were designed and examined based on the SAM substructure, which did not only give valuable insights into the structure activity relationship for DNMT2, but also revealed a remarkable correlation between MST and tritium incorporation assays during the screening efforts. On the other hand, determination of IC_{50} and K_D values using activity and ITC assays resulted in differing outcomes, conceivably due to the varying assay conditions, particularly with regard to a plausible impact of the tRNA molecule.

These analyses revealed that a Y-shape of the SAM-like inhibitors is crucial for addressing the enzyme. Herein, unsaturated residues displayed promising inhibition of DNMT2 with a series of alkyne derivatives outperforming other compounds. The best inhibitor of this first SAR study, **9c**, exhibited comparable IC_{50} and K_D values as the natural products SAH and SFG. Remarkably, partial selectivity of these compounds was observed, most of all for the tRNA MTases NSUN2 and NSUN6. An *in silico* analysis of the small molecule binding mode backed the experimental data and revealed additional insights into the interactions between compound and enzyme.

To further deepen the understanding of the interaction between inhibitors and DNMT2, a second series of compounds was investigated. Again, the Y-shaped SAM-substructure was utilised, but the inhibitors exclusively bore aromatic residues as their additional side chain. For this purpose, methylene as well as sulphonamide linkers were compared alongside a huge variety of differing ring substitution patterns. This demonstrated a general preference of benzylic derivatives over sulphonamide ones. Furthermore, the importance of a substitution on the aromatic ring's 4-position was acknowledged, preferentially comprising a chloro-residue.

The inhibition of sulphonamide derivatives correlated well with the ability of aromatic substituents to withdraw electrons from the ring, with the electron poorest derivative **16a** exhibiting an IC_{50} value in the range of SAH and SFG. This electron-deficient aromatic residue provides a feasible explanation for the time-dependent inhibition of **16a**, due to a possible interaction between DNMT2's catalytic cysteine and the electron-poor ring. With the evidence of RNA competition exhibited by aromatic derivatives, yet another mechanism was identified that could be exploited for future drug design.

While the above mentioned DNMT2 inhibitors did not outperform the natural products SAH and SFG significantly, at least two examples, **9c** and **16a**, demonstrated comparable affinity towards DNMT2, with compounds like **11a**, **13a** or **13b** likely revealing similar behaviour. More importantly, knowledge gained during the conducted SAR studies, including some compounds' potential to imply time-depending and RNA competing mechanisms, greatly facilitates future inhibitor design.

Nevertheless, upcoming endeavours for designing novel molecules should not only focus on the enhancement of their affinity, but also aim at selectivity issues, try to unveil the mechanisms behind

enzyme-small molecule interaction and importantly improve *in cellulo* efficacy. First data concerning selectivity was gathered during this study laying a solid basis for future efforts.

For the interaction between compounds and DNMT2, a profound knowledge was gained during this thesis. Due to the close structural similarity of the developed compounds with SAM, most likely the designed inhibitors address the SAM binding site. This assumption is backed by competition experiments conducted with ITC and *in silico* analyses. Further, compounds bearing aromatic residues stretch in the cytidine binding site to compete with the RNA substrate. However, the exact mechanism for the time-dependent inhibition remains elusive and further analysis is recommended to understand this phenomenon in detail.

While only minor effects of the investigated compounds in a cellular context were observed so far, this problem should be addressed with high priority, since compounds being active *in cellulo* would pave the way for their application as probes in living systems. To increase selectivity and cell permeability, the identification of novel scaffolds for DNMT2 inhibitors would be highly beneficial and with the insights gained during this thesis their development is facilitated.

The second approach taken for inhibitor development was the generation of a DNMT2 specific aptamer. During this research, SELEX pools created by the group of Professor ███ were evaluated using NGS. Subsequently, bioinformatical methods were applied to select sequences for further *in vitro* experiments. While a surprisingly high enrichment of two aptamers was observed, one of the sequences displayed higher reduction of DNMT2 activity than the complete SELEX pools investigated, indicating accurate *in silico* assumptions. First truncation of this aptamer did not result in RNA sequences with higher potency but revealed important SAR information for future experiments.

The observed lack of improvement of inhibition between SELEX rounds six, nine and twelve might indicate that the maximal aptamer affinity was already achieved early in the selection procedure and provides a possible explanation for the high enrichment. For a deeper insight, sequencing of multiple rounds of SELEX would be beneficial. To further improve the aptamer and gain a more detailed understanding regarding the SAR of the sequence, a reselection procedure was conducted by the ███ group during the writing of this thesis taking A2 as a basis, however the obtained pools are not analysed yet.

Optimisation of the aptamer *in vitro* should not only consider inhibition caused by the sequences, but also utilise binding assays. Additionally, the aptamer's selectivity is to be determined. After thorough *in vitro* characterisation and optimisation, profound emphasis should be taken towards *in cellulo* experiments exploiting the aptamer as a probe to help solving the DNMT2 enigma.

An approach combining small molecule and aptamer inhibitors would be the development of aptamer-drug-conjugates, a technique exploited previously (463). Even if a detailed understanding of binding modes for small molecules and aptamer is crucial for this approach, improvements for affinity as well as selectivity are expected.

Altogether, this work provides a solid first step towards the development of novel DNMT2 inhibitors by either small molecules or aptamers and certainly will facilitate future research directed in the manipulation of the epitranscriptome.

5 Materials and Methods

5.1 Materials

5.1.1 Instruments

Table 9. Instruments. Instruments used for conducting experiments described in this thesis.

Balances	
Mettler Toledo Excellence Plus	Mettler Toledo (Gießen, Germany)
Mettler Toledo PM460	Mettler Toledo (Gießen, Germany)
Sartorius Cubis Analytical Balance	Sartorius (Göttingen, Germany)
Centrifuges	
1–15 PK Sigma	Sigma (Osterode am Harz, Germany)
Heraeus Megafuge 8R	Thermo Scientific (Dreieich, Germany)
Eppendorf Centrifuge 5430 R	Eppendorf (Hamburg, Germany)
Eppendorf Centrifuge 5810 R	Eppendorf (Hamburg, Germany)
Sprout mini-centrifuge	Biozym (Hessisch Oldendorf, Germany)
Gel electrophoresis	
Aagarose gel chamber	PeqLab (Erlangen, Germany)
CAMAGTM UV Lamp 4	CAMAG (Muttenz, Switzerland)
Consort EV232 power supply	Consort (Turnhout, Belgium)
Electrophoresis Power Supply EPS 3501 XL	Amersham Pharmacia Biotech (Amersham, Great Britain)
Electrophoresis Power Supply EPS 3500 XL	Amersham Pharmacia Biotech Amersham, Great Britain)
LSG-400-20 NA vertical chamber	C.B.S. Scientific (San Diego, USA)
Model 250/2.5 power supply	BioRad (München, Germany)
Shaker (DOS-10L)	neoLab (Heidelberg, Germany)
TapeStation 4200	Agilent Technologies (Ratingen, Germany)
Typhoon TRIO+	GE Healthcare (Chicago, Illinois, USA)
General equipment	
FiveEasy™ FE20 pH meter	Mettler Toledo (Gießen, Germany)
Micropipettes, Pipetting Discovery Comfort (10 µL, 100 µL, 1000 µL)	Abimed (Langen, Germany)
NanoDrop ND 2000	PeqLab (Erlangen, Germany)
Pipetteboy Integra	VWR (Darmstadt, Germany)
Ultrapure water purification system Milli-Q	Millipore (Schwalbach, Germany)

Incubation	
BIOER ThermoCell	BIOER (Hangzhou, China)
IKA RH basic 2	IKA-Werke GmbH & CO. KG (Staufen, Germany)
Mixing Block MB-102	BIOER (Hangzhou, China)
Thermocycler peqSTAR	Peqlab (Erlangen, Germany)
Thermoshaker Plus	Eppendorf (Hamburg, Germany)
Vortex Mixer (7-2020)	neoLab (Heidelberg, Germany)
VWR Digital Heatblock	VWR International (Radnor, USA)
Ion exchange chromatography	
ÄKTA™ Start	VWR (Darmstadt, Germany)
Frac30 Fraktionssammler	VWR (Darmstadt, Germany)
HiTrap™ Q HP 5 mL	Cytiva (Freiburg, Germany)
Isotope laboratory	
TriCarb® Liquid Scintillation Analyzer 4810TR	PerkinElmer (Waltham, USA)

5.1.2 Chemicals and consumables

Table 10. Chemicals. Chemicals used for conducting experiments described in this thesis.

Chemicals	
Agarose	Biozym Scientific GmbH (Hessisch Oldendorf, Germany)
Agarose, low melting	Sigma-Aldrich (Taufkirchen, Germany)
NH_4OAc (ammonium acetate) for molecular biology, ≥98%	Sigma-Aldrich (Taufkirchen, Germany)
APS (ammonium persulfate), ≥98%, practical grade (p.a.)	Carl Roth (Karlsruhe, Germany)
ATP (adenosyl triphosphate, ≥90 %, lyophilized)	Carl Roth (Karlsruhe, Germany)
BSA (bovine serum albumin), BioReagent	Sigma-Aldrich (Taufkirchen, Germany)
CTP (cytidine triphosphate, 1g, ≥98%, lyophilized)	Carl Roth (Karlsruhe, Germany)
DMSO (dimethyl sulfoxide), american chemical society (ACS) reagent, ≥99.9%	Sigma-Aldrich (Taufkirchen, Germany)
DTT (dithiothreitol), molecular biology grade	Fermentas (St. Leon-Rot,Germany)
dNTP (deoxynucleotide triphospahte) Mix, 10 mM each	Thermo Fisher Scientific (Dreieich, Germany)
EDTA (ethylenediaminetetraacetic acid), 50 mM	Thermo Fisher Scientific (Dreieich, Germany)

Ethanol ≥99.5%, European Pharmacopoeia (Ph.Eur.), reinst	Carl Roth (Karlsruhe, Germany)
Formamide, BioBultra	Sigma-Aldrich (Taufkirchen, Germany)
GelRed® Nucleic Acid Stain, 3x in water	Biotium (Hayward, USA)
Glycerol, 99%	Grüssing GmbH (Filsum, Germany)
Glycogen, RNA grade	Thermo Fisher Scientific (Frankfurt, Germany)
GTP (guanosine triphosphate, 1g ≥90 %, lyophilized)	Carl Roth (Karlsruhe, Germany)
HEPES (4-(2-hydroxyethyl)-1-piperazineethane-sulfonic acid), ≥99.5%, BioScience-Grade	Carl Roth (Karlsruhe, Germany)
Hydrochloric acid. 37%, Ph.Eur.	VWR (Darmstadt, Germany)
KCl (potassium chloride), ≥99.5%	Carl Roth (Karlsruhe, Germany)
$MgCl_2$ (magnesium chloride) hexahydrate, ≥99%	Carl Roth (Karlsruhe, Germany)
NaCl (sodium chloride), BioXtra, ≥99.5%	Sigma-Aldrich (Taufkirchen, Germany)
PAGE denaturing gel premix, Sequenziergel-Konzentrat	Carl Roth (Karlsruhe, Germany)
PAGE gel diluent, Rotiphorese® Sequenziergel-Verdünner	Carl Roth (Karlsruhe, Germany)
PAGE gel buffer concentrate, Rotiphorese® Sequenziergel Puffer-Konzentrat	Carl Roth (Karlsruhe, Germany)
PAGE native gel premix, Rotiphorese® Gel40 (19:1)	Carl Roth (Karlsruhe, Germany)
SAM	New England Biolabs (Frankfurt am Main, Germany)
^{3}H- SAM, Adenosyl-L-methionine, S-[methyl-^{3}H], 250 µCi	Hartmann Analytics (Braunschweig, Germany)
Spermidine, trihydrochloride BioXtra, ≥99.5%	Sigma-Aldrich (Taufkirchen, Germany)
SYBR®Gold nucleic acid gel stain 10000x	Thermo Fisher Scientific (Frankfurt, Germany)
TCA (trichloroacetic acid), ≥99%, p.a.	Carl Roth (Karlsruhe, Germany)
TEMED, ≥99%, p.a.	Carl Roth (Karlsruhe, Germany)
Tris, Pufferan®, ≥99%	Carl Roth (Karlsruhe, Germany)
Tris-HCl, Pufferan®, ≥99%	Carl Roth (Karlsruhe, Germany)
Triton X-100, laboratory grade	Sigma-Aldrich (Taufkirchen, Germany)
ultra low range DNA ladder (ULR)	Thermo Fisher Scientific (Frankfurt, Germany)
UTP (uridine triphosphate, 100 mg, ≥90%, lyophilized)	Carl Roth (Karlsruhe, Germany)

Table 11. Consumables. Consumables used for conducting experiments described in this thesis.

Consumables

Eppendorf tubes (1.5, 2.0 mL)	Carl Roth (Karlsruhe, Germany)
Falcon® tubes (15, 50 mL)	CellStar (Frickenhausen, Germany)
Filtropur BT50, V25 and V50, 500 mL, 0.2 µm	Sarstedt (Nümbrecht, Germany)
Nanosep MF Centrifugal Devices 0.45 µm	VWR (Darmstadt, Germany)
PCR Softtubes	Biozym (Hessisch Oldendorf, Germany)
Pipette tips (10, 20, 100, 200, 1000 µL)	Carl Roth (Karlsruhe, Germany)
Scalpels B Braun™ Cutfix™	Thermo Fisher Scientific (Frankfurt, Germany)
Scintillation vials, Simport™ Scientific 6.5 ml HDPE Snaptwist™	Thermo Fisher Scientific (Frankfurt, Germany)
Scintillation cocktail, Ultima Gold™ MV	Perkin Elmer (Rodgau, Germany)
Serological Pipettes	Sarstedt (Nümbrecht, Germany)
Whatman® glass microfiber filters (GF/C, 25 mm)	Sigma-Aldrich (Taufkirchen, Germany)
Zymoclean™ Gel DNA Recovery Kit	Zymo Research (Freiburg, Germany)

5.1.3 Buffers

Table 12. Buffers. Buffers used for conducting experiments described in this thesis.

Buffer	Composition
10x DNase I buffer	100 mM Tris-HCl, pH 7.5, 25 mM $MgCl_2$, 1 mM $CaCl_2$ (Thermo Scientific, Dreieich Germany)
10x DNMT2 reaction buffer	1 M Tris-HCl, pH 8, 1 M NH_4OAc, 1 mM EDTA, 100 mM $MgCl_2$
4x ICB buffer	48 mM HEPES, pH 7.2, 40 mM NaCl, 540 mM KCl, 12 mM $MgCl_2$
IEX buffer A	20 mM HEPES (pH 7.2), 20 mM NaCl
IEX buffer B	20 mM HEPES (pH 7.2), 2 M NaCl
10x NSUN6 reaction buffer	500 mM Tris-HCl, pH 7, 500 mM NaCl, 50 mM $MgCl_2$
2x PAGE loading buffer, denaturing	90% v/v formamide in 1x TBE
5x PAGE loading buffer, native	80% v/v glycerol in 1x TBE
10x PCR reaction buffer	160 mM $(NH_4)_2SO_4$, 670 mM Tris-HCl, pH 8.8, 0.1%Tween 20 (Rapidozym, Berlin, Germany)
10x TBE buffer (ROTIPHORESE®)	1.0 M Tris-borat, pH8.3, 20 mM EDTA (Carl Roth, Karlsruhe, Germany)
5x transcription buffer	200 mM Tris-HCl (pH 8.8), 5 mM spermidine, 0.05% Triton X-100

5.1.4 Enzymes

Table 13. Enymes. Enzymes used for conducting experiments described in this thesis.

Enzyme	Supplier/Producer
DNase I (50 U µL⁻¹)	Thermo Fisher Scientific (Dreieich, Germany)
DNMT2	Prepared by ████████████, ██ ████████
NSUN6	Prepared by ████████████, ██ ████████
T7 RNA polymerase	Prepared by ████████████, ██ ██████.
T7 RNA polymerase (20 U µL⁻¹)	Thermo Fisher Scientific (Dreieich, Germany)
Taq DNA polymerase (5 U µL⁻¹)	New England Biolabs (Frankfurt am Main, Germany)

5.1.5 Oligonucleotides

Table 14. Oligonucleotides. Oligonucleotides used for conducting experiments described in this thesis.

Notation	Function	Sequence (5' to 3')	Supplier
MH53	Universal T7 forward primer	CGCGCGAAGCTTAATACGACTCACTATA	Biomers
MH1101	tRNA^{Asp} template	TGGCGGGCCGTCGGGGAATCGAACCCCGGTCTCC CGCGTGACAGGCGGGGATACTCACCACTATACTAA CGACCCTATAGTGAGTCGTATT	IBA
MH1102	tRNA^{Asp} reverse primer	TGGCGGGCCGTCG	IBA
MH1134	Forward primer aptamer	AATTCTAATACGACTCACTATAGGGAGAGGAGGGAG ATAGATATCAA	IBA
MH1135	Reverse primer aptamer	GTCCTGTGGCATCCACGAAA	IBA
MH1139	tRNA$^{Thr}_{AGU}$ reverse primer	TGGAGGCCCCGCTGGGAGTCGAA	IBA
MH1140	tRNA$^{Thr}_{AGU}$ template, incl. cNLB48	TAGTCGTAAGCTGATATGGCTGATTAGTCGGAAGCA TCGAACGCTGATTGGAGGCCCCGCTGGGAGTCGAA CCCAGGATCTCCTGTTTACTAGACAGGCGCTTTAAC CAACTAAGCTACGGAGCCTATAGTGAGTCGTATTA	IBA
MH1141	preQ$_1$ riboswitch reverse primer	TTAGTTTTTTATAGAGGGTG	IBA

MH1142	preQ$_1$ riboswitch template	TAGTCGTAAGCTGATATGGCTGATTAGTCGGAAGCA TCGAACGCTGATTTAGTTTTTTATAGAGGGTGTAGC TAGAACCTCTCCTATAGTGAGTCGTATTA	IBA
MH1150	SELEX sequencing primer N707	CAAGCAGAAGACGGCATACGAGATGTAGAGAGGTG ACTGGAGTTCAGACGTGTGCTCTTCCGATCTGTCCT GTGGCATCCA	IDT
MH1151	SELEX sequencing primer N711	CAAGCAGAAGACGGCATACGAGATTGCCTCTTGTG ACTGGAGTTCAGACGTGTGCTCTTCCGATCTGTCCT GTGGCATCCA	IDT
MH1152	SELEX sequencing primer N503	AATGATACGGCGACCACCGAGATCTACACTATCCTC TACACTCTTTCCCTACACGACGCTCTTCCGATCTAG GAGGGAGATAGAT	IDT
MH1153	SELEX sequencing primer N505	AATGATACGGCGACCACCGAGATCTACACGTAAGG AGACACTCTTTCCCTACACGACGCTCTTCCGATCTA GGAGGGAGATAGAT	IDT
MH1156	Aptamer 1 template, incl. cNLB48	GGGAGAGGAGGGAGATAGATATCAAGAGATACGCA CGTAGAAGGCAACTCACTGCCACATCCGGGTTTCG TGGATGCCACAGGACATCAGCGTTCGATGCTTCCG ACTAATCAGCCATATCAGCTTACGACTA	IDT
MH1157	Aptamer 2 template	GGGAGAGGAGGGAGATAGATATCAAGAGAAGAGTA TAATAGGCCGCCAGATATCACGACGGTCCCTTTCGT GGATGCCACAGGAC	IDT
MH1158	Aptamer 3 template	GGGAGAGGAGGGAGATAGATATCAATGACAGGGCA CAGAGAAGGCCGCCTCCCTACTTTTCGTTGTTTCGT GGATGCCACAGGAC	IDT
MH1159	Aptamer 4 template	GGGAGAGGAGGGAGATAGATATCAAGAAGAACAGC TACACGCAATCCTTCCGCCTTGTTGGTGCCTTTCGT GGATGCCAC AGGAC	IDT
MH1374	Forward truncation primer, short	AATTCTAATACGACTCACTATAGGGATATCAAGAGA AGAG	IDT
MH1375	Reverse truncation primer, short	GTGATATCTGGCGGCCTATTATACTC	IDT
MH1376	Forward truncation primer, medium	AATTCTAATACGACTCACTATAGGGAGATAGATATCA AGA	IDT
MH1376	Reverse truncation primer, medium	CCGTCGTGATATCTGGCGG	IDT

5.1.6   Software

Table 15. Software. Software used during this thesis.

Software	Supplier
ChemBioDraw Version 13.0.0.3015	CambridgeSoft/PerkinElmer (USA)
CorelDRAW V5 2020	Corel Corporation (Ottawa, Canada)
DRC Version 3.0-1 (RStudio Package)	Christian Ritz, Jens C. Strebig
FastAptamer	The Burke Lab (Columbia, USA)
FastQC	Babraham Bioinformatics (Cambridge, UK)
Galaxy Platform	Galaxy Community
ggPlot2 Version 3.3.5 (RStudio Package)	Hadley Wickham, Winston Chang, *et al*.
ImageJ V5	Wayne Rasband (Bethesda, Maryland, USA)
IrfanView	Irfan Skiljan
Jalview Version 2.11.1.0	The Barton Group (Dundee, UK)
Microsoft Office 365 for Enterprise	Microsoft (Redmond, USA)
PyMOL, Version 2.3.4	Schrödinger LLC (Braunschweig, Germay)
RRNA (RStudio Package)	John Paul Bida (Rochester, USA)
RStudio Version 4.0.4	RStudio Inc. (Boston, USA)
UNICORN™ start 1.1 control software	VWR (Darmstadt, Germany)
Trimmomatic	Usadel Lab (Aachen, Germany)

5.2   Methods

5.2.1   RNA synthesis and purification

Polymerase chain reaction. DNA templates for *in vitro* RNA synthesis were prepared using PCR. Reactions were carried out in a final volume of 200 µL in PCR reaction buffer with additional 3 mM MgCl$_2$, 400 µM dNTP-Mix, 2 µM of forward and reverse primers as well as 10 nM of the corresponding template. To this 0.05 U µL^{-1} Taq DNA polymerase (units specified by the supplier) were added. After an initial denaturation step for 2 min at 90 °C, 30 PCR cycles with 30 s annealing at temperatures specified in Table 16, 45 s elongation at 72 °C and 30 s denaturation at 90 °C were conducted with a final elongation step for 5 min.

Table 16. PCR settings. Combinations of templates and primer for IVT template generation together with used annealing temperatures.

Desired RNA species	Template	Forward primer	Reverse primer	Annealing temperature [° C]
tRNA^{Asp}	MH1102	MH53	MH1101	59
tRNA^{Thr}	MH1140	MH53	MH1139	59
preQ$_1$ riboswitch	MH1142	MH53	MH1141	45
A1	MH1156	MH1136	MH1137	59
A2	MH1157	MH1136	MH1137	59
A3	MH1158	MH1136	MH1137	59
A4	MH1159	MH1136	MH1137	59
T1	MH1157	MH1374	MH1375	57
T2	MH1157	MH1374	MH1377	57
T3	MH1157	MH1374	MH1137	57
T4	MH1157	MH1376	MH1375	57
T5	MH1157	MH1136	MH1375	57

In vitro transcription. To 1x transcription buffer, 30 mM MgCl$_2$, 5 mM DTT, 5 mM of each NTP, 2.5 µg mL^{-1} BSA and 400 µL of unpurified PCR products were added at room temperature to prevent DNA precipitation. Reactions were started with addition of T7 polymerase and carried out at 37 °C for 4 h. In the case of T7 polymerase produced by ███████████████, 50 µg mL^{-1} were added, while 0.5 U µL^{-1} were added in the case of commercial enzyme (units specified by the supplier).

Ethanol precipitation. For RNA precipitation, NH$_4$OAc was added to the samples to a final concentration of 0.5 M and 0.5–2 µL glycogen were added depending on the volume. Afterwards, 2.5–3 times volumes of cold ethanol were added to the mixture with subsequent incubation overnight at −20 °C. Samples were centrifuged with 13000 g for one hour at −4 °C and RNA pellets were washed once with 75% cold ethanol before centrifugation for 20 min with 13000 g at −4 °C. After drying the pellets on air, the RNA was solubilised in a suitable amount of MilliQ® water.

DNase digestion. After ethanol precipitation, crude *in vitro* transcription reactions were dissolved in 1x DNase I buffer and 1 U DNase I was added with subsequent incubation for 1 h at 37 °C.

Preparative denaturing PAGE. Transcription reactions which were DNase digested were purified using denaturing PAGE. Here, 50 mL of 10% denaturing PAGE premix (40% denaturing gel concentrate, 50% gel diluent, 10% gel buffer concentrate) was mixed with 25 μL TEMED before starting polymerisation by addition of 200 μL APS (10% solution, m/v).

Gels were cast between two glass plates (20 cm x 20 cm) and after polymerisation for roughly 15 min, gels were pre-run for around 15 min at 15 W in 1x TBE buffer.

Samples were loaded as a 1:1 mixture with 2x denaturing loading buffer and gels were run for 90 min at 15 W.

Preparative native PAGE. Transcription reactions which were not DNase digested beforehand were purified using native PAGE. Here, 50 mL of 10% native PAGE premix (25% native gel concentrate, 65% water, 10% 10x TBE) was mixed with 30 μL TEMED before starting polymerisation by addition of 500 μL APS (10% solution, m/v).

Gels were cast between two glass plates (20 cm x 20 cm) and after polymerisation for roughly 15 min, gels were pre-run for around 15 min at 15 W in 1x TBE buffer.

Samples were loaded as a 1:4 mixture with 5x native loading buffer and gels were run for 90 min at 15 W.

Gel excision. After conducting denaturing or native PAGE, RNA was visualised using UV shadowing at 254 nm. Corresponding bands were excised from the gel, smashed and subsequently frozen at −20 °C for at least 20 min. Afterwards, 200 μL of 0.5 M NH_4OAc were added and samples were shaken overnight at 700 rpm and 15 °C.

In the next step, samples were filtered using Nanosep® centrifugal filters and the flow through was ethanol precipitated as described before.

RNA concentration was determined using a NanoDrop device with a wavelength of 260 nm.

Ion exchange chromatography. Alternatively, *in vitro* transcribed RNA was purified by anion exchange chromatography on an ÄKTA™ start purification system connected to a 5 mL HiTrap™ Q column. The column was pre-equilibrated with IEX buffer A and up to 5 mL of transcription reaction were loaded on the column using a sample loop. Following gradient was applied with a flow rate of 5 mL min^{-1} using IEX buffers A and B: 1 column value of 100% IEX buffer A, 2 column volumes of 15% IEX buffer B, 3 column volumes of 15–40% IEX buffer B, 1.5 column volumes of 40% IEX buffer B and 3 column volumes of 100% IEX buffer B. Fractions of 1.2 mL were collected. RNA containing fractions were pooled and precipitated twice with ethanol as described before.

RNA concentration was determined using a NanoDrop device with a wavelength of 260 nm.

Analytical denaturing PAGE. To quality check RNA, denaturing PAGE was conducted. Here, 25 mL of 10% denaturing PAGE premix (40% denaturing gel concentrate, 50% gel diluent, 10% gel buffer concentrate) was mixed with 12.5 µL TEMED before starting polymerisation by addition of 25 µL APS (10% solution, m/v).

Gels were cast between two glass plates (20 cm x 13 cm) and after polymerisation for roughly 15 min, gels were pre-run for around 15 min at 15 W in 1x TBE buffer.

10 µL sample containing 0.5 µg–1 µg RNA was loaded as a 1:1 mixture with 2x denaturing loading buffer and gels were run for 25 min at 15 W.

Analytical native PAGE. To check for residual DNA, native PAGE was conducted. Here, 25 mL of 10% native PAGE premix (25% native gel concentrate, 65% water, 10% 10x TBE) was mixed with 15 µL TEMED before starting polymerisation by addition of 250 µL APS (10% solution, m/v).

Gels were cast between two glass plates (20 cm x 13 cm) and after polymerisation for roughly 15 min, gels were pre-run for around 15 min at 15 W in 1x TBE buffer.

10 µL sample containing 0.5–1 µg RNA was loaded as a 1:4 mixture with 5x native loading buffer and gels were run for 20 min at 15 W.

Visualisation of nucleic acids on gels. After stopping gel electrophoresis, gels were incubated in 100 mL 1x GelRed® for 15 min while shaking mildly. Following, gels were analysed on a Typhoon 9600 using laser emission of 532 nm and the emission filter 610 BP 30.

5.2.2   Tritium incorporation assay

DNMT2 activity assay. DNMT2 activity assays were carried out in 1x DNMT2 reaction buffer in the presence of 10 mM DTT. tRNA^{Asp} was heated up for 5 min to 75 °C and cooled down to room temperature before it was added to the reaction mixture to a final concentration of 5 µM. SAM was added as a mixture of ^{3}H-SAM and non-radioactive SAM to final concentrations of 0.9 µM and 0.025 µCi µL^{-1}. The amount of DMSO was adjusted to 5%. By adding 250 nM DNMT2, methylation reactions were started. Final volumes were 20 µL and reactions were conducted at 37 °C.

At 0 and 20 min, 8 µL were taken out of the reaction mixture and spotted on Whatman® glass microfiber filters. Substrate RNA was precipitated on Whatman® filters using 5% ice cold TCA for at least 15 min. First, filters were washed twice with 5% TCA at room temperature for 20 and 10 min and subsequently in ethanol for 10 min. After drying the filters under a heat lamp, they were put into scintillation vials and 3 mL of liquid scintillation cocktail was added. Scintillation was measured on a scintillation counter with a measurement time of 1 min.

NSUN6 activity assay. NSUN6 activity assays were carried out in 1x NSUN6 reaction buffer in the presence of 1 mM DTT. tRNA^{Thr} was heated up for 5 min to 75 °C and cooled down to room temperature before it was added to the reaction mixture with a final concentration of 1 µM. SAM was added as a mixture of ^{3}H-SAM and non-radioactive SAM to final concentrations of 1.2 µM and 0.038 µCi µL^{-1}. The

amount of DMSO was adjusted to 5%. By adding 30 nM NSUN6 methylation reactions were started. Final volumes were 20 µL and reactions were conducted at 37 °C.

At 0 and 20 min, 8 µL were taken out of the reaction mixture and spotted on Whatman® glass microfiber filters. Substrate RNA was precipitated on Whatman® filters using 5% ice cold TCA for at least 15 min. First, filters were washed twice with 5% TCA at room temperature for 20 and 10 min and subsequently in ethanol for 10 min. After drying the filters under a heat lamp, they were put into scintillation vials and 3 mL of liquid scintillation cocktail was added. Scintillation was measured on a scintillation counter with a measurement time of 1 min.

Compound Screening. For initial screenings, compounds were added to final concentrations of 100 µM to the reaction mixture. Percentage of inhibition was calculated by referencing obtained counts per minute (cpm) to a positive control conducted in the absence of compound. Errors refer to the standard deviation of three independent measurements. Negative controls were conducted in the absence of substrate tRNA^{Asp}.

IC$_{50}$ value determination. For IC$_{50}$ value determination, SAH, SFG and compounds **8b**, **9a**, **9b**, and **16a** were analysed at concentrations of 1000 µM, 500 µM, 100 µM, 50 µM, 10 µM, 5 µM and 1 µM and compound **9c** (experiment conducted by ██████████) at concentrations of 2500 µM, 833 µM, 250 µM, 83 µM, 25 µM, 8.3 µM, 2.5 µM, 0.83 µM and 0.25 µM. IC$_{50}$ values were calculated by exponential fitting of the relative enzymatic activities against the inhibitor concentrations using the LL.2 function of the drc package version 3.0-1 (464), in RStudio version 4.0.4 (465):

$$y = \frac{100}{1+e^{b(\log(x)-\log(e))}}, \text{ b= Hill coefficient, e = IC}_{50}.$$

IC$_{50}$ errors are given as standard errors of three independent measurements. Negative controls were conducted in the absence of substrate tRNA^{Asp}.

Time-dependency assay. To investigate potential time-dependent inhibition behaviour, the DNMT2 assay was conducted as described above with applying adaptations described in the following.

Here, the enzyme was added to a solution containing 1x DNMT2 reaction buffer and tRNA^{Asp} substrate either directly or after incubation for 75 min in 1x DNMT2 reaction buffer in the presence or absence of SAH, SFG and **8b** at 100 µM or **16a** at 5 µM.

Methylation reactions were started with addition of the radioactive/non-radioactive SAM mixture and standard procedure was followed as described above.

RNA concurrence. The concurrence between RNA and inhibitors was investigated using the DNMT2 activity assay as described above with applying adaptations described in the following.

Here, substrate tRNA^{Asp} was added to the assay at either 2.5 µM, 5 µM or 10 µM together with SAH, SFG, **8b**, **8c** and **11a** at a concentration of 100 µM or **16a** at a concentration of 2.5 µM.

Subsequent, the standard procedure was followed as described above, with positive controls without inhibitor addition conducted for every RNA concentration as reference.

Aptamer RNA as substrate. To investigate if aptamer RNAs can function as DNMT2 substrates they were subjected to DNMT2 activity assays instead of tRNA^{Asp} at concentrations of 50 µM.

Relative enzyme activity was calculated by referencing obtained cpm to a positive control conducted with tRNA^{Asp} as substrate at a concentration of 5 µM as described above. Here, addition of DMSO was omitted.

Aptamer screening. For aptamer screenings, aptamer RNAs were added to final concentrations of 50 µM to the reaction mixture if 5 µM of substrate tRNA^{Asp} was used.

If 3 µM of tRNA^{Asp} was used, aptamer RNAs were added at a concentration of 15 µM, 370 ng µL^{-1} or 420 ng µL^{-1} depending on the RNA species.

Percentage of inhibition was calculated by referencing obtained cpm to a positive control conducted in the absence of aptamer RNA.

Here, addition of DMSO was omitted. Errors refer to the standard deviation of three independent measurements. Negative controls were conducted in the absence of substrate tRNA^{Asp}.

5.2.3   Methods for SELEX analysis

Library preparation. Sequencing libraries were prepared by single step extension PCR. Reactions were carried out in a final volume of 100 µL in PCR reaction buffer with additional 3 mM MgCl$_2$, 300 µM dNTP-Mix, 0.5 µM of forward and reverse primers (pairing either N707 and N711 or N503 and N505, see Table 14) as well as 1 µL of PCR product obtained by SELEX cycle 12.

To this 0.05 U µL^{-1} Taq DNA polymerase (units specified by the supplier) were added. After an initial denaturation for 2 min at 90 °C, 20 PCR cycles with 30 s annealing at 62 °C, 45 s of elongation at 72 °C followed by denaturation for 30 s at 90 °C were conducted with a final elongation step for 5 min.

Preparative agarose gel electrophoresis. For purification of sequencing libraries, 1% agarose gels were prepared with low melting agarose. After mixing samples with denaturing loading dye, the gel was run in 1x TBE buffer at 120 V after loading PCR reactions.

Subsequently the gel was stained in 1x GelRed® for 20 min and analysed on a Typhoon 9600 fluorescent scanner using laser emission of 532 nm and the emission filter 610 BP 30.

Corresponding bands were excised from the gel using a printout of the visualised gel picture and DNA was extracted using the Zymoclean™ Gel DNA Recovery Kit according to the manufacturer's instructions. Briefly, three parts of agarose dissolving buffer were added to one part of gel slice and samples were incubated at 55 °C for 10 min. Afterwards, the mixtures were loaded on the kit's spin columns, washed twice with DNA washing buffer and eluted with DNA elution buffer.

Analytical agarose gel electrophoresis. DNA purity was assessed by analytical agarose gels. Here, 1% agarose gels were prepared using standard agarose prestained with 10 µL 10.000x SybrGold. 0.5 µg of DNA sample were loaded after mixing 1:1 with 2x denaturing loading dye and gels were run in 1x TBE at 120 V. Bands were visualised on a Typhoon 9600 fluorescent scanner using laser emission of 488/532 nm and the emission filter 520 BP.

Tape station analysis. Analysis of DNA was further conducted using a TapeStation 4200 according to the manufacturer's instructions.

Next generation sequencing. Sequencing was conducted by ▇▇▇▇▇▇▇ and ▇▇▇▇▇▇▇▇ (Biopôle, Nancy) and will only be briefly explained here. Sequencing libraries were analysed on a Illumina® MiSeq® device using paired-end sequencing with a read length of 75 bp.

Trimming and quality control of reads. Raw paired-end reads obtained from sequencing were merged and aptamer sequences were trimmed using Trimmomatic Galaxy Version 0.38.0 (466) provided by the Galaxy platform (467). Reads < 75 were discarded using Trimmomatic and read quality was assessed with FastQC Version 0.11.9 (468).

Sequence quantification and clustering. Sequence abundance was quantified with FastAptamer (443), using the count function according to the programmers' instructions. For cluster analysis, FastAptamer's cluster function was utilised setting Levenshtein distance to 4 and excluding reads with less than 10 reads per million.

Multiple sequence alignment. For multiple sequence alignment of all sequences reads with less than 100 reads per millions were discarded using FastAptamer's cluster function and reads were normalised to the lowest abundant sequence using RStudio (465). For unique sequences MSA sequences generated by FastAptamer count were used.
Thus generated sequence files (FASTA format) were loaded into Jalview Version 2.11.1.0 (446), the consensus annotation was exported and further analysed using RStudio (465).

RNA secondary structure prediction. RNA secondary structure prediction was conducted with the RNAFold webserver (450–452). Dot-Bracket notation was exported to RStudio where RNA structures were plotted using the RRNA package (469).

6 Appendix

Table 17. Prokaryotic MTase inhibitors. Collection of literature for prokaryotic RNA MTase inhibitors. In the "design strategy" column the original method for compound selection is given, while "evaluation method" gives an approximately listing of the experiments performed in the corresponding references. CADD = computer aided drug design, i.s. = *in silico*; i.vt. = *in vitro*; i.c. = *in cellulo*; i.vv. = *in vivo*. Table adapted from Fischer *et al.* (97) for which it was created with ███████████ and ██████████.

Enzyme/ Modification	Organism	Design strategy	Evaluation method	References
ErmC m^{6}A rRNA	*E. coli*	CADD	i.s., i.vt.	(273)
		CADD	i.s., i.vt.	(272)
	??	CADD	i.s., i.vt.	(271)
	Staphylococcus aureus/pyogenes	HTS	i.vt., i.vv.	(274)
ErmAM m^{6}A rRNA	??	NMR-based screening	i.vt.	(275)
TrmD m^{1}G$_{37}$ tRNA	*E.coli*	SAH analogue	i.vt.	(470)
		HTS	i.vt.	(232)
	Pseudomonas aeruginosa	HTS	i.vt.	(471)
		SAR, non SAH-like	i.vt.	(472)
	Mycobacterium tuberculosis	SAR, non SAH-like	i.vt.	(472)
	Mycobacterium tub. + abscessus + leprae	FBDD	i.vt., i.c.	(473)
	Haemophilus influenzae	HTS	i.vt.	(232)
	S. aureus	HTS	i.vt.	(232)
		SAR, non SAH-like	i.vt.	(472)
	Mycobacterium abscessus	FBDD	i.vt.	(474)
crude extract m^{5}U tRNA	*E. coli*	SAH analogue	i.vt.	(247)
RlmJ m^{6}A rRNA	*E. coli*	SAH analogue	i.vt.	(288)
crude extract unknwon modification tRNA		Purine & adenosine analogs	i.vt.	(475)

crude extract m^{1}A, m^{6}A, m$^6_2$A, m^{7}G tRNA, rRNA	*Streptomyces*	SAH analogue	i.vt.	(249)
Not specified		SFG, Azacytidin	i.c.	(476)
Dimethyladenosine transferase m^{6}A rRNA	*Chlamydia pneumoniae*	Similarity based VS	i.s., i.c.	(477)
rsmD like rRNA-MTase m^{2}G rRNA	*Wolbachia*	CADD	i.s., i.vv.	(478)

Table 18. Eukaryotic single cell MTase inhibitors. Collection of literature for eukarotic single cell RNA MTase inhibitors. In the "design strategy" column the original method for compound selection is given, while "evaluation method" gives an approximately listing of the experiments performed in the corresponding references. CADD = computer aided drug design, i.s. = *in silico*; i.vt. = *in vitro*; i.c. = *in cellulo*; i.vv. = *in vivo*. Table adapted from Fischer *et al*. (97), for which it was created with ██████████████████████ ██████.

Organism	Enzyme/ Modification	Design strategy	Evaluation method	References
Fungi, *Encephalitozoon cuniculi*	Ecm1 m^{7}G mRNA cap	SAH analogue	i.vt., i.c.	(277, 278)
		Nucleotide analogue	i.vt.	(236)
Fungi *C. albicans*	CCM1 m^{7}G mRNA cap	Natural products	i.c.	(276)
Yeast *S. cerevisiae*	ABD1 (*S.c.*) m^{7}G mRNA cap	Natural products	i.c.	(276)
Leishmania infantum	Cmt1 m^{7}G mRNA cap	SAH analogue	i.vt.	(479, 480)
Trypanosoma brucei	Cmt1 m^{7}G mRNA cap	SAH analogue	i.vt.	(480)

Table 19. Human MTase inhibitors. Collection of literature for human RNA MTase inhibitors. In the "design strategy" column the original method for compound selection is given, while "evaluation method" gives an approximately listing of the experiments performed in the corresponding references. CADD = computer aided drug design, i.s. = *in silico*; i.vt. = *in vitro*; i.c. = *in cellulo*; i.vv. = *in vivo*. Table adapted from Fischer *et al*. (97), for which it was created with ███████████.

Enzyme/ Modification	Design strategy	Evaluation method	References
METTL3-METTL14 m⁶A mRNA	CADD	i.s., i.vt., i.c.	(291)
	SAH analogue	i.vt.	(288)
		i.s., i.vt.	(289)
		i.s., i.vt., i.c.	(220, 290)
		i.vt., i.c.	R299
	Non SAH analogue	i.s., i.vt., i.c., i.vv.	(220)
		i.vt., i.c.	(292, 294, 481)

Table 20. Viral MTase inhibitors. Collection of literature for viral RNA MTase inhibitors. In the "design strategy" column the original method for compound selection is given, while "evaluation method" gives an approximately listing of the experiments performed in the corresponding references. CADD = computer aided drug design, i.s. = *in silico*; i.vt. = *in vitro*; i.c. = *in cellulo*; i.vv. = *in vivo*. Table adapted from Fischer *et al*. (97).

Organism	Enzyme/ Modification	Design strategy	Evaluation method	References
dengue virus (DENV)	NS5 m⁷G mRNA cap	CADD	i.vt.	(482)
			i.s., i.vt.	(483)
			i.vt., i.c.	(484)
		SAH analogue	i.vt.	(312)
			i.vt., i.c.	(485)
		LTS	i.vt.	(486)
		FBDD	i.vt.	(313)
			i.s., i.vt., i.c.	(314)
	NS5 2'-O mRNA cap	CADD	i.vt.	(482)
			i.s., i.vt.	(483, 487)

			i.vt., i.c.	(484)
			i.s., i.vt., i.c.	(233)
		Nucleotide analogue	i.vt	(488)
			i.vt.	(489)
			i.s., i.vt., i.c	(490)
		SAH analogue	i.vt., i.c.	(485)
			i.vt.	(312, 491)
		LTS	i.vt.	(486)
		FBDD	i.vt.	(313, 315)
			i.vt., i.c.	(316)
			i.s., i.vt., i.c.	(314)
	not determined	CADD	i.s.	(492–496)
			i.vt., i.c.	(497)
		Nucleotide analogue	i.vt., i.c.	(498, 499)
		LTS	i.s., i.c., i.vv.	(499)
		HTS	i.vt.	(500)
zika virus (ZIKV)	NS5 2'-O mRNA cap	Nucleotide analogue	i.s., i.vt.,i.c.	(490)
		FBDD	i.vt.	(315)
			i.s., i.vt., i.c.	(316)
	not determined	CADD	i.s.	(501–504)
			i.s., i.c.	(505)
			i.s., i.vt. i.c.	(497)
		SAH analogue	i.s., i.vt.	(506)
			i.c.	(507)
		HTS	i.s., i.vt.,i.c.	(508)
west nile virus (WNV)	NS5 m⁷G mRNA cap	CADD	i.vt.,i.c.	(483)
			i.s., i.vt.,i.c.	(484)

		Nucleotide analogue	i.s., i.vt.,i.c.	(509, 510)
		SAH analogue	i.s., i.vt.,i.c.	(485)
		HTS	i.vt., i.c.	(510)
	NS5 2'-O mRNA cap	CADD	i.vt.,i.c.	(483)
			i.s., i.vt.,i.c.	(484)
		Nucleotide analogue	i.s., i.vt.,i.c.	(509)
		SAH analogue	i.s., i.vt.,i.c.	(485)
		FBDD	i.vt.	(314)
	not determined	Nucleotide analogue	i.s., i.c.	(490, 498)
yellow fever virus (YFV)	NS5 m⁷G mRNA cap	CADD	i.vt.	(483, 484)
		SAH analogue	i.v., i.c.	(485)
	NS5 2'-O mRNA cap	CADD	i.vt.	(483, 484)
		SAH analogue	i.v., i.c.	(485)
		Nucleotide analogue	i.s., i.c.	(490)
	not determined	HTS	i.vt.	(511)
			i.s., i.vt.	(500)
wesselbron virus (WV)	NS5 m⁷G mRNA cap	CADD	i.s., i.v.	(482)
	NS5 2'-O mRNA cap	CADD	i.s., i.v.	(482)
japanese encephalitis virus (JEV)	not determined	CADD	i.c.	(484)
St. louis encephalitis virus (SLEV)	not determined	CADD	i.c.	(484)
severe acute respiratory syndrome coronavirus (SARS-CoV)	nsp14 m⁷G mRNA cap	SAH analogue	i.s., i.vt.	(328)
		LTS	i.vt.	(512)
		HTS	i.vt.	(433)
			i.vt., i.c.	(513)
	nsp16 2'-O mRNA cap	LTS	i.vt.	(512)
SARS-CoV-2	nsp14 m⁷G mRNA cap	CADD	i.s.	(514–520)
		SAH analogue	i.s., i.vt.	(325, 327)
			i.s., i.vt., i.c.	(326)
		HTS	i.vt.	(219)

			i.vt., i.c.	(521, 522)
	nsp16 2'-O mRNA cap	CADD	i.s.	(514, 519, 520, 523–546)
			i.s., i.vt.	(547)
		SAH analogue	i.s., i.vt., i.c.	(326)
		HTS	i.vt.	(548, 549)
chikungunya virus (CHIKV)	nsp1 m⁷G mRNA cap	HTS	i.c., i.vt.	(550)
		nucleoside analogue	i.c.	(551)
		CADD, nucleoside analogue	i.vt., i.c.	(552)
		natural products	i.vt.	(553)
		HTS	i.vt., i.c.	(554)
		HTS	i.c., i.vt.	(555)

Table 21. RNA sequences. RNA sequences used for conducting experiments described in this thesis.

RNA species	Template	Sequence (5' to 3')
tRNA^{Asp}	MH1102	GGGUCGUUAGUAUAG UGG UGA GUA UCC CCG CCU GUC ACG CGG GAG ACC GGG GUU CGA UUC CCC GAC GGC CCG CCA
tRNA^{Thr}	MH1140	GGCUCCGUAGCUUAGUUGGUUAAAGCGCCUGUCUAGUAAAC AGGAGAUCCUGGGUUCGACUCCCAGCGGGGCCUCCA
preQ$_1$ riboswitch	MH1142	GGAGAGGUUCUAGCUACACCCUCUAUAAAAAACUAA
A1	MH1156	GGGAGAGGAGGGAGATAGATATCAAGAGATACGCACGTAGAA GGCAACTCACTGCCACATCCGGGTTTCGTGGATGCCACAGGA C
A2	MH1157	GGGAGAGGAGGGAGATAGATATCAAGAGAAGAGTATAATAGG CCGCCAGATATCACGACGGTCCCTTTCGTGGATGCCACAGGA C
A3	MH1158	GGGAGAGGAGGGAGATAGATATCAATGACAGGGCACAGAGAA GGCCGCCTCCCTACTTTTCGTTGTTTCGTGGATGCCACAGGAC
A4	MH1159	GGGAGAGGAGGGAGATAGATATCAAGAAGAACAGCTACACGC AATCCTTCCGCCTTGTTGGTGCCTTTCGTGGATGCCACAGGAC
T1	MH1157	GGGAUAUCAAGAGAAGAGUAUAAUAGGCCGCCAGAUAUCAC
T2	MH1157	GGGAUAUCAAGAGAAGAGUAUAAUAGGCCGCCAGAUAUCAC GACGG
T3	MH1157	GGGAUAUCAAGAGAAGAGUAUAAUAGGCCGCCAGAUAUCAC GACGGUCCCUUUCGUGGAUGCCACAGGAC
T4	MH1157	GGGAGAUAGAUAUCAAGAGAAGAGUAUAAUAGGCCGCCAGA UAUCAC
T5	MH1157	GGGAGAGGAGGGAGAUAGAUAUCAAGAGAAGAGUAUAAUAG GCCGCCAGAUAUCAC

7 References

1. Brosius,J. and Raabe,C.A. (2016) What is an RNA? A top layer for RNA classification. *RNA Biol*, **13**, 140–144.

2. Statello,L., Guo,C.-J., Chen,L.-L. and Huarte,M. (2021) Gene regulation by long non-coding RNAs and its biological functions. *Nat Rev Mol Cell Biol*, **22**, 96–118.

3. Scull,C.E., Dandpat,S.S., Romero,R.A. and Walter,N.G. (2021) Transcriptional Riboswitches Integrate Timescales for Bacterial Gene Expression Control. *Front Mol Biosci*, **7**, 607158.

4. Wen,J.-T., Huang,Z.-H., Li,Q.-H., Chen,X., Qin,H.-L. and Zhao,Y. (2021) Research progress on the tsRNA classification, function, and application in gynecological malignant tumors. *Cell Death Discov*, **7**, 388.

5. Damase,T.R., Sukhovershin,R., Boada,C., Taraballi,F., Pettigrew,R.I. and Cooke,J.P. (2021) The Limitless Future of RNA Therapeutics. *Front Bioeng Biotechnol*, **9**, 628137.

6. Dana,H., Chalbatani,G.M., Mahmoodzadeh,H., Karimloo,R., Rezaiean,O., Moradzadeh,A., Mehmandoost,N., Moazzen,F., Mazraeh,A., Marmari,V., *et al.* (2017) Molecular Mechanisms and Biological Functions of siRNA. *Int J Biomed Sci*, **13**, 48–57.

7. Neumeier,J. and Meister,G. (2021) siRNA Specificity: RNAi Mechanisms and Strategies to Reduce Off-Target Effects. *Front Plant Sci*, **11**, 526455.

8. Hu,B., Zhong,L., Weng,Y., Peng,L., Huang,Y., Zhao,Y. and Liang,X.-J. (2020) Therapeutic siRNA: state of the art. *Signal Transduct Target Ther*, **5**, 101.

9. Park,J., Ahn,S.H., Shin,M.G., Kim,H.K. and Chang,S. (2020) tRNA-Derived Small RNAs: Novel Epigenetic Regulators. *Cancers (Basel)*, **12**, 2773.

10. Gapp,K. and Miska,E.A. (2016) tRNA fragments: novel players in intergenerational inheritance. *Cell Res*, **26**, 395–396.

11. Strzyz,P. (2020) CRISPR–Cas9 wins Nobel. *Nature Reviews Molecular Cell Biology*, **21**, 714.

12. Adli,M. (2018) The CRISPR tool kit for genome editing and beyond. *Nat Commun*, **9**, 1911.

13. Nance,K.D. and Meier,J.L. (2021) Modifications in an Emergency: The Role of N1-Methylpseudouridine in COVID-19 Vaccines. *ACS Cent Sci*, **7**, 748–756.

14. Smyth,R.P., Negroni,M., Lever,A.M., Mak,J. and Kenyon,J.C. (2018) RNA Structure-A Neglected Puppet Master for the Evolution of Virus and Host Immunity. *Front Immunol*, **9**, 2097.

15. Westhof,E. and Fritsch,V. (2000) RNA folding: beyond Watson-Crick pairs. *Structure*, **8**, R55–R65.

16. Ayon,N. (2020) Features, roles and chiral analyses of proteinogenic amino acids. *Molecular Science*, **7**, 229–268.

17. Boccaletto,P., Stefaniak,F., Ray,A., Cappannini,A., Mukherjee,S., Purta,E., Kurkowska,M., Shirvanizadeh,N., Destefanis,E., Groza,P., *et al.* (2022) MODOMICS: a database of RNA modification pathways. 2021 update. *Nucleic Acids Res*, **50**, D231–D235.

18. Cheng,H.-P., Yang,X.-H., Lan,L., Xie,L.-J., Chen,C., Liu,C., Chu,J., Li,Z.-Y., Liu,L., Zhang,T.-Q., *et al.* (2020) Chemical Deprenylation of N6-Isopentenyladenosine (i6A) RNA. *Angewandte Chemie International Edition*, **59**, 10645–10650.

19. Deutsch,C., el Yacoubi,B., de Crécy-Lagard,V. and Iwata-Reuyl,D. (2012) Biosynthesis of threonylcarbamoyl adenosine (t6A), a universal tRNA nucleoside. *J Biol Chem*, **287**, 13666–13673.

20. Yokoyama,S., Miyazawa,T., Iitaka,Y., Yamaizumi,Z., Kasai,H. and Nishimura,S. (1979) Three-dimensional structure of hyper-modified nucleoside Q located in the wobbling position of tRNA. *Nature*, **282**, 107–109.

21. Perche-Letuvée,P., Molle,T., Forouhar,F., Mulliez,E. and Atta,M. (2014) Wybutosine biosynthesis: structural and mechanistic overview. *RNA Biol*, **11**, 1508–1518.

22. Meyer,K.D., Saletore,Y., Zumbo,P., Elemento,O., Mason,C.E. and Jaffrey,S.R. (2012) Comprehensive analysis of mRNA methylation reveals enrichment in 3' UTRs and near stop codons. *Cell*, **149**, 1635–1646.

23. Dominissini,D., Moshitch-Moshkovitz,S., Schwartz,S., Salmon-Divon,M., Ungar,L., Osenberg,S., Cesarkas,K., Jacob-Hirsch,J., Amariglio,N., Kupiec,M., *et al.* (2012) Topology of the human and mouse m6A RNA methylomes revealed by m6A-seq. *Nature*, **485**, 201–206.

24. Meyer,K.D. and Jaffrey,S.R. (2014) The dynamic epitranscriptome: N6-methyladenosine and gene expression control. *Nat Rev Mol Cell Biol*, **15**, 313–326.

25. Saletore,Y., Meyer,K., Korlach,J., Vilfan,I.D., Jaffrey,S. and Mason,C.E. (2012) The birth of the Epitranscriptome: deciphering the function of RNA modifications. *Genome Biology*, **13**, 175.

26. Lewis,C.J.T., Pan,T. and Kalsotra,A. (2017) RNA modifications and structures cooperate to guide RNA-protein interactions. *Nat Rev Mol Cell Biol*, **18**, 202–210.

27. Wiener,D. and Schwartz,S. (2021) The epitranscriptome beyond m6A. *Nature Reviews Genetics*, **22**, 119–131.

28. Roundtree,I.A., Evans,M.E., Pan,T. and He,C. (2017) Dynamic RNA Modifications in Gene Expression Regulation. *Cell*, **169**, 1187–1200.

29. Boo,S.H. and Kim,Y.K. (2020) The emerging role of RNA modifications in the regulation of mRNA stability. *Exp Mol Med*, **52**, 400–408.

30. Schaefer,M., Kapoor,U. and Jantsch,M.F. (2017) Understanding RNA modifications: the promises and technological bottlenecks of the "epitranscriptome." *Open Biol*, **7**, 170077.

31. Barbieri,I. and Kouzarides,T. (2020) Role of RNA modifications in cancer. *Nature Reviews Cancer*, **20**, 303–322.

32. Meyer,K.D. (2019) m(6)A-mediated translation regulation. *Biochim Biophys Acta Gene Regul Mech*, **1862**, 301–309.

33. Jiang,X., Liu,B., Nie,Z., Duan,L., Xiong,Q., Jin,Z., Yang,C. and Chen,Y. (2021) The role of m6A modification in the biological functions and diseases. *Signal Transduct Target Ther*, **6**, 74.

34. Wang,S., Lv,W., Li,T., Zhang,S., Wang,H., Li,X., Wang,L., Ma,D., Zang,Y., Shen,J., *et al.* (2022) Dynamic regulation and functions of mRNA m6A modification. *Cancer Cell Int*, **22**, 48.

35. Wang,T., Kong,S., Tao,M. and Ju,S. (2020) The potential role of RNA N6-methyladenosine in Cancer progression. *Mol Cancer*, **19**, 88.

36. Vu,L.P., Pickering,B.F., Cheng,Y., Zaccara,S., Nguyen,D., Minuesa,G., Chou,T., Chow,A., Saletore,Y., MacKay,M., *et al.* (2017) The N(6)-methyladenosine (m(6)A)-forming enzyme METTL3 controls myeloid differentiation of normal hematopoietic and leukemia cells. *Nat Med*, **23**, 1369–1376.

37. Shi,H., Wei,J. and He,C. (2019) Where, When, and How: Context-Dependent Functions of RNA Methylation Writers, Readers, and Erasers. *Mol Cell*, **74**, 640–650.

38. Boriack-Sjodin,P.A., Ribich,S. and Copeland,R.A. (2018) RNA-modifying proteins as anticancer drug targets. *Nature Reviews Drug Discovery*, **17**, 435–453.

39. Zaccara,S., Ries,R.J. and Jaffrey,S.R. (2019) Reading, writing and erasing mRNA methylation. *Nature Reviews Molecular Cell Biology*, **20**, 608–624.

40. Livneh,I., Moshitch-Moshkovitz,S., Amariglio,N., Rechavi,G. and Dominissini,D. (2020) The m6A epitranscriptome: transcriptome plasticity in brain development and function. *Nature Reviews Neuroscience*, **21**, 36–51.

41. Freund,I., Eigenbrod,T., Helm,M. and Dalpke,A.H. (2019) RNA Modifications Modulate Activation of Innate Toll-Like Receptors. *Genes (Basel)*, **10**, 92.

42. Morais,P., Adachi,H. and Yu,Y.-T. (2021) The Critical Contribution of Pseudouridine to mRNA COVID-19 Vaccines. *Front Cell Dev Biol*, **9**, 789427.

43. Motorin,Y. and Helm,M. (2022) RNA nucleotide methylation: 2021 update. *WIREs RNA*, **13**, e1691.

44. Furuichi,Y. and Miura,K.-I. (1975) A blocked structure at the 5′ terminus of mRNA from cytoplasmic polyhedrosis virus. *Nature*, **253**, 374–375.

45. Furuichi,Y., Morgan,M., Muthukrishnan,S. and Shatkin,A.J. (1975) Reovirus messenger RNA contains a methylated, blocked 5'-terminal structure: m-7G(5')ppp(5')G-MpCp-. *Proc Natl Acad Sci U S A*, **72**, 362–366.

46. Shatkin,A.J. (1976) Capping of eucaryotic mRNAs. *Cell*, **9**, 645–653.

47. Furuichi,Y. (2015) Discovery of m(7)G-cap in eukaryotic mRNAs. *Proc Jpn Acad Ser B Phys Biol Sci*, **91**, 394–409.

48. Pelletier,J., Schmeing,T.M. and Sonenberg,N. (2021) The multifaceted eukaryotic cap structure. *WIREs RNA*, **12**, e1636.

49. Muthukrishnan,S., Both,G.W., Furuichi,Y. and Shatkin,A.J. (1975) 5′-Terminal 7-methylguanosine in eukaryotic mRNA is required for translation. *Nature*, **255**, 33–37.

50. Both,G.W., Furuichi,Y., Muthukrishnan,S. and Shatkin,A.J. (1975) Ribosome binding to reovirus mRNA in protein synthesis requires 5' terminal 7-methylguanosine. *Cell*, **6**, 185–195.

51. Nagarajan,V.K., Jones,C.I., Newbury,S.F. and Green,P.J. (2013) XRN 5'→3' exoribonucleases: structure, mechanisms and functions. *Biochim Biophys Acta*, **1829**, 590–603.

52. Cheng,H., Dufu,K., Lee,C.-S., Hsu,J.L., Dias,A. and Reed,R. (2006) Human mRNA Export Machinery Recruited to the 5' End of mRNA. *Cell*, **127**, 1389–1400.

53. Visa,N., Izaurralde,E., Ferreira,J., Daneholt,B. and Mattaj,I.W. (1996) A nuclear cap-binding complex binds Balbiani ring pre-mRNA cotranscriptionally and accompanies the ribonucleoprotein particle during nuclear export. *J Cell Biol*, **133**, 5–14.

54. Ramanathan,A., Robb,G.B. and Chan,S.-H. (2016) mRNA capping: biological functions and applications. *Nucleic Acids Res*, **44**, 7511–7526.

55. Bradrick,S.S. (2017) Causes and Consequences of Flavivirus RNA Methylation. *Front Microbiol*, **8**, 2374.

56. Chang,L.-J. and Chen,T.-H. (2021) NSP16 2'-O-MTase in Coronavirus Pathogenesis: Possible Prevention and Treatments Strategies. *Viruses*, **13**, 538.

57. Menachery,V.D., Debbink,K. and Baric,R.S. (2014) Coronavirus non-structural protein 16: evasion, attenuation, and possible treatments. *Virus Res*, **194**, 191–199.

58. Daffis,S., Szretter,K.J., Schriewer,J., Li,J., Youn,S., Errett,J., Lin,T.-Y., Schneller,S., Zust,R., Dong,H., *et al.* (2010) 2'-O methylation of the viral mRNA cap evades host restriction by IFIT family members. *Nature*, **468**, 452–456.

59. Motorin,Y. and Helm,M. (2011) RNA nucleotide methylation. *WIREs RNA*, **2**, 611–631.

60. Guy,M.P. and Phizicky,E.M. (2015) Conservation of an intricate circuit for crucial modifications of the tRNAPhe anticodon loop in eukaryotes. *RNA*, **21**, 61–74.

61. Guy,M.P., Podyma,B.M., Preston,M.A., Shaheen,H.H., Krivos,K.L., Limbach,P.A., Hopper,A.K. and Phizicky,E.M. (2012) Yeast Trm7 interacts with distinct proteins for critical modifications of the tRNAPhe anticodon loop. *RNA*, **18**, 1921–1933.

62. Han,L. and Phizicky,E.M. (2018) A rationale for tRNA modification circuits in the anticodon loop. *RNA*, **24**, 1277–1284.

63. Zhou,M., Long,T., Fang,Z.-P., Zhou,X.-L., Liu,R.-J. and Wang,E.-D. (2015) Identification of determinants for tRNA substrate recognition by Escherichia coli C/U34 2'-O-methyltransferase. *RNA Biol*, **12**, 900–911.

64. Kleiber,N., Lemus-Diaz,N., Stiller,C., Heinrichs,M., Mai,M.M.-Q., Hackert,P., Richter-Dennerlein,R., Höbartner,C., Bohnsack,K.E. and Bohnsack,M.T. (2022) The RNA methyltransferase METTL8 installs m(3)C(32) in mitochondrial tRNAs(Thr/Ser(UCN)) to optimise tRNA structure and mitochondrial translation. *Nat Commun*, **13**, 209.

65. Lentini,J.M., Bargabos,R., Chen,C. and Fu,D. (2022) Methyltransferase METTL8 is required for 3-methylcytosine modification in human mitochondrial tRNAs. *J Biol Chem*, **298**, 101788.

66. Schöller,E., Marks,J., Marchand,V., Bruckmann,A., Powell,C.A., Reichold,M., Mutti,C.D., Dettmer,K., Feederle,R., Hüttelmaier,S., *et al.* (2021) Balancing of mitochondrial translation through METTL8-mediated m^{3}C modification of mitochondrial tRNAs. *Molecular Cell*, **81**, 4810-4825.e12.

67. Schubert,H.L., Blumenthal,R.M. and Cheng,X. (2003) Many paths to methyltransfer: a chronicle of convergence. *Trends Biochem Sci*, **28**, 329–335.

68. Blanco,S. and Frye,M. (2014) Role of RNA methyltransferases in tissue renewal and pathology. *Curr Opin Cell Biol*, **31**, 1–7.

69. Lyko,F. (2018) The DNA methyltransferase family: a versatile toolkit for epigenetic regulation. *Nature Reviews Genetics*, **19**, 81–92.

70. Boriack-Sjodin,P.A. and Swinger,K.K. (2016) Protein Methyltransferases: A Distinct, Diverse, and Dynamic Family of Enzymes. *Biochemistry*, **55**, 1557–1569.

71. Fujioka,M. (1992) Mammalian small molecule methyltransferases: Their structural and functional features. *International Journal of Biochemistry*, **24**, 1917–1924.

72. Gao,J., Cahill,C.M., Huang,X., Roffman,J.L., Lamon-Fava,S., Fava,M., Mischoulon,D. and Rogers,J.T. (2018) S-Adenosyl Methionine and Transmethylation Pathways in Neuropsychiatric Diseases Throughout Life. *Neurotherapeutics*, **15**, 156–175.

73. Martin,J.L. and McMillan,F.M. (2002) SAM (dependent) I AM: the S-adenosylmethionine-dependent methyltransferase fold. *Current Opinion in Structural Biology*, **12**, 783–793.

74. Sun,Q., Huang,M. and Wei,Y. (2021) Diversity of the reaction mechanisms of SAM-dependent enzymes. *Acta Pharm Sin B*, **11**, 632–650.

75. Wlodarski,T., Kutner,J., Towpik,J., Knizewski,L., Rychlewski,L., Kudlicki,A., Rowicka,M., Dziembowski,A. and Ginalski,K. (2011) Comprehensive structural and substrate specificity classification of the Saccharomyces cerevisiae methyltransferome. *PLoS One*, **6**, e23168–e23168.

76. Yang,J., Kulkarni,K., Manolaridis,I., Zhang,Z., Dodd,R.B., Mas-Droux,C. and Barford,D. (2011) Mechanism of Isoprenylcysteine Carboxyl Methylation from the Crystal Structure of the Integral Membrane Methyltransferase ICMT. *Molecular Cell*, **44**, 997–1004.

77. Esakova,O.A., Grove,T.L., Yennawar,N.H., Arcinas,A.J., Wang,B., Krebs,C., Almo,S.C. and Booker,S.J. (2021) Structural basis for tRNA methylthiolation by the radical SAM enzyme MiaB. *Nature*, **597**, 566–570.

78. Forouhar,F., Kuzin,A., Seetharaman,J., Lee,I., Zhou,W., Abashidze,M., Chen,Y., Yong,W., Janjua,H., Fang,Y., *et al.* (2007) Functional insights from structural genomics. *Journal of Structural and Functional Genomics*, **8**, 37–44.

79. Kimura,S., Miyauchi,K., Ikeuchi,Y., Thiaville,P.C., Crécy-Lagard,V. de and Suzuki,T. (2014) Discovery of the β-barrel-type RNA methyltransferase responsible for N6-methylation of N6-threonylcarbamoyladenosine in tRNAs. *Nucleic Acids Res*, **42**, 9350–9365.

80. Currie,M.A., Brown,G., Wong,A., Ohira,T., Sugiyama,K., Suzuki,T., Yakunin,A.F. and Jia,Z. (2017) Structural and functional characterization of the TYW3/Taw3 class of SAM-dependent methyltransferases. *RNA*, **23**, 346–354.

81. Wolf,Y.I., Brenner,S.E., Bash,P.A. and Koonin,E. v (1999) Distribution of Protein Folds in the Three Superkingdoms of Life. *Genome Research*, **9**, 17–26.

82. Mosquera-Rendón,J., Cárdenas-Brito,S., Pineda,J.D., Corredor,M. and Benítez-Páez,A. (2014) Evolutionary and sequence-based relationships in bacterial AdoMet-dependent non-coding RNA methyltransferases. *BMC Res Notes*, **7**, 440.

83. Tkaczuk,K.L., Dunin-Horkawicz,S., Purta,E. and Bujnicki,J.M. (2007) Structural and evolutionary bioinformatics of the SPOUT superfamily of methyltransferases. *BMC Bioinformatics*, **8**, 73.

84. Smietanski,M., Werner,M., Purta,E., Kaminska,K.H., Stepinski,J., Darzynkiewicz,E., Nowotny,M. and Bujnicki,J.M. (2014) Structural analysis of human 2'-O-ribose methyltransferases involved in mRNA cap structure formation. *Nat Commun*, **5**, 3004.

85. Dillon,S.C., Zhang,X., Trievel,R.C. and Cheng,X. (2005) The SET-domain protein superfamily: protein lysine methyltransferases. *Genome Biol*, **6**, 227.

86. Vey,J.L. and Drennan,C.L. (2011) Structural insights into radical generation by the radical SAM superfamily. *Chem Rev*, **111**, 2487–2506.

87. Mehta,A.P., Abdelwahed,S.H., Mahanta,N., Fedoseyenko,D., Philmus,B., Cooper,L.E., Liu,Y., Jhulki,I., Ealick,S.E. and Begley,T.P. (2015) Radical S-adenosylmethionine (SAM) enzymes in cofactor biosynthesis: a treasure trove of complex organic radical rearrangement reactions. *J Biol Chem*, **290**, 3980–3986.

88. Hori,H. (2017) Transfer RNA methyltransferases with a SpoU-TrmD (SPOUT) fold and their modified nucleosides in tRNA. *Biomolecules*, **7**, 23.

89. Delk,A.S., Nagle,D.P. and Rabinowitz,J.C. (1980) Methylenetetrahydrofolate-dependent biosynthesis of ribothymidine in transfer RNA of Streptococcus faecalis. Evidence for reduction of the 1-carbon unit by FADH2. *Journal of Biological Chemistry*, **255**, 4387–4390.

90. Urbonavicius,J., Skouloubris,S., Myllykallio,H. and Grosjean,H. (2005) Identification of a novel gene encoding a flavin-dependent tRNA:m5U methyltransferase in bacteria--evolutionary implications. *Nucleic Acids Res*, **33**, 3955–3964.

91. Costi,M., Ferrari,S., Venturelli,A., Calò,S., Tondi,D. and Barlocco,D. (2005) Thymidylate Synthase Structure, Function and Implication in Drug Discovery. *Curr Med Chem*, **12**, 2241–2258.

92. Carreras,C.W. and Santi,D. v (1995) The catalytic mechanism and structure of thymidylate synthase. *Annual Review of Biochemistry*, **64**, 721–762.

93. Myllykallio Hannu, Skouloubris Skouloudis, Grosjean Henri and Liebl,U. (2009) Folate-Dependent Thymidylate-Forming Enzymes: Parallels between DNA and RNA Metabolic Enzymes and Evolutionary Implications. *Madame Curie Bioscience Database [Internet]. Austin (TX): Landes Bioscience*.

94. Doukov,T., Seravalli,J., Stezowski,J.J. and Ragsdale,S.W. (2000) Crystal structure of a methyltetrahydrofolate- and corrinoid-dependent methyltransferase. *Structure*, **8**, 817–830.

95. Nishimasu,H., Ishitani,R., Yamashita,K., Iwashita,C., Hirata,A., Hori,H. and Nureki,O. (2009) Atomic structure of a folate/FAD-dependent tRNA T54 methyltransferase. *Proc Natl Acad Sci U S A*, **106**, 8180–8185.

96. Koutmos,M., Datta,S., Pattridge,K.A., Smith,J.L. and Matthews,R.G. (2009) Insights into the reactivation of cobalamin-dependent methionine synthase. *Proc Natl Acad Sci U S A*, **106**, 18527–18532.

97. Fischer,T.R., Meidner,L., Schwickert,M., Weber,M., Zimmermann,R.A., Kersten,C., Schirmeister,T. and Helm,M. (2022) Chemical biology and medicinal chemistry of RNA methyltransferases. *Nucleic Acids Research*, 10.1093/nar/gkac224.

98. Schluckebier,G., Zhong,P., Stewart,K.D., Kavanaugh,T.J. and Abad-Zapatero,C. (1999) The 2.2 Å structure of the rRNA methyltransferase ErmC' and its complexes with cofactor and cofactor analogs: implications for the reaction mechanism11Edited by I. A. Wilson. *Journal of Molecular Biology*, **289**, 277–291.

99. Qiu,C., Sawada,K., Zhang,X. and Cheng,X. (2002) The PWWP domain of mammalian DNA methyltransferase Dnmt3b defines a new family of DNA-binding folds. *Nat Struct Biol*, **9**, 217–224.

100. Krafcikova,P., Silhan,J., Nencka,R. and Boura,E. (2020) Structural analysis of the SARS-CoV-2 methyltransferase complex involved in RNA cap creation bound to sinefungin. *Nat Commun*, **11**, 3717.

101. Nencka,R., Silhan,J., Klima,M., Otava,T., Kocek,H., Krafcikova,P. and Boura,E. (2022) Coronaviral RNA-methyltransferases: function, structure and inhibition. *Nucleic Acids Res*, **50**, 635–650.

102. Dixon,M.M., Huang,S., Matthews,R.G. and Ludwig,M. (1996) The structure of the C-terminal domain of methionine synthase: presenting S-adenosylmethionine for reductive methylation of B12. *Structure*, **4**, 1263–1275.

103. Schubert,H.L., Wilson,K.S., Raux,E., Woodcock,S.C. and Warren,M.J. (1998) The X-ray structure of a cobalamin biosynthetic enzyme, cobalt-precorrin-4 methyltransferase. *Nature Structural Biology*, **5**, 585–592.

104. Michel,G., Sauvé,V., Larocque,R., Li,Y., Matte,A. and Cygler,M. (2002) The Structure of the RlmB 23S rRNA Methyltransferase Reveals a New Methyltransferase Fold with a Unique Knot. *Structure*, **10**, 1303–1315.

105. Jacobs,S.A., Harp,J.M., Devarakonda,S., Kim,Y., Rastinejad,F. and Khorasanizadeh,S. (2002) The active site of the SET domain is constructed on a knot. *Nature Structural Biology*, **9**, 833–838.

106. Stephenson,R.C. and Clarke,S. (1992) Characterization of a rat liver protein carboxyl methyltransferase involved in the maturation of proteins with the -CXXX C-terminal sequence motif. *Journal of Biological Chemistry*, **267**, 13314–13319.

107. Kaminska,K.H., Purta,E., Hansen,L.H., Bujnicki,J.M., Vester,B. and Long,K.S. (2010) Insights into the structure, function and evolution of the radical-SAM 23S rRNA methyltransferase Cfr that confers antibiotic resistance in bacteria. *Nucleic Acids Res*, **38**, 1652–1663.

108. van den Wyngaert,I., Sprengel,J., Kass,S.U. and Luyten,W.H.M.L. (1998) Cloning and analysis of a novel human putative DNA methyltransferase. *FEBS Letters*, **426**, 283–289.

109. Yoder,J.A. and Bestor,T.H. (1998) A Candidate Mammalian DNA Methyltransferase Related to pmt1p of Fission Yeast. *Human Molecular Genetics*, **7**, 279–284.

110. Okano,M., Xie,S. and Li,E. (1998) Dnmt2 is not required for de novo and maintenance methylation of viral DNA in embryonic stem cells. *Nucleic Acids Res*, **26**, 2536–2540.

111. Jeltsch,A., Ehrenhofer-Murray,A., Jurkowski,T.P., Lyko,F., Reuter,G., Ankri,S., Nellen,W., Schaefer,M. and Helm,M. (2017) Mechanism and biological role of Dnmt2 in Nucleic Acid Methylation. *RNA Biol*, **14**, 1108–1123.

112. Jurkowski,T.P. and Jeltsch,A. (2011) On the evolutionary origin of eukaryotic DNA methyltransferases and Dnmt2. *PLoS One*, **6**, e28104–e28104.

113. Goll,M.G. and Bestor,T.H. (2005) Eukaryotic cytosine methyltransferases. *Annual Review of Biochemistry*, **74**, 481–514.

114. Schaefer,M. and Lyko,F. (2010) Solving the Dnmt2 enigma. *Chromosoma*, **119**, 35–40.

115. Shanmugam,R., Aklujkar,M., Schäfer,M., Reinhardt,R., Nickel,O., Reuter,G., Lovley,D.R., Ehrenhofer-Murray,A., Nellen,W., Ankri,S., *et al.* (2014) The Dnmt2 RNA methyltransferase homolog of Geobacter sulfurreducens specifically methylates tRNA-Glu. *Nucleic Acids Res*, **42**, 6487–6496.

116. Goll,M.G., Finn,K., A,M.K., A,Y.J., Chih-Lin,H., Xiaoyu,Z., G,G.K., E,J.S. and H,B.T. (2006) Methylation of tRNAAsp by the DNA Methyltransferase Homolog Dnmt2. *Science (1979)*, **311**, 395–398.

117. Dong,A., Yoder,J.A., Zhang,X., Zhou,L., Bestor,T.H. and Cheng,X. (2001) Structure of human DNMT2, an enigmatic DNA methyltransferase homolog that displays denaturant-resistant binding to DNA. *Nucleic Acids Res*, **29**, 439–448.

118. Li,S., Du,J., Yang,H., Yin,J., Ding,J. and Zhong,J. (2013) Functional and structural characterization of DNMT2 from Spodoptera frugiperda. *Journal of Molecular Cell Biology*, **5**, 64–66.

119. Schulz,E.C., Roth,H.M., Ankri,S. and Ficner,R. (2012) Structure analysis of Entamoeba histolytica DNMT2 (EhMeth). *PLoS One*, **7**, e38728–e38728.

120. Johannsson,S., Neumann,P., Wulf,A., Welp,L.M., Gerber,H.-D., Krull,M., Diederichsen,U., Urlaub,H. and Ficner,R. (2018) Structural insights into the stimulation of S. pombe Dnmt2 catalytic efficiency by the tRNA nucleoside queuosine. *Sci Rep*, **8**, 8880.

121. Schrödinger LLC (2019) The PyMOL Molecular Graphics System, Version 2.3.4.

122. Gana,R., Rao,S., Huang,H., Wu,C. and Vasudevan,S. (2013) Structural and functional studies of S-adenosyl-L-methionine binding proteins: a ligand-centric approach. *BMC Struct Biol*, **13**, 6.

123. Jeltsch,A. (2002) Beyond Watson and Crick: DNA Methylation and Molecular Enzymology of DNA Methyltransferases. *ChemBioChem*, **3**, 274–293.

124. Jurkowski,T.P., Meusburger,M., Phalke,S., Helm,M., Nellen,W., Reuter,G. and Jeltsch,A. (2008) Human DNMT2 methylates tRNA(Asp) molecules using a DNA methyltransferase-like catalytic mechanism. *RNA*, **14**, 1663–1670.

125. Bohnsack,K.E., Höbartner,C. and Bohnsack,M.T. (2019) Eukaryotic 5-methylcytosine (m5C) RNA Methyltransferases: Mechanisms, Cellular Functions, and Links to Disease. *Genes (Basel)*, **10**, 102.

126. Liu,Y. and Santi,D. v (2000) m5C RNA and m5C DNA methyl transferases use different cysteine residues as catalysts. *Proc Natl Acad Sci U S A*, **97**, 8263–8265.

127. Bujnicki,J.M., Feder,M., Ayres,C.L. and Redman,K.L. (2004) Sequence-structure-function studies of tRNA:m5C methyltransferase Trm4p and its relationship to DNA:m5C and RNA:m5U methyltransferases. *Nucleic Acids Res*, **32**, 2453–2463.

128. Katoh,M., Curk,T., Xu,Q., Zupan,B., Kuspa,A. and Shaulsky,G. (2006) Developmentally regulated DNA methylation in Dictyostelium discoideum. *Eukaryot Cell*, **5**, 18–25.

129. Krauss,V. and Reuter,G. (2011) Chapter 4 - DNA Methylation in Drosophila—A Critical Evaluation. In Cheng,X., Blumenthal,R.M. (eds), *Progress in Molecular Biology and Translational Science*. Academic Press, Vol. 101, pp. 177–191.

130. Gowher,H., Leismann,O. and Jeltsch,A. (2000) DNA of Drosophila melanogaster contains 5-methylcytosine. *EMBO J*, **19**, 6918–6923.

131. Lyko,F., Ramsahoye,B.H. and Jaenisch,R. (2000) DNA methylation in Drosophila melanogaster. *Nature*, **408**, 538–540.

132. Kunert,N., Marhold,J., Stanke,J., Stach,D. and Lyko,F. (2003) A Dnmt2-like protein mediates DNA methylation in Drosophila. *Development*, **130**, 5083–5090.

133. Hermann,A., Schmitt,S. and Jeltsch,A. (2003) The Human Dnmt2 Has Residual DNA-(Cytosine-C5) Methyltransferase Activity. *Journal of Biological Chemistry*, **278**, 31717–31721.

134. Geyer,K.K., Rodríguez López,C.M., Chalmers,I.W., Munshi,S.E., Truscott,M., Heald,J., Wilkinson,M.J. and Hoffmann,K.F. (2011) Cytosine methylation regulates oviposition in the pathogenic blood fluke Schistosoma mansoni. *Nat Commun*, **2**, 424.

135. Phalke,S., Nickel,O., Walluscheck,D., Hortig,F., Onorati,M.C. and Reuter,G. (2009) Retrotransposon silencing and telomere integrity in somatic cells of Drosophila depends on the cytosine-5 methyltransferase DNMT2. *Nature Genetics*, **41**, 696–702.

136. Kuhlmann,M., Borisova,B.E., Kaller,M., Larsson,P., Stach,D., Na,J., Eichinger,L., Lyko,F., Ambros,V., Söderbom,F., *et al.* (2005) Silencing of retrotransposons in Dictyostelium by DNA methylation and RNAi. *Nucleic Acids Res*, **33**, 6405–6417.

137. Claudio-Piedras,F., Recio-Tótoro,B., Condé,R., Hernández-Tablas,J.M., Hurtado-Sil,G. and Lanz-Mendoza,H. (2020) DNA Methylation in Anopheles albimanus Modulates the Midgut Immune Response Against Plasmodium berghei. *Front Immunol*, **10**, 3025.

138. Raddatz,G., Guzzardo,P.M., Olova,N., Fantappié,M.R., Rampp,M., Schaefer,M., Reik,W., Hannon,G.J. and Lyko,F. (2013) Dnmt2-dependent methylomes lack defined DNA methylation patterns. *Proc Natl Acad Sci U S A*, **110**, 8627–8631.

139. Schaefer,M. and Lyko,F. (2010) Lack of evidence for DNA methylation of Invader4 retroelements in Drosophila and implications for Dnmt2-mediated epigenetic regulation. *Nature Genetics*, **42**, 920–921.

140. Assaf,Z., E,M.I., Pedro,S. and Daniel,Z. (2010) Genome-Wide Evolutionary Analysis of Eukaryotic DNA Methylation. *Science (1979)*, **328**, 916–919.

141. Müller,S., Windhof,I.M., Maximov,V., Jurkowski,T., Jeltsch,A., Förstner,K.U., Sharma,C.M., Gräf,R. and Nellen,W. (2013) Target recognition, RNA methylation activity and transcriptional regulation of the Dictyostelium discoideum Dnmt2-homologue (DnmA). *Nucleic Acids Res*, **41**, 8615–8627.

142. Schaefer,M., Pollex,T., Hanna,K., Tuorto,F., Meusburger,M., Helm,M. and Lyko,F. (2010) RNA methylation by Dnmt2 protects transfer RNAs against stress-induced cleavage. *Genes Dev*, **24**, 1590–1595.

143. Becker,M., Müller,S., Nellen,W., Jurkowski,T.P., Jeltsch,A. and Ehrenhofer-Murray,A.E. (2012) Pmt1, a Dnmt2 homolog in Schizosaccharomyces pombe, mediates tRNA methylation in response to nutrient signaling. *Nucleic Acids Res*, **40**, 11648–11658.

144. Li,H., Zhu,D., Wu,J., Ma,Y., Cai,C., Chen,Y., Qin,M. and Dai,H. (2021) New substrates and determinants for tRNA recognition of RNA methyltransferase DNMT2/TRDMT1. *RNA Biology*, **18**, 2531–2545.

145. Chen,H., Yang,H., Zhu,X., Yadav,T., Ouyang,J., Truesdell,S.S., Tan,J., Wang,Y., Duan,M., Wei,L., *et al.* (2020) m(5)C modification of mRNA serves a DNA damage code to promote homologous recombination. *Nat Commun*, **11**, 2834.

146. Xue,S., Xu,H., Sun,Z., Shen,H., Chen,S., Ouyang,J., Zhou,Q., Hu,X. and Cui,H. (2019) Depletion of TRDMT1 affects 5-methylcytosine modification of mRNA and inhibits HEK293 cell proliferation and migration. *Biochemical and Biophysical Research Communications*, **520**, 60–66.

147. Dev,R.R., Ganji,R., Singh,S.P., Mahalingam,S., Banerjee,S. and Khosla,S. (2017) Cytosine methylation by DNMT2 facilitates stability and survival of HIV-1 RNA in the host cell during infection. *Biochemical Journal*, **474**, 2009–2026.

148. Kaiser,S., Jurkowski,T.P., Kellner,S., Schneider,D., Jeltsch,A. and Helm,M. (2017) The RNA methyltransferase Dnmt2 methylates DNA in the structural context of a tRNA. *RNA Biol*, **14**, 1241–1251.

149. Jurkowski,T.P., Shanmugam,R., Helm,M. and Jeltsch,A. (2012) Mapping the tRNA Binding Site on the Surface of Human DNMT2 Methyltransferase. *Biochemistry*, **51**, 4438–4444.

150. Easwaran,H.P., Schermelleh,L., Leonhardt,H. and Cardoso,M.C. (2004) Replication-independent chromatin loading of Dnmt1 during G2 and M phases. *EMBO Rep*, **5**, 1181–1186.

151. Bachman,K.E., Rountree,M.R. and Baylin,S.B. (2001) Dnmt3a and Dnmt3b Are Transcriptional Repressors That Exhibit Unique Localization Properties to Heterochromatin *. *Journal of Biological Chemistry*, **276**, 32282–32287.

152. Fisher,O., Siman-Tov,R. and Ankri,S. (2004) Characterization of cytosine methylated regions and 5-cytosine DNA methyltransferase (Ehmeth) in the protozoan parasite Entamoeba histolytica. *Nucleic Acids Res*, **32**, 287–297.

153. Schaefer,M., Steringer,J.P. and Lyko,F. (2008) The Drosophila cytosine-5 methyltransferase Dnmt2 is associated with the nuclear matrix and can access DNA during mitosis. *PLoS One*, **3**, e1414–e1414.

154. Rai,K., Chidester,S., Zavala,C. v, Manos,E.J., James,S.R., Karpf,A.R., Jones,D.A. and Cairns,B.R. (2007) Dnmt2 functions in the cytoplasm to promote liver, brain, and retina development in zebrafish. *Genes Dev*, **21**, 261–266.

155. Hopper,A.K. and Phizicky,E.M. (2003) tRNA transfers to the limelight. *Genes & Development*, **17**, 162–180.

156. Thiagarajan,D., Dev,R.R. and Khosla,S. (2011) The DNA methyltranferase Dnmt2 participates in RNA processing during cellular stress. *Epigenetics*, **6**, 103–113.

157. Agris,P.F., Vendeix,F.A.P. and Graham,W.D. (2007) tRNA's Wobble Decoding of the Genome: 40 Years of Modification. *Journal of Molecular Biology*, **366**, 1–13.

158. el Yacoubi,B., Bailly,M. and de Crécy-Lagard,V. (2012) Biosynthesis and Function of Posttranscriptional Modifications of Transfer RNAs. *Annual Review of Genetics*, **46**, 69–95.

159. Tuorto,F., Liebers,R., Musch,T., Schaefer,M., Hofmann,S., Kellner,S., Frye,M., Helm,M., Stoecklin,G. and Lyko,F. (2012) RNA cytosine methylation by Dnmt2 and NSun2 promotes tRNA stability and protein synthesis. *Nature Structural & Molecular Biology*, **19**, 900–905.

160. Shanmugam,R., Fierer,J., Kaiser,S., Helm,M., Jurkowski,T.P. and Jeltsch,A. (2015) Cytosine methylation of tRNA-Asp by DNMT2 has a role in translation of proteins containing poly-Asp sequences. *Cell Discov*, **1**, 15010.

161. Tuorto,F., Herbst,F., Alerasool,N., Bender,S., Popp,O., Federico,G., Reitter,S., Liebers,R., Stoecklin,G., Gröne,H.-J., *et al.* (2015) The tRNA methyltransferase Dnmt2 is required for accurate polypeptide synthesis during haematopoiesis. *EMBO J*, **34**, 2350–2362.

162. Müller,M., Hartmann,M., Schuster,I., Bender,S., Thüring,K.L., Helm,M., Katze,J.R., Nellen,W., Lyko,F. and Ehrenhofer-Murray,A.E. (2015) Dynamic modulation of Dnmt2-dependent tRNA methylation by the micronutrient queuine. *Nucleic Acids Res*, **43**, 10952–10962.

163. Thompson,D.M. and Parker,R. (2009) Stressing Out over tRNA Cleavage. *Cell*, **138**, 215–219.

164. Rashad,S., Niizuma,K. and Tominaga,T. (2020) tRNA cleavage: a new insight. *Neural Regen Res*, **15**, 47–52.

165. Sobala,A. and Hutvagner,G. (2013) Small RNAs derived from the 5' end of tRNA can inhibit protein translation in human cells. *RNA Biol*, **10**, 553–563.

166. Shen,L., Tan,Z., Gan,M., Li,Q., Chen,L., Niu,L., Jiang,D., Zhao,Y., Wang,J., Li,X., *et al.* (2019) tRNA-Derived Small Non-Coding RNAs as Novel Epigenetic Molecules Regulating Adipogenesis. *Biomolecules*, **9**, 274.

167. Durdevic,Z., Mobin,M.B., Hanna,K., Lyko,F. and Schaefer,M. (2013) The RNA Methyltransferase Dnmt2 Is Required for Efficient Dicer-2-Dependent siRNA Pathway Activity in Drosophila. *Cell Reports*, **4**, 931–937.

168. Durdevic,Z., Hanna,K., Gold,B., Pollex,T., Cherry,S., Lyko,F. and Schaefer,M. (2013) Efficient RNA virus control in Drosophila requires the RNA methyltransferase Dnmt2. *EMBO Rep*, **14**, 269–275.

169. Lewinska,A., Adamczyk-Grochala,J., Kwasniewicz,E., Deregowska,A., Semik,E., Zabek,T. and Wnuk,M. (2018) Reduced levels of methyltransferase DNMT2 sensitize human fibroblasts to oxidative stress and DNA damage that is accompanied by changes in proliferation-related miRNA expression. *Redox Biol*, **14**, 20–34.

170. Mytych,J., Lewinska,A., Bielak-Zmijewska,A., Grabowska,W., Zebrowski,J. and Wnuk,M. (2014) Nanodiamond-mediated impairment of nucleolar activity is accompanied by oxidative stress and DNMT2 upregulation in human cervical carcinoma cells. *Chemico-Biological Interactions*, **220**, 51–63.

171. Lewinska,A., Wnuk,M., Grabowska,W., Zabek,T., Semik,E., Sikora,E. and Bielak-Zmijewska,A. (2015) Curcumin induces oxidation-dependent cell cycle arrest mediated by SIRT7 inhibition of rDNA transcription in human aortic smooth muscle cells. *Toxicology Letters*, **233**, 227–238.

172. Mytych,J., Zebrowski,J., Lewinska,A. and Wnuk,M. (2017) Prolonged Effects of Silver Nanoparticles on p53/p21 Pathway-Mediated Proliferation, DNA Damage Response, and Methylation Parameters in HT22 Hippocampal Neuronal Cells. *Mol Neurobiol*, **54**, 1285–1300.

173. Lin,M.-J., Tang,L.-Y., Reddy,M.N. and Shen,C.-K.J. (2005) DNA Methyltransferase Gene dDnmt2 and Longevity of Drosophila. *Journal of Biological Chemistry*, **280**, 861–864.

174. Fisher,O., Siman-Tov,R. and Ankri,S. (2006) Pleiotropic phenotype in Entamoeba histolytica overexpressing DNA methyltransferase (Ehmeth). *Molecular and Biochemical Parasitology*, **147**, 48–54.

175. Hertz,R., Tovy,A., Kirschenbaum,M., Geffen,M., Nozaki,T., Adir,N. and Ankri,S. (2014) The Entamoeba histolytica Dnmt2 homolog (Ehmeth) confers resistance to nitrosative stress. *Eukaryot Cell*, **13**, 494–503.

176. Forbes,S.A., Beare,D., Gunasekaran,P., Leung,K., Bindal,N., Boutselakis,H., Ding,M., Bamford,S., Cole,C., Ward,S., *et al.* (2015) COSMIC: exploring the world's knowledge of somatic mutations in human cancer. *Nucleic Acids Res*, **43**, D805–D811.

177. Li,L.-L. and Wang,S.-S. (2017) DNA methyltransferase (DNMTs) expression in cervical cancer tissues and its relationship with HPV infection and tumor malignancy. *Journal of Hainan Medical University*, **23**, 136–139.

178. Tzelepi,V., Logotheti,S., Efstathiou,E., Troncoso,P., Aparicio,A., Sakellakis,M., Hoang,A., Perimenis,P., Melachrinou,M., Logothetis,C., *et al.* (2020) Epigenetics and prostate cancer: defining the timing of DNA methyltransferase deregulation during prostate cancer progression. *Pathology*, **52**, 218–227.

179. Elhardt,W., Shanmugam,R., Jurkowski,T.P. and Jeltsch,A. (2015) Somatic cancer mutations in the DNMT2 tRNA methyltransferase alter its catalytic properties. *Biochimie*, **112**, 66–72.

180. Bloniarz,D., Adamczyk-Grochala,J., Lewinska,A. and Wnuk,M. (2021) The lack of functional DNMT2/TRDMT1 gene modulates cancer cell responses during drug-induced senescence. *Aging*, **13**, 15833–15874.

181. Cheng,J.X., Chen,L., Li,Y., Cloe,A., Yue,M., Wei,J., Watanabe,K.A., Shammo,J.M., Anastasi,J., Shen,Q.J., *et al.* (2018) RNA cytosine methylation and methyltransferases mediate chromatin organization and 5-azacytidine response and resistance in leukaemia. *Nat Commun*, **9**, 1163.

182. Durdevic,Z. and Schaefer,M. (2013) Dnmt2 methyltransferases and immunity: An ancient overlooked connection between nucleotide modification and host defense? *BioEssays*, **35**, 1044–1049.

183. Bhattacharya,T., Rice,D.W., Crawford,J.M., Hardy,R.W. and Newton,I.L.G. (2021) Evidence of Adaptive Evolution in Wolbachia-Regulated Gene DNMT2 and Its Role in the Dipteran Immune Response and Pathogen Blocking. *Viruses*, **13**, 1464.

184. Zhang,G., Hussain,M., O'Neill,S.L. and Asgari,S. (2013) Wolbachia uses a host microRNA to regulate transcripts of a methyltransferase, contributing to dengue virus inhibition in Aedes aegypti. *Proc Natl Acad Sci U S A*, **110**, 10276–10281.

185. Bhattacharya,T., Yan,L., Crawford,J.M., Zaher,H., Newton,I.L.G. and Hardy,R.W. (2022) Differential viral RNA methylation contributes to pathogen blocking in Wolbachia-colonized arthropods. *PLoS Pathog*, **18**, e1010393–e1010393.

186. Baradaran,E., Moharramipour,S., Asgari,S. and Mehrabadi,M. (2019) Induction of DNA methyltransferase genes in Helicoverpa armigera following injection of pathogenic bacteria modulates expression of antimicrobial peptides and affects bacterial proliferation. *Journal of Insect Physiology*, **118**, 103939.

187. Ganesan,A., Arimondo,P.B., Rots,M.G., Jeronimo,C. and Berdasco,M. (2019) The timeline of epigenetic drug discovery: from reality to dreams. *Clin Epigenetics*, **11**, 174.

188. Jonkhout,N., Tran,J., Smith,M.A., Schonrock,N., Mattick,J.S. and Novoa,E.M. (2017) The RNA modification landscape in human disease. *RNA*, **23**, 1754–1769.

189. Chen,Q., Yan,W. and Duan,E. (2016) Epigenetic inheritance of acquired traits through sperm RNAs and sperm RNA modifications. *Nat Rev Genet*, **17**, 733–743.

190. Qi,C., Menghong,Y., Zhonghong,C., Xin,L., Yunfang,Z., Junchao,S., Gui-hai,F., Hongying,P., Xudong,Z., Ying,Z., *et al.* (2016) Sperm tsRNAs contribute to intergenerational inheritance of an acquired metabolic disorder. *Science (1979)*, **351**, 397–400.

191. Rassoulzadegan,M., Grandjean,V., Gounon,P., Vincent,S., Gillot,I. and Cuzin,F. (2006) RNA-mediated non-mendelian inheritance of an epigenetic change in the mouse. *Nature*, **441**, 469–474.

192. Liebers,R., Rassoulzadegan,M. and Lyko,F. (2014) Epigenetic regulation by heritable RNA. *PLoS Genet*, **10**, e1004296–e1004296.

193. Zhang,Y., Zhang,X., Shi,J., Tuorto,F., Li,X., Liu,Y., Liebers,R., Zhang,L., Qu,Y., Qian,J., *et al.* (2018) Dnmt2 mediates intergenerational transmission of paternally acquired metabolic disorders through sperm small non-coding RNAs. *Nat Cell Biol*, **20**, 535–540.

194. Sharma,U., Conine,C.C., Shea,J.M., Boskovic,A., Derr,A.G., Bing,X.Y., Belleannee,C., Kucukural,A., Serra,R.W., Sun,F., *et al.* (2016) Biogenesis and function of tRNA fragments during sperm maturation and fertilization in mammals. *Science*, **351**, 391–396.

195. Sarker,G., Sun,W., Rosenkranz,D., Pelczar,P., Opitz,L., Efthymiou,V., Wolfrum,C. and Peleg-Raibstein,D. (2019) Maternal overnutrition programs hedonic and metabolic phenotypes across generations through sperm tsRNAs. *Proc Natl Acad Sci U S A*, **116**, 10547–10556.

196. Swanson,G.M., Estill,M., Diamond,M.P., Legro,R.S., Coutifaris,C., Barnhart,K.T., Huang,H., Hansen,K.R., Trussell,J.C., Coward,R.M., *et al.* (2020) Human chromatin remodeler cofactor, RNA interactor, eraser and writer sperm RNAs responding to obesity. *Epigenetics*, **15**, 32–46.

197. Zhang,Y., Shi,J., Rassoulzadegan,M., Tuorto,F. and Chen,Q. (2019) Sperm RNA code programmes the metabolic health of offspring. *Nat Rev Endocrinol*, **15**, 489–498.

198. Wang,Y., Chen,Z.-P., Hu,H., Lei,J., Zhou,Z., Yao,B., Chen,L., Liang,G., Zhan,S., Zhu,X., *et al.* (2021) Sperm microRNAs confer depression susceptibility to offspring. *Sci Adv*, **7**, eabd7605.

199. Gapp,K., Jawaid,A., Sarkies,P., Bohacek,J., Pelczar,P., Prados,J., Farinelli,L., Miska,E. and Mansuy,I.M. (2014) Implication of sperm RNAs in transgenerational inheritance of the effects of early trauma in mice. *Nat Neurosci*, **17**, 667–669.

200. Rodgers,A.B., Morgan,C.P., Leu,N.A. and Bale,T.L. (2015) Transgenerational epigenetic programming via sperm microRNA recapitulates effects of paternal stress. *Proc Natl Acad Sci U S A*, **112**, 13699–13704.

201. Gapp,K., van Steenwyk,G., Germain,P.L., Matsushima,W., Rudolph,K.L.M., Manuella,F., Roszkowski,M., Vernaz,G., Ghosh,T., Pelczar,P., *et al.* (2020) Alterations in sperm long RNA contribute to the epigenetic inheritance of the effects of postnatal trauma. *Mol Psychiatry*, **25**, 2162–2174.

202. Kiani,J., Grandjean,V., Liebers,R., Tuorto,F., Ghanbarian,H., Lyko,F., Cuzin,F. and Rassoulzadegan,M. (2013) RNA-mediated epigenetic heredity requires the cytosine methyltransferase Dnmt2. *PLoS Genet*, **9**, e1003498–e1003498.

203. Hodgson,J. (2018) RNA epigenetics spurs investor interest, but uncertainties linger. *Nature Biotechnology*, **36**, 1123–1124.

204. Garber,K., Landhuis,E., Sheridan,C., Senior,M. and DeFrancesco,L. (2019) Nature Biotechnology's academic spinouts of 2018. *Nature Biotechnology*, **37**, 601–612.

205. Charlotte,S. (2019) Technology Feature | Epitranscriptomics: RNA revisited. *Science (1979)*, **364**, 696.

206. Ryan Cross (2019) Epitranscriptomics: The new RNA code and the race to drug it. *C&EN Global Enterprise*, **97**, 34–39.

207. Jin,W.-B., Wu,S., Jian,X.-H., Yuan,H. and Tang,G.-L. (2018) A radical S-adenosyl-L-methionine enzyme and a methyltransferase catalyze cyclopropane formation in natural product biosynthesis. *Nat Commun*, **9**, 2771.

208. Zhang,J. and Zheng,Y.G. (2016) SAM/SAH Analogs as Versatile Tools for SAM-Dependent Methyltransferases. *ACS Chem Biol*, **11**, 583–597.

209. Wise,C.K., Cooney,C.A., Ali,S.F. and Poirier,L.A. (1997) Measuring S-adenosylmethionine in whole blood, red blood cells and cultured cells using a fast preparation method and high-performance liquid chromatography. *Journal of Chromatography B: Biomedical Sciences and Applications*, **696**, 145–152.

210. Castro,R., Struys,E.A., Jansen,E.E.W., Blom,H.J., de Almeida,I.T. and Jakobs,C. (2002) Quantification of plasma S-adenosylmethionine and S-adenosylhomocysteine as their fluorescent 1,N6-etheno derivatives: an adaptation of previously described methodology. *Journal of Pharmaceutical and Biomedical Analysis*, **29**, 963–968.

211. Lin,Y., Fan,H., Frederiksen,M., Zhao,K., Jiang,L., Wang,Z., Zhou,S., Guo,W., Gao,J., Li,S., *et al.* (2012) Detecting S-adenosyl-l-methionine-induced conformational change of a histone methyltransferase using a homogeneous time-resolved fluorescence-based binding assay. *Analytical Biochemistry*, **423**, 171–177.

212. Albu,C., Litescu,S.C., Radu,G.L. and Y. Aboul-Enein,H. (2013) Validated HPLC-Fl Method for the Analysis of S-Adenosylmethionine and S-Adenosylhomocysteine Biomarkers in Human Blood. *Journal of Fluorescence*, **23**, 381–386.

213. Melnyk,S., Pogribna,M., Pogribny,I.P., Yi,P. and James,S.J. (2000) Measurement of plasma and intracellular S-adenosylmethionine and S- adenosylhomocysteine utilizing coulometric electrochemical detection: Alterations with plasma homocysteine and pyridoxal 5'-phosphate concentrations. *Clinical Chemistry*, **46**, 265–272.

214. Li,S., Gu,X.J., Hao,Q., Fan,H., Li,L., Zhou,S., Zhao,K., Chan,H.M. and Wang,Y.K. (2013) A liquid chromatography/mass spectrometry-based generic detection method for biochemical assay and hit discovery of histone methyltransferases. *Analytical Biochemistry*, **443**, 214–221.

215. King,R.C., Miller-Stein,C., Magiera,D.J. and Brann,J. (2002) Description and validation of a staggered parallel high performance liquid chromatography system for good laboratory practice level quantitative analysis by liquid chromatography/tandem mass spectrometry. *Rapid Communications in Mass Spectrometry*, **16**, 43–52.

216. Li,S., Hao,Q., Gounarides,J. and Wang,Y.K. (2012) Full utilization of a mass spectrometer using on-demand sharing with multiple LC units. *Journal of Mass Spectrometry*, **47**, 1074–1082.

217. Rohman,M. and Wingfield,J. (2016) High-Throughput Screening Using Mass Spectrometry within Drug Discovery. In Janzen,W.P. (ed), *High Throughput Screening: Methods and Protocols*. Springer New York, New York, NY, pp. 47–63.

218. Maegley,K.A., Krivacic,C., Bingham,P., Liu,W. and Brooun,A. (2015) Comparison of a High-Throughput Mass Spectrometry Method and Radioactive Filter Binding to Assay the Protein Methyltransferase PRMT5. *ASSAY and Drug Development Technologies*, **13**, 235–240.

219. Pearson,L.-A., Green,C.J., Lin,D., Petit,A.-P., Gray,D.W., Cowling,V.H. and Fordyce,E.A.F. (2021) Development of a High-Throughput Screening Assay to Identify Inhibitors of the SARS-CoV-2 Guanine-N7-Methyltransferase Using RapidFire Mass Spectrometry. *SLAS Discov*, **26**, 749–756.

220. Yankova,E., Blackaby,W., Albertella,M., Rak,J., de Braekeleer,E., Tsagkogeorga,G., Pilka,E.S., Aspris,D., Leggate,D., Hendrick,A.G., *et al.* (2021) Small-molecule inhibition of METTL3 as a strategy against myeloid leukaemia. *Nature*, **593**, 597–601.

221. Hendricks,C.L., Ross,J.R., Pichersky,E., Noel,J.P. and Zhou,Z.S. (2004) An enzyme-coupled colorimetric assay for S-adenosylmethionine-dependent methyltransferases. *Analytical Biochemistry*, **326**, 100–105.

222. Schulz,D. and Rentmeister,A. (2012) An enzyme-coupled high-throughput assay for screening RNA methyltransferase activity in E. Coli cell lysate. *RNA Biology*, **9**, 577–586.

223. Dorgan,K.M., Wooderchak,W.L., Wynn,D.P., Karschner,E.L., Alfaro,J.F., Cui,Y., Zhou,Z.S. and Hevel,J.M. (2006) An enzyme-coupled continuous spectrophotometric assay for S-adenosylmethionine-dependent methyltransferases. *Analytical Biochemistry*, **350**, 249–255.

224. Palmer,N.A., Sattler,S.E., Saathoff,A.J. and Sarath,G. (2010) A Continuous, Quantitative Fluorescent Assay for Plant Caffeic Acid O-Methyltransferases. *Journal of Agricultural and Food Chemistry*, **58**, 5220–5226.

225. Hemeon,I., Gutierrez,J.A., Ho,M.-C. and Schramm,V.L. (2011) Characterizing DNA methyltransferases with an ultrasensitive luciferase-linked continuous assay. *Anal Chem*, **83**, 4996–5004.

226. Ibáñez,G., McBean,J.L., Astudillo,Y.M. and Luo,M. (2010) An enzyme-coupled ultrasensitive luminescence assay for protein methyltransferases. *Analytical Biochemistry*, **401**, 203–210.

227. Tovy,A., Hofmann,B., Helm,M. and Ankri,S. (2010) In vitro tRNA methylation assay with the Entamoeba histolytica DNA and tRNA methyltransferase Dnmt2 (Ehmeth) enzyme. *J Vis Exp*, 10.3791/2390.

228. Hausmann,S. and Shuman,S. (2005) Giardia lamblia RNA cap guanine-N2 methyltransferase (Tgs2). *Journal of Biological Chemistry*, **280**, 32101–32106.

229. Benarroch,D., Jankowska-Anyszka,M., Stepinski,J., Darzynkiewicz,E. and Shuman,S. (2010) Cap analog substrates reveal three clades of cap guanine-N2 methyltransferases with distinct methyl acceptor specificities. *RNA*, **16**, 211–220.

230. Helm,M. and Attardi,G. (2004) Nuclear Control of Cloverleaf Structure of Human Mitochondrial tRNALys. *Journal of Molecular Biology*, **337**, 545–560.

231. Baker,M.R., Zarubica,T., Wright,H.T. and Rife,J.P. (2009) Scintillation proximity assay for measurement of RNA methylation. *Nucleic Acids Res*, **37**, e32–e32.

232. Hill,P.J., Abibi,A., Albert,R., Andrews,B., Gagnon,M.M., Gao,N., Grebe,T., Hajec,L.I., Huang,J., Livchak,S., *et al.* (2013) Selective Inhibitors of Bacterial t-RNA-(N1G37) Methyltransferase (TrmD) That Demonstrate Novel Ordering of the Lid Domain. *Journal of Medicinal Chemistry*, **56**, 7278–7288.

233. Podvinec,M., Lim,S.P., Schmidt,T., Scarsi,M., Wen,D., Sonntag,L.-S., Sanschagrin,P., Shenkin,P.S. and Schwede,T. (2010) Novel Inhibitors of Dengue Virus Methyltransferase: Discovery by in Vitro-Driven Virtual Screening on a Desktop Computer Grid. *Journal of Medicinal Chemistry*, **53**, 1483–1495.

234. Poh,W.J., Wee,C.P.P. and Gao,Z. (2016) DNA Methyltransferase Activity Assays: Advances and Challenges. *Theranostics*, **6**, 369–391.

235. Illamola,S.M., Echaabi,A.K., Mazeron,C., Deshayes,S., Loriot,M.A. and Pallet,N. (2019) Development and validation of a UPLC-UV method for the quantification of thiopurine methyltransferase enzyme activity in human erythrocytes. *Journal of Chromatography B*, **1113**, 91–97.

236. Kasprzyk,R., Fido,M., Mamot,A., Wanat,P., Smietanski,M., Kopcial,M., Cowling,V.H., Kowalska,J. and Jemi",lity,J. (2020) Direct High-Throughput Screening Assay for mRNA Cap Guanine-N7 Methyltransferase Activity. *Chemistry*, **26**, 11266–11275.

237. Cheng,C.C. (1972) Inhibitors of t-RNA O-Methyltransferase as Possible Antineoplastic Agents. *Journal of Pharmaceutical Sciences*, **61**, 645–649.

238. Michelot,R., Legraverend,M., Farrugia,G. and Lederer,E. (1976) Nouvelles études de l'inhibition d'une tRNA N2 guanine méthyltransférase par des analogues de la S-adénosyl-homocystéine et de la S-adénosyl-méthionine. *Biochimie*, **58**, 201–205.

239. Mertens,P.P.C. and Payne,C.C. (1983) The effects of S-Adenosyl methionine (AdoMet) and its analogues on the control of transcription and translation in vitro of the mRNA products of two cytoplasmic polyhedrosis viruses. *Virology*, **131**, 18–29.

240. Hildesheim,J., Goguillon,J.-F. and Lederer,E. (1973) Selective inhibitions of tRNA methyltransferases by S-adenosylhomocysteine and two of its analogues. *FEBS Letters*, **30**, 177–180.

241. Pugh,C.S.G., Borchardt,R.T. and Stone,H.O. (1977) Inhibition of Newcastle disease virion messenger RNA (guanine-7-)-methyltransferase by analogs of S-adenosylhomocysteine. *Biochemistry*, **16**, 3928–3932.

242. Chang,C.-D. and Coward,J.K. (1976) Analogues of S-adenosylhomocysteine as potential inhibitors of biological transmethylation. Synthesis of analogues with modifications at the 5'-thioether linkage. *Journal of Medicinal Chemistry*, **19**, 684–691.

243. Coward,J.K., Bussolotti,D.L. and Chang,C.-D. (1974) Analogs of S-adenosylhomocysteine as potential inhibitors of biological transmethylation. Inhibition of several methylases by S-tubercidinylhomocysteine. *Journal of Medicinal Chemistry*, **17**, 1286–1289.

244. Poldermans,B., Roza,L. and van Knippenberg,P.H. (1979) Studies on the function of two adjacent N6,N6-dimethyladenosines near the 3' end of 16 S ribosomal RNA of Escherichia coli. III. Purification and properties of the methylating enzyme and methylase-30 S interactions. *Journal of Biological Chemistry*, **254**, 9094–9100.

245. Gnegy,M.E. and Lotspeich,F.J. (1976) Inhibitors of tRNA methyltransferases. S-Adenosylsulfonium salts. *Journal of Medicinal Chemistry*, **19**, 1191–1195.

246. Hildesheim,J., Hildesheim,R., Blanchard,P., Farrugia,G. and Michelot,R. (1973) Studies on synthetic inhibitors of t-RNA methyl transferases: analogs of S-adenosyl homocysteine. *Biochimie*, **55**, 541–546.

247. Shugart,L. and Chastain,B. (1979) Escherichia coli tRNA (Uracil-5-)-Methyltransferase: Inhibition by Analogues of Adenosylhomocysteine. *Enzyme*, **24**, 353–357.

248. Segal,D.M. and Eichler,D.C. (1989) The specificity of interaction between S-adenosyl-l-methionine and a nucleolar 2′-O-methyltransferase. *Archives of Biochemistry and Biophysics*, **275**, 334–343.

249. Yebra,M.J., Sanchez,J., Martin,C.G., Hardisson,C. and Barbes,C. (1991) The effect of sinefungin and synthetic analogues on RNA AND DNA methyltransferases from Streptomyces. *THE JOURNAL OF ANTIBIOTICS*, **44**, 1141–1147.

250. Benghiat,E., Crooks,P.A., Goodwin,R. and Rottman,F. (1986) Inhibition of Vaccinia RNA Guanine 7-Methyltransferase by Compounds Designed as Multisubstrate Adducts. *Journal of Pharmaceutical Sciences*, **75**, 142–145.

251. Leboy,P.S., Glick,J.M., Steiner,F.G., Haney,S. and Borchardt,R.T. (1978) S-adenosylhomocysteine analogues as inhibitors of specific tRNA methylation. *Biochimica et Biophysica Acta (BBA) - Nucleic Acids and Protein Synthesis*, **520**, 153–163.

252. Pugh,C.S.G. and Borchardt,R.T. (1982) Effects of S-adenosylhomocysteine analogs on vaccinia viral mRNA synthesis and methylation. *Biochemistry*, **21**, 1535–1541.

253. Richon,V.M., Johnston,D., Sneeringer,C.J., Jin,L., Majer,C.R., Elliston,K., Jerva,L.F., Scott,M.P. and Copeland,R.A. (2011) Chemogenetic Analysis of Human Protein Methyltransferases. *Chemical Biology & Drug Design*, **78**, 199–210.

254. Hamill,R.L. and Hoehn,M.M. (1973) A9145, a new adenie-containing antifungal antibiotic, I. discovery and isolation. *The Journal of Antibiotics*, **26**, 463–465.

255. Macarron,R., Banks,M.N., Bojanic,D., Burns,D.J., Cirovic,D.A., Garyantes,T., Green,D.V.S., Hertzberg,R.P., Janzen,W.P., Paslay,J.W., *et al.* (2011) Impact of high-throughput screening in biomedical research. *Nature Reviews Drug Discovery*, **10**, 188–195.

256. Li,Q. (2020) Application of Fragment-Based Drug Discovery to Versatile Targets. *Front Mol Biosci*, **7**, 180.

257. Murray,C.W. and Rees,D.C. (2009) The rise of fragment-based drug discovery. *Nature Chemistry*, **1**, 187–192.

258. Erlanson,D.A., Fesik,S.W., Hubbard,R.E., Jahnke,W. and Jhoti,H. (2016) Twenty years on: the impact of fragments on drug discovery. *Nature Reviews Drug Discovery*, **15**, 605–619.

259. Leelananda,S.P. and Lindert,S. (2016) Computational methods in drug discovery. *Beilstein journal of organic chemistry*, **12**, 2694–2718.

260. Lyu,J., Wang,S., Balius,T.E., Singh,I., Levit,A., Moroz,Y.S., O'Meara,M.J., Che,T., Algaa,E., Tolmachova,K., *et al.* (2019) Ultra-large library docking for discovering new chemotypes. *Nature*, **566**, 224–229.

261. Hoffmann,T. and Gastreich,M. (2019) The next level in chemical space navigation: going far beyond enumerable compound libraries. *Drug Discovery Today*, **24**, 1148–1156.

262. Acharya,C., Coop,A., Polli,J.E. and Mackerell Jr,A.D. (2011) Recent advances in ligand-based drug design: relevance and utility of the conformationally sampled pharmacophore approach. *Curr Comput Aided Drug Des*, **7**, 10–22.

263. Lipinski,C.A., Lombardo,F., Dominy,B.W. and Feeney,P.J. (2001) Experimental and computational approaches to estimate solubility and permeability in drug discovery and development. *Advanced Drug Delivery Reviews*, **46**, 3–26.

264. Veber,D.F., Johnson,S.R., Cheng,H.-Y., Smith,B.R., Ward,K.W. and Kopple,K.D. (2002) Molecular Properties That Influence the Oral Bioavailability of Drug Candidates. *Journal of Medicinal Chemistry*, **45**, 2615–2623.

265. Oprea,T.I., Davis,A.M., Teague,S.J. and Leeson,P.D. (2001) Is There a Difference between Leads and Drugs? A Historical Perspective. *Journal of Chemical Information and Computer Sciences*, **41**, 1308–1315.

266. Brenk,R., Schipani,A., James,D., Krasowski,A., Gilbert,I.H., Frearson,J. and Wyatt,P.G. (2008) Lessons learnt from assembling screening libraries for drug discovery for neglected diseases. *ChemMedChem*, **3**, 435–444.

267. Baell,J. and Walters,M.A. (2014) Chemistry: Chemical con artists foil drug discovery. *Nature*, **513**, 481–483.

268. Ventola,C.L. (2015) The antibiotic resistance crisis: part 1: causes and threats. *P T*, **40**, 277–283.

269. Liu,M. and Douthwaite,S. (2002) Activity of the ketolide telithromycin is refractory to Erm monomethylation of bacterial rRNA. *Antimicrob Agents Chemother*, **46**, 1629–1633.

270. Denoya,C.D. and Dubnau,D. (1987) Site and substrate specificity of the ermC 23S rRNA methyltransferase. *J Bacteriol*, **169**, 3857–3860.

271. Kreander,K., Kurkela,M., Siiskonen,A., Vuorela,P. and Tammela,P. (2006) Identification of COMT and ErmC inhibitors by using a microplate assay in combination with library focusing by virtual screening. *Pharmazie*, **61**, 247–248.

272. Foik,I.P., Tuszynska,I., Feder,M., Purta,E., Stefaniak,F. and Bujnicki,J.M. (2018) Novel inhibitors of the rRNA ErmC' methyltransferase to block resistance to macrolides, lincosamides, streptogramine B antibiotics. *European Journal of Medicinal Chemistry*, **146**, 60–67.

273. Feder,M., Purta,E., Koscinski,L., Čubrilo,S., Maravic Vlahovicek,G. and Bujnicki,J.M. (2008) Virtual Screening and Experimental Verification to Identify Potential Inhibitors of the ErmC Methyltransferase Responsible for Bacterial Resistance against Macrolide Antibiotics. *ChemMedChem*, **3**, 316–322.

274. Clancy,J., Schmieder,B.J., Petitpas,J.W., Manousos,M., Williams,J.A., Faiella,J.A., Girard,A.E. and Mcguirk,P.R. (1995) Assays to Detect and Characterize Synthetic Agents that Inhibit the ErmCMethyltransferase. *NO. II THE JOURNAL OF ANTIBIOTICS*, **48**, 1273–1279.

275. Hajduk,P.J., Dinges,J., Schkeryantz,J.M., Janowick,D., Kaminski,M., Tufano,M., Augeri,D.J., Petros,A., Nienaber,V., Zhong,P., *et al.* (1999) Novel Inhibitors of Erm Methyltransferases from NMR and Parallel Synthesis. *Journal of Medicinal Chemistry*, **42**, 3852–3859.

276. Chrebet,G.L., Wisniewski,D., Perkins,A.L., Deng,Q., Kurtz,M.B., Marcy,A. and Parent,S.A. (2005) Cell-Based Assays to Detect Inhibitors of Fungal mRNA Capping Enzymes and Characterization of Sinefungin as a Cap Methyltransferase Inhibitor. *Journal of Biomolecular Screening*, **10**, 355–364.

277. Hausmann,S., Zheng,S., Fabrega,C., Schneller,S.W., Lima,C.D. and Shuman,S. (2005) Encephalitozoon cuniculi mRNA Cap (Guanine N-7) Methyltransferase: Methyl acceptor specificity, inhibition by S-adenosylmethionine analogs, and structure-guided mutational analysis. *Journal of Biological Chemistry*, **280**, 20404–20412.

278. Zheng,S., Hausmann,S., Liu,Q., Ghosh,A., Schwer,B., Lima,C.D. and Shuman,S. (2006) Mutational Analysis of Encephalitozoon cuniculimRNA Cap (Guanine-N7) Methyltransferase, Structure of the Enzyme Bound to Sinefungin, and Evidence That Cap Methyltransferase Is the Target of Sinefungin's Antifungal Activity. *Journal of Biological Chemistry*, **281**, 35904–35913.

279. Chen,Y.-S., Yang,W.-L., Zhao,Y.-L. and Yang,Y.-G. (2021) Dynamic transcriptomic m5C and its regulatory role in RNA processing. *WIREs RNA*, **12**, e1639.

280. Angelova,M.T., Dimitrova,D.G., Dinges,N., Lence,T., Worpenberg,L., Carré,C. and Roignant,J.-Y. (2018) The Emerging Field of Epitranscriptomics in Neurodevelopmental and Neuronal Disorders. *Front Bioeng Biotechnol*, **6**, 46.

281. Zaccara,S., Ries,R.J. and Jaffrey,S.R. (2019) Reading, writing and erasing mRNA methylation. *Nature Reviews Molecular Cell Biology*, **20**, 608–624.

282. Xue,C., Zhao,Y. and Li,L. (2020) Advances in RNA cytosine-5 methylation: detection, regulatory mechanisms, biological functions and links to cancer. *Biomark Res*, **8**, 43.

283. Ignatova,V. v, Kaiser,S., Ho,J.S.Y., Bing,X., Stolz,P., Tan,Y.X., Lee,C.L., Gay,F.P.H., Lastres,P.R., Gerlini,R., *et al.* (2020) METTL6 is a tRNA m(3)C methyltransferase that regulates pluripotency and tumor cell growth. *Sci Adv*, **6**, eaaz4551–eaaz4551.

284. Dunn,S., Lombardi,O., Lukoszek,R. and Cowling,V.H. (2019) Oncogenic PIK3CA mutations increase dependency on the mRNA cap methyltransferase, RNMT, in breast cancer cells. *Open Biol*, **9**, 190052.

285. Orellana,E.A., Liu,Q., Yankova,E., Pirouz,M., de Braekeleer,E., Zhang,W., Lim,J., Aspris,D., Sendinc,E., Garyfallos,D.A., *et al.* (2021) METTL1-mediated m7G modification of Arg-TCT tRNA drives oncogenic transformation. *Molecular Cell*, **81**, 3323-3338.e14.

286. Lin,S., Liu,Q., Lelyveld,V.S., Choe,J., Szostak,J.W. and Gregory,R.I. (2018) Mettl1/Wdr4-Mediated m7G tRNA Methylome Is Required for Normal mRNA Translation and Embryonic Stem Cell Self-Renewal and Differentiation. *Mol Cell*, **71**, 244-255.e5.

287. Delaunay,S. and Frye,M. (2019) RNA modifications regulating cell fate in cancer. *Nature Cell Biology*, **21**, 552–559.

288. Oerum,S., Catala,M., Atdjian,C., Brachet,F., Ponchon,L., Barraud,P., Iannazzo,L., Droogmans,L., Braud,E., Ethève-Quelquejeu,M., *et al.* (2019) Bisubstrate analogues as structural tools to investigate m(6)A methyltransferase active sites. *RNA Biol*, **16**, 798–808.

289. Bedi,R.K., Huang,D., Eberle,S.A., Wiedmer,L., Śledź,P. and Caflisch,A. (2020) Small-Molecule Inhibitors of METTL3, the Major Human Epitranscriptomic Writer. *ChemMedChem*, **15**, 744–748.

290. Moroz-Omori,E. v, Huang,D., Kumar Bedi,R., Cheriyamkunnel,S.J., Bochenkova,E., Dolbois,A., Rzeczkowski,M.D., Li,Y., Wiedmer,L. and Caflisch,A. (2021) METTL3 Inhibitors for Epitranscriptomic Modulation of Cellular Processes. *ChemMedChem*, **16**, 3035–3043.

291. Selberg,S., Blokhina,D., Aatonen,M., Koivisto,P., Siltanen,A., Mervaala,E., Kankuri,E. and Karelson,M. (2019) Discovery of Small Molecules that Activate RNA Methylation through Cooperative Binding to the METTL3-14-WTAP Complex Active Site. *Cell Reports*, **26**, 3762-3771.e5.

292. Dolbois,A., Bedi,R.K., Bochenkova,E., Müller,A., Moroz-Omori,E. v, Huang,D. and Caflisch,A. (2021) 1,4,9-Triazaspiro[5.5]undecan-2-one Derivatives as Potent and Selective METTL3 Inhibitors. *Journal of Medicinal Chemistry*, **64**, 12738–12760.

293. Śledź,P. and Jinek,M. (2016) Structural insights into the molecular mechanism of the m6A writer complex. *Elife*, **5**, e18434.

294. Burgess,H.M., Depledge,D.P., Thompson,L., Srinivas,K.P., Grande,R.C., Vink,E.I., Abebe,J.S., Blackaby,W.P., Hendrick,A., Albertella,M.R., *et al.* (2021) Targeting the m6A RNA modification pathway blocks SARS-CoV-2 and HCoV-OC43 replication. *Genes & Development*, **35**, 1005–1019.

295. Halstead,S.B. (1992) The XXth century dengue pandemic: need for surveillance and research. *World health statistics quarterly 1992 ; 45(2/3) : 292-298.*

296. Brito,A.F., Machado,L.C., Oidtman,R.J., Siconelli,M.J.L., Tran,Q.M., Fauver,J.R., Carvalho,R.D. de O., Dezordi,F.Z., Pereira,M.R., de Castro-Jorge,L.A., *et al.* (2021) Lying in wait: the resurgence of dengue virus after the Zika epidemic in Brazil. *Nat Commun*, **12**, 2619.

297. Hu,B., Guo,H., Zhou,P. and Shi,Z.-L. (2021) Characteristics of SARS-CoV-2 and COVID-19. *Nat Rev Microbiol*, **19**, 141–154.

298. Ferron,F., Decroly,E., Selisko,B. and Canard,B. (2012) The viral RNA capping machinery as a target for antiviral drugs. *Antiviral Res*, **96**, 21–31.

299. Liu,L., Dong,H., Chen,H., Zhang,J., Ling,H., Li,Z., Shi,P.-Y. and Li,H. (2010) Flavivirus RNA cap methyltransferase: structure, function, and inhibition. *Front Biol (Beijing)*, **5**, 286–303.

300. Dong,H., Zhang,B. and Shi,P.-Y. (2008) Flavivirus methyltransferase: a novel antiviral target. *Antiviral Res*, **80**, 1–10.

301. Pugh,C.S.G., Borchardt,R.T. and Stone,H.O. (1978) Sinefungin, a potent inhibitor of virion mRNA (guanine-7-)-methyltransferase, mRNA (nucleoside-2'-)-methyltransferase, and viral multiplication. *Journal of Biological Chemistry*, **253**, 4075–4077.

302. Serafinowski,P., Dorland,E., Harrap,K.R., Balzarini,J. and de Clercq,E. (1992) Synthesis and antiviral activity of some new S-adenosyl-L-homocysteine derivatives. *Journal of Medicinal Chemistry*, **35**, 4576–4583.

303. Pierson,T.C. and Diamond,M.S. (2020) The continued threat of emerging flaviviruses. *Nat Microbiol*, **5**, 796–812.

304. el Sahili,A. and Lescar,J. (2017) Dengue Virus Non-Structural Protein 5. *Viruses*, **9**, 91.

305. Dong,H., Ren,S., Zhang,B., Zhou,Y., Puig-Basagoiti,F., Li,H. and Shi,P.-Y. (2008) West Nile virus methyltransferase catalyzes two methylations of the viral RNA cap through a substrate-repositioning mechanism. *J Virol*, **82**, 4295–4307.

306. Zhao,R., Wang,M., Cao,J., Shen,J., Zhou,X., Wang,D. and Cao,J. (2021) Flavivirus: From Structure to Therapeutics Development. *Life (Basel)*, **11**, 615.

307. Dong,H., Chang,D.C., Xie,X., Toh,Y.X., Chung,K.Y., Zou,G., Lescar,J., Lim,S.P. and Shi,P.-Y. (2010) Biochemical and genetic characterization of dengue virus methyltransferase. *Virology*, **405**, 568–578.

308. Kroschewski,H., Lim,S.P., Butcher,R.E., Yap,T.L., Lescar,J., Wright,P.J., Vasudevan,S.G. and Davidson,A.D. (2008) Mutagenesis of the Dengue Virus Type 2 NS5 Methyltransferase Domain. *Journal of Biological Chemistry*, **283**, 19410–19421.

309. Zhou,Y., Ray,D., Zhao,Y., Dong,H., Ren,S., Li,Z., Guo,Y., Bernard,K.A., Shi,P.-Y. and Li,H. (2007) Structure and function of flavivirus NS5 methyltransferase. *J Virol*, **81**, 3891–3903.

310. Züst,R., Dong,H., Li,X.-F., Chang,D.C., Zhang,B., Balakrishnan,T., Toh,Y.-X., Jiang,T., Li,S.-H., Deng,Y.-Q., *et al.* (2013) Rational design of a live attenuated dengue vaccine: 2'-o-methyltransferase mutants are highly attenuated and immunogenic in mice and macaques. *PLoS Pathog*, **9**, e1003521–e1003521.

311. Dong,H., Liu,L., Zou,G., Zhao,Y., Li,Z., Lim,S.P., Shi,P.-Y. and Li,H. (2010) Structural and functional analyses of a conserved hydrophobic pocket of flavivirus methyltransferase. *J Biol Chem*, **285**, 32586–32595.

312. Lim,S.P., Sonntag,L.S., Noble,C., Nilar,S.H., Ng,R.H., Zou,G., Monaghan,P., Chung,K.Y., Dong,H., Liu,B., *et al.* (2011) Small molecule inhibitors that selectively block dengue virus methyltransferase. *J Biol Chem*, **286**, 6233–6240.

313. Coutard,B., Decroly,E., Li,C., Sharff,A., Lescar,J., Bricogne,G. and Barral,K. (2014) Assessment of Dengue virus helicase and methyltransferase as targets for fragment-based drug discovery. *Antiviral Research*, **106**, 61–70.

314. Benmansour,F., Trist,I., Coutard,B., Decroly,E., Querat,G., Brancale,A. and Barral,K. (2017) Discovery of novel dengue virus NS5 methyltransferase non-nucleoside inhibitors by fragment-based drug design. *European Journal of Medicinal Chemistry*, **125**, 865–880.

315. Coutard,B., Barral,K., Lichière,J., Selisko,B., Martin,B., Aouadi,W., Lombardia,M.O., Debart,F., Vasseur,J.-J., Guillemot,J.C., *et al.* (2017) Zika Virus Methyltransferase: Structure and Functions for Drug Design Perspectives. *J Virol*, **91**, e02202-16.

316. Hernandez,J., Hoffer,L., Coutard,B., Querat,G., Roche,P., Morelli,X., Decroly,E. and Barral,K. (2019) Optimization of a fragment linking hit toward Dengue and Zika virus NS5 methyltransferases inhibitors. *European Journal of Medicinal Chemistry*, **161**, 323–333.

317. Duan,W., Song,H., Wang,H., Chai,Y., Su,C., Qi,J., Shi,Y. and Gao,G.F. (2017) The crystal structure of Zika virus NS5 reveals conserved drug targets. *EMBO J*, **36**, 919–933.

318. Cui,J., Li,F. and Shi,Z.-L. (2019) Origin and evolution of pathogenic coronaviruses. *Nat Rev Microbiol*, **17**, 181–192.

319. Ma,Y., Wu,L., Shaw,N., Gao,Y., Wang,J., Sun,Y., Lou,Z., Yan,L., Zhang,R. and Rao,Z. (2015) Structural basis and functional analysis of the SARS coronavirus nsp14-nsp10 complex. *Proc Natl Acad Sci U S A*, **112**, 9436–9441.

320. Chen,Y., Cai,H., Pan,J., Xiang,N., Tien,P., Ahola,T. and Guo,D. (2009) Functional screen reveals SARS coronavirus nonstructural protein nsp14 as a novel cap N7 methyltransferase. *Proc Natl Acad Sci U S A*, **106**, 3484–3489.

321. Lu,Y., Cai,H., Lu,M., Ma,Y., Li,A., Gao,Y., Zhou,J., Gu,H., Li,J. and Gu,J. (2020) Porcine Epidemic Diarrhea Virus Deficient in RNA Cap Guanine-N-7 Methylation Is Attenuated and Induces Higher Type I and III Interferon Responses. *J Virol*, **94**, e00447-20.

322. Hsu,J.C.-C., Laurent-Rolle,M., Pawlak,J.B., Wilen,C.B. and Cresswell,P. (2021) Translational shutdown and evasion of the innate immune response by SARS-CoV-2 NSP14 protein. *Proc Natl Acad Sci U S A*, **118**, e2101161118.

323. Menachery,V.D., Yount Jr,B.L., Josset,L., Gralinski,L.E., Scobey,T., Agnihothram,S., Katze,M.G. and Baric,R.S. (2014) Attenuation and restoration of severe acute respiratory syndrome coronavirus mutant lacking 2'-o-methyltransferase activity. *J Virol*, **88**, 4251–4264.

324. Menachery,V.D., Gralinski,L.E., Mitchell,H.D., Dinnon 3rd,K.H., Leist,S.R., Yount Jr,B.L., Graham,R.L., McAnarney,E.T., Stratton,K.G., Cockrell,A.S., *et al.* (2017) Middle East Respiratory Syndrome Coronavirus Nonstructural Protein 16 Is Necessary for Interferon Resistance and Viral Pathogenesis. *mSphere*, **2**, e00346-17.

325. Otava,T., Šála,M., Li,F., Fanfrlík,J., Devkota,K., Perveen,S., Chau,I., Pakarian,P., Hobza,P., Vedadi,M., *et al.* (2021) The Structure-Based Design of SARS-CoV-2 nsp14 Methyltransferase Ligands Yields Nanomolar Inhibitors. *ACS Infect Dis*, **7**, 2214–2220.

326. Bobiļeva,O., Bobrovs,R., Kaņepe,I., Patetko,L., Kalniņš,G., Šišovs,M., Bula,A.L., Gri Nberga,S., Borodušķis,M.R., Ramata-Stunda,A., *et al.* (2021) Potent SARS-CoV-2 mRNA Cap Methyltransferase Inhibitors by Bioisosteric Replacement of Methionine in SAM Cosubstrate. *ACS Med Chem Lett*, **12**, 1102–1107.

327. Devkota,K., Schapira,M., Perveen,S., Khalili Yazdi,A., Li,F., Chau,I., Ghiabi,P., Hajian,T., Loppnau,P., Bolotokova,A., *et al.* (2021) Probing the SAM Binding Site of SARS-CoV-2 Nsp14 In Vitro Using SAM Competitive Inhibitors Guides Developing Selective Bisubstrate Inhibitors. *SLAS Discov*, **26**, 1200–1211.

328. Ahmed-Belkacem,R., Sutto-Ortiz,P., Guiraud,M., Canard,B., Vasseur,J.-J., Decroly,E. and Debart,F. (2020) Synthesis of adenine dinucleosides SAM analogs as specific inhibitors of SARS-CoV nsp14 RNA cap guanine-N7-methyltransferase. *Eur J Med Chem*, **201**, 112557.

329. Chang,L., Wei,S., T,B.S., G,S.D., Bin,L. and Yang,Y. (2021) Structural basis of mismatch recognition by a SARS-CoV-2 proofreading enzyme. *Science (1979)*, **373**, 1142–1146.

330. Scott,L.J. (2016) Azacitidine: A Review in Myelodysplastic Syndromes and Acute Myeloid Leukaemia. *Drugs*, **76**, 889–900.

331. Lu,L.-J.W. and Randerath,K. (1980) Mechanism of 5-Azacytidine-induced Transfer RNA Cytosine-5-methyltransferase Deficiency. *Cancer Research*, **40**, 2701.

332. Khoddami,V. and Cairns,B.R. (2013) Identification of direct targets and modified bases of RNA cytosine methyltransferases. *Nat Biotechnol*, **31**, 458–464.

333. Khoddami,V. and Cairns,B.R. (2014) Transcriptome-wide target profiling of RNA cytosine methyltransferases using the mechanism-based enrichment procedure Aza-IP. *Nature Protocols*, **9**, 337–361.

334. Schaefer,M., Hagemann,S., Hanna,K. and Lyko,F. (2009) Azacytidine Inhibits RNA Methylation at DNMT2 Target Sites in Human Cancer Cell Lines. *Cancer Research*, **69**, 8127.

335. Ke,M., Chen,Y., Wu,A., Sun,Y., Su,C., Wu,H., Jin,X., Tao,J., Wang,Y., Ma,X., *et al.* (2012) Short peptides derived from the interaction domain of SARS coronavirus nonstructural protein nsp10 can suppress the 2'-O-methyltransferase activity of nsp10/nsp16 complex. *Virus Res*, **167**, 322–328.

336. Wang,Y., Sun,Y., Wu,A., Xu,S., Pan,R., Zeng,C., Jin,X., Ge,X., Shi,Z., Ahola,T., *et al.* (2015) Coronavirus nsp10/nsp16 Methyltransferase Can Be Targeted by nsp10-Derived Peptide In Vitro and In Vivo To Reduce Replication and Pathogenesis. *J Virol*, **89**, 8416–8427.

337. Byun,J. (2021) Recent Progress and Opportunities for Nucleic Acid Aptamers. *Life (Basel)*, **11**, 193.

338. Tuerk,C. and Gold,L. (1990) Systematic Evolution of Ligands by Exponential Enrichment: RNA Ligands to Bacteriophage T4 DNA Polymerase. *Science (1979)*, **249**, 505–510.

339. Ellington,A.D. and Szostak,J.W. (1990) In vitro selection of RNA molecules that bind specific ligands. *Nature*, **346**, 818–822.

340. Yang,J. and Bowser,M.T. (2013) Capillary electrophoresis-SELEX selection of catalytic DNA aptamers for a small-molecule porphyrin target. *Anal Chem*, **85**, 1525–1530.

341. Wang,L., Lee,J.Y., Gao,L., Yin,J., Duan,Y., Jimenez,L.A., Adkins,G.B., Ren,W., Li,L., Fang,J., *et al.* (2019) A DNA aptamer for binding and inhibition of DNA methyltransferase 1. *Nucleic Acids Res*, **47**, 11527–11537.

342. Zhuo,Z., Yu,Y., Wang,M., Li,J., Zhang,Z., Liu,J., Wu,X., Lu,A., Zhang,G. and Zhang,B. (2017) Recent Advances in SELEX Technology and Aptamer Applications in Biomedicine. *Int J Mol Sci*, **18**, 2142.

343. Yan,J., Xiong,H., Cai,S., Wen,N., He,Q., Liu,Y., Peng,D. and Liu,Z. (2019) Advances in aptamer screening technologies. *Talanta*, **200**, 124–144.

344. Komarova,N. and Kuznetsov,A. (2019) Inside the Black Box: What Makes SELEX Better? *Molecules*, **24**, 3598.

345. Keefe,A.D., Pai,S. and Ellington,A. (2010) Aptamers as therapeutics. *Nat Rev Drug Discov*, **9**, 537–550.

346. Haßel,S.K. and Mayer,G. (2019) Aptamers as Therapeutic Agents: Has the Initial Euphoria Subsided? *Molecular Diagnosis & Therapy*, **23**, 301–309.

347. Ng,E.W.M., Shima,D.T., Calias,P., Cunningham,E.T., Guyer,D.R. and Adamis,A.P. (2006) Pegaptanib, a targeted anti-VEGF aptamer for ocular vascular disease. *Nature Reviews Drug Discovery*, **5**, 123–132.

348. Pinheiro,V.B., Taylor,A.I., Cozens,C., Abramov,M., Renders,M., Zhang,S., Chaput,J.C., Wengel,J., Peak-Chew,S.-Y., McLaughlin,S.H., *et al.* (2012) Synthetic genetic polymers capable of heredity and evolution. *Science*, **336**, 341–344.

349. Hernandez,F.J., Kalra,N., Wengel,J. and Vester,B. (2009) Aptamers as a model for functional evaluation of LNA and 2′-amino LNA. *Bioorganic & Medicinal Chemistry Letters*, **19**, 6585–6587.

350. Vater,A. and Klussmann,S. (2015) Turning mirror-image oligonucleotides into drugs: the evolution of Spiegelmer® therapeutics. *Drug Discovery Today*, **20**, 147–155.

351. Odeh,F., Nsairat,H., Alshaer,W., Ismail,M.A., Esawi,E., Qaqish,B., Bawab,A. al and Ismail,S.I. (2019) Aptamers Chemistry: Chemical Modifications and Conjugation Strategies. *Molecules*, **25**, 3.

352. Healy,J.M., Lewis,S.D., Kurz,M., Boomer,R.M., Thompson,K.M., Wilson,C. and McCauley,T.G. (2004) Pharmacokinetics and Biodistribution of Novel Aptamer Compositions. *Pharmaceutical Research*, **21**, 2234–2246.

353. Lee,C.H., Lee,S.-H., Kim,J.H., Noh,Y.-H., Noh,G.-J. and Lee,S.-W. (2015) Pharmacokinetics of a Cholesterol-conjugated Aptamer Against the Hepatitis C Virus (HCV) NS5B Protein. *Mol Ther Nucleic Acids*, **4**, e254–e254.

354. Ganson,N.J., Povsic,T.J., Sullenger,B.A., Alexander,J.H., Zelenkofske,S.L., Sailstad,J.M., Rusconi,C.P. and Hershfield,M.S. (2016) Pre-existing anti-polyethylene glycol antibody linked to first-exposure allergic reactions to pegnivacogin, a PEGylated RNA aptamer. *J Allergy Clin Immunol*, **137**, 1610-1613.e7.

355. Han,S.R. and Lee,S.-W. (2017) Inhibition of Japanese encephalitis virus (JEV) replication by specific RNA aptamer against JEV methyltransferase. *Biochemical and Biophysical Research Communications*, **483**, 687–693.

356. Jung,J.I., Han,S.R. and Lee,S.-W. (2018) Development of RNA aptamer that inhibits methyltransferase activity of dengue virus. *Biotechnology Letters*, **40**, 315–324.

357. Blundy,K., Clark,M. and Bashir,S. (2021) STORM Therapeutics publishes data in Nature showing its first-in-class inhibitor of METTL3 is effective as a new therapeutic strategy against AML. *STORM Therapeutics publishes data in Nature showing its first-in-class inhibitor of METTL3 is effective as a new therapeutic strategy against AML*.

358. Extance,A. (2021) Designing cancer drugs.

359. Rodríguez-Paredes,M. and Lyko,F. (2019) The importance of non-histone protein methylation in cancer therapy. *Nature Reviews Molecular Cell Biology*, **20**, 569–570.

360. Lerner,C., Masjost,B., Ruf,A., Gramlich,V., Jakob-Roetne,R., Zürcher,G., Borroni,E. and Diederich,F. (2003) Bisubstrate inhibitors for the enzyme catechol-O-methyltransferase (COMT): influence of inhibitor preorganisation and linker length between the two substrate moieties on binding affinity. *Organic & Biomolecular Chemistry*, **1**, 42–49.

361. Paulini,R., Lerner,C., Jakob-Roetne,R., Zürcher,G., Borroni,E. and Diederich,F. (2004) Bisubstrate Inhibitors of the Enzyme Catechol O-Methyltransferase (COMT): Efficient Inhibition Despite the Lack of a Nitro Group. *ChemBioChem*, **5**, 1270–1274.

362. Ellermann,M., Paulini,R., Jakob-Roetne,R., Lerner,C., Borroni,E., Roth,D., Ehler,A., Schweizer,W.B., Schlatter,D., Rudolph,M.G., *et al.* (2011) Molecular Recognition at the Active Site of Catechol-O-methyltransferase (COMT): Adenine Replacements in Bisubstrate Inhibitors. *Chemistry – A European Journal*, **17**, 6369–6381.

363. Anglin,J.L., Deng,L., Yao,Y., Cai,G., Liu,Z., Jiang,H., Cheng,G., Chen,P., Dong,S. and Song,Y. (2012) Synthesis and structure-activity relationship investigation of adenosine-containing inhibitors of histone methyltransferase DOT1L. *J Med Chem*, **55**, 8066–8074.

364. Jerabek-Willemsen,M., Wienken,C.J., Braun,D., Baaske,P. and Duhr,S. (2011) Molecular interaction studies using microscale thermophoresis. *Assay Drug Dev Technol*, **9**, 342–353.

365. Copeland,R.A. (2005) Evaluation of enzyme inhibitors in drug discovery 1st ed. Wiley-Interscience.

366. Lin,K. and Wu,G. (2019) Isothermal Titration Calorimetry Assays to Measure Binding Affinities In Vitro. In Hergovich,A. (ed), *The Hippo Pathway: Methods and Protocols*. Springer New York, New York, NY, pp. 257–272.

367. Kalliokoski,T., Kramer,C., Vulpetti,A. and Gedeck,P. (2013) Comparability of mixed IC_{50} data - a statistical analysis. *PLoS One*, **8**, e61007–e61007.

368. Chellamuthu,A. and Gray,S.G. (2020) The RNA Methyltransferase NSUN2 and Its Potential Roles in Cancer. *Cells*, **9**, 1758.

369. Trixl,L. and Lusser,A. (2019) The dynamic RNA modification 5-methylcytosine and its emerging role as an epitranscriptomic mark. *Wiley Interdiscip Rev RNA*, **10**, e1510–e1510.

370. Xue,C., Zhao,Y. and Li,L. (2020) Advances in RNA cytosine-5 methylation: detection, regulatory mechanisms, biological functions and links to cancer. *Biomark Res*, **8**, 43.

371. Shankar,S.R., Bahirvani,A.G., Rao,V.K., Bharathy,N., Ow,J.R. and Taneja,R. (2013) G9a, a multipotent regulator of gene expression. *Epigenetics*, **8**, 16–22.

372. Zhang,Z.-M., Lu,R., Wang,P., Yu,Y., Chen,D., Gao,L., Liu,S., Ji,D., Rothbart,S.B., Wang,Y., *et al.* (2018) Structural basis for DNMT3A-mediated de novo DNA methylation. *Nature*, **554**, 387–391.

373. Sweis,R.F., Pliushchev,M., Brown,P.J., Guo,J., Li,F., Maag,D., Petros,A.M., Soni,N.B., Tse,C., Vedadi,M., *et al.* (2014) Discovery and development of potent and selective inhibitors of histone methyltransferase g9a. *ACS Med Chem Lett*, **5**, 205–209.

374. Liu,R.-J., Long,T., Li,J., Li,H. and Wang,E.-D. (2017) Structural basis for substrate binding and catalytic mechanism of a human RNA:m5C methyltransferase NSun6. *Nucleic Acids Res*, **45**, 6684–6697.

375. Varadi,M., Anyango,S., Deshpande,M., Nair,S., Natassia,C., Yordanova,G., Yuan,D., Stroe,O., Wood,G., Laydon,A., *et al.* (2022) AlphaFold Protein Structure Database: massively expanding the structural coverage of protein-sequence space with high-accuracy models. *Nucleic Acids Res*, **50**, D439–D444.

376. Jumper,J., Evans,R., Pritzel,A., Green,T., Figurnov,M., Ronneberger,O., Tunyasuvunakool,K., Bates,R., Žídek,A., Potapenko,A., *et al.* (2021) Highly accurate protein structure prediction with AlphaFold. *Nature*, **596**, 583–589.

377. Yokochi,T. and Robertson,K.D. (2004) Dimethyl sulfoxide stimulates the catalytic activity of de novo DNA methyltransferase 3a (Dnmt3a) in vitro. *Bioorganic Chemistry*, **32**, 234–243.

378. Gros,C., Chauvigné,L., Poulet,A., Menon,Y., Ausseil,F., Dufau,I. and Arimondo,P.B. (2013) Development of a universal radioactive DNA methyltransferase inhibition test for high-throughput screening and mechanistic studies. *Nucleic Acids Res*, **41**, e185–e185.

379. Saavedra,O.M., Isakovic,L., Llewellyn,D.B., Zhan,L., Bernstein,N., Claridge,S., Raeppel,F., Vaisburg,A., Elowe,N., Petschner,A.J., *et al.* (2009) SAR around (l)-S-adenosyl-l-homocysteine, an inhibitor of human DNA methyltransferase (DNMT) enzymes. *Bioorganic & Medicinal Chemistry Letters*, **19**, 2747–2751.

380. Isakovic,L., Saavedra,O.M., Llewellyn,D.B., Claridge,S., Zhan,L., Bernstein,N., Vaisburg,A., Elowe,N., Petschner,A.J., Rahil,J., *et al.* (2009) Constrained (l-)-S-adenosyl-l-homocysteine (SAH) analogues as DNA methyltransferase inhibitors. *Bioorganic & Medicinal Chemistry Letters*, **19**, 2742–2746.

381. Liu,Q., Cai,X., Yang,D., Chen,Y., Wang,Y., Shao,L. and Wang,M.-W. (2017) Cycloalkane analogues of sinefungin as EHMT1/2 inhibitors. *Bioorganic & Medicinal Chemistry*, **25**, 4579–4594.

382. Rotili,D., Tarantino,D., Marrocco,B., Gros,C., Masson,V., Poughon,V., Ausseil,F., Chang,Y., Labella,D., Cosconati,S., *et al.* (2014) Properly substituted analogues of BIX-01294 lose inhibition of G9a histone methyltransferase and gain selective anti-DNA methyltransferase 3A activity. *PLoS One*, **9**, e96941–e96941.

383. Devkota,K., Lohse,B., Liu,Q., Wang,M.-W., Stærk,D., Berthelsen,J. and Clausen,R.P. (2014) Analogues of the Natural Product Sinefungin as Inhibitors of EHMT1 and EHMT2. *ACS Med Chem Lett*, **5**, 293–297.

384. Zheng,W., Ibáñez,G., Wu,H., Blum,G., Zeng,H., Dong,A., Li,F., Hajian,T., Allali-Hassani,A., Amaya,M.F., *et al.* (2012) Sinefungin derivatives as inhibitors and structure probes of protein lysine methyltransferase SETD2. *J Am Chem Soc*, **134**, 18004–18014.

385. Kilgore,J.A., Du,X., Melito,L., Wei,S., Wang,C., Chin,H.G., Posner,B., Pradhan,S., Ready,J.M. and Williams,N.S. (2013) Identification of DNMT1 selective antagonists using a novel scintillation proximity assay. *J Biol Chem*, **288**, 19673–19684.

386. Topliss,J.G. (1972) Utilization of operational schemes for analog synthesis in drug design. *Journal of Medicinal Chemistry*, **15**, 1006–1011.

387. Kuttruff,C. (2020) Topliss Tree and Topliss Scheme Posters.

388. Nepali,K., Lee,H.-Y. and Liou,J.-P. (2019) Nitro-Group-Containing Drugs. *Journal of Medicinal Chemistry*, **62**, 2851–2893.

389. Suhonen,A., Morgan,I.S., Nauha,E., Helttunen,K., Tuononen,H.M. and Nissinen,M. (2015) Effect of a Rigid Sulfonamide Bond on Molecular Folding: A Case Study. *Crystal Growth & Design*, **15**, 2602–2608.

390. Kumler,W.D. and Halverstadt,I.F. (1941) The Dipole Moment of Sulfanilamide and Related Compounds1,2. *J Am Chem Soc*, **63**, 2182–2187.

391. Edder,C., Piguet,C., Bernardinelli,G., Mareda,J., Bochet,C.G., Bünzli,J.-C.G. and Hopfgartner,G. (2000) Unusual Electronic Effects of Electron-Withdrawing Sulfonamide Groups in Optically and Magnetically Active Self-Assembled Noncovalent Heterodimetallic d−f Podates. *Inorganic Chemistry*, **39**, 5059–5073.

392. Hansch,Corwin., Leo,A. and Taft,R.W. (1991) A survey of Hammett substituent constants and resonance and field parameters. *Chemical Reviews*, **91**, 165–195.

393. Wilden,J.D. (2010) The Sulfonamide Motif as a Synthetic Tool. *Journal of Chemical Research*, **34**, 541–548.

394. Reddick,J.J., Cheng,J. and Roush,W.R. (2003) Relative Rates of Michael Reactions of 2'-(Phenethyl)thiol with Vinyl Sulfones, Vinyl Sulfonate Esters, and Vinyl Sulfonamides Relevant to Vinyl Sulfonyl Cysteine Protease Inhibitors. *Organic Letters*, **5**, 1967–1970.

395. Okbinoglu,T. and Kennepohl,P. (2021) Nature of S–N Bonding in Sulfonamides and Related Compounds: Insights into π-Bonding Contributions from Sulfur K-Edge X-ray Absorption Spectroscopy. *The Journal of Physical Chemistry A*, **125**, 615–620.

396. Schuster,I.I., Doss,S.H. and Roberts,J.D. (1978) Natural-abundance nitrogen-15 nuclear magnetic resonance spectroscopy. Electronic effects in benzenesulfonamides. *The Journal of Organic Chemistry*, **43**, 4693–4696.

397. Kletskov,A., Gil,D., Frontera,A., Zaytsev,V., Merkulova,N., Beltsova,K., Sinelshchikova,A., Grigoriev,M., Grudova,M. and Zubkov,F. (2020) Intramolecular sp2 -sp3 Disequalization of Chemically Identical Sulfonamide Nitrogen Atoms: Single Crystal X-Ray Diffraction Characterization, Hirshfeld Surface Analysis and DFT Calculations of N-Substituted Hexahydro-1,3,5-Triazines. *Crystals (Basel)*, **10**, 369.

398. Chataigner,I., Panel,C., Gérard,H. and Piettre,S.R. (2007) Sulfonyl vs. carbonyl group: which is the more electron-withdrawing? *Chemical Communications*, 10.1039/B705034H.

399. Breneman,C.M. and Weber,L.W. (1996) Charge and energy redistribution in sulfonamides undergoing conformational changes. Hybridization as a controlling influence over conformer stability. *Canadian Journal of Chemistry*, **74**, 1271–1282.

400. Keeley,A., Ábrányi-Balogh,P., Hrast,M., Imre,T., Ilaš,J., Gobec,S. and Keserű,G.M. (2018) Heterocyclic electrophiles as new MurA inhibitors. *Arch Pharm (Weinheim)*, **351**, 1800184.

401. Ullman,B.R., Aja,T., Chen,N., Diaz,J.-L., Gu,X., Herrmann,J., Kalish,V.J., Karanewsky,D.S., Kodandapani,L., Krebs,J.J., *et al.* (2005) Structure–activity relationships within a series of caspase inhibitors. Part 2: Heterocyclic warheads. *Bioorganic & Medicinal Chemistry Letters*, **15**, 3632–3636.

402. Keeley,A., Ábrányi-Balogh,P. and Keserű,G.M. (2018) Design and characterization of a heterocyclic electrophilic fragment library for the discovery of cysteine-targeted covalent inhibitors. *Medchemcomm*, **10**, 263–267.

403. Tiwari,R., Miller,P.A., Cho,S., Franzblau,S.G. and Miller,M.J. (2014) Syntheses and Antituberculosis Activity of 1,3-Benzothiazinone Sulfoxide and Sulfone Derived from BTZ043. *ACS Med Chem Lett*, **6**, 128–133.

404. Barthels,F., Meyr,J., Hammerschmidt,S.J., Marciniak,T., Räder,H.-J., Ziebuhr,W., Engels,B. and Schirmeister,T. (2022) 2-Sulfonylpyrimidines as Privileged Warheads for the Development of S. aureus Sortase A Inhibitors. *Front Mol Biosci*, **8**, 804970.

405. Bunnett,J.F. (1958) Mechanism and reactivity in aromatic nucleophilic substitution reactions. *Quarterly Reviews, Chemical Society*, **12**, 1–16.

406. Klein,P., Johe,P., Wagner,A., Jung,S., Kühlborn,J., Barthels,F., Tenzer,S., Distler,U., Waigel,W., Engels,B., *et al.* (2020) New Cysteine Protease Inhibitors: Electrophilic (Het)arenes and Unexpected Prodrug Identification for the Trypanosoma Protease Rhodesain. *Molecules*, **25**, 1451.

407. Lux,G., Langer,A., Pschenitza,M., Karsunke,X., Strasser,R., Niessner,R., Knopp,D. and Rant,U. (2015) Detection of the Carcinogenic Water Pollutant Benzo[a]pyrene with an Electro-Switchable Biosurface. *Analytical Chemistry*, **87**, 4538–4545.

408. Li,S., Gu,X.J., Hao,Q., Fan,H., Li,L., Zhou,S., Zhao,K., Chan,H.M. and Wang,Y.K. (2013) A liquid chromatography/mass spectrometry-based generic detection method for biochemical assay and hit discovery of histone methyltransferases. *Analytical Biochemistry*, **443**, 214–221.

409. Yang,X.-L., Otero,F.J., Ewalt,K.L., Liu,J., Swairjo,M.A., Köhrer,C., RajBhandary,U.L., Skene,R.J., McRee,D.E. and Schimmel,P. (2006) Two conformations of a crystalline human tRNA synthetase-tRNA complex: implications for protein synthesis. *EMBO J*, **25**, 2919–2929.

410. McPherson,A. and Gavira,J.A. (2014) Introduction to protein crystallization. *Acta Crystallogr F Struct Biol Commun*, **70**, 2–20.

411. Ke,A. and Doudna,J.A. (2004) Crystallization of RNA and RNA–protein complexes. *Methods*, **34**, 408–414.

412. Greenfield,N.J. (2006) Using circular dichroism spectra to estimate protein secondary structure. *Nat Protoc*, **1**, 2876–2890.

413. Petit,C.M., Zhang,J., Sapienza,P.J., Fuentes,E.J. and Lee,A.L. (2009) Hidden dynamic allostery in a PDZ domain. *Proc Natl Acad Sci U S A*, **106**, 18249–18254.

414. Kajihara,D., Abe,R., Iijima,I., Komiyama,C., Sisido,M. and Hohsaka,T. (2006) FRET analysis of protein conformational change through position-specific incorporation of fluorescent amino acids. *Nature Methods*, **3**, 923–929.

415. Clayden,J., Warren,S. and Greeves,N. (2012) Organic Chemistry 2nd ed. Oxford University Press, London.

416. Schirmeister,T., Kesselring,J., Jung,S., Schneider,T.H., Weickert,A., Becker,J., Lee,W., Bamberger,D., Wich,P.R., Distler,U., *et al.* (2016) Quantum Chemical-Based Protocol for the Rational Design of Covalent Inhibitors. *J Am Chem Soc*, **138**, 8332–8335.

417. Jung,S., Fuchs,N., Johe,P., Wagner,A., Diehl,E., Yuliani,T., Zimmer,C., Barthels,F., Zimmermann,R.A., Klein,P., *et al.* (2021) Fluorovinylsulfones and -Sulfonates as Potent Covalent Reversible Inhibitors of the Trypanosomal Cysteine Protease Rhodesain: Structure–Activity Relationship, Inhibition Mechanism, Metabolism, and In Vivo Studies. *Journal of Medicinal Chemistry*, **64**, 12322–12358.

418. Williams,J.W., Morrison,J.F. and Duggleby,R.G. (1979) Methotrexate, a high-affinity pseudosubstrate of dihydrofolate reductase. *Biochemistry*, **18**, 2567–2573.

419. Klein,P., Barthels,F., Johe,P., Wagner,A., Tenzer,S., Distler,U., Le,T.A., Schmid,P., Engel,V., Engels,B., *et al.* (2020) Naphthoquinones as Covalent Reversible Inhibitors of Cysteine Proteases-Studies on Inhibition Mechanism and Kinetics. *Molecules*, **25**, 2064.

420. Campuzano,I.D.G., San Miguel,T., Rowe,T., Onea,D., Cee,V.J., Arvedson,T. and McCarter,J.D. (2015) High-Throughput Mass Spectrometric Analysis of Covalent Protein-Inhibitor Adducts for the Discovery of Irreversible Inhibitors: A Complete Workflow. *Journal of Biomolecular Screening*, **21**, 136–144.

421. Chen,G., Fan,M., Liu,Y., Sun,B., Liu,M., Wu,J., Li,N. and Guo,M. (2019) Advances in MS Based Strategies for Probing Ligand-Target Interactions: Focus on Soft Ionization Mass Spectrometric Techniques. *Front Chem*, **7**, 703.

422. Browne,C.M., Jiang,B., Ficarro,S.B., Doctor,Z.M., Johnson,J.L., Card,J.D., Sivakumaren,S.C., Alexander,W.M., Yaron,T.M., Murphy,C.J., *et al.* (2019) A Chemoproteomic Strategy for Direct and Proteome-Wide Covalent Inhibitor Target-Site Identification. *J Am Chem Soc*, **141**, 191–203.

423. Morrison,J.F. (1982) The slow-binding and slow, tight-binding inhibition of enzyme-catalysed reactions. *Trends in Biochemical Sciences*, **7**, 102–105.

424. Daigle,S.R., Olhava,E.J., Therkelsen,C.A., Majer,C.R., Sneeringer,C.J., Song,J., Johnston,L.D., Scott,M.P., Smith,J.J., Xiao,Y., *et al.* (2011) Selective killing of mixed lineage leukemia cells by a potent small-molecule DOT1L inhibitor. *Cancer Cell*, **20**, 53–65.

425. Pappalardi,M.B., Keenan,K., Cockerill,M., Kellner,W.A., Stowell,A., Sherk,C., Wong,K., Pathuri,S., Briand,J., Steidel,M., *et al.* (2021) Discovery of a first-in-class reversible DNMT1-selective inhibitor with improved tolerability and efficacy in acute myeloid leukemia. *Nat Cancer*, **2**, 1002–1017.

426. Dumat,B., Bood,M., Wranne,M.S., Lawson,C.P., Larsen,A.F., Preus,S., Streling,J., Gradén,H., Wellner,E., Grøtli,M., *et al.* (2015) Second-Generation Fluorescent Quadracyclic Adenine Analogues: Environment-Responsive Probes with Enhanced Brightness. *Chemistry – A European Journal*, **21**, 4039–4048.

427. Santhosh,C. and Mishra,P.C. (1991) Electronic spectra of 2-aminopurine and 2,6-diaminopurine: phototautomerism and fluorescence reabsorption. *Spectrochimica Acta Part A: Molecular Spectroscopy*, **47**, 1685–1693.

428. Luan,Y., Blazer,L.L., Hu,H., Hajian,T., Zhang,J., Wu,H., Houliston,S., Arrowsmith,C.H., Vedadi,M. and Zheng,Y.G. (2016) Design of a fluorescent ligand targeting the S-adenosylmethionine binding site of the histone methyltransferase MLL1. *Org Biomol Chem*, **14**, 631–638.

429. Lea,W.A. and Simeonov,A. (2011) Fluorescence polarization assays in small molecule screening. *Expert Opin Drug Discov*, **6**, 17–32.

430. Wranne,M.S., Füchtbauer,A.F., Dumat,B., Bood,M., El-Sagheer,A.H., Brown,T., Gradén,H., Grøtli,M. and Wilhelmsson,L.M. (2017) Toward Complete Sequence Flexibility of Nucleic Acid Base Analogue FRET. *J Am Chem Soc*, **139**, 9271–9280.

431. Matveeva,E.G., Morisseau,C., Goodrow,M.H., Mullin,C. and Hammock,B.D. (2009) Tryptophan fluorescence quenching by enzyme inhibitors as a tool for enzyme active site structure investigation: epoxide hydrolase. *Curr Pharm Biotechnol*, **10**, 589–599.

432. Nasri,R., Bidel,L.P.R., Rugani,N., Perrier,V., Carrière,F., Dubreucq,E. and Jay-Allemand,C. (2019) Inhibition of CpLIP2 Lipase Hydrolytic Activity by Four Flavonols (Galangin, Kaempferol, Quercetin, Myricetin) Compared to Orlistat and Their Binding Mechanisms Studied by Quenching of Fluorescence. *Molecules*, **24**, 2888.

433. Aouadi,W., Eydoux,C., Coutard,B., Martin,B., Debart,F., Vasseur,J.J., Contreras,J.M., Morice,C., Quérat,G., Jung,M.-L., *et al.* (2017) Toward the identification of viral cap-methyltransferase inhibitors by fluorescence screening assay. *Antiviral Res*, **144**, 330–339.

434. Kimos,M., Burton,M., Urbain,D., Caudron,D., Martini,M., Famelart,M., Gillard,M., Barrow,J. and Wood,M. (2015) Development of an HTRF Assay for the Detection and Characterization of Inhibitors of Catechol-O-Methyltransferase. *Journal of Biomolecular Screening*, **21**, 490–495.

435. Maia,E.H.B., Assis,L.C., de Oliveira,T.A., da Silva,A.M. and Taranto,A.G. (2020) Structure-Based Virtual Screening: From Classical to Artificial Intelligence. *Front Chem*, **8**, 343.

436. Kontoyianni,M. (2017) Docking and Virtual Screening in Drug Discovery. In Lazar,I.M., Kontoyianni,M., Lazar,A.C. (eds), *Proteomics for Drug Discovery: Methods and Protocols*. Springer New York, New York, NY, pp. 255–266.

437. Lill,M. (2013) Virtual Screening in Drug Design. In Kortagere,S. (ed), *In Silico Models for Drug Discovery*. Humana Press, Totowa, NJ, pp. 1–12.

438. Breuers,S., Bryant,L.L., Legen,T. and Mayer,G. (2019) Robotic assisted generation of 2'-deoxy-2'-fluoro-modifed RNA aptamers - High performance enabling strategies in aptamer selection. *Methods*, **161**, 3–9.

439. Bendak,K., Loughlin,F.E., Cheung,V., O'Connell,M.R., Crossley,M. and Mackay,J.P. (2012) A rapid method for assessing the RNA-binding potential of a protein. *Nucleic Acids Res*, **40**, e105–e105.

440. Jaeschke,A., Harvey,N.R., Tsurkan,M., Werner,C., Griffiths,L.R., Haupt,L.M. and Bray,L.J. (2021) Techniques for RNA extraction from cells cultured in starPEG-heparin hydrogels. *Open Biol*, **11**, 200388.

441. Quang,N.N., Miodek,A., Cibiel,A. and Ducongé,F. (2017) Selection of Aptamers Against Whole Living Cells: From Cell-SELEX to Identification of Biomarkers. In Tiller,T. (ed), *Synthetic Antibodies: Methods and Protocols*. Springer New York, New York, NY, pp. 253–272.

442. Komarova,N., Barkova,D. and Kuznetsov,A. (2020) Implementation of High-Throughput Sequencing (HTS) in Aptamer Selection Technology. *Int J Mol Sci*, **21**, 8774.

443. Alam,K.K., Chang,J.L. and Burke,D.H. (2015) FASTAptamer: A Bioinformatic Toolkit for High-throughput Sequence Analysis of Combinatorial Selections. *Mol Ther Nucleic Acids*, **4**, e230–e230.

444. Levenshtein,V.I. (1965) Binary codes capable of correcting deletions, insertions, and reversals. *Dokl. Akad. Nauk SSSR*, **10**, 845–848.

445. Schmitz,A., Weber,A., Bayin,M., Breuers,S., Fieberg,V., Famulok,M. and Mayer,G. (2021) A SARS-CoV-2 Spike Binding DNA Aptamer that Inhibits Pseudovirus Infection by an RBD-Independent Mechanism*. *Angew Chem Int Ed Engl*, **60**, 10279–10285.

446. Waterhouse,A.M., Procter,J.B., Martin,D.M.A., Clamp,M. and Barton,G.J. (2009) Jalview Version 2--a multiple sequence alignment editor and analysis workbench. *Bioinformatics*, **25**, 1189–1191.

447. Roth,A., Winkler,W.C., Regulski,E.E., Lee,B.W.K., Lim,J., Jona,I., Barrick,J.E., Ritwik,A., Kim,J.N., Welz,R., *et al.* (2007) A riboswitch selective for the queuosine precursor preQ1 contains an unusually small aptamer domain. *Nature Structural & Molecular Biology*, **14**, 308–317.

448. Jacobson,D.R. and Saleh,O.A. (2017) Counting the ions surrounding nucleic acids. *Nucleic Acids Res*, **45**, 1596–1605.

449. Le,T.T., Chumphukam,O. and Cass,A.E.G. (2014) Determination of minimal sequence for binding of an aptamer. A comparison of truncation and hybridization inhibition methods. *RSC Advances*, **4**, 47227–47233.

450. Gruber,A.R., Lorenz,R., Bernhart,S.H., Neuböck,R. and Hofacker,I.L. (2008) The Vienna RNA websuite. *Nucleic Acids Res*, **36**, W70–W74.

451. Mathews,D.H., Disney,M.D., Childs,J.L., Schroeder,S.J., Zuker,M. and Turner,D.H. (2004) Incorporating chemical modification constraints into a dynamic programming algorithm for prediction of RNA secondary structure. *Proc Natl Acad Sci U S A*, **101**, 7287–7292.

452. Lorenz,R., Bernhart,S.H., Höner Zu Siederdissen,C., Tafer,H., Flamm,C., Stadler,P.F. and Hofacker,I.L. (2011) ViennaRNA Package 2.0. *Algorithms Mol Biol*, **6**, 26.

453. Eddy,S.R. (2014) Computational analysis of conserved RNA secondary structure in transcriptomes and genomes. *Annu Rev Biophys*, **43**, 433–456.

454. Ekland,E.H. and Bartel,D.P. (1995) The secondary structure and sequence optimization of an RNA ligase ribozyme. *Nucleic Acids Res*, **23**, 3231–3238.

455. Boese,B.J., Corbino,K. and Breaker,R.R. (2008) In vitro selection and characterization of cellulose-binding RNA aptamers using isothermal amplification. *Nucleosides Nucleotides Nucleic Acids*, **27**, 949–966.

456. Trachman 3rd,R.J., Autour,A., Jeng,S.C.Y., Abdolahzadeh,A., Andreoni,A., Cojocaru,R., Garipov,R., Dolgosheina,E. v, Knutson,J.R., Ryckelynck,M., *et al.* (2019) Structure and functional reselection of the Mango-III fluorogenic RNA aptamer. *Nat Chem Biol*, **15**, 472–479.

457. Weber,A.M., Kaiser,J., Ziegler,T., Pilsl,S., Renzl,C., Sixt,L., Pietruschka,G., Moniot,S., Kakoti,A., Juraschitz,M., *et al.* (2019) A blue light receptor that mediates RNA binding and translational regulation. *Nat Chem Biol*, **15**, 1085–1092.

458. Feig,A.L. (2009) Studying RNA-RNA and RNA-protein interactions by isothermal titration calorimetry. *Methods Enzymol*, **468**, 409–422.

459. Cléry,A., Sohier,T.J.M., Welte,T., Langer,A. and Allain,F.H.T. (2017) switchSENSE: A new technology to study protein-RNA interactions. *Methods*, **118–119**, 137–145.

460. Germer,K., Leonard,M. and Zhang,X. (2013) RNA aptamers and their therapeutic and diagnostic applications. *Int J Biochem Mol Biol*, **4**, 27–40.

461. Deprey,K., Batistatou,N. and Kritzer,J.A. (2020) A critical analysis of methods used to investigate the cellular uptake and subcellular localization of RNA therapeutics. *Nucleic Acids Res*, **48**, 7623–7639.

462. Litke,J.L. and Jaffrey,S.R. (2019) Highly efficient expression of circular RNA aptamers in cells using autocatalytic transcripts. *Nat Biotechnol*, **37**, 667–675.

463. Kim,D.-H., Seo,J.-M., Shin,K.-J. and Yang,S.-G. (2021) Design and clinical developments of aptamer-drug conjugates for targeted cancer therapy. *Biomater Res*, **25**, 42.

464. Ritz,C. (2016) Package 'drc.'

465. RStudio Team (2021) RStudio: Integrated Development Environment for R.

466. Bolger,A.M., Lohse,M. and Usadel,B. (2014) Trimmomatic: a flexible trimmer for Illumina sequence data. *Bioinformatics*, **30**, 2114–2120.

467. Afgan,E., Baker,D., van den Beek,M., Blankenberg,D., Bouvier,D., Čech,M., Chilton,J., Clements,D., Coraor,N., Eberhard,C., *et al.* (2016) The Galaxy platform for accessible, reproducible and collaborative biomedical analyses: 2016 update. *Nucleic Acids Res*, **44**, W3–W10.

468. Andrew,S., Lindenbaum,P., Howard,B. and Ewels,P. (2011) FastQC: A Quality Control Tool for High Throughput Sequence Data [Online].

469. Bida,J.P. and Maher 3rd,L.J. (2012) Improved prediction of RNA tertiary structure with insights into native state dynamics. *RNA*, **18**, 385–393.

470. Lahoud,G., Goto-Ito,S., Yoshida,K.-I., Ito,T., Yokoyama,S. and Hou,Y.-M. (2011) Differentiating analogous tRNA methyltransferases by fragments of the methyl donor. *RNA*, **17**, 1236–1246.

471. Zhong,W., Koay,A., Ngo,A., Li,Y., Nah,Q., Wong,Y.H., Chionh,Y.H., Ng,H.Q., Koh-Stenta,X., Poulsen,A., *et al.* (2019) Targeting the Bacterial Epitranscriptome for Antibiotic Development: Discovery of Novel tRNA-(N1G37) Methyltransferase (TrmD) Inhibitors. *ACS Infectious Diseases*, **5**, 326–335.

472. Zhong,W., Pasunooti,K.K., Balamkundu,S., Wong,Y.H., Nah,Q., Gadi,V., Gnanakalai,S., Chionh,Y.H., McBee,M.E., Gopal,P., *et al.* (2019) Thienopyrimidinone Derivatives That Inhibit Bacterial tRNA (Guanine37-N(1))-Methyltransferase (TrmD) by Restructuring the Active Site with a Tyrosine-Flipping Mechanism. *J Med Chem*, **62**, 7788–7805.

473. Thomas,S.E., Whitehouse,A.J., Brown,K., Burbaud,S., Belardinelli,J.M., Sangen,J., Lahiri,R., Libardo,M.D.J., Gupta,P., Malhotra,S., *et al.* (2020) Fragment-based discovery of a new class of inhibitors targeting mycobacterial tRNA modification. *Nucleic Acids Res*, **48**, 8099–8112.

474. Whitehouse,A.J., Thomas,S.E., Brown,K.P., Fanourakis,A., Chan,D.S.-H., Libardo,M.D.J., Mendes,V., Boshoff,H.I.M., Floto,R.A., Abell,C., *et al.* (2019) Development of Inhibitors against Mycobacterium abscessus tRNA (m(1)G37) Methyltransferase (TrmD) Using Fragment-Based Approaches. *J Med Chem*, **62**, 7210–7232.

475. Wainfan,E. and Landsberg,B. (1973) Inhibition of transfer ribonucleic acid methylating enzymes by cytotoxic analogs of adenosine. *Biochemical Pharmacology*, **22**, 493–500.

476. Fernandez,M., Soliveri,J., Novella,I.S., Yebra,M.J., Barbés,C. and Sánchez,J. (1995) Effect of 5-azacytidine and sinefungin on streptomyces development. *Gene*, **157**, 221–223.

477. Alvesalo,J.K.O., Siiskonen,A., Vainio,M.J., Tammela,P.S.M. and Vuorela,P.M. (2006) Similarity Based Virtual Screening: A Tool for Targeted Library Design. *Journal of Medicinal Chemistry*, **49**, 2353–2356.

478. Rana,A.K., Chandra,S., Siddiqi,M.I. and Misra-Bhattacharya,S. (2013) Molecular characterization of an rsmD-like rRNA methyltransferase from the Wolbachia endosymbiont of Brugia malayi and antifilarial activity of specific inhibitors of the enzyme. *Antimicrob Agents Chemother*, **57**, 3843–3856.

479. Bhattacharya,A., Sharma,M., Pakkinathan,C., Rosen,B.P., Leprohon,P. and Ouellette,M. (2019) Genomewide Analysis of Mode of Action of the S-Adenosylmethionine Analogue Sinefungin in Leishmania infantum. *mSystems*, **4**, e00416-19.

480. Hall,M.P. and Ho,C.K. (2006) Characterization of a Trypanosoma brucei RNA cap (guanine N-7) methyltransferase. *RNA*, **12**, 488–497.

481. Lee,J.-H., Kim,S., Jin,M.S. and Kim,Y.-C. (2022) Discovery of substituted indole derivatives as allosteric inhibitors of m6A-RNA methyltransferase, METTL3-14 complex. *Drug Development Research*, **n/a**.

482. Milani,M., Mastrangelo,E., Bollati,M., Selisko,B., Decroly,E., Bouvet,M., Canard,B. and Bolognesi,M. (2009) Flaviviral methyltransferase/RNA interaction: structural basis for enzyme inhibition. *Antiviral Res*, **83**, 28–34.

483. Brecher,M., Chen,H., Liu,B., Banavali,N.K., Jones,S.A., Zhang,J., Li,Z., Kramer,L.D. and Li,H. (2015) Novel Broad Spectrum Inhibitors Targeting the Flavivirus Methyltransferase. *PLoS One*, **10**, e0130062–e0130062.

484. Brecher,M., Chen,H., Li,Z., Banavali,N.K., Jones,S.A., Zhang,J., Kramer,L.D. and Li,H. (2015) Identification and Characterization of Novel Broad-Spectrum Inhibitors of the Flavivirus Methyltransferase. *ACS Infect Dis*, **1**, 340–349.

485. Chen,H., Zhou,B., Brecher,M., Banavali,N., Jones,S.A., Li,Z., Zhang,J., Nag,D., Kramer,L.D., Ghosh,A.K., *et al.* (2013) S-adenosyl-homocysteine is a weakly bound inhibitor for a flaviviral methyltransferase. *PLoS One*, **8**, e76900–e76900.

486. Barral,K., Sallamand,C., Petzold,C., Coutard,B., Collet,A., Thillier,Y., Zimmermann,J., Vasseur,J.-J., Canard,B., Rohayem,J., *et al.* (2013) Development of specific dengue virus 2′-O- and N7-methyltransferase assays for antiviral drug screening. *Antiviral Research*, **99**, 292–300.

487. Luzhkov,V.B., Selisko,B., Nordqvist,A., Peyrane,F., Decroly,E., Alvarez,K., Karlen,A., Canard,B. and Åqvist,J. (2007) Virtual screening and bioassay study of novel inhibitors for dengue virus mRNA cap (nucleoside-2′O)-methyltransferase. *Bioorganic & Medicinal Chemistry*, **15**, 7795–7802.

488. Benarroch,D., Egloff,M.-P., Mulard,L., Guerreiro,C., Romette,J.-L. and Canard,B. (2004) A Structural Basis for the Inhibition of the NS5 Dengue Virus mRNA 2'-O-Methyltransferase Domain by Ribavirin 5'-Triphosphate *. *Journal of Biological Chemistry*, **279**, 35638–35643.

489. Selisko,B., Peyrane,F.F., Canard,B., Alvarez,K. and Decroly,E. (2010) Biochemical characterization of the (nucleoside-2′O)-methyltransferase activity of dengue virus protein NS5 using purified capped RNA oligonucleotides 7MeGpppACn and GpppACn. *Journal of General Virology*, **91**, 112–121.

490. Thames,J.E., Waters 3rd,C.D., Valle,C., Bassetto,M., Aouadi,W., Martin,B., Selisko,B., Falat,A., Coutard,B., Brancale,A., *et al.* (2020) Synthesis and biological evaluation of novel flexible nucleoside analogues that inhibit flavivirus replication in vitro. *Bioorg Med Chem*, **28**, 115713.

491. Lim,S.P., Wen,D., Yap,T.L., Yan,C.K., Lescar,J. and Vasudevan,S.G. (2008) A scintillation proximity assay for dengue virus NS5 2′-O-methyltransferase—kinetic and inhibition analyses. *Antiviral Research*, **80**, 360–369.

492. Lim,S.V., Rahman,M.B.A. and Tejo,B.A. (2011) Structure-based and ligand-based virtual screening of novel methyltransferase inhibitors of the dengue virus. *BMC Bioinformatics*, **12 Suppl 13**, S24–S24.

493. Powers,C.N. and Setzer,W.N. (2016) An In-Silico Investigation of Phytochemicals as Antiviral Agents Against Dengue Fever. *Comb Chem High Throughput Screen*, **19**, 516–536.

494. Tambunan,U.S.F., Zahroh,H., Utomo,B.B. and Parikesit,A.A. (2014) Screening of commercial cyclic peptide as inhibitor NS5 methyltransferase of Dengue virus through Molecular Docking and Molecular Dynamics Simulation. *Bioinformation*, **10**, 23–27.

495. Tambunan,U.S.F., Nasution,M.A.F., Azhima,F., Parikesit,A.A., Toepak,E.P., Idrus,S. and Kerami,D. (2017) Modification of S-Adenosyl-l-Homocysteine as Inhibitor of Nonstructural Protein 5 Methyltransferase Dengue Virus Through Molecular Docking and Molecular Dynamics Simulation. *Drug Target Insights*, **11**, 1177392817701726–1177392817701726.

496. Idrus,S., Tambunan,U.S.F. and Zubaidi,A.A. (2012) Designing cyclopentapeptide inhibitor as potential antiviral drug for dengue virus ns5 methyltransferase. *Bioinformation*, **8**, 348–352.

497. Spizzichino,S., Mattedi,G., Lauder,K., Valle,C., Aouadi,W., Canard,B., Decroly,E., Kaptein,S.J.F., Neyts,J., Graham,C., *et al.* (2020) Design, Synthesis and Discovery of N,N'-Carbazoyl-aryl-urea Inhibitors of Zika NS5 Methyltransferase and Virus Replication. *ChemMedChem*, **15**, 385–390.

498. Vernekar,S.K. v, Qiu,L., Zhang,J., Kankanala,J., Li,H., Geraghty,R.J. and Wang,Z. (2015) 5'-Silylated 3'-1,2,3-triazolyl Thymidine Analogues as Inhibitors of West Nile Virus and Dengue Virus. *J Med Chem*, **58**, 4016–4028.

499. Boonyasuppayakorn,S., Saelee,T., Visitchanakun,P., Leelahavanichkul,A., Hengphasatporn,K., Shigeta,Y., Huynh,T.N.T., Chu,J.J.H., Rungrotmongkol,T. and Chavasiri,W. (2020) Dibromopinocembrin and Dibromopinostrobin Are Potential Anti-Dengue Leads with Mild Animal Toxicity. *Molecules*, **25**, 4154.

500. Geiss,B.J., Thompson,A.A., Andrews,A.J., Sons,R.L., Gari,H.H., Keenan,S.M. and Peersen,O.B. (2009) Analysis of flavivirus NS5 methyltransferase cap binding. *J Mol Biol*, **385**, 1643–1654.

501. Santos,F.R.S., Lima,W.G., Maia,E.H.B., Assis,L.C., Davyt,D., Taranto,A.G. and Ferreira,J.M.S. (2020) Identification of a Potential Zika Virus Inhibitor Targeting NS5 Methyltransferase Using Virtual Screening and Molecular Dynamics Simulations. *Journal of Chemical Information and Modeling*, **60**, 562–568.

502. Byler,K.G., Ogungbe,I.V. and Setzer,W.N. (2016) In-silico screening for anti-Zika virus phytochemicals. *J Mol Graph Model*, **69**, 78–91.

503. Ramharack,P. and Soliman,M.E.S. (2018) Zika virus NS5 protein potential inhibitors: an enhanced in silico approach in drug discovery. *Journal of Biomolecular Structure and Dynamics*, **36**, 1118–1133.

504. Singh,J., Kumar,M., Mansuri,R., Sahoo,G.C. and Deep,A. (2016) Inhibitor designing, virtual screening, and docking studies for methyltransferase: A potential target against dengue virus. *J Pharm Bioallied Sci*, **8**, 188–194.

505. Stephen,P., Baz,M., Boivin,G. and Lin,S.-X. (2016) Structural Insight into NS5 of Zika Virus Leading to the Discovery of MTase Inhibitors. *J Am Chem Soc*, **138**, 16212–16215.

506. Jain,R., Butler,K. v, Coloma,J., Jin,J. and Aggarwal,A.K. (2017) Development of a S-adenosylmethionine analog that intrudes the RNA-cap binding site of Zika methyltransferase. *Sci Rep*, **7**, 1632.

507. Tao,Z., Cao,R., Yan,Y., Huang,G., Lv,K., Li,W., Geng,Y., Zhao,L., Wang,A., He,Q., *et al.* (2018) Design, synthesis and in vitro anti-Zika virus evaluation of novel Sinefungin derivatives. *European Journal of Medicinal Chemistry*, **157**, 994–1004.

508. Song,W., Zhang,H., Zhang,Y., Chen,Y., Lin,Y., Han,Y. and Jiang,J. (2021) Identification and Characterization of Zika Virus NS5 Methyltransferase Inhibitors. *Front Cell Infect Microbiol*, **11**, 665379.

509. Chen,H., Liu,L., Jones,S.A., Banavali,N., Kass,J., Li,Z., Zhang,J., Kramer,L.D., Ghosh,A.K. and Li,H. (2013) Selective inhibition of the West Nile virus methyltransferase by nucleoside analogs. *Antiviral Res*, **97**, 232–239.

510. Puig-Basagoiti,F., Qing,M., Dong,H., Zhang,B., Zou,G., Yuan,Z. and Shi,P.-Y. (2009) Identification and characterization of inhibitors of West Nile virus. *Antiviral Res*, **83**, 71–79.

511. Falk,S.P. and Weisblum,B. (2014) Aptamer Displacement Screen for Flaviviral RNA Methyltransferase Inhibitors. *Journal of Biomolecular Screening*, **19**, 1147–1153.

512. Bouvet,M., Debarnot,C., Imbert,I., Selisko,B., Snijder,E.J., Canard,B. and Decroly,E. (2010) In vitro reconstitution of SARS-coronavirus mRNA cap methylation. *PLoS Pathog*, **6**, e1000863–e1000863.

513. Sun,Y., Wang,Z., Tao,J., Wang,Y., Wu,A., Yang,Z., Wang,K., Shi,L., Chen,Y. and Guo,D. (2014) Yeast-based assays for the high-throughput screening of inhibitors of coronavirus RNA cap guanine-N7-methyltransferase. *Antiviral Res*, **104**, 156–164.

514. Gorgulla,C., Padmanabha Das,K.M., Leigh,K.E., Cespugli,M., Fischer,P.D., Wang,Z.-F., Tesseyre,G., Pandita,S., Shnapir,A., Calderaio,A., *et al.* (2021) A multi-pronged approach targeting SARS-CoV-2 proteins using ultra-large virtual screening. *iScience*, **24**, 102021.

515. Gurung,A.B. (2020) In silico structure modelling of SARS-CoV-2 Nsp13 helicase and Nsp14 and repurposing of FDA approved antiviral drugs as dual inhibitors. *Gene Rep*, **21**, 100860.

516. Selvaraj,C., Dinesh,D.C., Panwar,U., Abhirami,R., Boura,E. and Singh,S.K. (2021) Structure-based virtual screening and molecular dynamics simulation of SARS-CoV-2 Guanine-N7 methyltransferase (nsp14) for identifying antiviral inhibitors against COVID-19. *J Biomol Struct Dyn*, **39**, 4582–4593.

517. Liu,C., Zhu,X., Lu,Y., Zhang,X., Jia,X. and Yang,T. (2021) Potential treatment with Chinese and Western medicine targeting NSP14 of SARS-CoV-2. *J Pharm Anal*, **11**, 272–277.

518. Martin,W.R. and Cheng,F. (2020) Repurposing of FDA-Approved Toremifene to Treat COVID-19 by Blocking the Spike Glycoprotein and NSP14 of SARS-CoV-2. *J Proteome Res*, **19**, 4670–4677.

519. Gentile,D., Fuochi,V., Rescifina,A. and Furneri,P.M. (2020) New Anti SARS-Cov-2 Targets for Quinoline Derivatives Chloroquine and Hydroxychloroquine. *Int J Mol Sci*, **21**, 5856.

520. Halder,U.C. (2021) Predicted antiviral drugs Darunavir, Amprenavir, Rimantadine and Saquinavir can potentially bind to neutralize SARS-CoV-2 conserved proteins. *Journal of biological research (Thessalonike, Greece)*, **28**, 18.

521. Basu,S., Mak,T., Ulferts,R., Wu,M., Deegan,T., Fujisawa,R., Wei Tan,K., Lim,C.T., Basier,C., Canal,B., *et al.* (2021) Identifying SARS-CoV-2 antiviral compounds by screening for small molecule inhibitors of Nsp14 RNA cap methyltransferase. *Biochemical Journal*, **478**, 2481–2497.

522. Kasprzyk,R., Spiewla,T.J., Smietanski,M., Golojuch,S., Vangeel,L., de Jonghe,S., Jochmans,D., Neyts,J., Kowalska,J. and Jemielity,J. (2021) Identification and evaluation of potential SARS-CoV-2 antiviral agents targeting mRNA cap guanine N7-Methyltransferase. *Antiviral Res*, **193**, 105142.

523. Kousar,K., Majeed,A., Yasmin,F., Hussain,W. and Rasool,N. (2020) Phytochemicals from Selective Plants Have Promising Potential against SARS-CoV-2: Investigation and Corroboration through Molecular Docking, MD Simulations, and Quantum Computations. *Biomed Res Int*, **2020**, 6237160.

524. Dutta,M. and Iype,E. (2021) Peptide inhibitors against SARS-CoV-2 2'-O-methyltransferase involved in RNA capping: A computational approach. *Biochem Biophys Rep*, **27**, 101069.

525. Khan,R.J., Jha,R.K., Amera,G.M., Jain,M., Singh,E., Pathak,A., Singh,R.P., Muthukumaran,J. and Singh,A.K. (2021) Targeting SARS-CoV-2: a systematic drug repurposing approach to identify promising inhibitors against 3C-like proteinase and 2'-O-ribose methyltransferase. *J Biomol Struct Dyn*, **39**, 2679–2692.

526. Tazikeh-Lemeski,E., Moradi,S., Raoufi,R., Shahlaei,M., Janlou,M.A.M. and Zolghadri,S. (2021) Targeting SARS-COV-2 non-structural protein 16: a virtual drug repurposing study. *J Biomol Struct Dyn*, **39**, 4633–4646.

527. Rasool,N., Yasmin,F., Sahai,S., Hussain,W., Inam,H. and Arshad,A. (2021) Biological perspective of thiazolide derivatives against Mpro and MTase of SARS-CoV-2: Molecular docking, DFT and MD simulation investigations. *Chem Phys Lett*, **771**, 138463.

528. Aldahham,B.J.M., Al-Khafaji,K., Saleh,M.Y., Abdelhakem,A.M., Alanazi,A.M. and Islam,M.A. (2020) Identification of naphthyridine and quinoline derivatives as potential Nsp16-Nsp10 inhibitors: a pharmacoinformatics study. *Journal of Biomolecular Structure and Dynamics*, 10.1080/07391102.2020.1851305.

529. Sharma,K., Morla,S., Goyal,A. and Kumar,S. (2020) Computational guided drug repurposing for targeting 2'-O-ribose methyltransferase of SARS-CoV-2. *Life Sci*, **259**, 118169.

530. Q Almeida-Neto,F.W., Castro Matos,M.G., Marinho,E.M., Marinho,M.M., Róseo Paula Pessoa Bezerra de Menezes,R., Sampaio,T.L., Bandeira,P.N., Celedonio Fernandes,C.F., Magno Rodrigues Teixeira,A., Marinho,E.S., *et al.* (2021) In silico study of the potential interactions of 4'-acetamidechalcones with protein targets in SARS-CoV-2. *Biochem Biophys Res Commun*, **537**, 71–77.

531. Singh,R., Bhardwaj,V.K., Sharma,J., Purohit,R. and Kumar,S. (2021) In-silico evaluation of bioactive compounds from tea as potential SARS-CoV-2 nonstructural protein 16 inhibitors. *J Tradit Complement Med*, 10.1016/j.jtcme.2021.05.005.

532. Maurya,A.K. and Mishra,N. (2021) In silico validation of coumarin derivatives as potential inhibitors against Main Protease, NSP10/NSP16-Methyltransferase, Phosphatase and Endoribonuclease of SARS CoV-2. *J Biomol Struct Dyn*, **39**, 7306–7321.

533. Vijayan,V., Pant,P., Vikram,N., Kaur,P., Singh,T.P., Sharma,S. and Sharma,P. (2021) Identification of promising drug candidates against NSP16 of SARS-CoV-2 through computational drug repurposing study. *Journal of Biomolecular Structure and Dynamics*, **39**, 6713–6727.

534. Liang,J., Pitsillou,E., Burbury,L., Hung,A. and Karagiannis,T.C. (2021) In silico investigation of potential small molecule inhibitors of the SARS-CoV-2 nsp10-nsp16 methyltransferase complex. *Chem Phys Lett*, **774**, 138618.

535. Kadioglu,O., Saeed,M., Greten,H.J. and Efferth,T. (2021) Identification of novel compounds against three targets of SARS CoV-2 coronavirus by combined virtual screening and supervised machine learning. *Comput Biol Med*, **133**, 104359.

536. el Hassab,M.A., Ibrahim,T.M., Al-Rashood,S.T., Alharbi,A., Eskandrani,R.O. and Eldehna,W.M. (2021) In silico identification of novel SARS-COV-2 2'-O-methyltransferase (nsp16) inhibitors: structure-based virtual screening, molecular dynamics simulation and MM-PBSA approaches. *J Enzyme Inhib Med Chem*, **36**, 727–736.

537. Chandra,A., Chaudhary,M., Qamar,I., Singh,N. and Nain,V. (2021) In silico identification and validation of natural antiviral compounds as potential inhibitors of SARS-CoV-2 methyltransferase. *J Biomol Struct Dyn*, 10.1080/07391102.2021.1886174.

538. Jiang,Y., Liu,L., Manning,M., Bonahoom,M., Lotvola,A., Yang,Z. and Yang,Z.-Q. (2020) Structural analysis, virtual screening and molecular simulation to identify potential inhibitors targeting 2'-O-ribose methyltransferase of SARS-CoV-2 coronavirus. *J Biomol Struct Dyn*, 10.1080/07391102.2020.1828172.

539. Maurya,S.K., Maurya,A.K., Mishra,N. and Siddique,H.R. (2020) Virtual screening, ADME/T, and binding free energy analysis of anti-viral, anti-protease, and anti-infectious compounds against NSP10/NSP16 methyltransferase and main protease of SARS CoV-2. *J Recept Signal Transduct Res*, **40**, 605–612.

540. Omotuyi,I.O., Nash,O., Ajiboye,B.O., Olumekun,V.O., Oyinloye,B.E., Osuntokun,O.T., Olonisakin,A., Ajayi,A.O., Olusanya,O., Akomolafe,F.S., *et al.* (2021) Aframomum melegueta secondary metabolites exhibit polypharmacology against SARS-CoV-2 drug targets: in vitro validation of furin inhibition. *Phytotherapy Research*, **35**, 908–919.

541. Encinar,J.A. and Menendez,J.A. (2020) Potential Drugs Targeting Early Innate Immune Evasion of SARS-Coronavirus 2 via 2'-O-Methylation of Viral RNA. *Viruses*, **12**, 525.

542. Mahalapbutr,P., Kongtaworn,N. and Rungrotmongkol,T. (2020) Structural insight into the recognition of S-adenosyl-L-homocysteine and sinefungin in SARS-CoV-2 Nsp16/Nsp10 RNA cap 2'-O-Methyltransferase. *Comput Struct Biotechnol J*, **18**, 2757–2765.

543. Jaan,S., Waheed,S., Bashir,S., Javed,M.S., Amjad,A., Nishan,U., Nawaz,H. and Shah,M. (2021) Virtual Screening and Molecular Docking of FDA Approved Antiviral Drugs for the Identification of

Potential Inhibitors of SARS-CoV-2 RNA-MTase Protein. *International Journal of Advanced Biological and Biomedical Research*, **9**, 105–118.

544. Saliu,T.P., Umar,H.I., Ogunsile,O.J., Okpara,M.O., Yanaka,N. and Elekofehinti,O.O. (2021) Molecular docking and pharmacokinetic studies of phytocompounds from Nigerian Medicinal Plants as promising inhibitory agents against SARS-CoV-2 methyltransferase (nsp16). *J Genet Eng Biotechnol*, **19**, 172.

545. Malik,A., Kohli,M., Jacob,N.A., Kayal,A., Raj,T.K., Kulkarni,N. and Chandramohan,V. (2021) In silico screening of phytochemical compounds and FDA drugs as potential inhibitors for NSP16/10 5' methyl transferase activity. *Journal of Biomolecular Structure and Dynamics*, 10.1080/07391102.2021.2005680.

546. Kumar,M., Roy,A., Rawat,R.S., Alok,A., Tetala,K.K.R., Biswas,N.R., Kaur,P. and Kumar,S. (2021) Identification and structural studies of natural inhibitors against SARS-CoV-2 viral RNA methyltransferase (NSP16). *Journal of Biomolecular Structure and Dynamics*, 10.1080/07391102.2021.1997821.

547. Alzahrani,A.Y., Shaaban,M.M., Elwakil,B.H., Hamed,M.T., Rezki,N., Aouad,M.R., Zakaria,M.A. and Hagar,M. (2021) Anti-COVID-19 activity of some benzofused 1,2,3-triazolesulfonamide hybrids using in silico and in vitro analyses. *Chemometr Intell Lab Syst*, **217**, 104421.

548. Khalili Yazdi,A., Li,F., Devkota,K., Perveen,S., Ghiabi,P., Hajian,T., Bolotokova,A. and Vedadi,M. (2021) A High-Throughput Radioactivity-Based Assay for Screening SARS-CoV-2 nsp10-nsp16 Complex. *SLAS Discov*, **26**, 757–765.

549. Perveen,S., Khalili Yazdi,A., Devkota,K., Li,F., Ghiabi,P., Hajian,T., Loppnau,P., Bolotokova,A. and Vedadi,M. (2021) A High-Throughput RNA Displacement Assay for Screening SARS-CoV-2 nsp10-nsp16 Complex toward Developing Therapeutics for COVID-19. *SLAS Discov*, **26**, 620–627.

550. Bullard-Feibelman,K.M., Fuller,B.P. and Geiss,B.J. (2016) A Sensitive and Robust High-Throughput Screening Assay for Inhibitors of the Chikungunya Virus nsP1 Capping Enzyme. *PLoS One*, **11**, e0158923–e0158923.

551. Kovacikova,K., Morren,B.M., Tas,A., Albulescu,I.C., van Rijswijk,R., Jarhad,D.B., Shin,Y.S., Jang,M.H., Kim,G., Lee,H.W., *et al.* (2020) 6'-β-Fluoro-Homoaristeromycin and 6'-Fluoro-Homoneplanocin A Are Potent Inhibitors of Chikungunya Virus Replication through Their Direct Effect on Viral Nonstructural Protein 1. *Antimicrob Agents Chemother*, **64**, e02532-19.

552. Mudgal,R., Mahajan,S. and Tomar,S. (2020) Inhibition of Chikungunya virus by an adenosine analog targeting the SAM-dependent nsP1 methyltransferase. *FEBS Lett*, **594**, 678–694.

553. Kaur,R., Mudgal,R., Narwal,M. and Tomar,S. (2018) Development of an ELISA assay for screening inhibitors against divalent metal ion dependent alphavirus capping enzyme. *Virus Research*, **256**, 209–218.

554. Feibelman,K.M., Fuller,B.P., Li,L., LaBarbera,D. v and Geiss,B.J. (2018) Identification of small molecule inhibitors of the Chikungunya virus nsP1 RNA capping enzyme. *Antiviral Res*, **154**, 124–131.

555. Abdelnabi,R., Kovacikova,K., Moesslacher,J., Donckers,K., Battisti,V., Leyssen,P., Langer,T., Puerstinger,G., Quérat,G., Li,C., *et al.* (2020) Novel Class of Chikungunya Virus Small Molecule Inhibitors That Targets the Viral Capping Machinery. *Antimicrob Agents Chemother*, **64**, e00649-20.

8 List of publications

8.1 Scientific publications

(1) Fabian Barthels, Stefan J. Hammerschmidt, **<u>Tim R. Fischer</u>**, Collin Zimmer, Elisabeth Kallert, Mark Helm, Christian Kersten, Tanja Schirmeister (2022) A low-cost 3D-printable differential scanning fluorometer for protein and RNA melting experiments. *HardwareX*, **11**, e00256.

Under revision:

(2) Marvin Schwickert,[‡] **<u>Tim R. Fischer,[‡]</u>** Robert A. Zimmermann,[‡] Sabrina N. Hoba, J. Laurenz Meidner, Marlies Weber, Moritz Weber, Martin M. Stark Jonas Koch, Christian Kersten, Frank Lyko, Mark Helm and Tanja Schirmeister (2022) Discovery of potent inhibitors of DNA methyltransferase 2, an epitranscriptomic modulator and potential target for cancer treatment. *J. Med. Chem.*, currently under revision.

[‡]These authors contribute equally.

8.2 Review articles

(3) **<u>Tim R. Fischer</u>**, Laurenz Meidner, Marvin Schwickert, Marlies Weber, Robert A. Zimmermann, Christian Kersten, Tanja Schirmeister* and Mark Helm (2022) Chemical biology and medicinal chemistry of RNA methyltransferases. *Nucleic Acid Res.*, gkac224.

9 Curriculum Vitae